ISSN 1694-7398
e-ISSN
journals.manas.edu.kg

December 2019
Volume 7, Issue 2

# MJEN

# MANAS JOURNAL OF ENGINEERING

BISHKEK

Kyrgyz - Turkish Manas University
Manas Journal of Engineering (MJEN)

ISSN: 1694- 7398
e-ISSN: 1694- 7398
Year: 2019
Volume: 7
Issue: 2
http://journals.manas.edu.kg
journals@manas.edu.kg

**PUBLICATION PERIOD**

Manas Journal of Engineering (MJEN) is published twice year, MJEN is a peer reviewed journal.



CORRESPONDENCE ADDRESS
Kyrgyz Turkish Manas University
Mira Avenue 56 Bishkek, KYRGYZSTAN
URL: http://journals.manas.edu.kg
e-mail: journals@manas.edu.kg
Tel : +996 312 492763- Fax: +996 312 541935

Kyrgyz - Turkish Manas University
Manas Journal of Engineering (MJEN)

# Contents

MANAS Journal of Engineering
ISSN 1694-7398 | e-ISSN 1694-7398

*Volume 7 (Issue 2) (2019) Pages 68-73*

# Phenol recovery and removal from aqueous solutions by emulsion liquid membranes

Durdu Topkara[1], Osman Tutkun[2,*], Janarbek Izakov[3], Nurzat Shaykieva[3]

[1]Sakarya University, Faculty of Science, 54187 Adapazarı, Türkiye

[2]Kyrgyz-Turkish Manas University, Dept. Chem. Eng., Bishkek, Kyrgyzstan, osman.tutkun@manas.edu.kg, ORCID: 0000-0001-6585-9228

[3]Kyrgyz-Turkish Manas University, Dept. Env. Eng., Bishkek, Kyrgyzstan

**ABSTRACT**

Emulsion type liquid membrane process is a new and effective method for separation of mixtures with applications in the nuclear industry, hydrometallurgy and wastewater treatment. The emulsified liquid membrane is made by forming an emulsion of two immiscible phases and then dispersing the emulsion in a third phase (i.e. continuous or feed phase). Phenol is mainly found in the wastewaters of such industries as petroleum refineries and petrochemicals. In addition phenol is also contained in the wastewaters of industries of resins, explosives, paper, plastics, glass and rubbers. Numerous solvent extraction techniques using various ligands are also used as commercial in such processes as hydrometallurgy and wastewater treatment. However one of the disadvantage of solvent extraction is the necessity of solvents and ligands of large quantities. Water-oil-water (W/O/W) type of liquid membrane system provides excellent separation techniques and thus this causes a substantial reduction in the amount of ligands and solvents, Liquid membrane phase consist of a surfactant (Span 80) and solvent (kerosene). In this study the most important parameters that provide the extraction of phenol from aqueous solutions and their effect on extraction efficiency were examined by liquid membrane process. These parameters are determined to be as membrane viscosity, treatment ratio (feed volume/emulsion volume), surfactant concentration, feed concentration and pH, mixing speed and phase ratio (stripping solution volume / membrane volume). The phenol was extracted from the aqueous feed solutions in which phenol concentration ranged from 100 to 550 mg/L. Optimum parameters were found to be as: pH = 4; phase ratio, $\phi = 1$; mixing speed (300 rpm); 3 % Span 80 and 2 % NaOH. Under the suitable conditions, about 96 % of the phenol in the feed solutions could be removed from the solution It has been possible that the phenol concentration were reduced from 550 mg/L to 5-10 mg/L within two minutes.

**ARTICLE INFO**

***Research article***

*Received: 19.11.2019*
*Accepted: 02.12.2019*

***Keywords:***
*Emulsion liquid membranes,*
*phenol recovery,*
*phenol removal,*
*4-aminoantipyrine,*
*phenol extraction,*
*Span 80*

**Corresponding author*

## 1. Introduction

Phenol and its derivatives are used as raw materials for manufacturing a wide variety of useful chemicals including coal gasification, petrochemical, wood products, paints, dyes, polymers, pharmaceuticals and pesticides. The discharges from oil refineries and coal conversion processes are also rich in these contaminants. They are released in industrial wastewater and domestic water, and may directly or indirectly cause serious health and odour problems. As a result, phenols and phenolic compounds are prevalent industrial effluents and major source of water pollution. Therefore, both US Environmental Protection Agency (EPA) and the European Union (EU) directive number 80/778/EC consider phenol as a priority pollutant [1-4]. Most of the overall world production of phenol, which was $7.78 \times 10^6$ tons in 2001, is related to the production of bisphenol A (39%), phenolic resins (27%), and the others [5].

The various techniques available for the treatment of phenolic effluents can be subdivided into two main categories: destruction and recovery methods. Among the destruction methods, there are biological treatments [7-8], incineration, ozonisation in the presence of UV radiation, and oxidation with wet air [6]. Treatment times with chemical or biological methods may be quite high and total mineralization of the effluent stream may not be possible. Existing wastewater treatment methods such as adsorption on activated carbon and chemical oxidation suffer from limitations, such as limited

applicability and low efficiency, hence imparting the need research into alternative treatment techniques such as membrane processes[13]. On the other hand, recovery methods include liquid-liquid extraction [3,9], ionic exchange with resins [10]. Solvent extraction is the most often used technique to recover phenol ($pK_a$ =10.0) in its neutral form [11]. This method requires expensive and hazardous organic solvents, which are undesirable for health and environment [12].

Development of new low-cost processes capable to substitute existing separation and purification technologies is a challenging task. Membrane technologies is used in many industrial sectors as important alternative to the classical separation and purification processes. The emulsion liquid membrane (ELM) technique has been regarded as an advance in relation to solvent extraction for separating and concentrating metal ions from aqueous dilute solutions. In this respect, liquid membranes have shown a great potential, especially in cases where solute concentrations are relatively low and other techniques cannot be applied efficiently since they combine the process of extraction and stripping in a single unit operation. The extraction chemistry is basically the same as that in solvent extraction, but the transport is governed by kinetics rather than equilibrium parameters, that is, it is governed by a non-equilibrium mass transfer. Moreover, the large specific interfacial areas associated with ELMs result in higher permeation rates, which together with the reaction rather than equilibrium restrain, enable the achievement of higher solute concentrations in fewer separation stages, maintaining the high selectivity of solvent extraction [14]. Several studies have reported the extraction of phenols by emulsion liquid membranes [13,15-18] and by supported liquid membranes [2-3,12].

In this study the most important parameters that provide the extraction of phenol from aqueous solutions and their effect on extraction efficiency were examined by liquid membrane process. These parameters are determined to be as membrane viscosity, treatment ratio (feed volume / emulsion volume), surfactant concentration, feed concentration and pH, mixing speed and phase ratio (stripping solution volume/membrane volume)..

## 2. Experimental

### *2.1 Chemicals*

Surface active reagent sorbitan monooleate (Span 80, Fluka), petroleum fractions (kerosene, Tupras, Turkiye), stripping solution (NaOH, Merck), 4-aminoantipyrine, $K_3Fe(CN)_6$, $K_2HPO_4$ and $NH_3$ (all being Merck) for phenol analysis were used. All salts and reagents were of analytical grade and used for without further purification.

### *2.2 Experimental Procedure*

The liquid membrane phase is composed of a surfactant (Span 80) and a solvent. The surfactant is a sorbitanmonooleate which is commercially known as Span 80. The solvent is a commercial kerosene, obtained from Tupras Corp., Turkiye (density 830 kg/m$^3$ and viscosity 1.6 mPa.s at 20 $^o$C). Batch extraction experiments of phenol were conducted in a 600 mL-glass beaker, stirred vessel with four Teflon-coated baffle plates. A Teflon turbine impeller was used. Phenol stock solutions were prepared by dissolving analytical grade phenol, purchased from Merck, in double-disttilled water. Various feed solutions were prepared by diluting the stock solutions as desired.

The extraction of phenol using emulsion type of liquid membrane (ELM) involves three steps, namely preparation of ELM, extraction of the solute (phenol) from the feed solution by contacting the emulsion, and separation of liquid emulsion from external phase by settling, as shown in Fig. 1.

Sodium hydroxide solutions were used for strip phase. Feed mixture was prepared from the stock solution of phenol. The buffer soution was essential for phenol extraction to maintain the desired feed pH, which was very critical. Unless otherwise stated, pH of feed solution, mixing speed and volume ratio of strip phase/membrane phase/feed phase ($V_s/V_m/V_F$) were kept constant. The 25-mL of strip was added dropwise to the 25 to 30 mL-membrane phase, stirred at 1900 for the period of 20 minutes and passed through a burette in about 8 minutes. The prepared W/O emulsion was immediately dispersed into a 500-mL feed solution. The uptake of phenol was monitored by removing 1-2 mL of samples of the feed phase periodically for analysis with a UV-VIS spectrophotometer (Shimadzu, Japan). All the extraction experiments were carried out batchwise and at the ambient temperature of 20±1 $^o$C. The aqueous phase pH measurements were determined with a pH meter (Thermo Scientific Inc., Eutech 150 & 450 Series, Singapore).

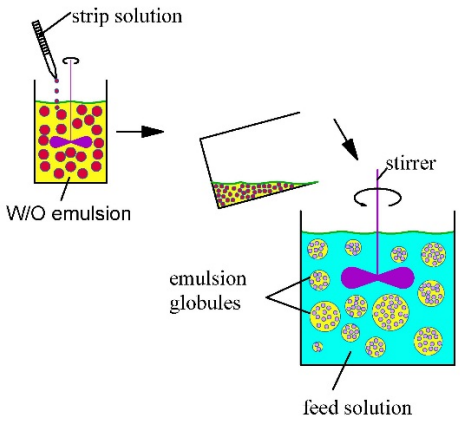


**Figure 1.** *The preparation of a W-O-W type of emulsion liquid membrane*

### 2.3. Determination of phenol concentration

The determination of phenol was determined according to the method of Annadurai et al. (19), based on rapid condensation with 4-aminoantipyrine (4-AAP) followed by oxidation with alkaline potassium ferricyanide giving red color detected UV-Vis spectrophotometer at 510 nm wavelength. The reaction is as follows:

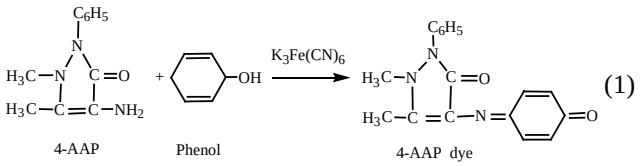


(1)

In order not to be a color change in the solution, the phenol samples have to be read within 30 minutes. The 2-mL samples taken are diluted to 100 mL in volumetric flasks, before the 2.5 mL of 0.50 M $NH_4OH$ solution is added to each of the flasks, and pH of the solution is adjusted to $7.9 \mp 0.1$ using a phosphate buffer. 1 mL of 4-aminoantipyrine solution is added to all samples and is well mixed. 15 minutes later, absorbances of all the samples are measured by a UV-Vis spectrophotometer at 510 nm wavelength against the blank. Before the measurements are taken, the spectrophotometer is calibrated using standard phenol solutions and the obtained relation is given by Eqn. (2) as

$$y = 7.962x + 0.1388 \quad (2)$$

where $y$: phenol concentration, mg/L, and $x$: absorbance of sample.

## 3. Results and discussion

### 3.1. Effect of surfactant concentration

The effect of surfactant concentration on the behavior of the rate extraction and phenol removal was studied in the range of 1 through 3 wt % Span 80, as shown in Fig. 2. From 2, the percentage removal of phenol in 5 min increased from 89.4 to 96.2 % with an increase in the Span 80 from 1 to 3 wt %. After 5 min, as the time increased the membrane stability tended to slightly decreased, as a result the emulsion stability increases as the surfactant concentration increases.

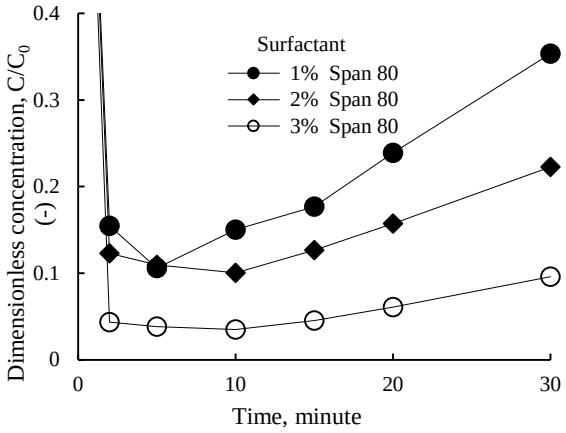


**Figure 2.** *Effect of surfactant (Span 80) on the rate of extraction (Feed conc.: 565.4 mg/L; strip solution: 25 mL 2 wt % NaOH; treatment ratio ($V_F/V_E$): 5/1; phase ratio: 1/1; pH: 4; mixing speed: 400 min$^{-1}$)*

### 3.2. Effect of mixing speed

To investigate the mixing speed on removal of phenol the mixing speed increased from 300 to 400 min$^{-1}$, as shown in Fig. 3. It is observed from Fig. 3 that mixing speed at 300 min$^{-1}$ provides maximum removal of phenol with higher emulsion stability. From Fig. 3, initially, that is, in the first 5 min the percentage of phenol removal slightly increases, but later there is a notable increase in the extraction efficiency. The reason for that might be, with an increase in the mixing speed relatively smaller emulsion globules may have formed, and thus the phenol removal rate or mass transfer increases. However, after 15 min, the emulsion globules tend to break up, and as a result the extraction efficiency decreases.

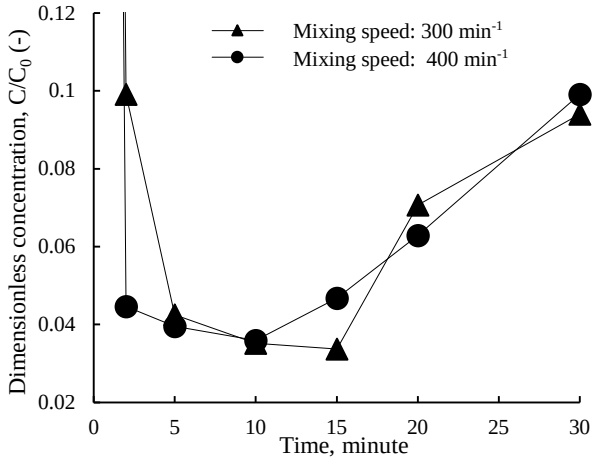


**Figure 3.** *Effect of mixing speed on the rate of extraction (Feed conc.: 548.8 mg/L; surfactant conc.: 3 wt % Span 80; strip solution: 25 mL 2 wt % NaOH; treatment ratio ($V_F/V_E$): 5/1; phase ratio: 1/1; pH: 4)*

### 3.3. Effect of external solution pH

The effect of external phase pH on removal rate of phenol was studied in the range of 2 through 6, as shown in Fig. 4. From Fig. 4, it is clearly evident that the most favorable case was obtained at pH 4, adjusted by concentrated hydrochloric acid. Similar behavior was also experienced and reported elsewhere (18). However, at pH 4 when the pH adjustment was made by $H_2SO_4$ instead of HCl, the percentage of phenol removal significantly deteriorated. At pH 4, the removal efficiency of phenol remained to be constant between 10 and 20 min, being about 95 %.

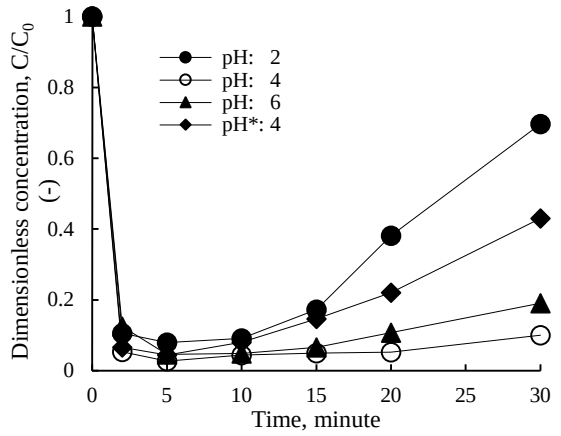


**Figure 4.** *Effect of external phase pH (Feed conc.: 542 mg/L; surfactant conc.: 3 wt % Span 80; strip solution: 25 mL 2 wt % NaOH; mixing speed: 300 min$^{-1}$; treatment ratio ($V_F/V_E$): 5/1; phase ratio: 1/1; Note: pH 4* was adjusted using concentrated $H_2SO_4$)*

### 3.4. Effect of treatment ratio

The effect of external phase to emulsion volume ratio (treatment ratio) in the range from 4 to 7 was studied on the removal of phenol and emulsion stability, and the results are indicated in Fig. 5. With an increase in the treatment ratio from 4 to 7 (v/v), decrease in removal of phenol from 96.0 to 89 in the first 5 min. From Fig. 5, if the phenol removals for three treatment ratios in 5 min are compared, the phenol extraction efficiency decreased from 96.0 to 89.6 %. However, the membrane stability tends to break up and deteriorates as time as the time goes on.

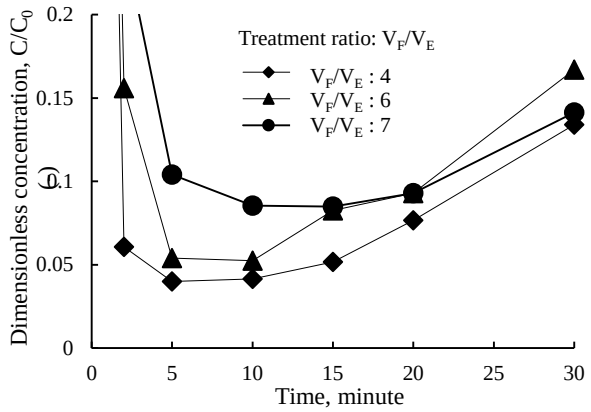


**Figure 5.** *Effect of treatment ratio on the rate of extraction (Feed conc.: 500 mg/L; surfactant conc.: 3 wt % Span 80; strip solution: 25 mL 2 wt % NaOH; mixing speed: 300 min$^{-1}$; phase ratio: 1/1; pH: 4)*

### 3.5. Effect of phase ratio ($V_s/V_m$)

The effect of internal to membrane phase volume ratio, on removal of phenol and emulsion stability was studied experimentally in the range of 0.8 to 1.4, as shown in Fig. 6. As seen from Fig. 6, the best phase ratio was obtained at $\phi$=1.0. The percentage removal of phenol increased from 95.3 to 92.6 %, as the ratio increased from 0.8 to 1.4 in the first 5 min. At the phase ratio of 1.0, the percentage of phenol removal from 5 to 20 min gradually decreases.

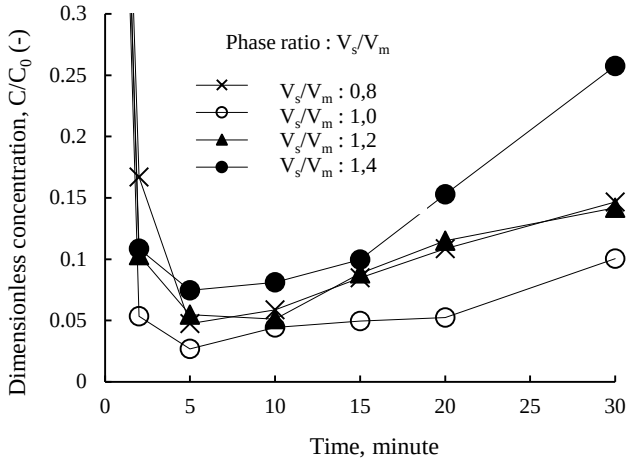


**Figure 6.** *Effect of phase ratio on the rate of extraction (Feed conc.: 542.4 mg/L; surfactant conc.: 3 wt % Span 80; strip solution: 25 mL 2 wt % NaOH; mixing speed: 300 min$^{-1}$; treatment ratio ($V_F/V_E$): 5/1; phase ratio: 1/1; pH: 4)*

### 3.6. Effect of strip solution concentration

The rol of stripping agent in strip phase in phenol removal was investigated in the concentration range from 0.5 through 2 wt % NaOH, and the results obtained are given in Fig. 7. As observed from Fig. 7, the percentage removal of phenol

increased from 91.2 to 96.6 % in 15 min. NaOH in the strip solution gives the following reaction:

$$C_6H_5OH + NaOH \rightarrow C_6H_5ONa + H_2O \qquad (3)$$

The reaction prevents the phenol from returning to the feed solution through the membrane phase. 2 % strip solution of NaOH was found to be more appropriate for the phenol extraction.

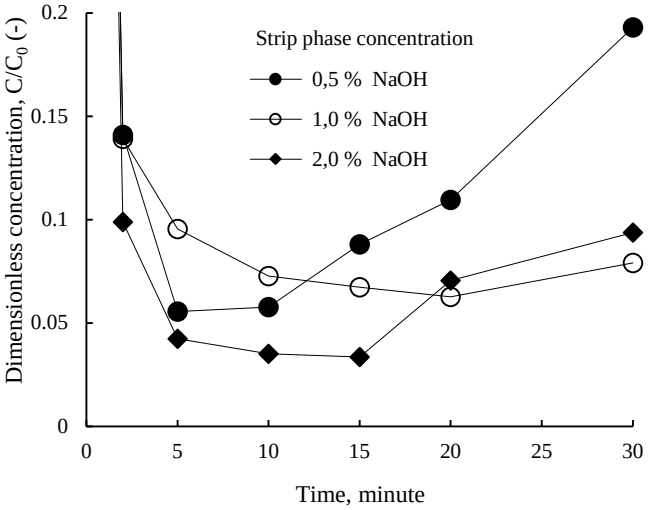


**Figure 7.** *Effect of strip solution (NaOH) on the rate of extraction (Feed conc.: 550 mg/L; surfactant conc.: 3 wt % Span 80; mixing speed: 300 min$^{-1}$; treatment ratio ($V_F/V_E$): 5/1; phase ratio: 1/1; pH: 4)*

### *3.7. Effect of external solution concentration*

Effect of initial phenol concentration in the feed solution on the extent of extraction is shown in Fig. 8, using the optimum parameters. The phenol concentration in the external or feed phase ranging from 100 to 550 mg/L is presented in Fig. 8. In 5 min, the percentage of phenol removal from 100 through 550 mg/L of the external phase concentrations is about 96.0 %. As the time passes from 5 to 20 min, the phenol removal decreases down to about 90 %.

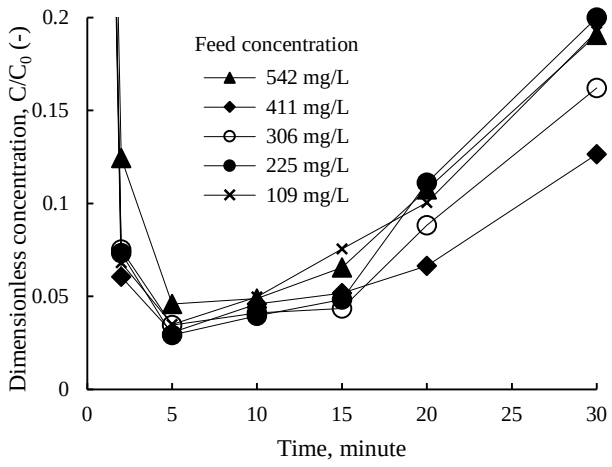


**Figure 8.** *Effect of initial phenol concentration in the external phase (Feed concs.: 100-550 mg/L; surfactant conc.: 3 wt % Span 80; mixing speed: 300 min$^{-1}$; strip solution: 25 mL 2 wt % NaOH; treatment ratio ($V_F/V_E$): 5/1; phase ratio: 1/1; pH: 4)*

## 4. Conclusion

Removal of phenol from aqueous solutions, containing 550 mg/L phenol, using an emulsion liquid membrane (ELM) was investigated. EML consisted of surfactant Span 80, and diluent kerosene of a petroleum fraction, NaOH solutions was used as strip phase. Such parameters as surfactant (Span 80) concentration, feed solution pH and concentration, mixing speed, treatment ratio, internal phase ratio, and strip phase concentration were studied and from this study following conclusions could be drawn:

1. As the surfactant concentration increased from 1 to 3 wt %, the membrane stability increased, as a result extraction efficiency also raised.

2. As the mixing speed increased from 300 to 400 rpm, the extraction efficiency in the first 5 minutes increased, but later due to the breakages of the emulsion globules, the membrane stability was reduced, as a result the efficiency decreased.

3. As the feed solution pH increased from 2 to 6, the extraction efficiency also increased, pH 4 gave the highest efficiency, that is, feed solution pH is of great significance.

4. As the treatment ratio ($V_F/V_E$), that is the ratio of feed volume to emulsion volume, increased from 4/1 to 7/1, the extraction efficiency decreased from 96 % to 89.6 %.

5. As the phase ratio $\phi$ ($V_s/V_m$), that is, the ratio of strip phase volume to membrane volume, increased from 0.8 to 1.4, the highest efficiency was obtained at $\phi = 1$, being 90 %.

6. As the strip solution (NaOH) concentration increased from 0.5 to 2 %, the highest extraction efficiency was obtained at 2 wt % of NaOH concentration.

7. The optimum conditions, from examining the experimental parameters, were as follows :

- Diluent: Petroleum fraction kerosene
- Surfactant: 3 wt % Span 80
- Feed solution pH: 4.0.
- Strip phase concentration: 2 wt % NaOH
- Treatment ratio : 4
- Phase ratio $\phi$ ($V_s/V_m$): 1.0
- Mixing speed : 300 $min^{-1}$

8. At the optimum conditions, as the phenol concentration in feed phase increased from 108 mg/L to 550 mg/L, the extraction efficiency in this direction decreased. However, for 542.4 mg/L of phenol concentration, 95.5 % of phenol was extracted in 5 minutes, for 108.5 mg/L of phenol feed concentration, 96.5 % of phenol was removed or extracted from the feed solution in 5 minutes.

**Acknowledgements**

The authors wish to thank to the Kyrgyz-Turkish Manas University, Kyrgyzstan for providing facilities and financial support.

**References**

[1]. Gonzalez-Munoz M.J., Luque S., Alvares J.R., Coca J. "Recovery of phenol from aqueous solutions using hollow fibre contactars", J. Memb. Sci., 213, (2013), 181-193.

[2]. Praveen P., Loh K.-C, "Trioctyl phosphine oxide-impregnated hollow fiber membranes for removal of phenol from wastewater", J. Memb. Sci., 437, (2013), 1-6.

[3]. Zidi C., Tayeb R., Ben Sik Ali M., Dhahbi M. "Liquid-liquid extraction and transport across supported liquid membrane of phenol using tributyl phosphate", J. Memb. Sci., 360, (2010), 334-340.

[4]. Hill G.H., Robinson C.W. "Substrate inhibition kinetics: degradation kinetics by *Pseudomonas Putida*", Biotechnol. Bioeng., 17, (1975), 1599-1615.

[5]. Anonymous, Phenol, Chem. Week 64, (2002), 31.

[6]. Saxena S.C., Jotshi C.K. "Management and combustion of hazardous wastes", Prog. Energy Combust. Sci., 22, (1996), 401-425.

[7]. Zilli M., Converti A., Flickinger M.C., in: Drew S.W. (Eds.), The Encyclopedia of Bioprocess Technology: Fermentation, Biocatalysis, and Bioseparation, Wilew, New York, (1999).

[8]. Zilli M., Fabiano B., Ferraiolo A., Converti A. "Micro-kinetic investigation on phenol uptake from air by biofiltration: Influence of superficial gas flow rate and inlet pollutant concentration", Biotechnol. Bioeng., 49, (1996), 391-398.

[9]. Jiang H., Fang Y., Fu Y., Guo Q.-X. "Studies on the extraction of phenol in wastewater", J. Hazard. Mat. B, 101, (2003), 179-190.

[10]. Palepu D.T., Chauhan S.P., Amanth K.P., in: Freeman H.M. (Ed.), Industrial Pollution Prevention Handbook, McGraw-Hill, New York, (1995).

[11]. King C.J., Senetar J.J., in: Marinsky J.A., Marcus Y. (Eds.), Solvent Extraction of Industrial Organic Substances, Ion Exchange and Solvent Extraction, Vol. 10, Dekker, New York, (1988), 35-61.

[12]. Zidi C., Tayeb R., Dhahbi M. "Extraction of phenol from aqueous solutions by means of supported liquid membrane (MLS) containing tri-n-octyl phosphine oxide (TOPO)", J. Hazard. Mat., 194, (2011), 62-68.

[13]. Chaouchi S., Hamdaoui O. "Removal of 4-nitrophenol from water by emulsion liquid membrane", Desal. Water Treat, (2015), 1-5.

[14]. Draxler J., Furst W., Marr R. "Separation of metal species by emulsion liquid membranes", J. Memb. Sci., 38, (1988), 281-293.

[15]. Reis M.T.A., Freitas O.M.F., Agarwal S., Ferreira L.M., Rosinda M., Ismael M.R.C., Machado R., Carvalho J.M.R. "Removal of phenols from aqueous solutions by emulsion liquid membranes", J. Hazard. Mat., 192, (2011), 986-994.

[16]. Kargari A. "Simultaneous extraction and stripping of 4-chlorophenol from aqueous solutions by emulsion liquid membrane", Desal. Water Treat, 51, (2013), 2275-2279.

[17]. Rosly M.B., Jusoh N., Othman N., Rahman H.A., Noah N.F.M., Sulaiman R.N.R. "Effect and optimization parameters of phenol removal in emulsion liquid membrane process via fractional-factorial design", Chem. Eng. Res. Design, 145. (2019). 268-278.

[18]. Balasubramanian A., Venkatesan S. "Removal of phenolic compounds from aqueous solutions using Aliquat 336 as a carrier in emulsion liquid membrane", Korean J. Chem. Eng., 29, (11), (2012), 1622-1627.

[19]. Annadurai G., Rajehbabu S., Mahesh K.P.O., Murugen T. "Adsorption and biodegradation of phenol by chitosan-immobilized *pseudomonas putida* (NICM 2174)", Bioprocess Eng., 22, (2000), 493-501

MANAS Journal of Engineering
ISSN 1694-7398 | e-ISSN 1694-7398

*Volume 7 (Issue 2) (2019) Pages 74-88*

# A review study on the using of diethyl ether in diesel engines: effects on smoke and PM emissions

İsmet Sezer

Gumushane University, Baglarbasi Street 29100 Gumushane, Turkey, isezer@gumushane.edu.tr, ORCID: 0000-0001-7342-9172

**ABSTRACT**

This study was compiled from the results of various researches performed on using diethyl ether as a fuel or fuel additive in diesel engines. Three different techniques are used for the reduction of the harmful exhaust emissions of diesel engines. The first technique for the reduction of harmful emissions is improved the combustion by modification of engine design and fuel injection system, but this process is expensive and time consuming. The second technique is the using various exhaust gas devices like catalytic converter and diesel particulate filter. However, the use of these devices affects negatively diesel engine performance. The final technique to reduce emissions and also improve diesel engine performance is the use of various alternative fuels or fuel additives. The major pollutants of diesel engines are oxide of nitrogen (NOx) and smoke or particulate matter (PM). It is very difficult to reduce NOx and PM simultaneously in practice. Most of the researchers declare that the best way to reduce is the use of various alternative fuels i.e. natural gas, biogas, biodiesel or using the additives with alternative fuels or conventional diesel fuel. Therefore, it is very important that the results of various studies on alternative fuels or fuel additives are evaluated together to practice applications. Especially, this study focus on the use of diethyl ether in diesel engines as fuel or fuel additive in various diesel engine fuels. This review study investigates the effects of diethyl ether addition on the smoke and PM emissions.

**ARTICLE INFO**

***Review article***

*Received: 27.08.2019*
*Accepted: 12.11.2019*

***Keywords:***
*Diesel engine performance, diethyl ether, fuel additives, PM emissions*

## 1. Introduction

Diesel engines are widely used in both light and heavy-duty vehicles [1]. They are reliable, robust and the most efficient internal combustion engines [2]. However, diesel engines are suffer form their high emission drawbacks like particulate matters (PM), total gaseous hydrocarbons (THC), nitrogen oxides (NOx), sulfur oxides (SOx) and smoke [3, 4]. It is seemed that the most suitable way to reduce of these emissions is the using of alternative fuels made from renewable sources instead of the commercial fuels [5]. However, complete replacement of fossil fuels with renewable alternative fuels will require to a comprehensive modification of the engine hardware and their combustion in the engine results in operational and technical limitations [6]. The fuel side modification techniques such as blending, emulsification and oxygenation are the easy way for emission reduction without any modification on the engine hardware. Modification of diesel fuel to reduce exhaust emission can be performed by increasing the cetane number, reducing fuel sulphur, reducing aromatic content, increasing fuel volatility and decreasing the fuel density to have the compromise between engine performance and engine out emissions, one such change has been the possibility of using diesel fuels with oxygenates [7]. Among different alternative fuels, oxygenated fuel is a kind of alternative fuel. Diethylene glycol dimethyl ether (DGM), dimethoxy methane (DMM), dimethyl ether (DME), methyl tertiary butyl ether (MTBE), dibutyl ether (DBE), dimethyl carbonate (DMC), methanol, ethanol and diethyl ether (DEE) have played their role to reduce diesel emissions [7, 8, 9]. These fuels can either be used as a blend with conventional diesel fuel or pure. These additives can also be used in combination with biodiesel [10]. The presence of oxygen in the fuel molecular structure plays an important role to reduce PM and other harmful emissions from diesel engines. However, NOx emissions can be reduced in some cases and be increased depending on the engine operating conditions [11, 12]. Especially, DEE is a suitable fuel for diesel engines due to it is a cetane improver besides an oxygenated fuel [13]. Therefore, this review study is devoted to use of DEE in diesel engines as fuel or fuel additive in various diesel engine fuels.

## 2. Properties of diethyl ether

Diethyl ether is the simplest ether expressed by its chemical formula $CH_3CH_2$-O-$CH_2CH_3$, consisting of two ethyl groups bonded to a central oxygen atom as seen in Fig. 1.

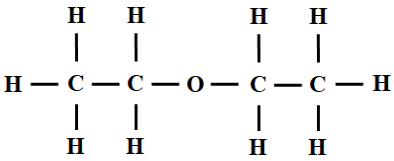

**Figure 1.** *Diethyl ether chemical structure [3]*

Diethyl ether (DEE) is regarded as one of the promising alternative fuels or an oxygen additive for diesel engines with its advantages of a high cetane number and oxygen content. DEE is liquid at the ambient conditions, which makes it attractive for fuel storage and handling. DEE is produced from ethanol by dehydration process as seen in Fig. 2 so it is a renewable fuel [14].

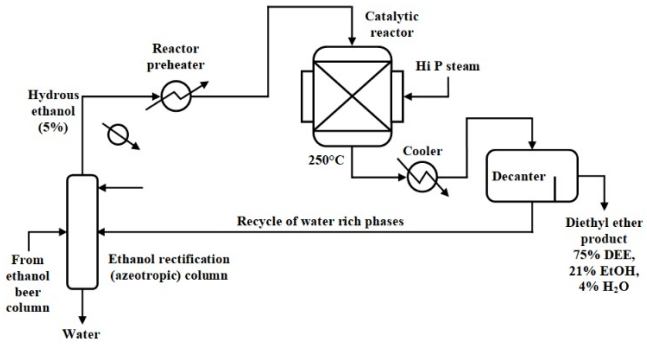


**Figure 2.** *Production of diethyl ether from ethanol [14]*

As shown in Table 1, DEE has several favorable properties, including exceptional cetane number, reasonable energy density, high oxygen content, low autoignition temperature and high volatility. Therefore, it can be assist to improving of engine performance and reducing the cold starting problem and emissions when using as a pure or an additive in diesel engines [14, 15].

**Table 1.** *The main fuel properties of diesel fuel and DEE [15].*

| Property | Diesel | DEE |
|---|---|---|
| Chemical formula | $C_xH_y$ | $C_4H_{10}O$ |
| Molecular weight | 190-220 | 74 |
| Density of liquid at NTP* (kg/L) | ~0.84 | 0.71 |
| Viscosity at NTP* (cP) | 2.6 | 0.23 |
| Oxygen content (wt %) | - | 21 |
| Sulfur content (ppm) | ~250 | - |
| Boiling temperature (°C) | 180-360 | 34.6 |
| Autoignition temperature in air (°C) | 315 | 160 |
| Flammability limit in air (vol %) | 0.6-6.5 | 1.9-9.5 |
| Stoichiometric air-fuel ratio ($AFR_s$) | 14.6 | 11.1 |
| Heat of vaporization at NTP* (kJ/kg) | 250 | 356 |
| Lower heating value (MJ/kg) | 42.5 | 33.9 |
| Cetane number (CN) | 40-55 | 125 |

*NTP: Normal temperature and pressure

There are some challenges with DEE such as storage stability, flammability limits and lower lubricity. Storage stability of DEE and DEE blends are of concern because of a tendency to oxidize, forming peroxides in storage. It is suggested that antioxidant additives may be available to prevent storage oxidation. Flammability limits for DEE as seen in Table 1 are broader than that of diesel fuel, but the rich flammability limit of DEE is in question [14].

## 3. Studies on diethyl ether in literature

There are a number of studies in literature on the use DEE in diesel engines as a fuel or fuel additive in various diesel engine fuels. For example; as pure, with diesel fuel, with diesel-ethanol blends, with diesel-ferric chloride blends, with diesel-kerosene blends, with diesel-acetylene gas dual fuel, with biogas, with liquefied petroleum gas, with diesel-natural gas dual fuel, with ethanol, with various biodiesel fuels, with biogas-biodiesel blends, with water-biodiesel emulsion fuel, with various biodiesel-diesel blends, with ethanol-biodiesel-diesel blends and methanol-biodiesel-diesel blends [16-113].

## 4. PM and smoke emissions

Rakopoulos et al declared that the soot emitted by all DEE-diesel blends was lower than neat diesel fuel. The reduction was higher for higher the percentage of DEE in the blend. This might be attributed to the engine running overall leaner, with the combustion being now assisted by the presence of oxygen in DEE even in locally rich zones, which seemed to have the dominating influence. This decrease in smoke emissions was significant for the higher load and modest for lower loads as seen in Fig. 3(a) [17]. Banapurmath et al declared that smoke is direct indication of incomplete combustion in the engine and is formed in fuel rich regions in the combustion chamber. Smoke emission was higher at low loads, which might be due to short combustion cycle at high speed, long delay period and

shortage of oxygen which might be due to improper mixing or usage of rich fuel. The smoke emissions were reduced with DEE blends. This might be due to overall leaning operation of the engine as the combustion was assisted by the presence of the fuel-bound oxygen of DEE. Additionally, high volatility of DEE had a remarkable effect on the reduction of smoke emissions, especially at high engine loads; hence DEE20 blend showed the lowest smoke emissions as seen in Fig. 3(b) [22].

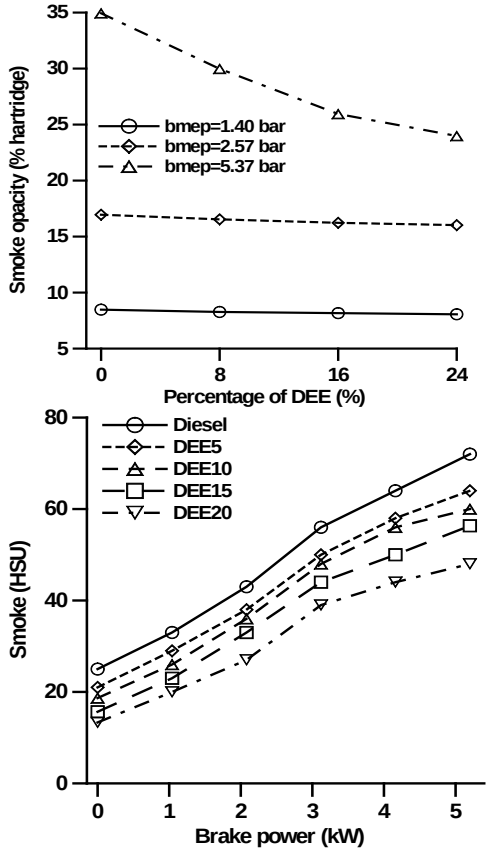


**Figure 3.** *Effect of diethyl ether additive on smoke emissions of diesel fuel [17, 22]*

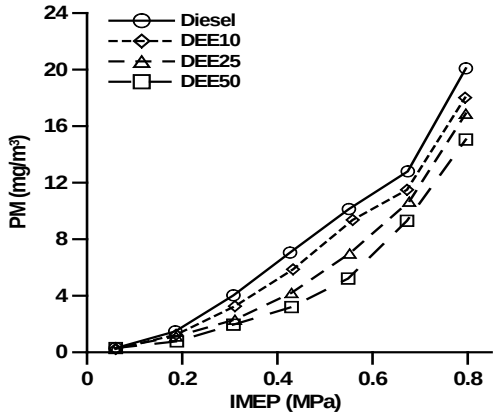


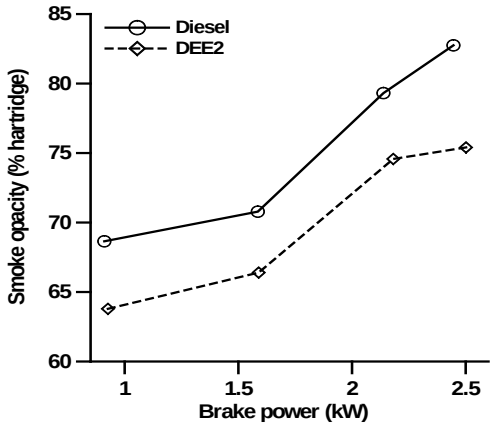


**Figure 4.** *Effect of diethyl ether additive on PM emissions [23] and smoke emissions [28] of diesel fuel*

Lee and Kim declared that diesel particulate matter (PM) consists principally of combustion generated carbonaceous material (soot) on which some organic compounds have absorbed. Unsaturated hydrocarbons, such as polycyclic aromatic hydrocarbons (PAHs) and acetylene, are the most likely precursors of soot particles. PM tended to increase with increasing engine load for all the tested fuels because the volume for fuel-rich regions became large as the amount of fuel injected increased with increased engine load. This resulted in high PM emissions due to the worsening air-fuel mixing in the combustion chamber. Also, diesel had the highest PM, which decreased with increasing DEE content as seen in Fig. 4(a). This might be attributed to the high volatility and the presence of fuel bound oxygen in DEE. DEE is more volatile and has a lower self-ignition temperature than pure diesel. So, DEE enabled better mixing of the air-fuel mixture and provided more complete combustion. The presence of fuel bound oxygen in the blended fuels created locally lean fuel-air mixture environments and aided in the oxidation of unsaturated hydrocarbons during the diffusion flame phase rather than allowing them to act as precursors of soot particles [23]. Saravanan et al declared that the incomplete combustion of the fuel hydrocarbon increases the smoke opacity. The increase of DEE in diesel fuel increased the smoke opacity. This might be due to the phase separation of the blend [24]. Balamurugan and Nalini declared that the addition of DEE with diesel decreased the smoke density appreciably as seen in Fig. 4(b). This was because of the increase in combustion efficiency and the release of more $CO_2$ due to increase in cetane number of the blend by blending of DEE with diesel [28]. Madhu et al declared DEE-diesel blends gave better smoke reduction which indicated that there was better combustion. Smoke emission showed minimum levels for DEE15, which was 17% less than diesel fuel. As the fuel injection pressure increased, smoke emission reduced. It was also found that with increase in composition of DEE at any injection pressure, the smoke levels were found reduced. DEE, being a volatile fuel could overcome poor mixing of the

fuel with air and leaded to improvement in diffusive combustion [29]. Cinar et al declared that smoke emissions were reduced with increasing in the premixed DEE fuel ratio. In HCCI-DI engine, premixed fuel charge was homogeneously introduced into the cylinder. Therefore, rich fuel regions in combustion chamber were minimized and formation of soot precursors was prevented. Also, DEE fuel was oxygenated and it had low carbon to hydrogen ratio. It had positive effect on the elimination of soot formation. Smoke emissions were decreased up to 76% with increase in the premixed fuel ratio of DEE as seen in Fig. 5(a) [32].

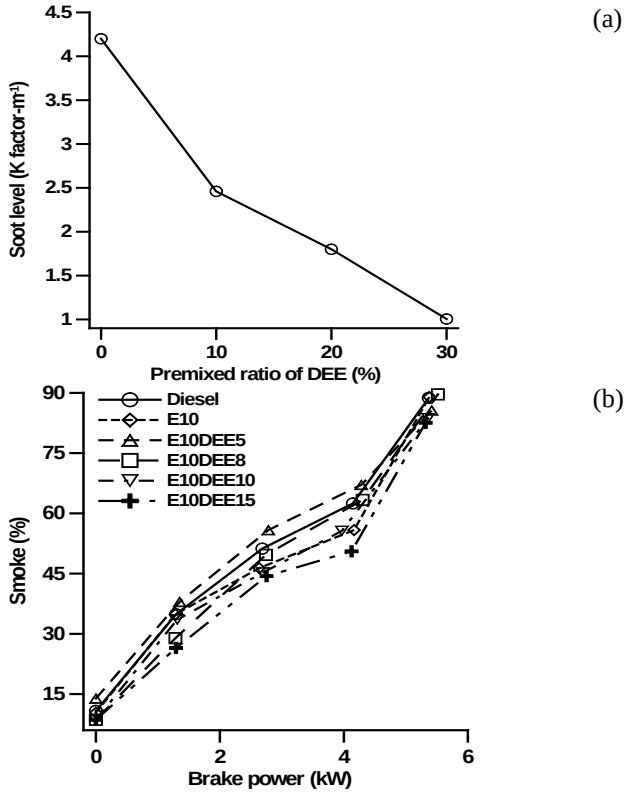


**Figure 5.** *Effect of diethyl ether premixed ratio on smoke emissions of diesel fuel [32] and ethanol-diesel blend [33]*

Iranmanesh declared that the general trend of smoke opacity displayed a reduction with addition of oxygenates as seen in Fig. 5(b) due to oxygen content in ethanol and DEE which helped in an improved combustion than neat diesel fuel. Since the smoke was produced mainly in the diffusive combustion phase, the addition of oxygenated fuel leaded to an improvement in diffusive combustion. On the other hand, enhancing the oxygen content in the charge, could overcome poor mixing of the fuel with air, which was responsible for smoke formation in diesel engines. E10DEE15 blend showed the lowest smoke opacity at all of the load conditions [33]. Sudhakar and Sivaprakasam declared that smoke density decreased for all test fuels while compare with diesel as seen in Fig. 6(a). The maximum decreased percentage 32 was achieved for 30% injection of DEE. This was due to the oxygen enrichment of ethanol and DEE improved reactions in diffusion phase of combustion reflected in reduction in smoke density [35]. Sudhakar and Sivaprakasam declared that smoke density of E15 decreased. The increasing percentage of DEE injection without EGR decreased the smoke density. However, the increasing percentage of hot EGR was resulted increased smoke density than in the case of without EGR [36].

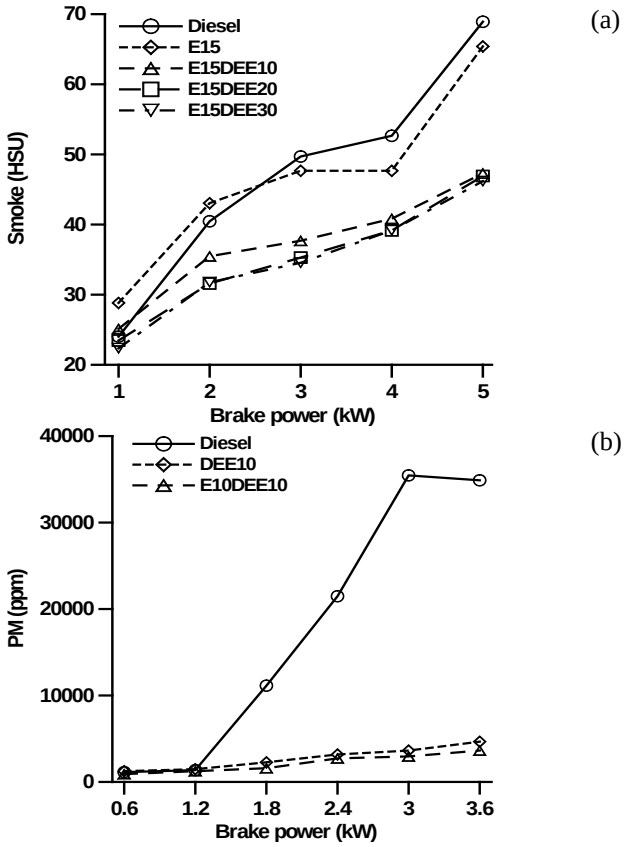


**Figure 6.** *Effect of diethyl ether premixed ratio on smoke emissions of ethanol-diesel blend [35] and PM emissions of ethanol-diesel blend [37]*

Paul et al declared that PM emission from the engine had drastically reduced with all the blends at medium and high load conditions. At low loads, diesel-DEE blends showed reduced or similar PM emission rates as compared to diesel. This might be due to lower in-cylinder temperature and pressure that reduced the quality of combustion. At medium and high load conditions, the PM emission from the engine decreased for all the tested fuel blends as seen in Fig. 6(b). The high cetane number and 21.6% oxygen content of DEE was advantageous to the combustion as the former reduced the ignition delay and the later helped in better combustion of the charge. As a result, the carbon and soot elements burned and reduced the PM emission. This was reflected in the drastic reduction in PM emission with diesel-DEE blends. It was also found that addition of ethanol further reduced the PM emission. This was because combustion of ethanol liberated the 'OH' radicals into the combustion chamber. These 'OH' radicals are instrumental in soot decomposition in diffusion

flame. Hence, with the increase of ethanol content in fuel, the PM emission reduced invariably [37]. Patnaik et al declared that the smoke opacity was reduced for DEE15 blend by 72% compared to diesel fuel at higher engine load as seen in Fig 7(a). The blend of DEE advanced the combustion by reducing ignition delay which leaded to increase in combustion time resulting in the reduction of soot formation. The molecular oxygen content of DEE depromoted the formation of smoke during the diffusion phase of combustion [41]. Rakopoulos declared that the soot emitted by the DEE blends was lower than those of the neat biodiesel and diesel as seen in Fig. 7(b). This might be attributed to the presence of extra fuel bound oxygen in the blends even at locally fuel rich zones [50].

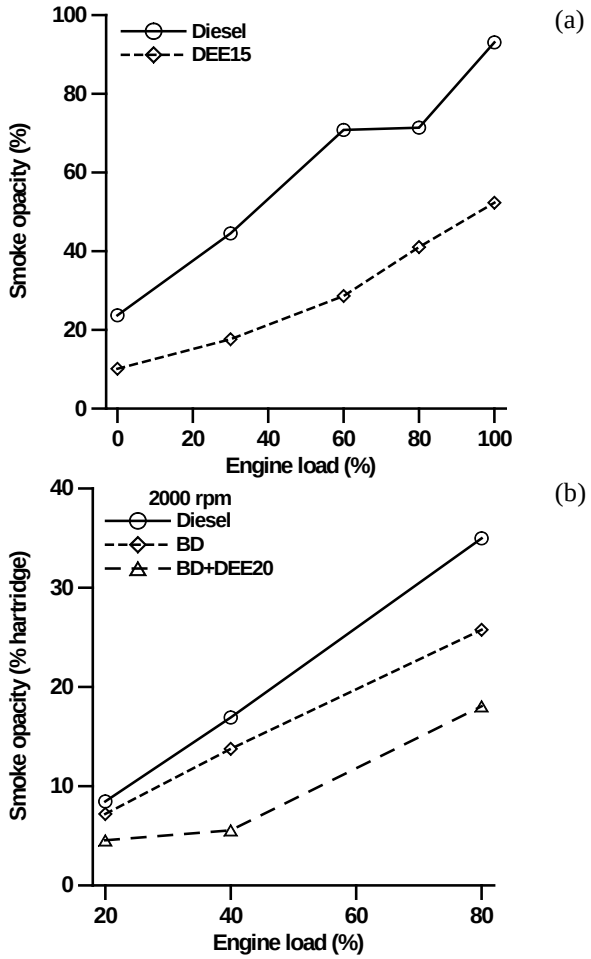


**Figure 7.** *Effect of diethyl ether on smoke emissions of diesel fuel [41] and biodiesel fuel [50]*

Jawre and Lawankar declared that smoke intensity with diesel fuel was higher than biodiesel and DEE blends as seen in Fig. 8(a). Smoke was formed due to incomplete combustion of fuel. Oxygen content in biodiesel was higher than diesel fuel. Improved and complete combustion could be the reasons for obtaining lower smoke emission values with biodiesel. Addition of DEE to biodiesel also improved oxygen content and reduced viscosity. Smoke emission with DEE10 and DEE15 blend gave lower value smoke and it was lower by 21% and 28% compared to biodiesel [55]. Sivalakshmi and Balusamy declared that the smoke intensity decreased by 10% for DEE5 blend comparing to that of biodiesel as seen in Fig. 8(b). Smoke was formed at rich region, the improvement in spray atomization and fuel-air mixing with the addition of diethyl ether decreased the rich mixture region and decreased the smoke emission. However, in case of DEE10 and DEE15 blends, the smoke intensity seemed to increase but it was still lower than that of biodiesel and diesel. This might be due to phase separation of the blend, which resulted in incomplete combustion of fuel [59].

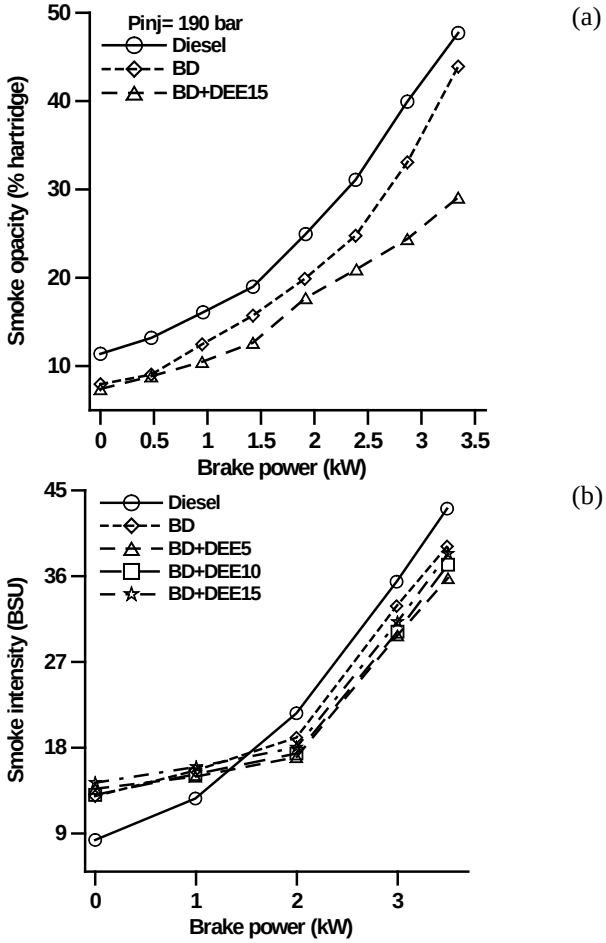


**Figure 8.** *Effect of diethyl ether on smoke emissions of biodiesel fuel [55, 59]*

Rajan et al declared that the smoke emission decreased with increase of DEE in the blends with biodiesel at full load as seen in Fig. 9(a). The maximum smoke emissions for 10% and 15% DEE were 3.4 BSU and 3.2 BSU, respectively, whereas the same for diesel and neat biodiesel were 3.6 BSU and 3.8 BSU, respectively, at full load. The 10% reduction in smoke emission for biodiesel with 15% DEE might be due to the presence of more oxygen in the DEE which made the combustion complete and also since the biodiesel fuel itself contained 11% oxygen in it which might promote the oxidation of soot during the combustion process [64]. Geo et

al declared that the smoke emission was 6.1 BSU (Bosch smoke units) with neat biodiesel and 3.4 BSU with diesel at full load as seen in Fig. 9(b). With neat biodiesel due to its heavier molecular structure and high viscosity, atomization became poor and leaded to higher smoke emission. There was a drastic reduction in smoke emission of the engine fuelled with DEE operation. Smoke decreased from 6.1 BSU to 4 BSU with DEE at a flow rate of 200 g/h at peak output. The volatility and oxygen enrichment provided by DEE was beneficial in improving the fuel evaporation and smoke reduction. Also high cetane number of the DEE resulted in shorter ignition delay. Shorter ignition delay reduced the accumulation of fuel in the combustion chamber and reduced the smoke emission. Thus, a small quantity of oxygenates injected with vegetable oil could be effective in reducing smoke emission [65].

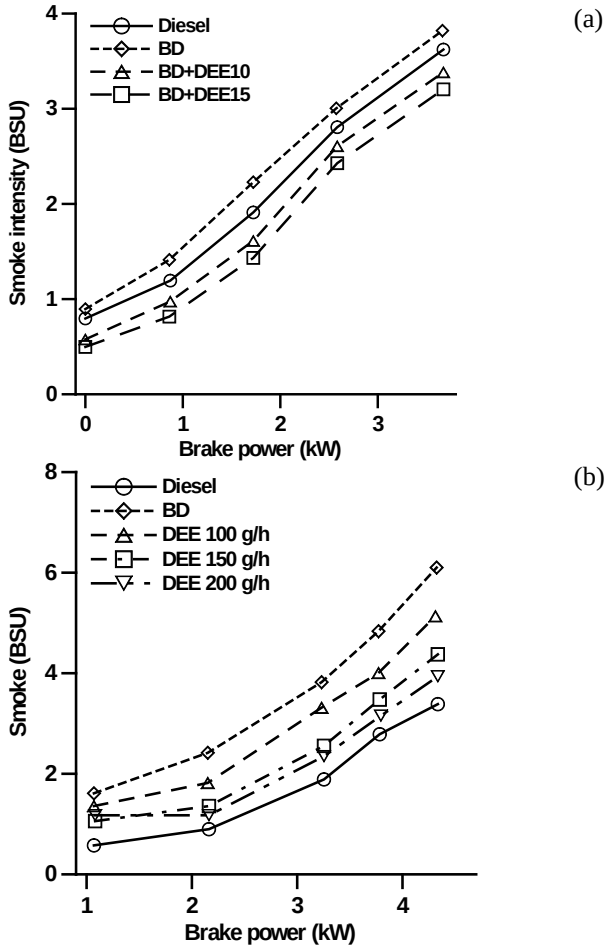


**Figure 9.** *Effect of diethyl ether on smoke emissions of biodiesel fuel [64, 65]*

Hariharan et al declared that smoke was due to the incomplete combustion of unsaturated hydrocarbons like polycyclic aromatic hydrocarbons that were present in the fuel. Smoke varied according to the type of fuel used, its composition, its carbon content and C/H ratio. It could be observed from Fig. 10(a) that smoke increased with increase in the induction of DEE. For diesel operation, smoke emission varied from 0 at no load to 1.45 BSU at full load. It varied from 0.55 BSU at no load to 2.2 BSU at full load with biodiesel-DEE mode at 65 g/h of DEE induction, from 1.8 BSU at no load to 3.2 BSU at full load at 130 g/h and from 0.45 BSU at no load to 2.4 BSU at full load at 170 g/h. Smoke would be higher for fuels that have a value of hydrogen to carbon ratio lesser than 2. Current biodiesel had hydrogen to carbon ratio of 1.4. This was the main reason for a significant change in smoke emission for biodiesel-DEE operation than diesel fuel. Since biodiesel had higher aromatic content, the presence of unsaturated hydrocarbon like poly aromatic hydrocarbon resulted in higher smoke. Slow combustion of the biodiesel during the diffusion combustion phase and the pyrolysis of fuel at high temperature were also the reasons for higher smoke emission for biodiesel-DEE operation particularly at full load [66]. Devaraj et al declared that the smoke opacity of any fuel increased with the increase in load as seen in Fig. 10(b). The smoke opacity of biodiesel was higher than that of diesel due to heavier molecules. The smoke opacity level was 1.7% for 20% load and 53.5% at full load, in case of diesel. In case of biodiesel, the value was 2% at 20% load and 55.1% at full load. The smoke opacity for DEE5 and DEE10 at 20% load is 9.5% and 9.9% and at full load, it is 49.2% and 55.1%. The addition of DEE with biodiesel showed reduction in smoke opacity. This is due to the higher oxygen content of DEE depromoted the formation of smoke during the diffusion phase of combustion. The smoke opacity at high load obtained for DEE5 and DEE10 showed that there was an increment in smoke opacity. This indicated that beyond certain limit the addition of DEE had no effect in reduction of smoke opacity [67].

Sachuthananthan and Jeyachandran declared that smoke emission for 30% water-biodiesel emulsion was 2.5 BSU at full load and for 10% DEE it was 1.8 BSU and for 15% DEE it was 1.6 BSU as seen in Fig. 11(a).

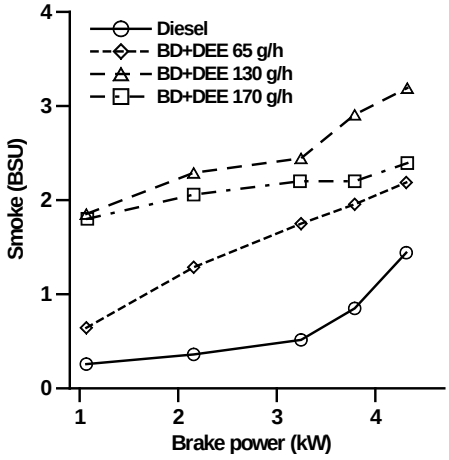

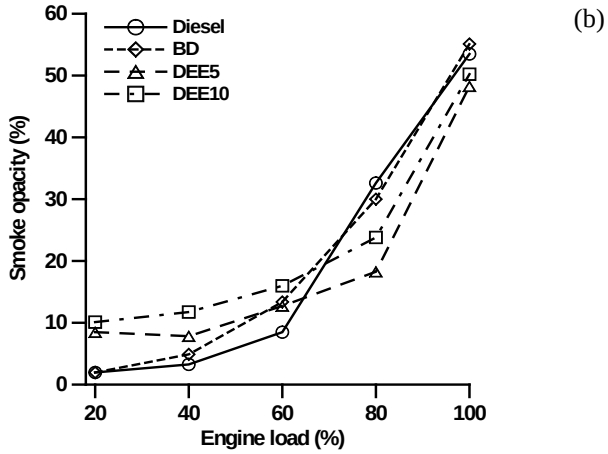


**Figure 10.** *Effect of diethyl ether on smoke emissions of biodiesel fuel [66, 67]*

This reduction in smoke emission for water-biodiesel emulsion with DEE was due to presence of 21.6% oxygen by mass in DEE which made the combustion complete and also since the biodiesel fuel itself contains 11% oxygen in it which might promoted the oxidation of soot during the combustion process [70]. Kumar et al declared that BD has prolonged aromatic chain-like structure and it has poor combustion. Thus, it results in more amounts of smoke level increases it may be due to poor atomization of the BD. It is observed that the smoke opacity of BD20 blend is higher than diesel. Result shows at full loading condition smoke level of BD20 is 3.96 FSN whereas for diesel its level is 3.15 FSN as seen in Fig. 11(b). After addition of DEE with BD20 it is reduced. It has been found that smoke level of BD20DEE15 is 3.38 FSN. This is because improved viscosity resulting improve combustion rate of the DEE blends [74].

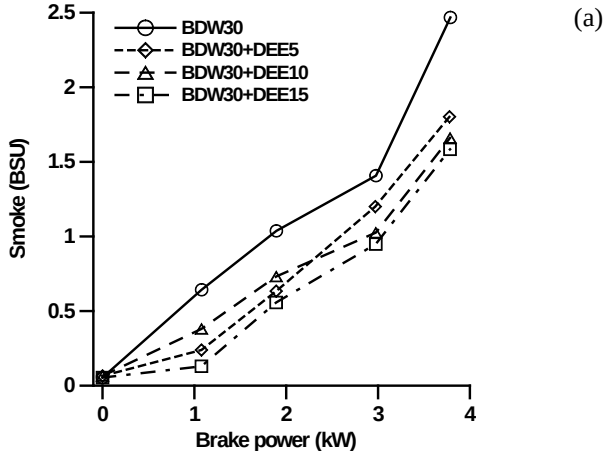


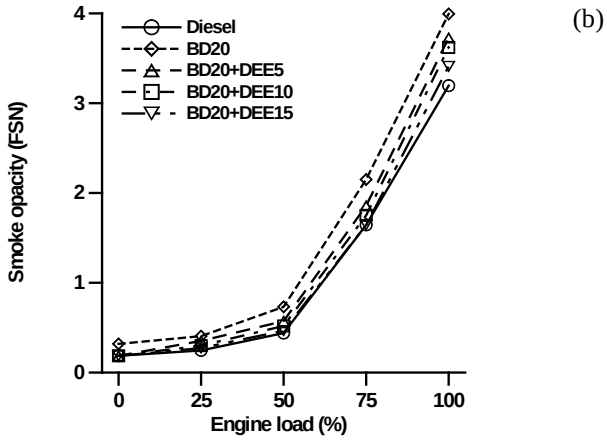


**Figure 11.** *Effect of diethyl ether on smoke emissions of biodiesel-water emulsified fuel [70] and diesel-biodiesel blends [74]*

Srihari et al declared that smoke level for all the blends are fairly lower than that of diesel as seen in Fig. 12(a). But, at low and medium loads smoke level seems to be almost the same for all the blends. Nevertheless, for DEE10 and DEE15 the smoke level is low for all the loads when compared to that of the others. Thus, DEE10 and DEE15 can be considered as better options as far as smoke concentration is concerned. Here, in the case of DEE15 a reduction in smoke concentration of 50% and 32% is observed when compared to that of diesel and BD20 at full load. The corresponding values for DEE10 are 30% and 38.5%. The reason for this reduction in smoke concentration can be attributed to the reduction in density due to the addition of DEE and the corresponding altered spray pattern leading to better fuel-air mixing process. Another reason could be the absence of fuel rich zone in the cylinder that leads to reduced smoke [76].

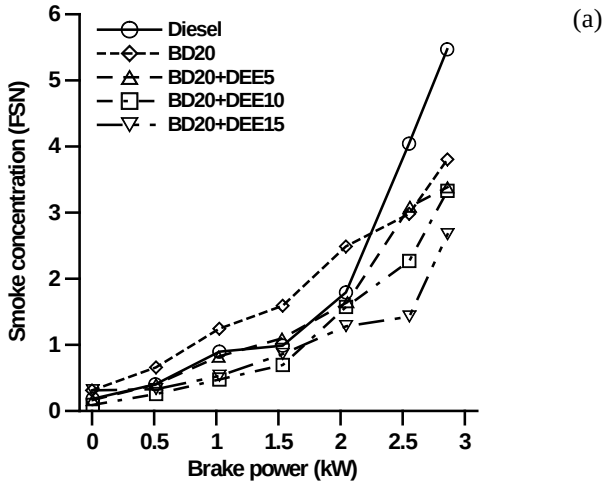

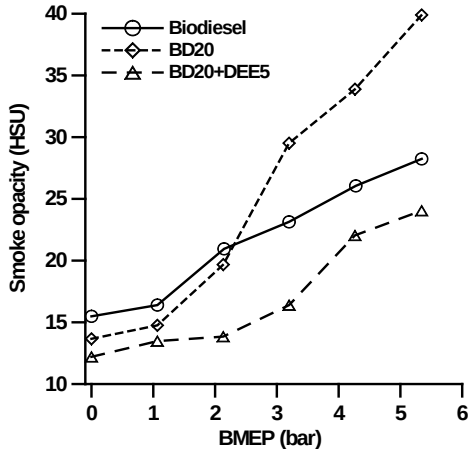


**Figure 12.** *Effect of diethyl ether on smoke emissions of diesel-biodiesel blends [76, 81]*

The smoke opacity exhibited by different fuels is plotted in Fig. 12(b). It can be seen that the values are on the lower side for the BD20 blend with DEE additive. Lowest values are observed for the case of BD20 with DEE5 and highest being BD. Improved and complete combustion could be the reasons for obtaining lower smoke opacity values with DEE additive. Therefore, it can be concluded here that DEE has proven to be eco-friendly additive to improve the performance and emissions of BD20 blend [81]. It is observed from Fig. 13(a) that the smoke emission is decreased with increase of DEE in BD20 blend at full load. The maximum smoke emissions for DEE10 and DEE15 are 3.4BSU and 3.2BSU, whereas they are 3.6BSU and 3.8BSU for diesel and BD20 blend respectively at full load. The 10% reduction in smoke emission for BD20 with DEE15 may be due to the presence of more oxygen in the DEE which makes the combustion complete and also since the biodiesel fuel itself contains 11% oxygen in it which may promote the oxidation of soot during the combustion process [83]. The smoke emissions variation is shown in Fig. 13(b). The smoke is formed due to incomplete combustion. It is obvious that the smoke emissions are reduced with DEE additive. This may be attributed to the engine running overall leaner with the combustion being now assisted by the presence of the fuel-bound oxygen of the diethyl ether even in locally rich zones. Additionally, diethyl ether has a remarkable effect on the reduction of smoke emissions due to it is evaporating easily, especially at high engine loads. So, DEE5 blend shows the lowest smoke emissions at all engine loads [85].

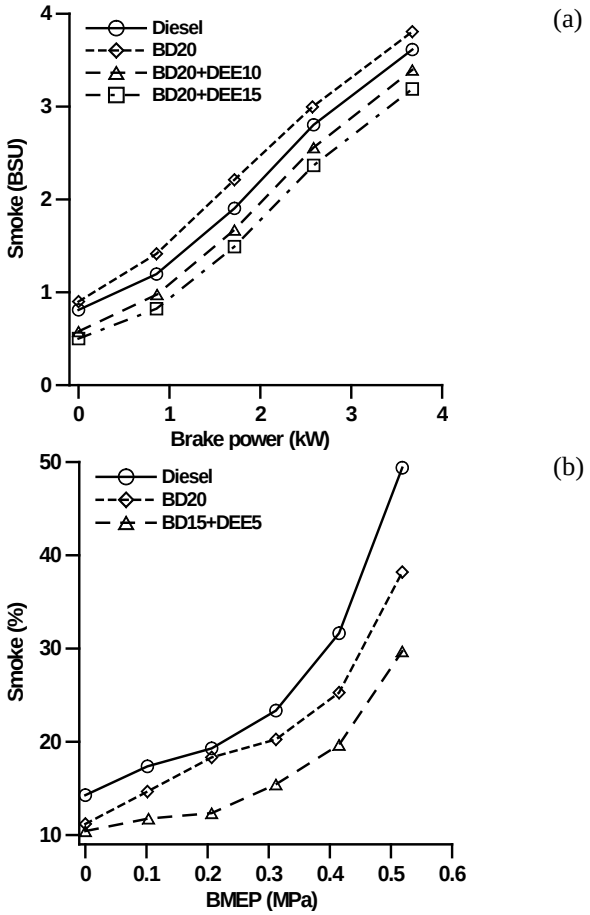


**Figure 13.** *Effect of diethyl ether on smoke emissions of diesel-biodiesel blends [83, 85]*

Smoke density of DEE5 is generally lower than that of BD20 and diesel as seen in Fig. 14(a). That is, lesser amount of unburned hydrocarbon presents in the engine exhaust gas. Thus, the lower smoke density values are achieved with DEE blends as compared to that of biodiesel and diesel [87]. Fig. 14(b) illustrates the smoke opacity of the test fuels. BD20 gave about 6.2% decreased smoke opacity than diesel fuel. It can be attributed to advanced start of combustion of BD20 for higher cetane number. Hence, the combustion started early, it allowed more time for the oxidation of soot. Soot formation takes place generally at the initial premixed combustion phase when the fuel-air equivalence ratio remains at stoichiometry. Therefore, higher oxygen content of BD20 provided oxygen in the fuel rich zones and reduced smoke opacity especially at higher speeds. BD15DEE5 and BD10DEE10 reduced smoke opacity about 30% and 38.5% on average than BD20. Therefore, it is obvious that such oxygenated blends reduced the probability of rich fuel zone formation and assisted to decrease the soot emission [91].

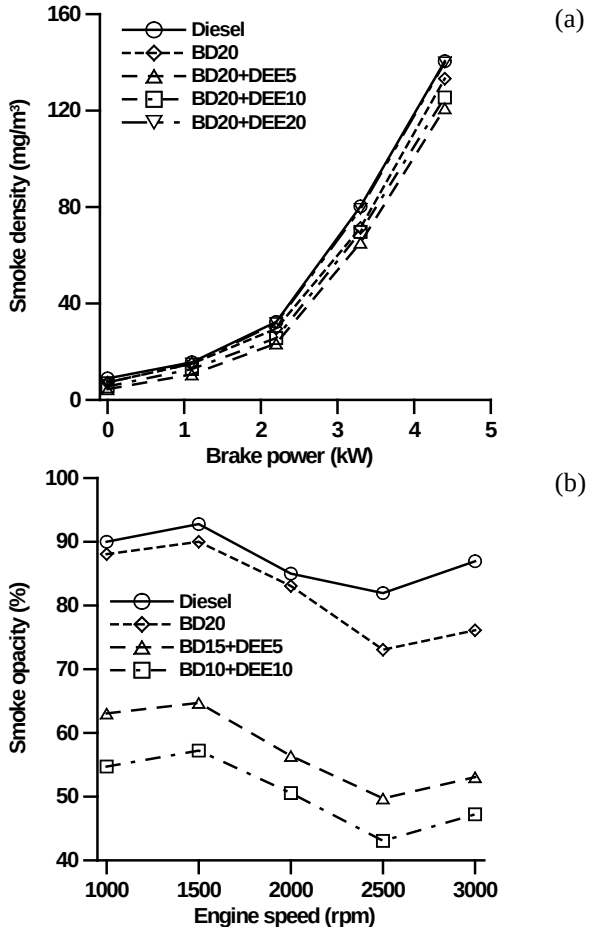


**Figure 14.** *Effect of diethyl ether on smoke emissions of diesel-biodiesel blends [87, 91]*

Smoke emission in diesel engines occurs due to the incomplete combustion inside the combustion chamber and is normally formed in the rich zone. The variation of smoke emission, with brake power for diesel, BD40 and DEE4 blends are depicted in Fig. 15(a). The smoke emission increases with increasing load. This is due to the increase in the mass of fuel consumed when brake power is increased. The smoke emission for BD40 blend is the highest at full load. The smoke emission reduces with adding of DEE to BD40 blend. The volatility and oxygen enrichment provided by DEE is beneficial to improving the fuel evaporation and smoke reduction. The smoke emissions of DEE4 are approximately 21% lower compared to that of diesel, and about 34% lower compared to that of the BD40 blend at full load [107].

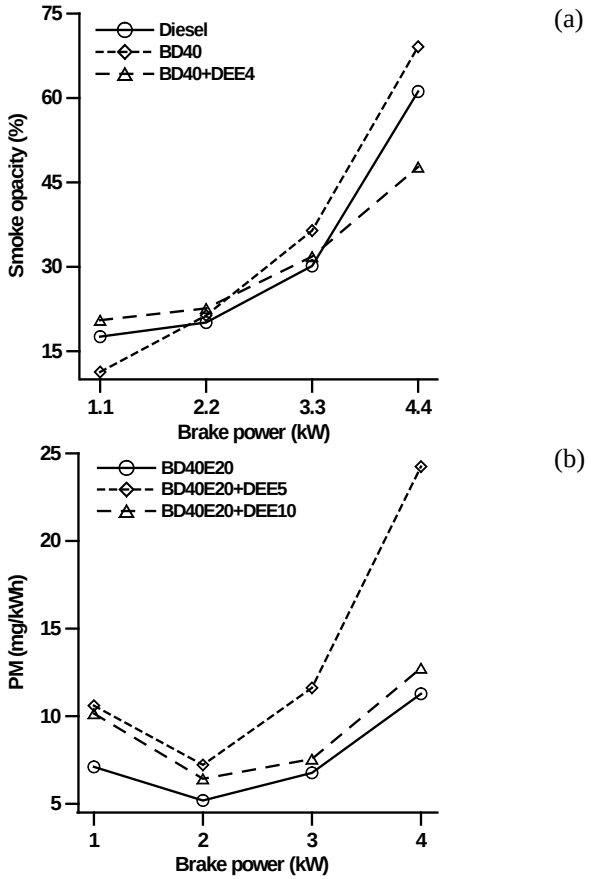


**Figure 15.** *Effect of diethyl ether on smoke emissions of diesel-biodiesel blends [107] and PM emissions biodiesel-ethanol blends [110]*

Particulate matter (PM) is generated as a result of insufficient $O_2$ content in fuel rich zones, especially during heterogeneous combustion. In general, in comparison with diesel, oxygenate blends lowers the PM emissions due to reduced aromatics, C/H ratio and the presence of readily available $O_2$, which improves the combustion rate followed by lower PM formation. From Fig. 15(b), DEE10 blend has highest PM in comparison with other fuels. At lower loads, PM formation is less owing to less fuel fraction burnt, whereas PM formation increases with increasing load due to excess fuel accumulation resulting in higher burn duration. At all engine loads, the presence of DEE additive has raised the PM emission in comparison with BD40E20 blend [110].

## 5. Conclusion

The effect of diethyl ether addition to various diesel engine fuels and fuel blends is investigated on the PM and smoke emissions in this review study. The following conclusions can be summarized as results of the study.

- Smoke, soot or particulate matter is direct indication of incomplete combustion in the engine and these are formed in fuel rich regions in the combustion chamber.

- Smoke emissions increase with increasing engine speed and load due to short combustion duration, long delay period and shortage of oxygen as the amount of fuel injected increased.
- DEE addition various diesel engine fuels reduces the PM and smoke emissions by enabling better mixing of air-fuel mixture and providing more complete combustion due to high cetane number and oxygen content of DEE. The improvement in spray atomization and fuel-air mixing with the addition of diethyl ether decreased the rich mixture region and decreased the smoke emission. High volatility of DEE also has a remarkable effect on the reduction of smoke emissions. Moreover, DEE has positive effect on the elimination of soot formation because of the low carbon to hydrogen ratio.
- In some studies, the increase of DEE in the blend increases the smoke emissions due to the phase separation of the blend. This shows that DEE addition beyond certain limit has no effect in reduction of smoke opacity. On the other hand, the increasing of hot EGR causes the increasing of smoke emissions than in the case of without EGR.
- The neat biodiesel fuels generate the higher smoke emissions by causing poor atomization due to its heavier molecular structure, high viscosity and the presence of unsaturated hydrocarbons. However, important improvements achieve with biodiesel-diesel blends and DEE addition in smoke emission.

**ABBREVIATIONS**

| | |
|---|---|
| BD | : Biodiesel |
| BD–D | : Biodiesel–diesel blends |
| BSU | : Bosch smoke units |
| C/H | : Carbon to hydrogen ratio |
| CNSO | : Cashew nut shell oil |
| D | : Diesel |
| D–BD–DEE | : Diesel–biodiesel–diethyl ether blends |
| DBE | : Dibutyl ether |
| DEE | : Diethyl ether |
| DGM | : Diethylene glycol dimethyl ether |
| DMC | : Dimethyl carbonate |
| DME | : Dimethyl ether |
| DMM | : Dimethoxy methane |
| E | : Ethanol |
| EGR | : Exhaust gas recirculation |
| FSN | : Filter smoke number |
| HCCI | : Homogenous charge compression ignition |
| K | : Kerosene |
| kW | : Kilowatt |
| MTBE | : Methyl tertiary butyl ether |
| NG | : Natural gas |
| PAHs | : Polycyclic aromatic hydrocarbons |
| PCCI | : Partially charge compression ignition |
| PM | : Particulate matter |
| ppm | : Parts per million |
| SOx | : Sulphur oxides |
| THC | : Total gaseous hydrocarbons |

**References**


[1]. Manikandan R., Sethuraman N., "Experimental investigation of nano additive ceric oxide ($CeO_2$)-ethanol blend on single cylinder four stroke diesel engine", International Journal of Recent Development in Engineering and Technology, 3(2), (2014), 24-28.

[2]. Londhekar A.G., Kongre S.C., "Effects of different additives on performance and emission of biodiesel fuelled compression ignition engine", International Journal of Science and Research, 6(2), (2017), 1947-1952.

[3]. Hagos F.Y., Ali O.M., Mamat R., Abdullah A.A., "Effect of emulsification and blending on the oxygenation and substitution of diesel fuel for compression ignition engine", Renewable and Sustainable Energy Reviews, 75, (2017), 1281-1294.

[4]. Patil R.N., Marlapalle B.G., "Karanja (pongamia pinnata) biodiesel as an alternative fuel for DICI engine: A review", International Journal of Research in Aeronautical and Mechanical Engineering, 4(1), (2016), 96-101.

[5]. Geng P., Cao E., Tan Q., Wei L., "Effects of alternative fuels on the combustion characteristics and emission products from diesel engines: A review", Renewable and Sustainable Energy Reviews, 71, (2017), 523-534.

[6]. Kumar B.R., Saravanan S., "Use of higher alcohol biofuels in diesel engines: A review", Renewable and Sustainable Energy Reviews, 60, (2016), 84-115.

[7]. Patil A.R., Taji S.G., "Effect of oxygenated fuel additive on diesel engine performance and emission: a review", Journal of Mechanical and Civil Engineering, X, (2013), 30-35.

[8]. Senthilkumar R., Ramadoss K., Manimaran R., Prabu M., "Emission, combustion, performance and characteristics of a CI engine using MTBE blended diesel fuel", in International Conference on Advances in Engineering, Science and Management (lCAESM), March 30-31, (2012), 360-364.

[9]. Saravanakumar L, Bapu B.R.R., Prasad B.D., "Performance and emission characteristics of a CI engine operating on methyl esters blended diesel with di-methyl carbonate additives", International Energy Journal, 14, (2014), 121-132.

[10]. Jawre S.S., Bhagat A., Moghe S.M., Pakhale V.A., "Diethyl ether as additive and its effect on diesel engine performance-a review", Global Research and Development Journal for Engineering, 1(5), (2016), 27-31.

[11]. Chauhan B.S., Singh R.K., Cho H.M., Lim H.C., "Practice of diesel fuel blends using alternative fuels: A

review", Renewable and Sustainable Energy Reviews, 59, (2016), 1358-1368.

[12]. Valipour A., "A review on effect of fuel additives on combustion, performance and emission characteristics of diesel and biodiesel fuelled engine", International Journal of Application or Innovation in Engineering & Management, 3(1), (2014), 366-273.

[13]. Krishnamoorthi M., Malayalamurthi R., "A review on effect of diethyl ether additive on combustion, performance and emission characteristics of a diesel and biodiesel/vegetable oil fuelled engine", Advances in Natural and Applied Sciences, 10(7), (2016), 9-17.

[14]. Bailey B., Eberhardt J., Goguen S., Erwin J., "Diethyl ether (DEE) as a renewable diesel fuel", Society of Automotive Engineering, Paper no: 972978, (1997).

[15]. Sezer I., "Thermodynamic, performance and emission investigation of a diesel engine running on dimethyl ether and diethyl ether," International Journal of Thermal Sciences, 50, (2011), 1594-1603.

[16]. Mohan B., Yang W., Yu W., Tay K.L., "Numerical analysis of spray characteristics of dimethyl ether and diethyl ether fuel", Applied Energy, 185, (2017), 1403-1410.

[17]. Rakopoulos D.C., Rakopoulos C.D., Giakoumis E.G., Dimaratos A.M., "Characteristics of performance and emissions in high-speed direct injection diesel engine fueled with diethyl ether/diesel fuel blends", Energy, 43, (2012), 214-224.

[18]. Rakopoulos D.C., Rakopoulos C.D., Giakoumis E.G., Dimaratos A.M., "Studying combustion and cyclic irregularity of diethyl ether as supplement fuel in diesel engine", Fuel, 109, (2013), 325-335.

[19]. Patil K.R., Thipse S.S., "The effect of injection timing on the performance and emission of direct injection CI engine running on diethyl ether-diesel blends", International Journal of Automotive and Mechanical Engineering, 13(3), (2016), 3773-3787.

[20]. Rathod P.H., Darunde D.S., "Experimental investigation and performance analysis of diethyl ether (DEE) and tert-amyl ethyl ether (TAEE) blend with diesel in C.I.D.I. engine: a review", International Journal of Research In Science & Engineering, 2(1), (2015), 137-142.

[21]. Karthik A.V., Kumar S.P., " Experimental study of 4-stroke diesel engine blending with alternate fuel diethyl ether (DEE) and exhaust gas recirculation (EGR) system", International Journal of Engineering Science and Computing, 6, (2016), 7054-7058.

[22]. Banapurmath N.R., Khandal S.V., Ranganatha S.L., Chandrashekar T.K., "Alcohol (ethanol and diethyl ethyl ether)-diesel blended fuels for diesel engine applications-a feasible solution", Advances in Automobile Engineering, 4(1), (2015), 1-8.

[23]. Lee S., Kim T.Y., "Performance and emission characteristics of a DI diesel engine operated with diesel/DEE blended fuel", Applied Thermal Engineering, 121, (2017), 454-461.

[24]. Saravanan D., Vijayakumar T., Thamaraikannan M., "Experimental analysis of combustion and emissions characteristics of CI engine powered with diethyl ether blended diesel as fuel", Research Journal of Engineering Sciences, 1(4), (2012), 41-47.

[25]. Ibrahim A., "Investigating the effect of using diethyl ether as a fuel additive on diesel engine performance and combustion", Applied Thermal Engineering, 107, (2016), 853-862.

[26]. Likhitha S.S.S., Prasad B.D., Kumar R.V., "Investigation on the effect of diethyl ether additive on the performance of variable compression ratio diesel engine", International Journal of Engineering Research, 3(1), (2014), 11-15.

[27]. Kumar R.S., Nagaprasad K.S., "Investigation on diesel engine performance by injecting di-ethyl ether as an additive with exhaust gas recirculation using diesel particulate filter", International Journal of Innovative Research in Science, Engineering and Technology, 3(8), (2014), 15192-15200.

[28]. Balamurugan T., Nalini R., "Comparative study on performance and emission in four stroke diesel engine using different blended fuel", International Journal of Current Research and Development, 4(1), (2016), 58-64.

[29]. Madhu S., Chaitanya A.V.K., Bridjesh P., "Effects of diethyl ether on performance and emission characteristics of a diesel engine using toroidal profile bowl piston by varying injection pressure", International Journal of Mechanical Engineering and Technology, 8(6), (2017), 96-106.

[30]. Danesha D., Manjunath H., "Production and characterization of biodiesel from Simarouba Glauca seed oil with diethyl ether as an additive and its performance and emission evaluation on single cylinder, four stroke C.I engine", International Journal of Research in Engineering and Technology, 5(13), (2016), 64-68.

[31]. Prasadarao B.V.V., Haribabu N., Ramana M.V., "The role of oxygenated fuel additive (DEE) along with palm methyl ester and diesel to estimate performance and emission analysis of DI-diesel engine", International Journal of Engineering Research & Technology, 3(1), (2014), 1-9.

[32]. Cinar C., Can Ö., Sahin F., Yucesu H.S., "Effects of premixed diethyl ether (DEE) on combustion and exhaust emissions in a HCCI-DI diesel engine", Applied Thermal Engineering, 30, (2010), 360-365.

[33]. Iranmanesh M., "Experimental investigations about the effect of new combination of biofuels on simultaneous reduction of $NO_x$ and smoke emissions in DI-diesel engine", International Journal of Automotive Engineering, 3(2), (2013), 379-392.

[34]. Sudhakar S., Sivaprakasam S., "Experimental investigation on combustion characteristics in DI diesel engine using diethyl ether fumigation with ethanol blended diesel", International Journal of Renewable Energy Research, 4(4), (2014), 872-878.

[35]. Sudhakar S., Sivaprakasam S., "Effects of diethyl ether fumigation in DI diesel engine using bio ethanol blended diesel", International Journal of Innovation and Scientific Research, 11(1), (2014), 65-71.

[36]. Sudhakar S., Sivaprakasam S., "The effect of exhaust gas recirculation on diethyl ether fumigation in DI diesel engine with ethanol blended diesel", International Journal of Engineering Research & Technology, 3(10), (2014), 538-548.

[37]. Paul A., Bose P.K., Panua R.S., Debroy D., "Study of performance and emission characteristics of a single cylinder CI engine using diethyl ether and ethanol blends", Journal of the Energy Institute, 88, (2015), 1-10.

[38]. Paul A., Panua R.S., Debroy D., Bose P.K., "Effect of diethyl ether and ethanol on performance, combustion, and emission of single cylinder compression ignition engine", International Journal of Ambient Energy, 38(1), (2017), 2-13.

[39]. Lukhman M.M., Sadees P., Pradeep V., Murali M., "Experimental investigation on diethyl ether as an ignition improver in diesel- ethanol emulsified fuel for C.I. engine", in International Conference on Systems, Science, Control, Communication, Engineering and Technology, (2016), 554-560.

[40]. Kumar M.M., Reddy S.S.K., "Performance characteristics of single cylinder DI diesel engine by using di-ethyl ether as an additive with diesel ethanol blend", International Journal of Science, Engineering and Technology Research, 4(9), (2015), 3272-3275.

[41]. Patnaik P.P., Jena S.P., Acharya S.K., Das H.C., "Effect of $FeCl_3$ and diethyl ether as additives on compression ignition engine emissions", Sustainable Environment Research, 27, (2017), 154-161.

[42]. Patil K.R., Thipse S.S., "Experimental investigation of CI engine combustion, performance and emissions in DEE-kerosene-diesel blends of high DEE concentration", Energy Conversion and Management, 89, (2015), 396-408.

[43]. Mahla S.K., Kumar S., Shergill H., Kumar A., "Study the performance characteristics of acetylene gas in dual fuel engine with diethyl ether blends", International Journal on Emerging Technologies, 3(1), (2012), 80-83.

[44]. Sudheesh K., Mallikarjuna J.M., "Diethyl ether as an ignition improver for biogas homogeneous charge compression ignition (HCCI) operation-an experimental investigation", Energy, 35, (2010), 3614-3622.

[45]. Jothi N.K.M., Nagarajan G., Renganarayanan S., "Experimental studies on homogeneous charge CI engine fueled with LPG using DEE as an ignition enhancer", Renewable Energy, 32, (2007), 1581-1593.

[46]. Karabektas M., Ergen G., Hosoz M., "The effects of using diethylether as additive on the performance and emissions of a diesel engine fuelled with CNG", Fuel, 115, (2014), 855-860.

[47]. Polat S., "An experimental study on combustion, engine performance and exhaust emissions in a HCCI engine fuelled with diethyl ether-ethanol fuel blends", Fuel Processing Technology, 143, (2016), 140-150.

[48]. Mack J.H., Buchholz B.A., Flowers D.L., Dibble R.W., "The effect of the di-tertiary butyl peroxide (DTBP) additive on HCCI combustion of fuel blends of ethanol and diethyl ether", Society of Automotive Engineering, Paper no: 2005-01-2135, (2015).

[49]. Pranesh G., Samuel P.M., Thankachan B., Manimaran M., Silambarasan R., "Performance and emission characteristics of blending diethyl ether in cotton seed oil methyl ester using a direct injection diesel engine", International Journal on Applications in Mechanical and Production Engineering, 1(6), (2015), 14-16.

[50]. Rakopoulos D.C., "Combustion and emissions of cottonseed oil and its bio-diesel in blends with either n-butanol or diethyl ether in HSDI diesel engine", Fuel, 105, (2013), 603-613.

[51]. Rakopoulos D.C., Rakopoulos C.D., Kyritsis D.C., "Butanol or DEE blends with either straight vegetable oil or biodiesel excluding fossil fuel: Comparative effects on diesel engine combustion attributes, cyclic variability and regulated emissions trade-off", Energy, 115, (2016), 314-325.

[52]. Rakopoulos D.C., Rakopoulos C.D., Giakoumis E.G., Papagiannakis R.G., Kyritsis D.C., "Influence of properties of various common bio-fuels on the combustion and emission characteristics of high-speed DI (direct injection) diesel engine: Vegetable oil, bio-diesel, ethanol, n-butanol, diethyl ether", Energy, 73, (2014), 354-366.

[53]. Krishna R., Bandewar A.G., Dongare V.K., "Experimental investigations of blending diethyl ether in karanja vegetable oil using a multi-cylinder diesel engine", International Journal of Research and Innovative Technology, 1(5), (2014), 70-73.

[54]. Singh I., Sahni V., "Performance analysis of the compression ignition engine using karanja biodiesel with additive diethyl ether", in Int'l Conference on Aeronautical, Automotive and Manufacturing Engineering, (2015) 9-12.

[55]. Jawre S.S., Lawankar S.M., "Performance analysis of Kusum methyl ester as alternative bio-fuel in diesel engine with diethyl ether as additive", International Journal of Innovative Research & Development, 3(5), (2014), 139-144.

[56]. Jawre S.S., Lawankar S.M., "Experimental analysis of performance of diesel engine using kusum methyl ester with diethyl ether as additive", International Journal of Engineering Research and Applications, 4(5), (2014), 106-111.

[57]. Rao K.P., Reddi V.L., "Performance evaluation of diesel engine with biodiesel along with additive for replacing diesel fuel", International Journal of Chemical Science, 14(4), (2016), 2379-2388.

[58]. Babu P.R., Rao K.P., Rao B.V.A., "The role of oxygenated fuel additive (DEE) along with mahuva methyl ester to estimate performance and emission analysis of DI-diesel engine", International Journal of Thermal Technologies, 2(1), (2012), 119-123.

[59]. Sivalakshmi S., Balusamy T., "Effect of biodiesel and its blends with diethyl ether on the combustion, performance and emissions from a diesel engine", Fuel, 106, (2013), 106-110.

[60]. Ali O.M., Mamat R., Faizal C.K.M., "Effects of diethyl ether additives on palm biodiesel fuel characteristics and low temperature flow properties", International Journal of Advanced Science and Technology, 52, (2013), 111-120.

[61]. Ali O.M., Yusaf T., Mamat R., Abdullah N.R., Abdullah A.A., "Influence of chemical blends on palm oil methyl esters' cold flow properties and fuel characteristics", Energies, 7, (2014), 4364-4380.

[62]. Kumar J.S., Prasad S.V.M., "Experimental study on performance characteristics of C.I. engine fueled with biodiesel and its blends diethyl ether", International Journal & Magazine of Engineering, Technology, Management and Research, 1(8), (2014), 36-40.

[63]. Satyanarayanamurthy YVV. Experimental investigations of real time secondary co-injection of water-diethyl ether solution in DI-diesel engine fuelled with palm kernel methyl ester. Journal of Engineering Science and Technology; 7 (6): (2012), 711-721.

[64]. Rajan K., Prabhahar M., Senthilkumar K.R., "Experimental studies on the performance, emission and combustion characteristics of a biodiesel-fuelled (pongamia methyl ester) diesel engine with diethyl ether as an oxygenated fuel additive", International Journal of Ambient Energy, 37(5), (2016), 439-445.

[65]. Geo V.E., Nagarajan G., Nagalingam B., "Studies on improving the performance of rubber seed oil fuel for diesel engine with DEE port injection", Fuel, 89, (2010), 3559-3567.

[66]. Hariharan S., Murugan S., Nagarajan G., "Effect of diethyl ether on tyre pyrolysis oil fueled diesel engine", Fuel, 104, (2013), 109-115.

[67]. Devaraj J., Robinson Y., Ganapathi P., "Experimental investigation of performance, emission and combustion characteristics of waste plastic pyrolysis oil blended with diethyl ether used as fuel for diesel engine", Energy, 85, (2015), 304-309.

[68]. Kaimal V.K., Vijayabalan P., "An investigation on the effects of using DEE additive in a DI diesel engine fuelled with waste plastic oil", Fuel, 180, (2016), 90-96.

[69]. Barik D., Murugan S., "Effects of diethyl ether (DEE) injection on combustion performance and emission characteristics of Karanja methyl ester (KME)–biogas fueled dual fuel diesel engine", Fuel, 164, (2016), 286-296.

[70]. Sachuthananthan B., Jeyachandran K., "Combustion, performance and emission characteristics of water-biodiesel emulsion as fuel with DEE as ignition improver in a DI diesel engine", Journal of Environmental Research and Development, 2(2), (2007), 164-172.

[71]. Krishnamoorthi M., Malayalamurthi R., "Experimental investigation on performance, emission behavior and exergy analysis of a variable compression ratio engine fueled with diesel-aegle marmelos oil-diethyl ether blends", Energy, 128, (2017), 312-328.

[72]. Roy M.M., Calder J., Wang W., Mangad A., Diniz F.C. M., "Cold start idle emissions from a modern Tier-4 turbo-charged diesel engine fueled with diesel-biodiesel, diesel-biodiesel-ethanol, and diesel-biodiesel-diethyl ether blends", Applied Energy, 180, (2016), 52-65.

[73]. Kumar A., Rajan K., Naraynan M.R., Kumar K.R.S., "Performance and emission characteristics of a DI diesel engine fuelled with Cashew Nut Shell Oil (CNSO)-diesel blends with Diethyl ether as additive", Applied Mechanics and Materials, 787, (2015), 746-750.

[74]. Kumar A., Rajan K., Kumar K.R.S., Maiyappan K., Rasheed U. T., "Green fuel utilization for diesel engine, combustion and emission analysis fuelled with CNSO diesel blends with diethyl ether as additive", Materials Science and Engineering, 197, (2017), 1-10.

[75]. Ganesha T., Chethan K.S., "An experimental investigation of the performance and emission of diesel engine fueled with cashew shell oil methyl ester (CSOME) and it's blend with diethyl ether and conventional diesel", Imperial Journal of Interdisciplinary Research, 2(9), (2016), 922-929.

[76]. Srihari S., Thirumalini S., Prashanth K., "An experimental study on the performance and emission characteristics of PCCI-DI engine fuelled with diethyl ether-biodiesel-diesel blends", Renewable Energy, 107, (2017), 440-447.

[77]. Karthick D., Dwarakesh R., Premnath., "Combustion and emission characteristics of jatropha blend as a biodiesel for compression ignition engine with variation of compression ratio", International Review of Applied Engineering Research, 4(1), (2014), 39-46.

[78]. Satya V.P.U., Murthy K.M., Rao G.A.P., "Effective utilization of B20 blend with oxygenated additives", Thermal Science, 15(4), (2011), 1175-1184.

[79]. Abraham B.C., Thomas A.J., "Performance evaluation of biodiesel with a combustion enhancer additive", International Journal of Mechanical Engineering and Technology, 6(8), (2015), 118-125.

[80]. Firew D., Babu N. R., Didwania M., "The performance evaluation of diethyl-ether (DEE) additive with diesel blends using diesel engine test rig", International Journal of Scientific & Engineering Research, 7(6), (2016), 23-29.

[81]. Prasad U.S.V., Madhu Murthy K., Amba Prasad R.G., "Effect of oxygenated additives on control of emissions in a DI diesel engine using biodiesel-diesel blends", International Conference on Mechanical, Automobile and Robotics Engineering, (2012), 256-260.

[82]. Biradar C.H., Subramanian K.A., Dastidar M.G., "Performance improvement and emissions reduction of a DI diesel engine for use of karanja biodiesel-diesel blend (B20) using diethyl ether", Society of Automotive Engineers, Paper no: 2011-26-0004, (2011).

[83]. Manickam A.R., Rajan K., Manoharan N., Senthil Kumar K. R., "Experimental analysis of a diesel engine fuelled with biodiesel blend using di-ethyl ether as fuel additives", International Journal of Engineering and Technology, 6(5), (2014), 2412-2420.

[84]. Channe P.K., Kulkarni R.K., "Performance testing of diesel engine using KME and DEE blends with kerosene: a review", International Journal of Mechanical Engineering, 3(6), (2015), 1-5.

[85]. Nagdeote D.D., Deshmukh M.M., "Experimental study of diethyl ether and ethanol additives with biodiesel-diesel blended fuel engine", International Journal of Emerging Technology and Advanced Engineering, 2(3), (2012), 195-199.

[86]. Vadivel N., Somasundaram P., Krishnamoorthi M., "Performance and emission characteristics of a CI engine fueled with diesel -biodiesel (mahua/mustard) blend with diethyl ether additive", Journal of Chemical and Pharmaceutical Sciences, 7, (2015), 109-115.

[87]. Mallikarjun M.V., Mamilla V.R., Rao G.L.N., "NOx emission control techniques when CI engine is fuelled with blends of mahua methyle esters and diesel", International Journal of Engineering Sciences & Emerging Technologies, 4(2), (2013), 96-104.

[88]. Sudhakar S., Sivaprakasam S., "Potential of diethyl ether blends with biodiesel in DI diesel engine-an experimental investigation", International Journal of Research in Engineering & Advanced Technology, 2(5), (2014), 1-6.

[89]. Krishnamoorthi M., "Exergy analysis of diesel engine powered by diesel-mustard biodiesel blend with diethyl ether as additive", Journal of Chemical and Pharmaceutical Research, 7(8), (2015), 809-816.

[90]. Sathiyamoorthi R., Sankaranarayanan G., Pitchandi K., "Combined effect of nanoemulsion and EGR on combustion and emission characteristics of neat lemongrass oil (LGO)-DEE-diesel blend fuelled diesel engine", Applied Thermal Engineering, 112, (2017), 1421-1432.

[91]. Imtenan S., Masjuki H.H., Varman M., Rizwanul Fattah I. M., Sajjad H., Arbab M. I., "Effect of n-butanol and diethyl ether as oxygenated additives on combustion-emission-performance characteristics of a multiple cylinder diesel engine fuelled with diesel-jatropha biodiesel blend", Energy Conversion and Management, 94, (2015), 84-94.

[92]. Akshatha D.S., Manavendra G., Kumarappa S., "Performance evaluation of Neem biodiesel on CI engine with diethyl ether as additive", International Journal of Innovative Research in Science, Engineering and Technology 2(8), (2013), 3729-3736.

[93]. Kumar J.V., Rao C.J., "Experimental investigation of performance and emission characteristics of diesel engine working on diesel and neem oil blend with diethyl ether as additive", International Journal of Technological Exploration and Learning, 3(5), (2014), 581-588.

[94]. Annamalai K., Kumar A.R.P., Premkartik K., "Adelfa (NOME-Nerium Oil Methyl Ester) with DEE as the fuel additive for NOx reduction in DI Diesel engines-An experimental investigation", Journal of Scientific & Industrial Research, 73, (2014), 627-632.

[95]. Ali O.M., Mamat R., Masjuki H.H., Abdullah A.A., "Analysis of blended fuel properties and cycle-to-cycle variation in a diesel engine with a diethyl ether additive", Energy Conversion and Management, 108, (2016), 511-519.

[96]. Ali O.M., Mamat R., Najafi G., Yusaf T., Ardebili S.M. S., "Optimization of biodiesel-diesel blended fuel properties and engine performance with ether additive using statistical analysis and response surface methods", Energies, 8, (2015), 14136-14150.

[97]. Ali O.M., Mamat R., Abdullah N.R., Abdullah A.A., "Investigation of blended palm biodiesel-diesel fuel properties with oxygenated additive", Journal of Engineering and Applied Sciences, 11(8), (2016), 5289-5293.

[98]. Imtenan S., Masjukia H.H., Varmana M., Arbaba M.I., Sajjada H., Rizwanul Fattaha I. M., Abedina M. J., Md. Hasib A. S., "Emission and performance improvement analysis of biodiesel-diesel blends with additives", Procedia Engineering, 90, (2014), 472-477.

[99]. Imtenan S., Varman M., Masjuki H.H., Kalam M.A., Sajjad H., Arbab M.I., "Effect of DEE as an oxygenated additive on palm biodiesel-diesel blend in the context of combustion and emission characteristics on a medium duty diesel engine", 4th International Conference on Environmental, Energy and Biotechnology, 85, (2015), 100-104.

[100]. Varaprasad K.S., Rao H.S.B., "Experimental investigation on engine performance and exhaust emission analysis of diesel engine operating on palm oil biodiesel blends with diethyl ether as an additive", International Journal of Research and Innovation, (2017).

[101]. Muneeswaran R., Thansekhar M.R., Varatharajan K., "Effect of diethyl ether addition to palm stearin biodiesel blends on NOx emissions from a diesel engine", Asian Journal of Research in Social Sciences and Humanities, 6(9), (2016), 1382-1394.

[102]. Samuel K.J., Raj R.T.K., Sreenivasulu N., Rajasekhar Y., Edison G., Saco S.A., "An experimental study on performance and emissions of a direct ignition diesel engine with crude pongamia, pongamia methyl ester and diethyl ether blended with diesel", International Journal of Renewable Energy Research, 6(4), (2016), 1506-1515.

[103]. Pugazhvadivu M., Rajagopan S., "Investigations on a diesel engine fuelled with biodiesel blends and diethyl ether as an additive", Indian Journal of Science and Technology, 2(5), (2009), 31-35.

[104]. Muneeswaran R., Thansekhar M.R., "Reduction of NOx emission in biodiesel (soyabean) fuelled DI diesel engine by cetane improver", Journal of Engineering and Applied Sciences, 10(7), (2015), 2968-2973.

[105]. Navaneethakrishnan P., Vasudevan D., "Experimental study on performance and exhaust emission characteristics of a C.I. engine fuelled with tri compound oxygenated diesel fuel blends", Indian Journal of Science and Technology, 8(4), (2015), 307-313.

[106]. Tudu K., Murugan S., Patel S.K., "Effect of diethyl ether in a DI diesel engine run on a tyre derived fuel-diesel blend", Journal of the Energy Institute, 89, (2016), 525-535.

[107]. Murugan S., Tudu K., Patel S.K., "Performance and emission studies of a naturally aspirated diesel engine", Journal of Clean Energy Technologies, 5(5), (2017), 359-365.

[108]. Krishnamoorthi M., Natarajan A., "Performance and emission characteristics of a CI engine fueled with diesel-waste fried oil blend with DEE as additive", International Journal for Research in Applied Science & Engineering Technology, 3(5), (2015), 65-72.

[109]. Senthil R., Sivakumar E., Silambarasan R., "Effect of diethyl ether on the performance and emission characteristics of a diesel engine using biodiesel-eucalyptus oil blends", RSC Advances, 5, (2015), 54019-54027.

[110]. Venu H., Madhavan V., "Effect of diethyl ether and $Al_2O_3$ nano additives in diesel-biodiesel-ethanol blends: performance, combustion and emission characteristics", Journal of Mechanical Science and Technology, 31(1), (2017), 409-420.

[111]. Venu H., Madhavan V., "Effect of nano additives (titanium and zirconium oxides) and diethyl ether on biodiesel-ethanol fuelled CI engine", Journal of Mechanical Science and Technology, 30(5), (2016), 2361-2368.

[112]. Qi D.H., Chen H., Geng L.M., Bian Y.Z., "Effect of diethyl ether and ethanol additives on the combustion and emission characteristics of biodiesel-diesel blended fuel engine", Renewable Energy, 36, (2011), 1252-1258.

[113]. Venu H., Madhavan V., "Influence of diethyl ether (DEE) addition in ethanol-biodiesel-diesel (EBD) and methanol-biodiesel-diesel (MBD) blends in a diesel engine", Fuel, 189, (2017), 377-390.

MANAS Journal of Engineering
ISSN 1694-7398 | e-ISSN 1694-7398

*Volume 7 (Issue 2) (2019) Pages 89-93*

# Mechanical and microstructural characterization of rubber particle reinforced thermoplastic for automobile bumper application

Muideen Adebayo Bodude[1], Theddeus Tochukwu Akano[2,*], Adebayo Felix Owa[3]

[1]Department of Metallurgical and Materials Engineering, University of Lagos, Akoka, Lagos, Nigeria. mbodude@unilag.edu.ng

[2]Department of Systems Engineering, University of Lagos, Akoka, Lagos, Nigeria. takano@unilag.edu.ng, ORCID: 0000-0002-6998-0743

[3]Department of Materials and Metallurgical Engineering, Federal University Oye-Ekiti, Ekiti State, Nigeria

**ABSTRACT**

Thermoplastic elastomer composite produced from low-density polyethylene (LD-PE) mixed with 150 µm pulverised rubber particles in varied proportions (5%, 10%, 15%, 20% and 25%) using stir casting technique was characterized for mechanical properties in relation to the base polyethylene. Tensile, impact, flexural, and hardness tests were conducted to investigate the mechanical properties of the elastomer. The results obtained showed that the reinforcement with up to 20% wt of pulverised rubber particle generated a composite with a higher modulus of elasticity of 374MPa and hardness of 14.06BHN relative to those of the base material which are 227 MPa and 11.48 BHN respectively. However, the bending strength and the impact energy of the generated composite are 40MPa and 19.5 J, which are lower than those of the base material, which are 57 MPa and 20 J. This may be due to insufficient adhesion between the phases of the matrix and reinforcement.

**ARTICLE INFO**

***Research article***

*Received: 30.10.2019*
*Accepted: 02.12.2019*

***Keywords:***
*Elastomer,*
*automobile tyres,*
*mechanical properties,*
*stir casting,*
*thermoplastic,*
*polymeric composite*

*Corresponding author

## 1. Introduction

Polymer modification for improved properties and applications are currently being researched worldwide [1–4] investigated the bonding characteristics of ground rubber (GR) blended with isotactic polypropylene (PP) and discovered that properties comparable with commercial thermoplastic vulcanizates were achieved when creating bonds between the rubber particles and the thermoplastic matrix. Xin *et al.* [5] prepared expanded composites from GR/PP using a single-screw foam extrusion setup and chemical blowing agent. Guo *et al.* [6] prepared and characterised thermoplastic elastomers from scrap rubber powder, and linear low-density polyethylene (PE-LLD) treated with dual compatibiliser consisting of PE-LLD grafted with maleic anhydride, methyl methacrylate and butyl acrylate and epoxidised natural rubber (ENR). Their findings revealed that the mechanical properties, especially elongation at break improved phenomenally after compatibilisation. Grigoryeva *et al.* [7] prepared thermoplastic elastomers based on recycled PE-HD, ethylene-propylene-diene terpolymer (EPDM) and ground tyre rubber (GR) treated with bitumen. The authors concluded that bitumen acts as an effective devulcanizing agent in the GR treatment stage. Li *et al.* [8] synthesised PE-HD/ground rubber powder (GR) composites modified with various elastomers (ethylene-propylene copolymer, EPDM, ethylene-octylene copolymer) and dicumyl peroxide and/or dimethyl silicon oil. The rheological behaviour, dynamic mechanical properties, and morphology observation suggested that an enhanced adhesion between GR and polymer matrix formed in the modified PE-HD/GR composites.

Naskar *et al.* [9] used rubber hydrocarbon of ground rubber tyre (GRT) as a partial substitute for EPDM in a dynamically vulcanised EPDM/acrylic-modified PE-HD blend. The 60:40 rubber/plastic blends were found to behave like a thermoplastic elastomer, and it was observed that 50 wt. % of EPDM can be replaced by GRT without deterioration of properties. Low-density polyethylene (LD-PE) can be used for blending with ground waste rubber as well. Kumar *et al.* [10]

nvestigated TPEs based on ground tyre rubber (GTR, particle size 0.4 - 0.7 mm, untreated or thermomechanically decomposed), LD-PE and fresh rubber (natural rubber, styrene-butadiene rubber, EPDM) prepared with and without dynamic curing via sulfur or peroxide. Recipes containing decomposed GTR and EPDM gave the best performance. This was attributed to the dual compatibiliser effect of EPDM. Nevatia *et al.* [11] prepared thermoplastic elastomeric compositions from reclaimed rubber and scrap LD-PE. The 50:50 rubber-plastic ratio proved to be the best for processability and ultimate elongation.

A branch of waste tyre management is material recycling. Waste rubber is ground (at ambient temperature or cryogenically), and the product has vast application possibilities. It can be used to construct playground, parking lots, or produce railroad sleepers, bank stabilisers, noise barriers etc. A route to a high level of quality is offered by blending rubber powder with thermoplastics to form materials similar to thermoplastic elastomers.

This work is aimed at producing thermoplastic reinforced with rubber obtained from waste automobile tyre with a view to producing elastomer usable for such applications as automobile bumper, cable and wire, jacketing, hydraulic engine mount and head shield where high hardness, high young's modulus and good flexural and impact strengths are required.

## 2. Materials and methods

### *2.1. Materials*

The low-density polyethylene (LD-PE) pellets used were purchased from a commercial polymer Market in Ojota, Lagos Nigeria on which FTIR test was conducted to ascertain its chemical composition. Grounded Rubber Tyre waste was obtained from a local rubber factory. The rubber waste chips were passed through a conventional high powered, locally fabricated grinding mill. Natural Rubber was also obtained from the same rubber factory. This was also cut into a smaller piece. The compositional analysis of the ground rubber (waste tyre) is presented in Table 1.

### *2.2. Methods*

#### *2.2.1. Sample preparation*

Ground rubber powder was sieved using ASTM Standard sieve of 100 BSS to obtain the particle size of 150 µm. The calculated amount of this powder, the natural rubber as well as the polyethylene pellets was weighed and charged in the stir casting machine maintained at 200$^{O}$C and continuously stirred until the homogeneous melt is obtained. The molten elastomer is then poured in the already prepared wooden mould and allowed to solidify.

**Table 1.** *Chemical Analysis of Rubber Used for Automobile Tyre [12]*

| Ingredient | Composition |
|---|---|
| Natural rubber | 43%w |
| Synthethic rubber (styrene butadiene) rubber and butadiene rubber) | <22.8%w |
| Vulcanizing agent (sulphur) | <0.8%w |
| Accelerators (MBT/TMT) | <0.8%w |
| Inorganic activators (Calcium/zinc oxide) | <3.3%w |
| Carbon black | <27%w |
| Plasticizer(mineral oil) | |
| Antioxidant and antiozonant | <1.3%w |
| Other components | <1% |

#### *2.2.2. Microstructural analysis*

The optical microscopy of the samples was conducted by grinding and polishing the surfaces of the samples followed by observation using an optical microscope focused at a magnification of 200 to reveal the internal structure of the composites. The micrograph is thus obtained by the camera attached to the machine.

#### *2.2.3. Mechanical tests*

Three samples each were used for the mechanical tests reported below. The average of the values obtained was however used for the analysis. The resistance of the elastomers samples to indentation and penetration (Hardness test) were measured using Brinell hardness tester. The hardness was indicated by the diameter of the indentation made on the sample by a 10mm ball indenter pressed on the sample by a load of 1000N for 10seconds. The tensile test samples were prepared as a dumbbell test pieces and the testing procedure was carried out in accordance with the ASTM E8 specification. The test sample was held in the grips of Instron 3369M Tensometer and subjected to tensile load until it fractures.

The flexural test was conducted using the 3-point ASTM standard specification method. The maximum stress absorbed to failure by the material was recorded along with other relevant data obtained from the test. The stress at fracture is known as the flexural strength, fracture strength, modulus of rupture, or the bending strength. The Izod impact test was carried out on the notched samples held in a vice while a heavy pendulum, mounted on ball bearings was allowed to strike the samples after swinging from a fixed height. The energy absorbed in breaking the sample is thus indicated on the machine as the impact energy. The impact energy is an indication of the fracture toughness of the material.

*2.2.4. Fourier Transform Infrared Spectroscopy (FTIR) test*

The functional group of the low-density polyethylene was determined using the FTIR test. This was done to ascertain the quality of the material. An infrared (IR) spectrum, which consists of a plot of stretching frequency (in $cm^{-1}$) versus intensity (as measured by percentage transmittance) was obtained from this test. The peaks in IR spectrum reveal the functional groups present in the molecule.

## 3. Results and discussion

The absorbance spectrum indicated in Fig. 1 corresponds to Isocyanate functional group. This confirmed the quality of the low-density polyethylene (LD-PE) used as a matrix for this study.

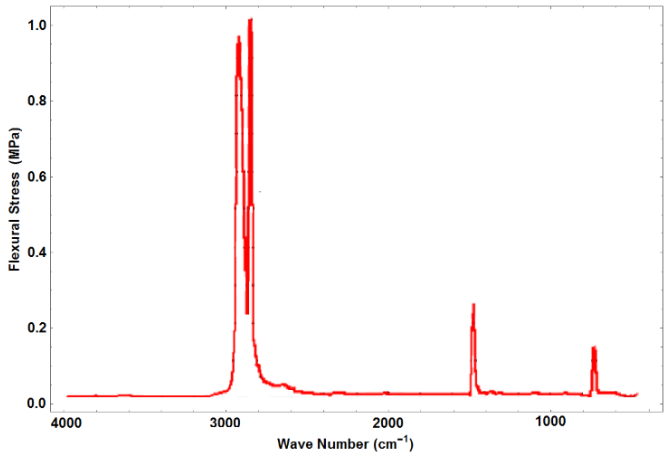


**Figure 1**. *FTIR of Polyethylene*

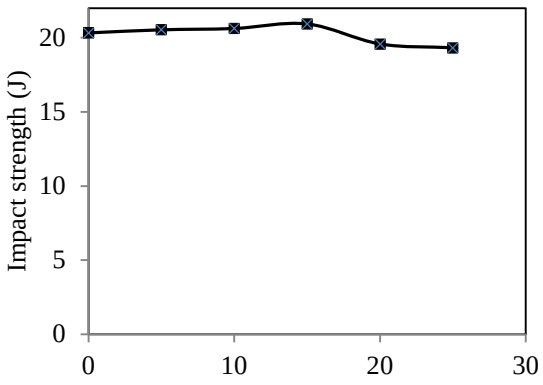


(a) Filler Concentration (%)

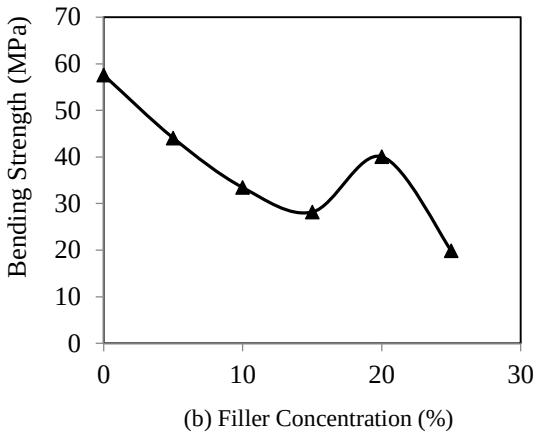


(b) Filler Concentration (%)

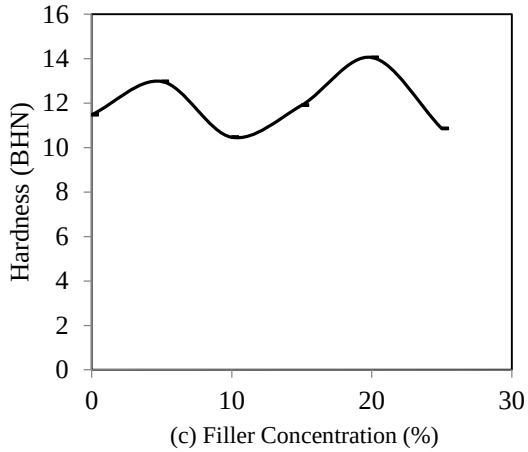


(c) Filler Concentration (%)

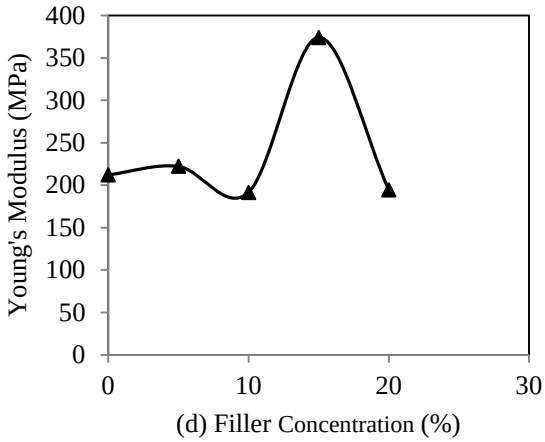


(d) Filler Concentration (%)

**Figure 2.** *Mechanical properties variation with filler concentration*

The plots of filler concentration against the mechanical property parameters are shown in Figs. 2(a)-(d). From Fig. 2(a), the impact strengths of the composites increase slightly with an increase in filler concentration to 20.94J at 15% filler and drop subsequently upon an increase in filler concentration. While Fig. 2(b) shows the plots of bending strength of the composite against filler concentration. This figure shows that the bending strength of the elastomer fell

between 0 - 5% filler concentration and continued with the trend up to 15% but peaked at 20% and decreased again at 25% rubber particle addition. This unstable behaviour may be attributed to the fact that as the amount of reinforcement increases, there is a reduction in the total surface area available for matrix-filler interaction. Fig. 2(c) indicates the graph of the composites hardness versus the filler concentration. From this plot, the base material has hardness value of 11.48BHN and this slight increase to 12.98BHN when 5% of ground rubber filler was added and it dropped to 10.47 with 10% filler. However, it attained the highest of 14.06BHN when 20% filler was added. Fig. 2(c) shows the young's modulus of elasticity of the composite against the filler concentration. The modulus follows the same trend as the bending strength. However, both the young's modulus and the hardness values increased while the bending and impact strengths reduced with increasing rubber particles filler addition. This shows the dependence of all these parameters on the percentage proportion of the filler. Fig. 3 shows the flexural stress-strain behaviours of all the samples. The Figure shows that all the samples reinforced (composites) have better flexural strength than the control sample (LD-PE). While the plots of filler concentrations against flexural test results are shown in Figs. 4 and 5. From these Figures sample with 5% filler addition has the highest flexural strength of 44.06MPa, while the sample with 20% filler addition exhibited significantly high flexural strength (40.07MPa) even though these values are lower than that of LD-PE which is 57.58MPa.

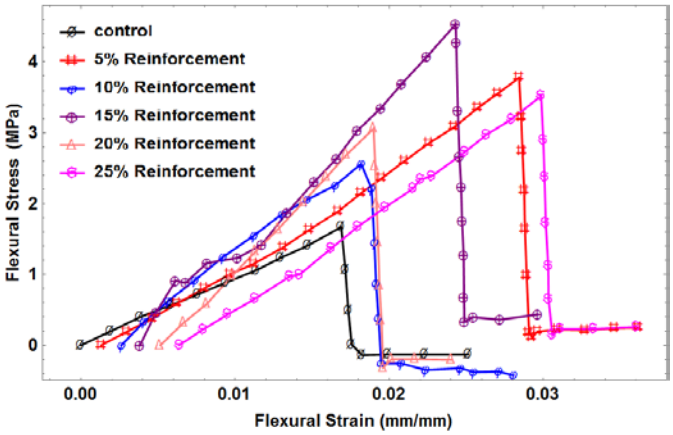


**Figure 3**. *Flexural stress-strain of the rubber particle reinforced elastomer*

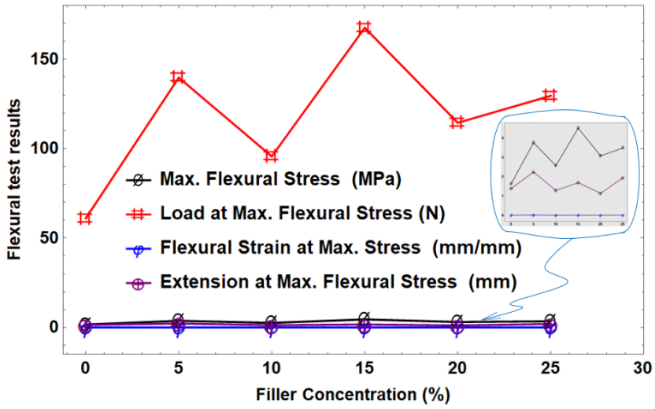


**Figure 4.** *Filler Concentration against various flexural test results*

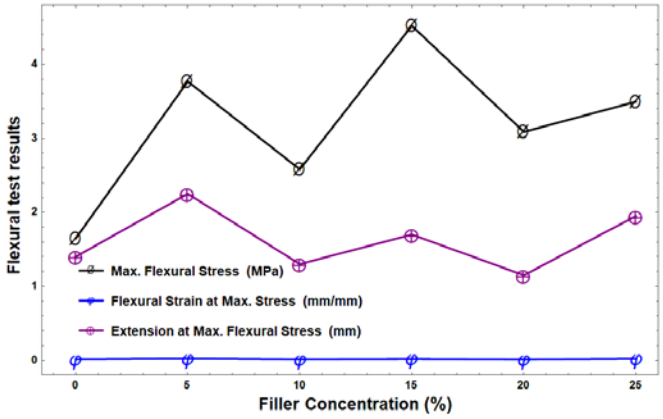


**Figure 5.** *Filler Concentration against various flexural test results from Fig.4*

The microstructures of the samples from 0 - 25% filler additions are shown in Fig. 6. The filler appears as additional black particles which already exist in the LD-PE. It can be seen that the volume of the particle increases with percent filler addition and their dispersion within the matrix is generally uniform. The rubbers are well agglomorated and evenly distributed within the matrix as displayed in Fig.6.

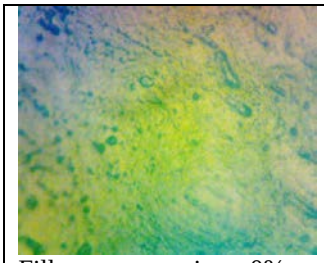

Filler concentration - 0%

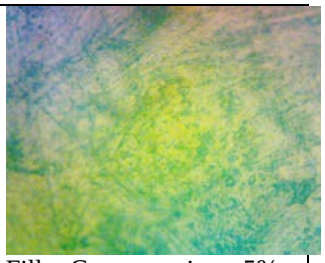

Filler Concentration - 5%

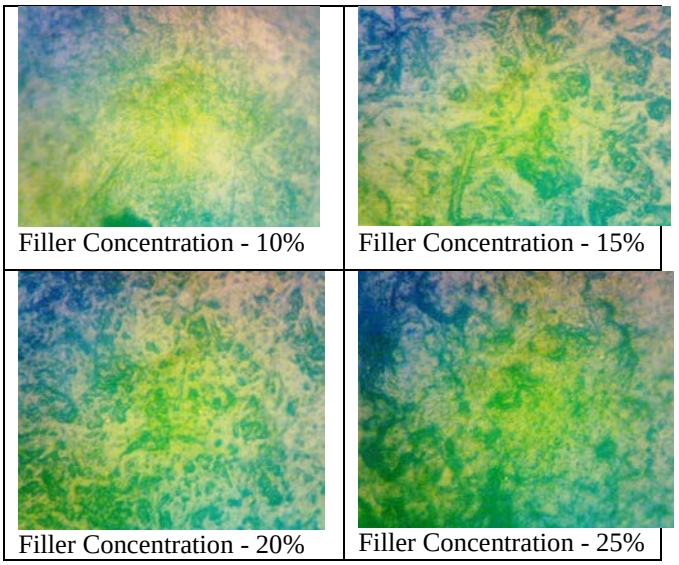


**Figure 6**. *Optical micrographs of LD-PE thermoplastic elastomer*

## 4. Conclusion

It was noticed that the least hardness value of 10.47 BHN was obtained in the composite with 10% ground rubber particle addition while the highest hardness value of 14.06 BHN was obtained in composite with 20% ground rubber particle addition.The above behavior may be due to the fact that at 20% filler addition the microstructure comprises of highly homogeneous mixture of the rubber particle and the matrices. The filler is evenly distributed in the structure as shown in Fig. 5. The highest young's modulus value of 374 MPa was obtained in composite with 20% filler addition. The highest impact energy of 20.94 J was obtained in composite with 15% rubber filler concentration. It was also observed that composite with 5% rubber particle addition showed the highest flexural strength of 44.06 MPa before shattering relative to other composite samples.

**Nomenclature**

| | |
|---|---|
| LD-PE | Low density polyethylene |
| PE-LLD | Linear low-density polyethylene |
| PE-HD | High density polyethylene |
| GRT | Ground rubber tire |
| FTIR | Fourier transform Infrared spectroscopy |
| EPDM | Ethylene propylene-diene terpolymer |
| MPa | Mega Pascal |
| J | Joule |
| ENR | Epoxidized natural rubber |
| GR | Ground rubber |
| PP | Polypropylene |

## References

[1]. Egodage SM, Harper JF, Walpalage S. "The development of rubber-thermoplastic blends from ground tyre rubber and waste polypropylene", J Natl Sci Found Sri Lanka (2009), 37.

[2]. Hrdlicka Z, Kuta A, Hajek J. "Thermoplastic elastomer blends based on waste rubber and low-density polyethylene", Polimery, 55, (2010), 832–8.

[3]. Michael H, Scholz H, Mennig G. "Blends from recycled rubber and thermoplastics", Kautschuk Gummi Kunststoffe, 52, (1999), 510–3.

[4]. Mennig G, Michael H, Rzymski WM, Scholz H. "Thermoplastic elastomers from polypropylene-powdered rubber scrap blends", Polimery, 42, (1997), 491–3.

[5]. Zhang ZX, Zhang SL, Kim JK. "Evaluation of mechanical, morphological and thermal properties of waste rubber tire powder/LLDPE blends", E-Polymers (2008), 8.

[6]. Guo B, Cao Y, Jia D, Qiu Q. "Thermoplastic Elastomers .Derived from Scrap Rubber Powder/LLDPE Blend with LLDPE-graft-(Epoxidized Natural Rubber) Dual Compatibilizer", Macromol Mater Eng, 7, (2004), 289-360.

[7]. Tolstov A, Grigoryeva O, Fainleib A, Danilenko I, Spanoudaki A, Pissis P, et al. Reactive Compatibilization of Polyethylene/Ground Tire Rubber Inhomogeneous Blends via Interactions of Pre-Functionalized Polymers in Interface. Macromol. Symp., vol. 254, Wiley Online Library; (2007), 226–32.

[8]. Li Y, Zhang Y, Zhang Y. "Mechanical properties of high-density polyethylene/scrap rubber powder composites modified with ethylene–propylene–diene terpolymer, dicumyl peroxide, and silicone oil", J Appl Polym Sci, 88, (2003), 2020–7.

[9]. Naskar AK, De SK, Bhowmick AK. "Thermoplastic elastomeric composition based on maleic anhydride–grafted ground rubber tire", J Appl Polym Sci, 84, (2002), 370–8.

[10]. Kumar CR, Fuhrmann I, Karger-Kocsis J. "LDPE-based thermoplastic elastomers containing ground tire rubber with and without dynamic curing", Polym Degrad Stab, 76, (2002), 137–44.

[11]. Nevatia P, Banerjee TS, Dutta B, Jha A, Naskar AK, Bhowmick AK. "Thermoplastic elastomers from reclaimed rubber and waste plastics", J Appl Polym Sci., 83, (2002), 2035–42.

[12]. Evans A, Evans R. "The composition of a tyre: typical components". Waste Resour Action Program, (2006), 5.

MANAS Journal of Engineering
ISSN 1694-7398 | e-ISSN 1694-7398

*Volume 7 (Issue 2) (2019) Pages 94-98*

# Design, fabrication and performance analysis of TTD structures for S-band active phased array RF beamforming networks

Ahmet Hastürk[1], Nursel Akçam[2], Tayfun Okan[3,*]

[1]Aselsan Inc., Ankara, Turkey, hasturkk.ahmet@gmail.com,

[2]Gazi University, Electrical and Electronics Enginering Department, Ankara, Turkey, ynursel@gazi.edu.tr, ORCID: 0000-0003-0585-3988

[3]University of Turkish Aeronautical Association, Electrical and Electrinics Engineering Department, Ankara, Turkey, tokan@thk.edu.tr, ORCID: 0000-0002-9913-0803

**ABSTRACT**

In this study an eight-channel active analog beamforming structure is designed and developed in subsystems by using an Applied Wave Research (AWR) simulation program. This structure works in S-band and contains true-time-delay (TTD) systems. The simulation results and the results obtained from the manufactured structure are compared. In the comparison, the TTD values for different time delay steps and phase difference measurements between channels are analyzed and interpreted. The test results show that desired performance is obtained from the designed and manufactured PCB. However, it is observed that feeding each antenna element with single channel beamforming board would be more appropriate.

**ARTICLE INFO**

***Research article***

*Received: 28.03.2019*
*Accepted: 15.10.2019*

***Keywords:***
*Active phased array, beamforming, true-time-delay (TTD), phase shift, single pole four throw (SP4T).*

*Corresponding author

## 1. Introduction

In electronic warfare (EW) systems, electronic scanning featured active phased-array beamforming systems are one of the most important structures necessary for vital functions like: self-protection and counter measure. The performance of these structures directly affects the performance of whole system. To be able to involve targets in different positions, the antenna beam should be directional. EW systems can be classified into two groups with respect to the type of beamforming as: mechanically directed systems [1] and phased array systems [1-5]. A large scaled, mechanically directed antenna and to feed that antenna a high powered RF amplifier is needed to generate a beam in conventional methods [1]. Only one beam can be generated when beamforming is done mechanically which takes milliseconds. On the other hand, in phased array systems the beamforming is done by exciting more than one antenna element in different phases [1]. Since beams are directed electronically with phase shifters in these systems, the time necessary for beamforming is in the order of microseconds. This provides efficiency in comparison to mechanically directed systems.

Phased array structures are divided into two with respect to feeding status of antenna element as: passive phased array and active phased array structures. The advantage of active phased array structures against passive phased array ones is that they are able to control amplitude of each antenna element individually. Compared to passive phased array structures less powered transceiver modules are used to feed these antennas [1].

Photonic TTD beamformers provide solutions to many drawbacks for wireless radar and satellite communication systems. But with the increasing number of antennas, scalability limitations may arise. In [2] a concept of a photonic TTD beamforming network for phased array antennas (PAA) is presented. Rotman lens which increases the capabilities of multibeam antennas and photonic beamforming are compared in [3] for wideband radio frequency (RF) beamforming. In [4] optical phase-lock-loop (OPLL) is used to achieve tunable time delays and laser diodes are used to generate RF signal. This is the first example of an OPLL being used in TTD setup. An optical TTD beamformer is reported in [6, 7, 8] for various systems and in all successful results have been achieved. A

compact and high frequency TTD beamformer is applied by using bidirectional reflectance of the fiber gratings in [9]. In [10], a combination of time switching with non-orthogonal multiple access is reported by Gao *et al.* in order to cancel the inter-cluster interference.

In this study, an eight-channel active beamforming structure is designed by using Applied Wave Research (AWR) simulation program. The designed and manufactured beamforming printed circuit board (PCB) operates in the S-band and contains true-time-delay (TTD) systems. A good matching is observed, when the simulation results and the results obtained from the manufactured structure are compared with respect to TTD values for different time delay steps, and phase difference between channels.

## 2. Analog beamforming

In most of the phased array structures only one beamforming technique is used which is either analog, digital [11] or photonic [12]. On the other hand, there are some examples of hybrid systems in which more than one of these techniques are used [5]. The complexity of RF circuit can be reduced and same performance can be provided with the hybrid beamforming. An investigation is made [5] to prevent reduction in system bandwidth, where long delays are produced digitally and short delays with analog electric circuits.

The phase value necessary for each antenna element is given by analog or digital phase shifters in analog beamforming technique, the block diagram of which is given in Fig. 1. When a breakdown occurs in one of the modules, the system continues to work properly with less performance; since each antenna is fed with a separate module. Phase shifters add a constant phase difference to the signal through the operating frequency band, without changing the signals amplitude. Theoretically, if the signal entering to the phase shifter is $Ve^{j0}$, then the signal in the output is $Ve^{-j\phi}$ [13]. In phased array systems, phase shifters are used to add proper phases to antenna elements in order to perform beamforming electronically.

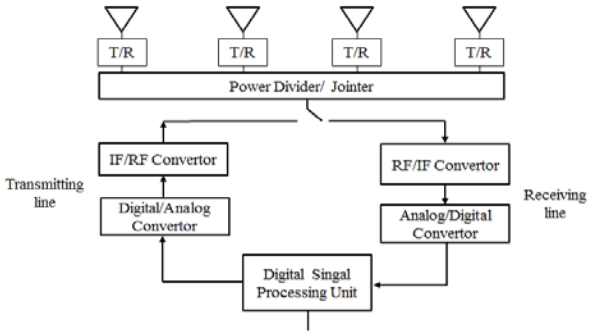


**Figure 1**. *Block diagram of analog beamforming structure.*

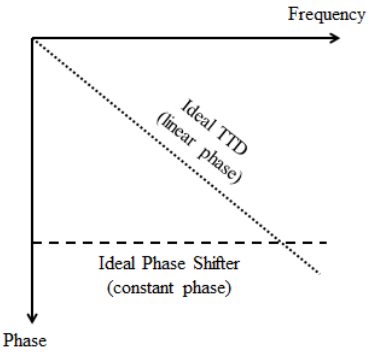


**Figure 2**. *Comparison between TTD and phase shifter.*

In analog beamforming, if the broadcasting frequency band is wide and the array is formed with multiple elements, TTD structures are used to reduce the loss of earnings caused by beam shifting. As TTD structures are independent of frequency, loss of earnings emerged during beamforming in wide band systems can be removed easily. Unlike phase shifter, there is an inverse relationship between frequency and phase for TTD which can be seen in Fig. 2. TTD expression can be identified in terms of time and phase as [1]:

$$\Delta t = \frac{dsin(\theta)}{c} \quad (1)$$

$$\Delta\phi = 2\pi f \Delta t = \frac{2\pi dsin(\theta)}{\lambda} \quad (2)$$

where $\theta$ is the direction or steering angle, $c$ is the speed of light, $d$ is the distance between antenna elements, and $f$ indicates the frequency. Time delay $\tau = \frac{i \times d \times \sin(\theta)}{c}$ indicates that TTD value is independent of frequency [14].

## 3. Numerical results

In this study, a structure with eight channels is designed and manufactured for beamforming process. The designed and manufactured beamforming PCB is shown in Fig. 3. As seen from the manufactured structure, the components of the beamforming circuit have a physically symmetrical design.

Because of material over-density on the PCB, any short circuit that is possible to occur during alignment process may affect whole operating performance. For beamforming process each channel passes through power divider part of the structure. That is why an RF performance decrease in any channel will affect the overall performance of the system; since the channels are interactive of each other. The HMC594LC3B and HMC232LP4 amplifiers are used to compensate the interruption losses of the phase shifter and attenuator, and also to achieve the desired gain. Moreover, the LFCN3800 filter is used to provide the desired S-band frequency (2-4 GHz). In Fig. 3, the part of the circuit used for phase and amplitude

adjustment is given, where the aforementioned phase shifters and adjustable attenuator is implemented.

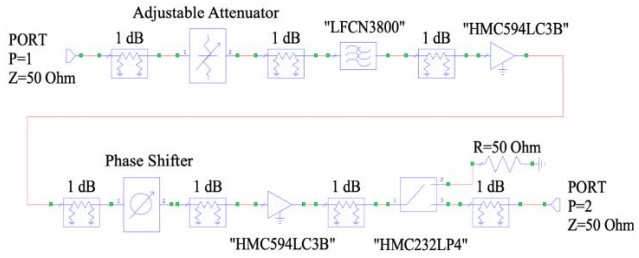


**Figure 3**. *Circuit schematic for the phase and amplitude adjustment block.*

As seen in Fig. 4, this design study consists of three blocks; which are phase and amplitude setting block, first TTD block and second TTD block. Each TTD block contains two levels in itself and connected to other TTD blocks with a time delay by using single pole four throw (SP4T) switching mechanisms. In switched time delay, when lines of switches are directly connected to each other via transmission lines, there occurs no time delay. This condition is accepted as reference channel, and the calculations are made with respect to this reference channel. In the measurements, some bits are unable to give the expected delays. The reason for that is the coupling effect; which is occurred as lines of switches with same lengths are inclined toward each other.

First TTD block measurements are made for 100, 200, 300 ps time delay steps as shown in Fig. 5. The measurements are made between 2-4 GHz frequency range, since the structure operates at S-band. The maximum difference between measured TTD values and simulation results is 10 ps. Similarly, second TTD block measurements are made for the time delay steps values of: 100, 200, 400 ps. Second block of the system has two levels. First and second level of second block TTD test results are depicted in Fig. 6(a) and (b), respectively. As seen from the graphs, very close results are obtained between measured and simulated values, where the maximum difference is 15 ps. This shows the accuracy and usability of the proposed system.

According to the simulation results, the phase difference between channels is expected to be in the same phase for each channel. On the other hand, when measurement results in Fig. 7 are analyzed, at the end of the band in some of the channels there occurs 20 degrees of phase difference. The line length of each channel is expected to be equal; however, for the manufactured PCB, some lines are not in equal length with a very small difference. This is one of the reasons for the phase difference between channels. Secondly, since RF connectors and other circuit materials are not precisely soldered and contacted to the PCB, it also causes the phase difference between channels.

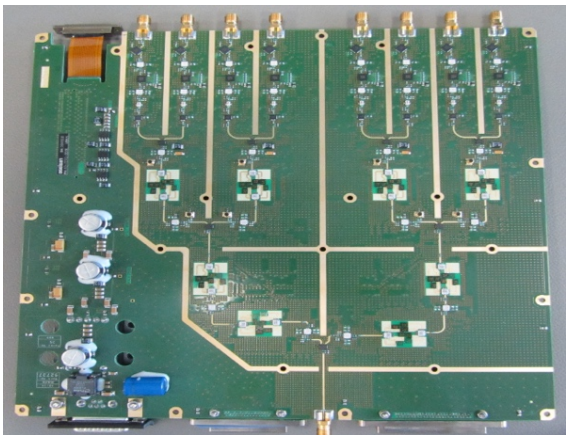

**Figure 4**. *Manufactured beamforming PCB.*

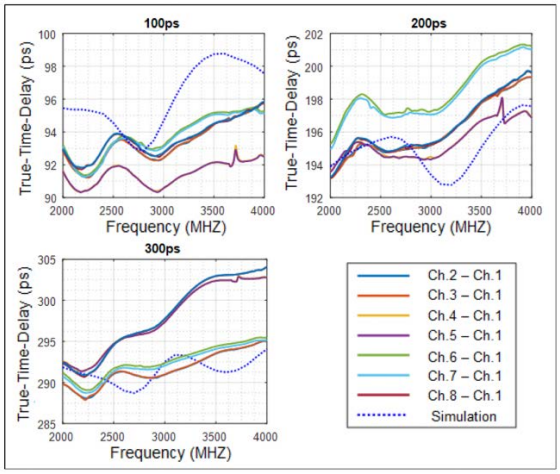


**Figure 5**. *First block TTD test results.*

(a)

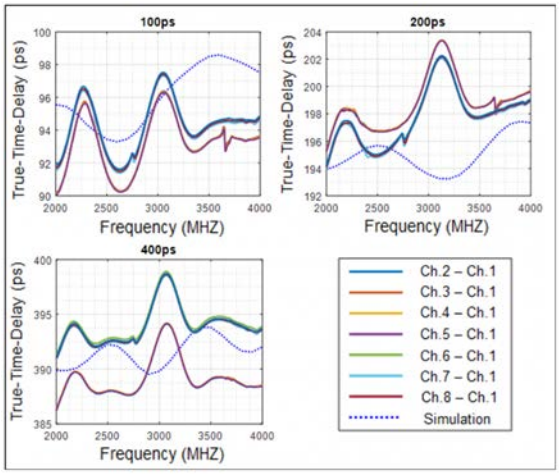

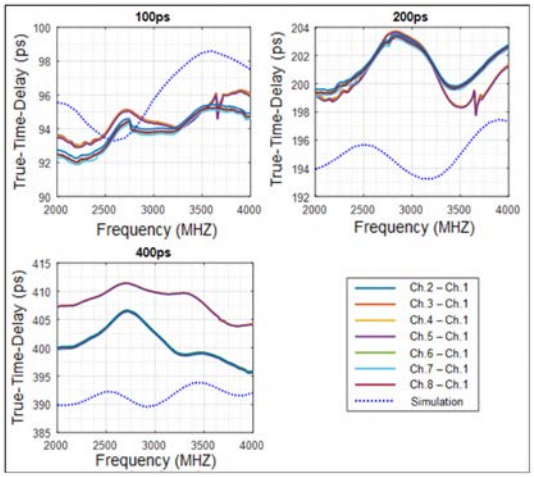


**Figure 6**. ***(a)*** *First level of second block TTD test results.* ***(b)*** *Second level of second block TTD test results.*

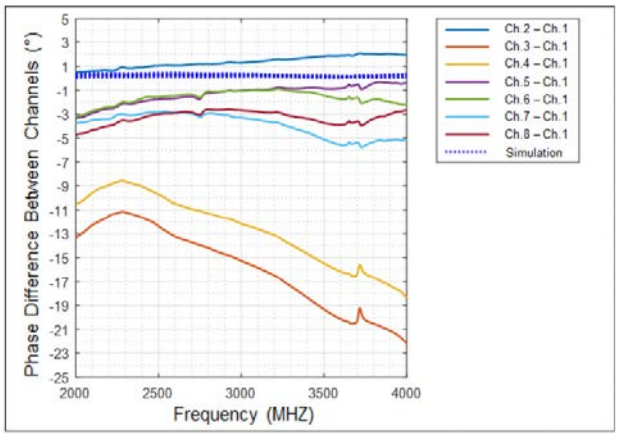


**Figure 7**. *Phase difference test results between channels.*

## 4. Conclusion

In this study a novel analog beamforming structure is designed in sub-blocks by using a simulation program, which is also manufactured as a PCB. Measurements of TTD and phase difference between channels are made for different time delay steps. When the simulation results are compared with the measured ones, the maximum time differences between them are: 10 ps for first level TTD with 100, 200, 300 ps time delay steps; 15 ps for each block of second level TTD with 100, 200, 400 ps time delay steps. According to measurement results, 20 degrees of phase difference is observed at the end of the bands for some channels. Test results confirm the success in the performance and accuracy of the manufactured PCB. Furthermore, similar values are obtained for the simulated design and manufactured PCB. However, it is observed that for the reported system, feeding each antenna element with single channel beamforming board would be more appropriate. This helps to achieve more successful results with (b) less time difference between the simulated and fabricated system.

## References

[1]. Balanis C.A., Antenna Theory: Analysis and Design. New York: Wiley, 1997.

[2]. Duarte V.C., Drummond M.V. and Nogueira R.N., "Coherent photonic tru-time-delay beamforming system for a phased array antenna receiver", in 18th International Conference on Transparent Optical Networks (ICTON), (2016), 1-5.

[3]. Rotman R., Rotman S., Rotman W., Raz O. and Tur M., "Wideband RF beamforming: the Rotman lens vs. photonic beamforming", in IEEE Antennas and Propagation Society International Symposium, vol. 2B, (2005), 23-26.

[4]. Rideout H.R., Seregelyi J.S. and Yao J., "A True Time Delay Beamforming System Incorporating a Wavelength Tunable Optical Phase-Lock Loop", Journal of Lightwave Technology, 25, (2007), 1761-1770.

[5]. Morgan L. and Andersson H., "An efficient beamforming method using a combination of analog true time and digital delay", in IEEE Radar Conference, (2002), 260-265.

[6]. Walden R.H., "Performance Trends for Analog-to Digital Converters", IEEE Communications Magazine, 37, (1999), 96-101.

[7]. Capmany J. and Novak D., "Microwave photonics combines two worlds", Nature Photonics, 1, (2007), 319-330.

[8]. Shin D.H., Yom I.B. and Kim D.W., "4–20 GHz GaAs True-Time Delay Amplifier MMIC", IEEE Microwave and Wireless Components Letters, 27, (2017), 1119-1121.

[9]. Yi X., Huang T.X.H., Minasian R.A., "Photonic Beamforming Based on Programmable Phase Shifters With Amplitude and Phase Control", IEEE Photonics Technology Letters, 23, (2011), 1286-1288.

[10]. Gao X., Huang S., Wei Y., Gao C., Zhou J., Zhang H. and Gu W., "A high-resolution compact optical true-time delay beamformer using fiber Bragg grating and highly dispersive fiber", Optical Fiber Technology, 20, (2014), 478-482.

[11]. Yang D. H. and Lin W. P., "Phased-array beam steering using optical true time delay technique", Optics Communications, 350, (2015), 90-96.

[12]. Fan C., Huang S., Gao X., Zhou J., Gu W. and Zhang H., “Compact high frequency true-time-delay beamformer using bidirectional reflectance of the fiber gratings”, Optical Fiber Technology, 19, (2013), 60-65.

[13]. Li X., Zhao S., Zhu Z., Liu Y., Zhao J. and Miao X., “Power fading elimination and linearization for a dispersive optical true time delay using carrier phase shifting and optical sideband processing”, Optik, 126, (2015), 3949-3953.

[14]. Hiep P. T. and Hoang, T. M., “Non-orthogonal multiple access and beamforming for relay network with RF energy harvesting”, ICT Express, in press, (2019), 1-5.

MANAS Journal of Engineering
ISSN 1694-7398 | e-ISSN 1694-7398

*Volume 7 (Issue 2) (2019) Pages 99-113*

# Calculating slope gradient variations in the submarine landforms by R and Python statistical libraries

Polina Lemenkova

Ocean University of China, College of Marine Geo-sciences. Address: 238 Songling Road, Laoshan, 266100, Qingdao, Shandong Province, People's Republic of China, pauline.lemenkova@gmail.com, ORCID 0000-0002-5759-1089

**ABSTRACT**

This research focuses on the analysis of the submarine geomorphology in the Mariana Trench located in west Pacific Ocean. The research question is to identify variations in the geomorphic form and bathymetry in different segments of the trench. Technically, the paper applies Python and R programming statistical libraries for geospatial modelling of the data sets. The methodological approach of the statistical data analysis by scripting libraries aimed to visualize geomorphic variations in the 25 transect profiles of the trench. Multiple factors affect submarine geomorphology causing variations in the gradient slope: geological settings (rock composition, structure, permeability, erodibility of the materials), submarine erosion, gravity flows of water streams, tectonics, sediments from the volcanic arcs, transported by transverse submarine canyons. Understanding changes in geomorphic variations is important for the correct geospatial analysis. However, modelling such a complex structure as hadal trench requires numerical computation and advanced statistical analysis of the data set. Such methods are proposed by R and Python programming languages. Current research presented usage of statistical libraries for the data processing: Matplotlib, NumPy, SciPy, Pandas, Seaborn, StatsModels by Python. The research workflow includes following steps: Partial least squares regression analysis; Ordinary Least Square (OLS); Violin plots and Bar plots for analysis of ranges of the bathymetric data; Isotonic Regression by StatsModels library; Data distribution analysis by Bokeh and Matplotlib libraries; Circular bar plots for sorting data by R; Euler-Venn diagrams for visualizing overlapping of attributes and factors by Python. As a result of the data analysis, the geomorphology of the trench slopes in 25 transecting profiles was modelled. The results achieved by the statistical data modelling show differences in the gradient slope in various segments of the trench depending on its spatial location. This shows complex geological structure of the trench. The paper contributes towards the methodological development of the data analysis in marine geology through the stepwise workflow explanations with a case study of Python and R applications

**ARTICLE INFO**

***Research article***

*Received: 04.05.2019*
*Accepted: 15.10.2019*

***Keywords:***
*Python,*
*R,*
*geomorphology,*
*data analysis,*
*statistics,*
*Mariana trench*

## 1. Introduction

The geomorphology of the ocean trenches and continental-shelf submarine canyons plays crucial role for the deep-sea ecosystems, because, along with other environmental factors, steep gradient slopes create conditions for the downward transport from the flat abyssal plains and accumulation of the organic matter and sediments along the hadal trench axis [1, 2, 3]. Therefore, understanding geomorphic slope processes is of particular interest to the geoscientists, since slopes form conditions for the ecosystem life [4] and reflect changes in lithology [5]. However, the geomorphology of the submarine slopes of the ocean trenches is often overlooked, due to the unreachable nature of the study object that can only be studied by means of the remote sensing and computer based modelling.

Existing studies on the landform geomorphology are mostly focused on the landforms structure and variations, land surface processes [6], classification of the geomorphic classes as land forms existing on the Earth in general [7, 8, 9, 10]. Nevertheless, the submarine landforms as a particular class of the geomorphic shapes on the ocean seafloor have lesser attention comparing to the land geomorphology. Some existing works report recent findings on the on hadal trench geomorphology used in the current work [11, 12, 13, 14, 15, 16, 17, 18]. The particular focus of this study lies on the calculations of the slope gradients and classification of the

hadal trench's slope steepness by multi-disciplinary approach of GIS and data analysis using programming libraries. Estimation of slopes and ranking data were performed by R language with auxiliary statistical analysis by Python libraries.

## 2. Methods and materials

The methodology of this work is illustrated by the workflow chart (Fig. 1). The core methods used in this work are based on the machine learning algorithms provided by Python and R programming languages and statistical libraries.

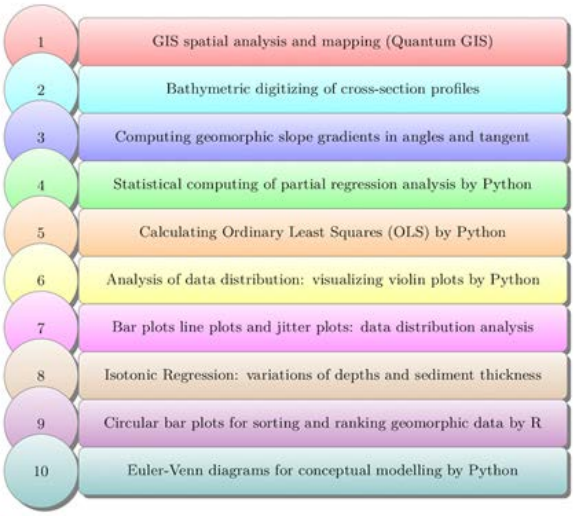


**Figure 1**. *The methodological workflow in 10 steps.*

The research started from the installing Python and necessary libraries. Following steps are described in the relevant subsections below.

### *2.1. Spatial data processing using GIS*

The first step included GIS based analysis performed in QGIS where geospatial layers were stored, re-projected and visualized. These include vector .shp files of thematic data: geology, bathymetry, tectonics, sediment thickness covering study area of Mariana Trench, Pacific Ocean (Fig. 2). The next step included plotting profiles crossing the study area (Fig. 3) plotted by 'ProfileFromPoints' QGIS plugin. The data pool now consisted in 25 cross-section profiles within a 1.000km length each and a distance of 100 between each couple in the area which extend from Philippine Sea crossing Mariana Trench (Fig. 2) in a perpendicular direction. The visualization of the profiles and calculations of the deepest gradient slope angle by profiles are shown on the facetted plot of Fig. 3 for each profile, respectively. The attributes values of the the digitized layers were stored in a table (.csv) and exported to R and Python libraries for further processing.

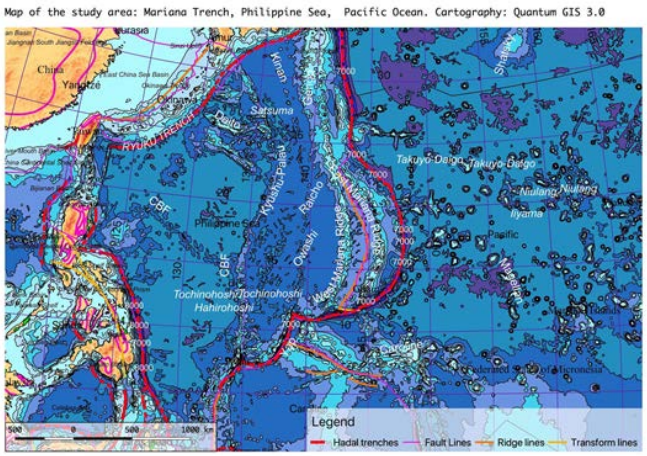


**Figure 2.** *Study area: Mariana Trench. Geomorphic and geological features.*

### *2.2. Installing tools and preparing data*

The following step consists in the statistical data processing by libraries StatsModels, Matplotlib, Pandas, using existing methodologies on Python data processing [19, 20, 21, 22]. The general syntax of Python and solutions of the statistical algorithms by libraries were derived from the existing literature on data science [23, 24, 25, 26, 27, 28] and modified for the particular case study. The research is technically based on versions of Python 3.7.2 and R 3.6.1. The installation of the Python libraries and dependancies was done via the command line of the bash terminal. Because this process is not trivial, a brief explanation of the crucial installation steps is provided below. Upon installing core package of Python, the settings tools were adjusted. The package installer for Python 'pip' 19.0.3 and Xcode were installed. These steps are illustrated in the following command: $ curl https://bootstrap.pypa.io/get-pip.py -o get-pip.py $ python get-pip.py $ xcode-select –install

Then, important Python libraries were installed via the console utility 'pip'. First, NumPy, a Python's package for the scientific computing providing fast N-dimensional array processing. Second, a SciPy package version 1.1.0, depending on NumPy 1.14.5, was installed. SciPy was used for the computations. Third, Pandas 1.11.0, the package for data manipulation in tabular format was installed. Plotting packages for data visualization, Matpotlib and Seaborn, were installed via pip using commands lines, stepwise: $ pip install scipy $ pip install numpy $ python3 -m pip install pandas $ sudo python3 -m pip install matplotlib $ python3 -m pip install seaborn

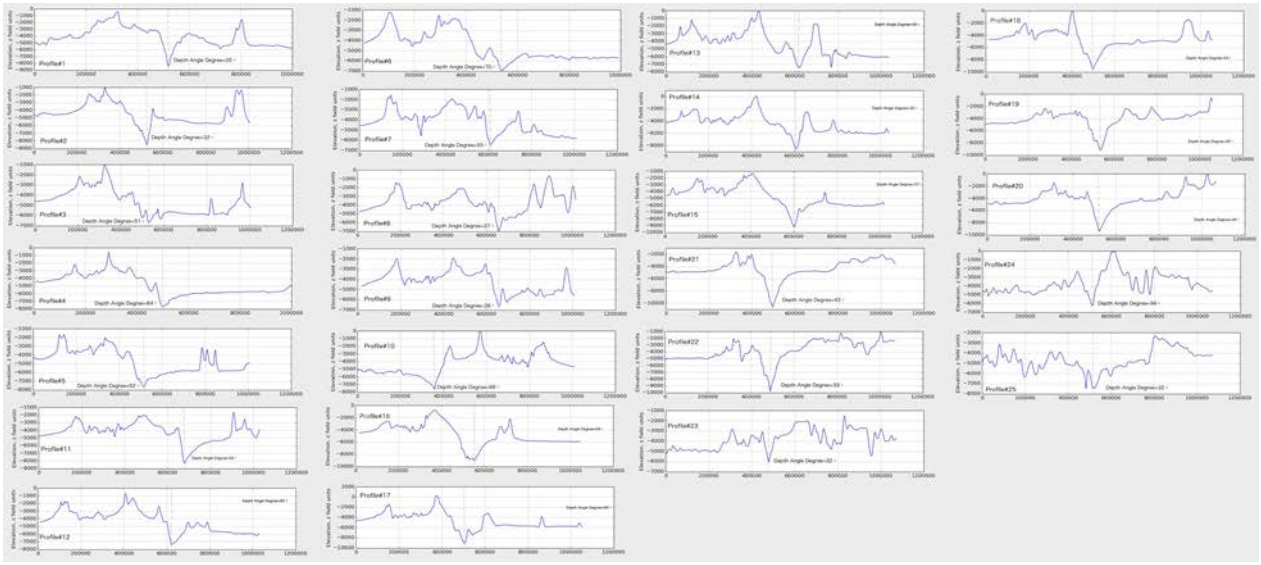

**Figure 3.** *25 cross-sectioning profiles transecting Marian*

a Trench in perpendicular direction.
The advantages of the Matplotlib library of Python for geographic studies consists in its versatility and capability of creating a variety of plots. Seaborn package is build atop the Matplotlib. It combines the power of the Matplotlib with more intuitive approach for data visualization.

After all necessary libraries were installed, the statistical analysis was performed using previously made geographic dataset on the Mariana Trench. Importing data using table with variables was done using Pandas library, installed in the previous step. The data were stored and transformed in the .csv file format. The table was received from the QGIS project containing vector layers and attribute tables. The Pandas ability to read-in, manipulate and write data to and from csv file is a key feature enabling effective data analysis. Three data frames are data type for storing tabular 2D data in Pandas. Using read_csv() function the files were read into Pandas DataFrames.

### *2.3. Using Python Pandas library for logical queries for geospatial analysis in data frame*

A Pandas library of Python was used for manipulations with geological data: loading from the csv table, viewing and editing its content, analysing data range and structure, selecting target rows and columns, automatization of the data processing, manipulation and inquiries, examining the descriptive statistics on data. Therefore, the start of this project initialized with the loading an existing geospatial data set into Pandas environment.

First, the csv file was imported into Pandas Data Frame using command: df = pd.read_csv("Tab-Bathy.csv"). The table for the bathymetry had 517 rows and 18 columns. Second, the data were analysed using logical queries by Pandas. Selecting necessary columns or rows and their attributes in Pandas is relatively straightforward. Thus, using 'iloc' and 'loc' as operations for retrieving data from data frames, necessary columns were selected for modelling by logical selections. For example, X = df.iloc[ : , 1:13] was done to select 12 first columns in the Bathymetry table. Alternative syntax would be (for the case of 4 columns) X = df.iloc[ : , [1, 2, 3, 4]] for smaller data sets where the number of columns can be defined manually. Similarly, selecting necessary row during the data analysis was done using loc[] function, e.g. B = df.loc[12] returned the bathymetric observation nr. 13 (starting from 0). For instance, selecting the slope classes fir geomorphic analysis across the trench was done using following Python code:

```
very_steep = data['slope_class'] == 10,
extreme = data['slope_class'] == 9,
strong = data['slope_class'] == 8,
```

which returns a boolean expression of True/False for all 25 profiles.

Selecting a particular profile and corresponding geologic columns for this profile was done using following code snippet (example of profile nr. 15):

```
profile_15 = data. loc[data['profile'] == 15, ['sedim_thick', 'slope_angle', 'igneous_volc']]
```

Analysing geological data set was done through logical queries by Pandas. E.g. to find maximal depths, or to find a profile that has the thickest layer of sediments is done by the code lines:

```
# What is the maximal bathymetric depth? data['Min'].min()
    [Out 3]: 10.600 m.
# What is the maximal sediment thickness?
    data['sedim_thick'].max() [Out 3]: 142
# What is the maximal slope angle steepness?
    data['slope_angle'].max()
```

[Out 3]: 70
Other examples of the logical queries:
# How many bathymetric data['plate_pacif'].value_counts() observations are there for each tectonic plate?
# How many data belong to each of the slope class? data['slope_class'].value_counts()
# Summary displaying statistics for the selected variable: Mariana Plate data['sedim_thick'].describe()
This returns a descriptive statistics on the column of sediment thickness (Name: sedim_thick, dtype: float64)
# Splitting data into groups ba variables was done using groupby():
data.groupby(['slope_class']).groups.keys()
[Out 4]: dict_keys([6, 7, 8, 9, 10]) # that is, 5 slope classes of the geomorphic steepness.
# Analysing how many profiles have specific slope steepness using groupby(): data.groupby('slope_class', as_index=False)[['profile']].sum() # produces Pandas DataFrame
Similar logical queries are possible through Pandas environment. All scripting was done on Jupyter Notebook. The tables were examined to correctly process columns and rows. Thus, a df.shape function was used to know the number of rows and columns; df.ndim – to check up the dimension of the array; df.head() and df.tail() for analysis of the first and last rows in the data frame. The types of each column were checked using '.dtypes' function.

### *2.4. Partial least squares regression analysis*

Partial least squares regression analysis was performed in Python library StatsModels to estimate the relationships between two factors of the data set: slope gradient angle steepness as independent variable and sediment thickness as dependent variable, by four tectonic plates. The results are presented as a facetted plot on Fig. 4. Geological materials deposited during transit downward the slope is presented by a mixture of rock and sediment derived from the abyssal plain [29]. Therefore, as can be seen from the Fig. 4, the slope gradient and sediment thickness have certain correlation of the observed and predicted values. Moreover, the dependences between the shape of the profiles varies due to the effects from the external factors and location of the segment on one of the four tectonic plates: Mariana, Caroline, Pacific and Philippine Sea.

### *2.5. Ordinary Least Square (OLS) by Python*

The Ordinary Least Square (OLS) method of the statistical analysis aims at estimating the unknown parameters in a linear regression model [30]. It produced (Fig. 5) the best possible coefficient estimating that the model satisfies the OLS assumptions for the linear regression.

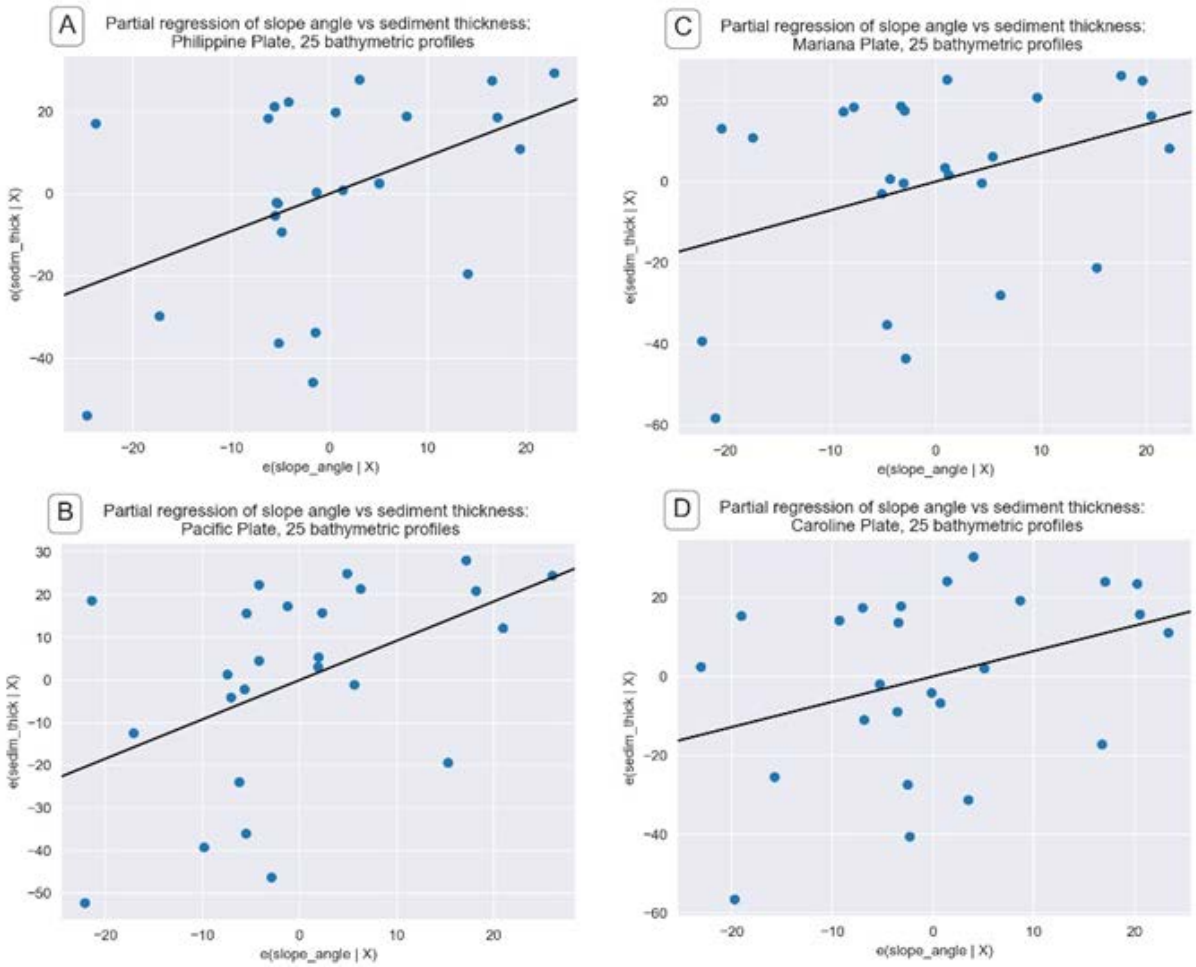


**Figure 4.** *Partial regression analysis for the slope gradient of the profiles by tectonic plates*.

The calculation of the OLS minimizes the sum of the squares of the differences between the observed and predicted variables in the dataset on Mariana Trench geomorphology. The predicted values are given by a plot visualizing linear partial regression analysis of a set of explanatory variables, presented as bathymetric profiles and their depths (Fig. 4). The Fig. 5 shows a screenshot of the OLS's execution and results by Python's StatsModels library.

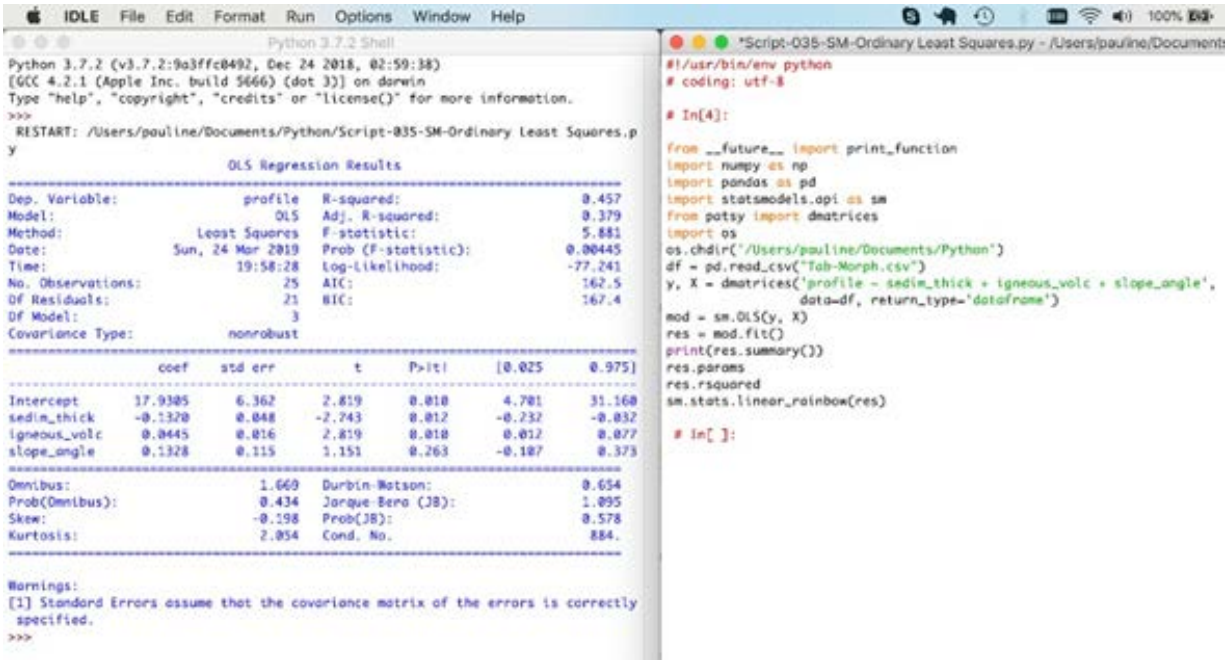


**Figure 5.** *Ordinary Least Square calculation by Python library StatsModel, for the Mariana Trench project on the geomorphic analysis of the profiles*.

### *2.6. Violin plots for descriptive statistical analysis of the bathymetry*

The 'violin' plots illustrated on Fig. 6 represent statistical analysis of the bathymetric data by profiles. The name 'violin' plots is derived due to the visual similarity of the plot to the music instrument. The violin plot illustrates statistical values for each profile: markers indicating median, interquartile range box plot, rotated smoothed probability Kernel Density Plot (KDE) on each side (curved shape on each profile) of the bathymetric data at different profiles (Fig. 6).

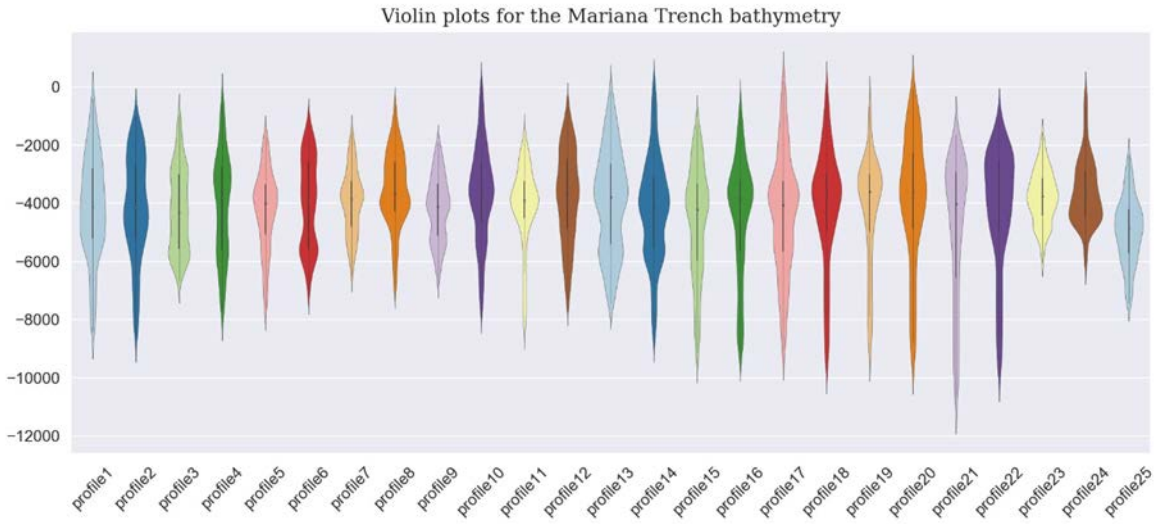


**Figure 6**. *Statistics on the bathymetry by violin plots: median, KDE, means of the profiles*

### *2.7. Bar plots: ranges of the bathymetric depths*

The data distribution are presented on Fig. 7, made by Python library Matplotlib. By profiles, they ranged from -10.600m (maximal depth in this data set) to -3150m (the shallowest point in the data set). The maximum depths in the profiles were found in profiles Nr. 20, 21, 19, 14 (Fig. 7, right, sorted bathymetry), and the minimal depths (i.e. the shallowest) consist the first group, that is profiles 24, 23, 22 and 10 (Fig.

7, right, sorted bathymetry). The deepest part of the trench is located in the south-west and central segments where the trench crosses Philippine and Pacific Plates. The moderate depths correlate with Mariana Plate and the majority of the Philippine Plate. The depths ranges detected across the profiles of the present study are also higher in the southern part of the trench than in northern one (Fig. 7). In general, the central part of the Mariana Trench has variations in depth. However, the general trend shows the increased depths towards the southern part were the depths are higher than in the northern segments. By comparing the profiles Nr. 3, 4, 9, 12 from the Pandas array (Fig. 7, coloured green) with profiles Nr. 18, 16, 15, 13 (coloured orange on Fig. 7), it is clear that depths increase reaching their maximal values in the following group (Profiles Nr. 20, 21, 19, 14, group coloured blue, Fig. 7, right).

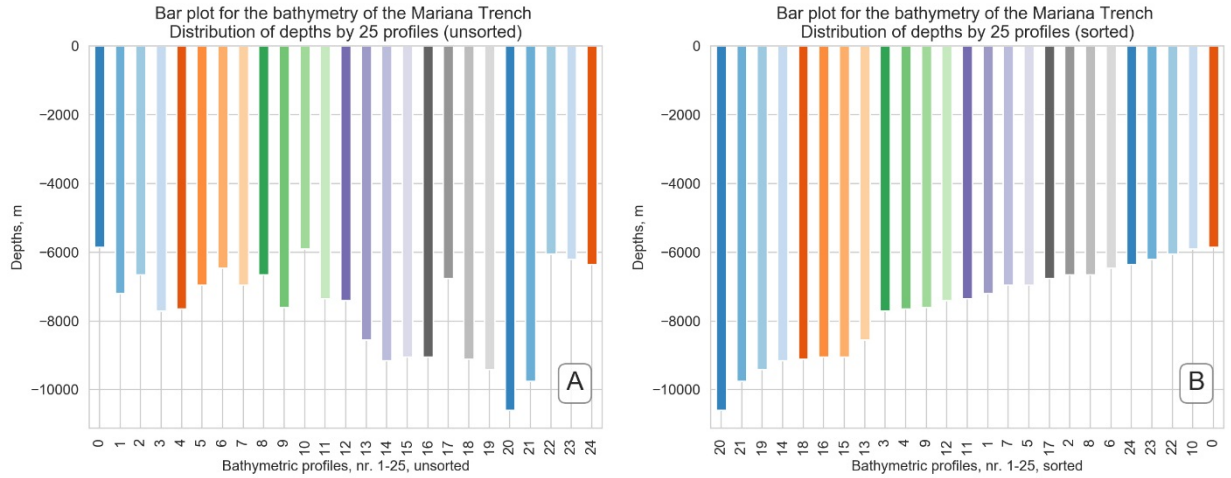


**Figure 7**. *Data distribution analysis: ranges of the maximal depths. Python library: Matplotlib*

*2.8. Isotonic Regression by Python's library StatsModels*

The statistical method of the isotonic regression (Fig. 8) was applied as a non-metric multidimensional scaling aimed at fitting a line to a sequence of the observations. The conditions are that the line has variation in forms, non-decreasing and non-increasing across the samples and the line lies most close to the observations pool. The concept of the isotonic regression was introduced by [31] and further developed by [32]. The principle of the computation algorithm of the isotonic regression lies in the following formula (1) of the problem of quadratic program (QP):

$$min \sum wi*(xi-ai)2 \; subject{:}xi \leq xj \; forall(i,j) \in E \qquad (1)$$

where, *x(i)* and *x(j)* are constraints; *E* are the edges or the is the set of pairs (i, j) for each constraint; *w* is a weights vector; *n* is a number of observations. The isotonic estimator, *g* minimizes the weighted least squares-like condition (2):

$$ming \in A \sum wi*(g(xi)-f(xi))2 \qquad (2)$$

where, A is the set of all piecewise linear, non-decreasing continuous functions; f is a known function. Further references on isotonic regression and its applications are given by [33]. The presented plot of the isotonic regression (Fig. 8) shows a non-decreasing approximation of the function while minimizing the mean squared error on the bathymetric data set. The benefit of this kind of a model applied for the Mariana Trench analysis consists in the flexibility of the model: the function does not assume any form for the target function, i.e. linearity. Thus, the real data of the observed bathymetric profiles can be compared with the isotonic curves (Fig. 8). Further references are given by [34].

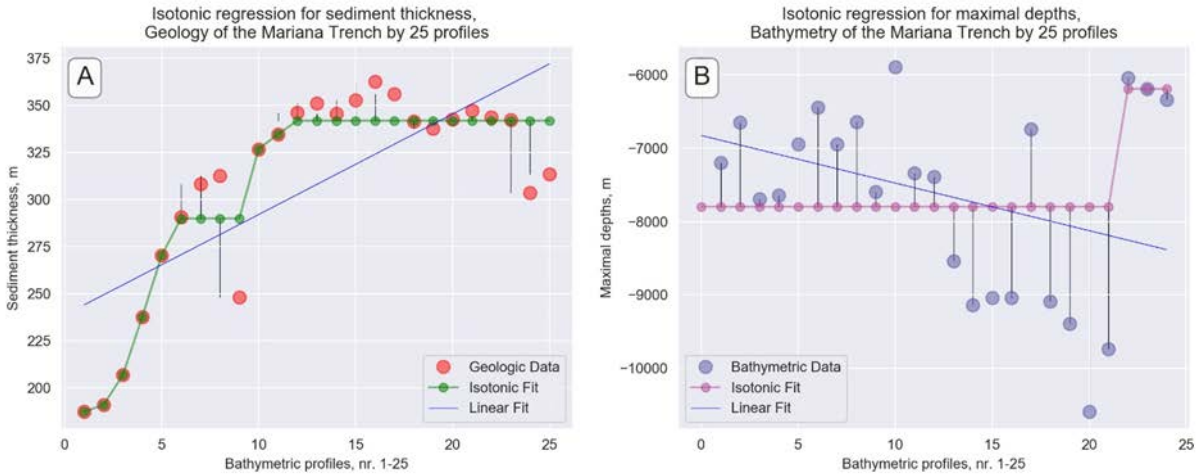


**Figure 8**. *Isotonic regression for the selected variables: geological data on sediment thickness layer (A) and maximal depths recorded by 25 profiles (B). Python library: StatsModels.*

### *2.9. Data distribution analysis by Python's libraries Bokeh and Matplotlib*

Now we can have a more detailed look on the profiles' shape and outline (Fig. 9). While Fig. 7 shows maximal depths by profiles (i.e. each profile has only one dot point on the plot), Fig. 9 illustrates the cross-section profiles by 518 samples in each profile using a 'stepwise' visualization.

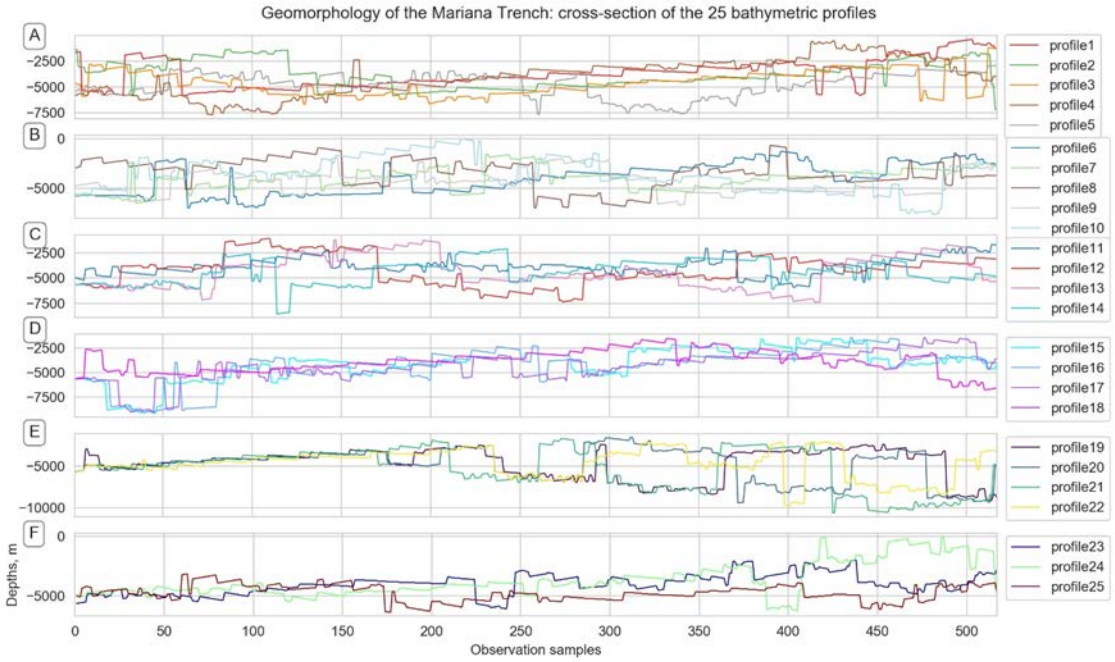


**Figure 9.** *Visualization of the cross-section profiles, Mariana Trench*

A jitter plot (Fig. 10) plotted using Python library Bokeh is visualizing overlapped samples by profiles. It shows concentration of the most frequent, repeated depths by profiles. Comparing to the Fig. 7 and Fig. 9 focused on the data range, Fig. 10 shows analysis of frequency.

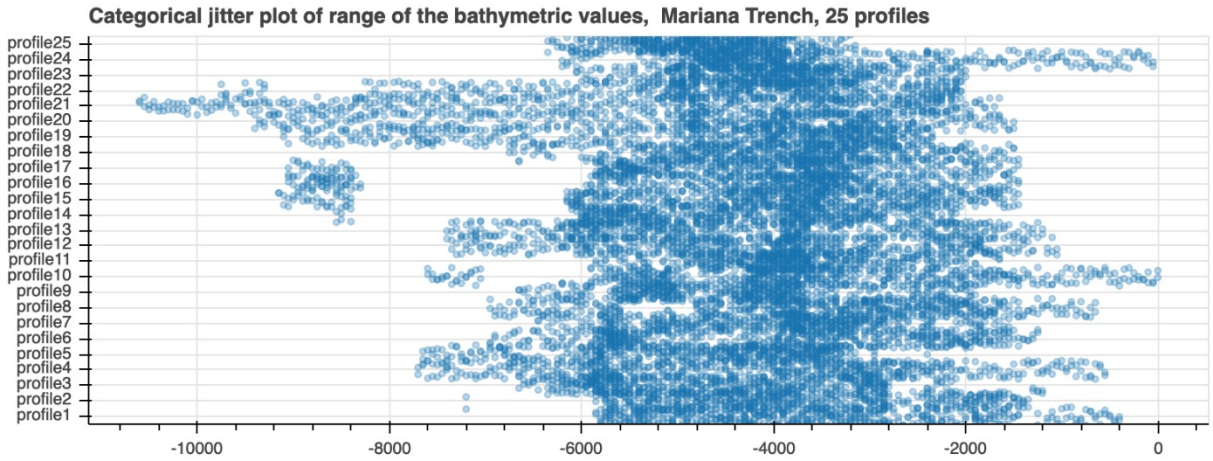


**Figure 10**. *Data distribution analysis: ranges of the maximal depths. Python library: Bokeh*.

Here we can see (Fig. 10) that the most deep values are notable for the profiles 21 and 22 (upper left part of the graph), where the deepest place on the Earth is located: the Challenger Deep. In general, the graph shows distribution of the bathymetric data by the cross-section profiles.

*2.10. Circular bar plots for sorting data*

If we want to have more detailed insight into the bathymetry and geologic settings of the geospatial data set, we can extend other functions of spatial analysis embedded in R plotting. Hence, the variations in the sediment thickness by profiles were studied, in addition to the slope degree by four tectonic plates that Mariana Trench crosses: Mariana, Caroline, Pacific, Philippine Sea [35] .To enable multiple comparisons of the variables, existing methodology [36, 37] was used to analyse the distribution of the observation points across these plates (Fig. 11). The least points are located on the Caroline Plate, south-western part of the trench (cyan coloured lines on the Fig. 11). The most dense distribution of the samples is observed on Mariana Plate (purple colour, Fig. 11) and Philippine Sea Plates (magenta colour, Fig. 11). As for Pacific Plate, there is a absence of the samples on the central part of the trench between the profiles Nr. 15 to 19 where the trench has a curvature (Fig. 2).

Ranking geologic data has a step in geomorphic analysis where the levels of the slope degree are determined by the geospatial impact. Therefore, geomorphic variations typically necessitate an additional sub-task of the geological analysis of the study area. For example, if a certain segment of the trench is located near the active volcanic area the sedimentation rates may increase significantly in this particular region. A {tidyverse} R package, was used to visualize a circular plot showing the comparative analysis of the bathymetric ranged by the sediment thickness. The algorithms and syntax of R coding was applied from the R manuals and available materials. Variations in the slope gradient steepness in the Mariana Trench subduction system are caused by various factors, among which sediment dispersal: longitudinal transport of sediments along the trench and transverse transport into the forearc basins. As a result of these physical processes, Mariana Trench formed as the most significant elongate depressions on the Earth seafloor with a deepest place detected in the Challenger Deep [38].

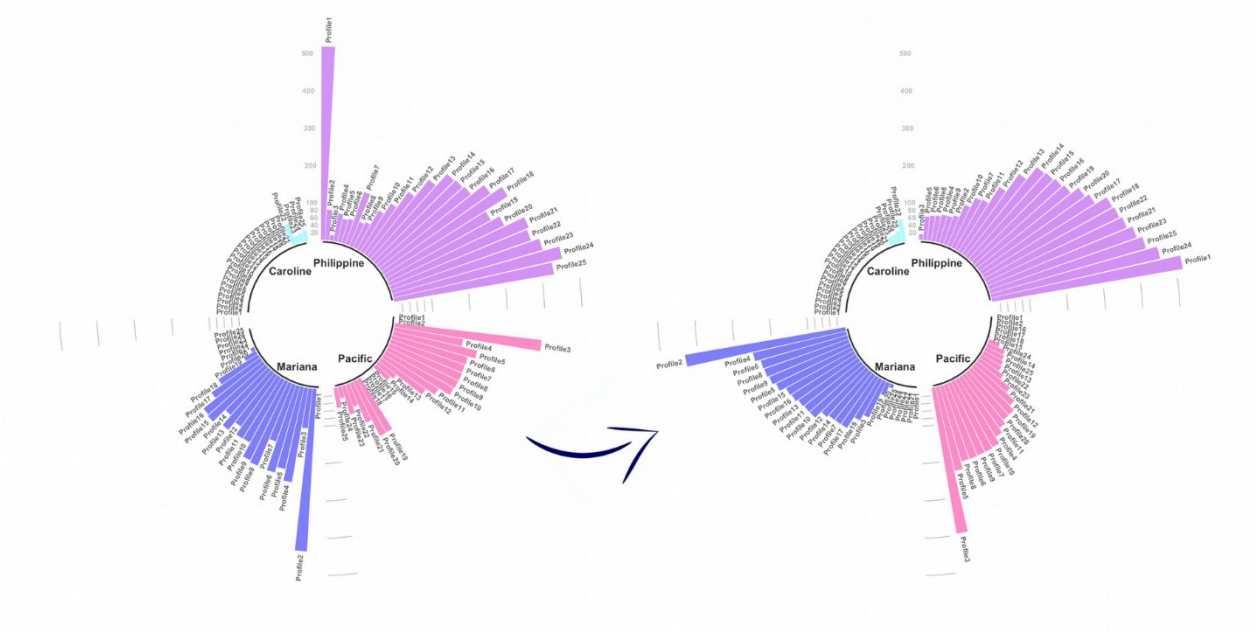


**Figure 11**. *Unsorted (left) and sorted (right) distribution of the profiles according to the sediment thickness, circular plot by tidyverse library, R.*

*2.11. Euler-Venn diagrams for visualizing overlapping of attributes and factors*

The Euler-Venn diagram shows four cases where overlapping in values or concepts can be visualized. The Fig. 12, subplot A shows cumulative total sediment thickness by tectonic plates. The subplot B shows detected igneous volcanic spots. Subplot C shows slope degree and D shows methodological overlay showing the approaches of this work: GIS data mapping and digitizing, geological analysis and Python and R programming languages.

## 3. Results

Python and R based data analysis presented in this research resulted in following findings. Among various shapes of the profiles (Fig. 9) the section of profiles 19, 20, 21 and 22 (Fig. 9, E) had initially uniform shape of the geomorphology that decreased abruptly after the samples 200. The unevenness of the profiles can be explained by the changes geologic conditions and transfer to the neighbour tectonic plate (from the Philippine to the Pacific Plate, and from Mariana to the Philippine Plate). Fig. 9 and 10 illustrate comparison of the data distribution by profiles, made by Python libraries Bokeh and Matplotlib.

The groups of profiles 23, 24 and 25, (Fig. 9, F) have similar geomorphic shapes: the first part of the profiles is relatively even while the southern part is notable for the increased depths. This analyses can be drawn from Fig. 9. The profiles are coloured with the shared X axis for better visualization. The increase of depths by profiles can be influenced by multiple factors: geographic location and subducting tectonic plates, geologic settings, sedimentation, etc. The geomorphic shapes in the seafloor of the Mariana Trench subduction system vary by four tectonic plates: Mariana, Caroline, Pacific and the Philippine Sea. The Caroline Plate has the least sampling points due to the location in the south-west of the trench. The majority of the samples are located on the Mariana and the Philippine Sea, followed by the moderate number on the Pacific Plate.

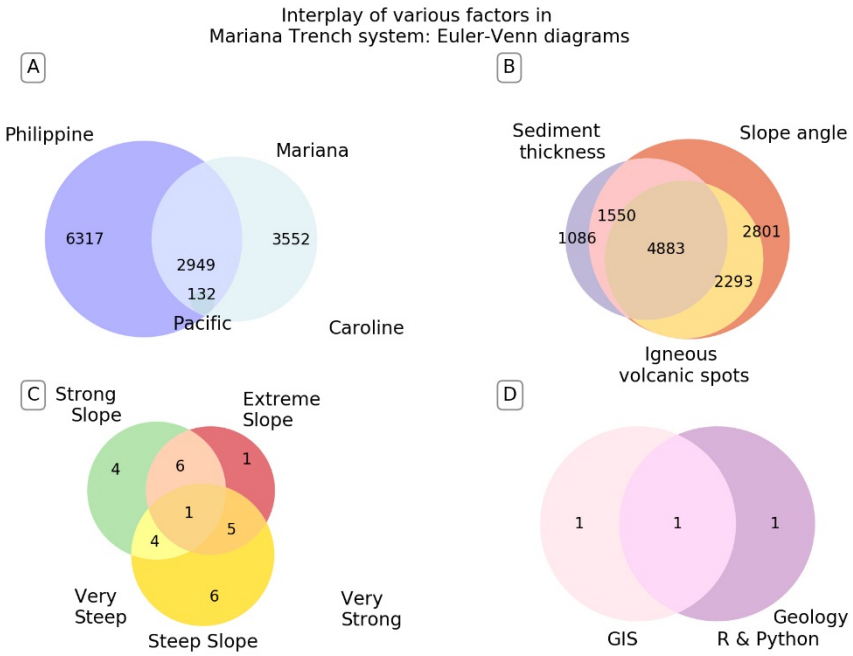


**Figure 12**. *Modelling intersection and correlation by various factors in the project Mariana Trench by Euler-Venn diagrams. A): Bathymetric observations by plates, cumulative computing; B): Sediment thickness, slope degree and closeness of the volcanic spots; C): Subdivision of the slope steepness by classes; D): Methodological approaches*.

The following results are received on sediment thickness based on the data modelling, Fig. 11. The profiles Nr. 1, 24, 25, 23 are notable for the high sediment thickness on the Philippine Plate, profiles Nr. 2, 4, 6, 8 have the highest values for the Mariana Trench, profiles Nr. 3, 5, 8, 6 have the highest values of the sediment thickness for the Pacific Plate, etc. As can be seen from the Fig. 8, the profiles located on the Caroline plate have the least values, since this part of the trench has only a few bathymetric points from the sample pool that cross the Caroline Plate. This can be explained by the fact that sediment thickness is indirectly impacted by the variations in slope degree that creates conditions for the sediment accumulation.

The methodological goal of this research was to identify variations of the steepness in various segments of the trench. The slope steepness degrees and depths were analysed and determined using statistical analysis by libraries of Python and R programming languages. The results revealed that the most steep part of the trench is located in its south-west, north-west and central segments (profiles Nr. 3, 7, 9, 23, 24) where trench crosses Philippine and Pacific tectonic plates. This segment of the trench can be characterised by the largest local depths and sharp abrupt changes in the geomorphic shape. The highest depth gradient can be seen at the profile Nr. 21 is at the distance of 10.600 m from the seal level. The middle moderate slope degrees (Profiles Nr. 1, 11, 4, 5, 10) correlate with the areas where the trench crosses Mariana Plate. These geomorphic segments have relatively balanced bathymetric elevations records ranging from -7.600 m (profile Nr. 11), -7.750 m (profile Nr. 4), -7.800 m (profile Nr. 5), -7.750 m (profile Nr. 10), to -6.200 m (profile Nr. 1). The modelled depths are shown in on Fig. 5 (jitter plot showing depths ranges).

Finally, the profiles with the least slope degree Nr. 21, 22, 18, 20 are mostly located in the southern segments where trench crosses Caroline Plate. Mostly, the depth values of deeper than -9600 m below the sea level prevails on the bathymetric model for the deepest depth range (Fig. 5), representing the depths of the very steep slopes of the Mariana Trench. Correlation between the geomorphic shape with geologic settings and geographic location revealed that submarine geomorphology of the Mariana Trench is generally influenced by the geospatial settings of the underlying tectonic plates. They affect its shape and cause variation of the steepness across the trench segments. The variation of the shape form is affected by the location of the trench crescent.

## 4. Recommendations

As a recommendation for the future similar research, it can be noted that it is necessary to select statistical methods the most suitable to the modelling type: data ranking, data distribution (e.g. box plots or 'violin' plots, linear regression or isotonic regression), correlation matrix or correlogram ellipses, etc. Differences in modelling geomorphological variation may result from the application of various methods and algorithms

or different approaches proposed by selected libraries of programming languages (R, Python or Octave), software, e.g., Gretl [39] or SPSS [40]. To achieve the optimal results, it is crucial to follow methodological principles, select correct statistical algorithms for better data visualisation.

Modelling submarine geomorphology can be done using various approaches: by the deepest values (i.e. each profile can have only one dot point), by showing the full profile line in its length, by circular plots, bar plot, dot plots, as demonstrated. The extra- or interpolation of the depths may possibly increase random errors due to the complex nature of the physical landscapes. It can be either the effects of the environmental factors over the structure of the profile (e.g. tectonic slab movement affecting the shape of the trench segment) or mathematical approaches of the selected algorithm for depths approximation. For better quality of the data set, the profiles should be taken at equal lengths and equal distance in between each two. The whole length of the trench should be covered by the profiles. In difficult segments (e.g., where trench crosses several tectonic plates), is is possible to do more dense digitizing. However, in this case it would be reasonable to enlarge the scale of this particular area as a separate fragment.

## 5. Discussion

Slope gradients are of particular interest for the geomorphological and bathymetric modelling. Slopes of the Mariana Trench are formed by twofold interconnected factors: primary slopes and decreasing slopes caused by the erosion and modification of the first ones. The submarine erosion of the slopes is triggered by the sediment failures and active erosion caused by gravity flows. Factors affecting slope morphology are diverse. Geological factors, such as rock composition, structure, permeability and erodibility of the slope materials (rock) that controls the detachability of the materials from the slope by a set of physical processes. Other factors include inner features of rocks and sediments structure: degree of consolidation, cohesiveness, grain size and geometry (angularity or roundness). As demonstrated in the research, a set of the slopes by 25 cross-sectioning profiles illustrates the shape formed as a results of the internal structure and external processes of the sediment transport and submarine erosion. Various geospatial factors cause formation of the slopes in Mariana Trench, and cause changes in gradient. A complex pattern of the erosional moats and depositions of the sediment drifts along the profiles cause varieties in the profile shapes (Fig. 3).

Submarine erosion has origin in sediment failures and gravity flows by the water streams, erosional processes causing formation of the submarine canyon valleys [41, 42]. However, it should be noted that submarine geomorphology and bathymetric landforms along the trench may in turn affect hydrological processes by accelerating currents. Other factors that contribute to the formation of the slopes and slightly affect variations in their gradient: benthos, tectonics faults and plates [43], volcanic activities [44], contribution from the alluvial submarine fans, etc. Mariana Trench is a large subduction zone with depths exceeding 11 km. In these areas, cross-sections of the trench illustrate a complex association of the processes of subduction and the deposition of the deep-water sediments. The sediment that fill up the trench area are derived mainly from the volcanic arcs and basins, being transported by the transverse canyons [45].

Understanding such a complex set of processes and dynamics of the submarine geomorphology prerequisite an interdisciplinary approach. Therefore, besides the general geological knowledge and a set of data, quantitative numerical modelling of the processes is a requirement for the correct modelling. Existing papers report questions of the geomorphic analysis, bathymetric and environmental mapping [46, 47, 48]. The advantage of using machine learning approach lies is the increase precision of the results, free from the subjective errors.

Current research shown Python and R based statistical modelling of the complex geological processes that include several variables aimed at processing data sets for submarine geomorphic modelling. Prognosis of the geological processes is possible by means of R and Python based data analysis and plotting. Their libraries are based on the existing statistical and mathematical methods of data processing [49, 50, 51]. Using numerical methods by R and Python libraries, current study indicated geomorphic variations of the profiles affected by geologic and tectonic factors. The study demonstrated effective usage of the statistical methods and advantages of the multi-disciplinary implementation of the IT methods in marine geology.

## 6. Conclusion

Since rapid development of the programming and machine learning in the last 20 years, some papers reported using Python and R. Testing functionality of various packages, algorithms and modelling methods of these languages, these works have challenged data science and brought fresh ideas in methodology of geosciences. However, insufficient attention was done so far to the statistical data processing by Python and R specifically in marine geology. Some research examples demonstrate application of the traditional GIS methods and mapping for spatial environmental analysis [52, 53]. In marine geology, despite obvious importance of the linkage between the GIS analysis and Python and R statistical libraries, enough case studies are not yet available. This paper contributed in this field by connecting scripting based data analysis with geospatial modelling. Technical application of Python and R statistical libraries enabled successful for modelling of the geomorphic variations of the hadal trench. The study contributed towards methodological development

of the applied statistical analysis by Python and R in marine geology.

**Acknowledgement**

This research was funded by the China Scholarship Council (CSC), State Oceanic Administration (SOA), Marine Scholarship of China, Grant Nr. 2016SOA002, People's Republic of China.

**References**

[1]. Jamieson A.J., Fujii T., Mayor D.J., Solan M., Priede, I. G. "Hadal trenches: the ecology of the deepest places on Earth", Trends in Ecology and Evolution, 25 (3), (2009), 190-197.
doi: 10.1016/j.tree.2009.09.009

[2]. Lemenkova P. "Factor Analysis by R Programming to Assess Variability Among Environmental Determinants of the Mariana Trench", Turkish Journal of Maritime and Marine Sciences, 4, (2018), 146–155.
doi: 10.6084/m9.figshare.7358207

[3]. Lemenkova P. "R scripting libraries for comparative analysis of the correlation methods to identify factors affecting Mariana Trench formation", Journal of Marine Technology and Environment, 2, (2018), 35-42.
doi: 10.6084/m9.figshare.7434167

[4]. Duineveld G. "Activity and composition of the benthic fauna in the Whittard Canyon and the adjacent continental slope (NE Atlantic)", Oceanologica Acta, 24, (2001), 69–83.

[5]. McCullagh P. Slopes, in: FitzGerald, B.P. (ed.), Modern Concepts in Geomorphology, (1988).

[6]. Ritter D.F., Kochel C.R., Miller J.R. Process Geomorphology (3rd Edition): Wm. C. Brown Publishers, Dubuque, IA, (2002), 544.

[7]. Chorley R.J., Schumm S.A., Sugden D.E. Geomorphology. London: Methuen and Co. Ltd. (1984).

[8]. Summerfield M.A. Global Geomorphology. New York: John Wiley and Sons, (1991).

[9]. Easterbrook D.J. Surface Processes and Landforms: Macmillan Pub. Co., (1993).

[10]. Bloom A. Geomorphology, A systematic analysis of Late Cenozoic landforms, 3rd ed. Prentice Hall, Upper Saddle River, N.J., (1998).

[11]. Harris P. T., Macmillan-Lawler M., Rupp J., Baker E.K. Geomorphology of the oceans. Marine Geology, 352, (2014), 4–24.

[12]. Wilson M.F.J., O'Connell,B., Brown,C., Guinan,J.C., Grehan A.J. "Multiscale terrain analysis of multibeam bathymetry data for habitat mapping on the continental slope", Marine Geodesy 30, (2007), 3–35.

[13]. Lemenkova P. "Hierarchical Cluster Analysis by R language for Pattern Recognition in the Bathymetric Data Frame: a Case Study of the Mariana Trench, Pacific Ocean. Virtual Simulation, Prototyping and Industrial Design". Proceedings of the 5th Int'l Sci.-Pract. Conference, 2(5), (2018), Ed. M. N. Krasnyansky, Tambov: TSTU Press, 147–152.
doi: 10.6084/m9.figshare.7531550

[14]. Pickering K.T., Hiscott R.N. Deep marine systems: processes, deposits, environments, tectonics and sedimentation. Wiley, Chichester, (2015).

[15]. Wu S., Takahashi N., Tokuyama H., Wong H.K. "Geomorphology, sedimentary processes and development of the Zenisu deep-sea channel, northern Philippine Sea", Geo-Marine Letters, 25(4), (2005), 230-240.
doi: 10.1007/s00367-005-0210-9

[16]. Lemenkova P. "An Empirical Study of R Applications for Data Analysis in Marine Geology", Marine Science and Technology Bulletin, 8(1), (2019), 1-9.
doi: 10.33714/masteb.486678

[17]. Okada H. "Anatomy of trench-slope basins: examples from the Nankai trough", Palaeogeography, Palaeoclimatology, Palaeoecology, 71 (1-2), (1989), 3-13.
doi: 10.1016/0031-0182(89)90026-6

[18]. Yu H.S. "Geological characteristics and distribution of submarine physiographic features in the Taiwan region", Marine Georesources and Geotechnology, 21 (3-4), (2003), 139–153.
doi: 10.1080/ 713773391

[19]. VanderPlas, J. Python Data Science Handbook. Essential Tools for Working with Data. O'Reilly, (2016).

[20]. McKinney W. PyData Development Team. Pandas: powerful Python data analysis toolkit Release 0.24.0. [Online] http://www.python.org [Accessed: 10 April 2019].

[21]. Lemenkova P. "Processing oceanographic data by Python libraries NumPy, SciPy and Pandas", Aquatic Research, 2, (2019), 73-91.
doi: 10.3153/AR19009

[22]. Duchesnay E., Löfstedt T. Statistics and Machine Learning in Python Release 0.2, 2019. [Online] http://www.python.org [Accessed: 10 April 2019].

[23]. R Development Core Team. R: A Language and Environment for Statistical Computing. R Foundation

for Statistical Computing. Vienna, Austria, (2014). http://www.R-project.org [Accessed: 13 March. 2019].

[24]. Lemenkova P. "K-means Clustering in R Libraries {cluster} and {factoextra} for Grouping Oceanographic Data", International Journal of Informatics and Applied Mathematics, 2(1), (2019), 1-26.
doi: 10.6084/m9.figshare.9891203

[25]. Rossum, G. van. Python Programming Language, 2011. https://www.python.org/ [Accessed: 10 April 2019].

[26]. Rossetier D.G. Tutorial: An example of statistical data analysis using the R environment for statistical computing, (2017).

[27]. NumPy community. NumPy Reference. Release 1.16.1, (2019), https://www.python.org/ [Accessed: 10 April 2019].

[28]. Lemenkova P. "Testing Linear Regressions by StatsModel Library of Python for Oceanological Data Interpretation", Aquatic Sciences and Engineering, 34, (2019), 51–60.
doi: 10.26650/ASE2019547010

[29]. Crozier M. Slope Evolution, in Goudie, A.S., ed., Encyclopedia of Geomorphology, Volume 2, Routledge, New York, NY, (2004).

[30]. Savage L.J. The Foundations of Statistics, 2nd revised ed., Dover, New Yor, (1972).

[31]. Kruskal J.B. "Nonmetric Multidimensional Scaling: A numerical method", Psychometrika, 29 (2), (1964), 115–129.
doi:10.1007/BF02289694

[32]. Best M.J. Chakravarti N. "Active set algorithms for isotonic regression; a unifying framework", Mathematical Programming, 47 (1–3), (1990), 425–439.
doi:10.1007/BF01580873

[33]. Wu W.B., Woodroofe M., Mentz G. "Isotonic regression: Another look at the changepoint problem", Biometrika, 88 (3), (2001), 793–804.
doi:10.1093/biomet/88.3.793

[34]. Leeuw J. de Hornik K., Mair P. "Isotone Optimization in R: Pool-Adjacent-Violators Algorithm (PAVA) and Active Set Methods", Journal of Statistical Software, 32 (5), (2009), 1–24.
doi:10.18637/jss.v032.i05.

[35]. Lemenkova P. Scatterplot Matrices of the Geomorphic Structure of the Mariana Trench at Four Tectonic Plates (Pacific, Philippine, Mariana and Caroline): a Geostatistical Analysis by R. In: Problems of Tectonics of Continents and Oceans. Proceedings of the 51st Tectonics Meeting, Ed. Degtyarev, K. E. (1) RAS Institute of Geology. Moscow: GEOS, (2019), 347–352.
doi: 10.6084/m9.figshare.7699787.v1

[36]. Bretz F., Hothorn T. aWestfall P. Multiple Comparisons Using R. Taylor and Francis Group, LLC. (2011).

[37]. Lemenkova P. "Statistical Analysis of the Mariana Trench Geomorphology Using R Programming Language", Geodesy and Cartography, 45(2), (2019), 57–84.
doi: 10.3846/gac.2019.3785

[38]. Gardner J.V., Armstrong A.A., Calder B.R. Beaudoin J. So. "How Deep Is the Mariana Trench?", Marine Geodesy, 37, (2014), 1-13,
doi: 10.1080/01490419.2013.837849

[39]. Lemenkova P. "Regression Models by Gretl and R Statistical Packages for Data Analysis in Marine Geology", International Journal of Environmental Trends, 3(1), (2019), 39–59.
doi: 10.6084/m9.figshare.8313362.v1

[40]. Lemenkova P. "Numerical Data Modelling and Classification in Marine Geology by the SPSS Statistics", International Journal of Engineering Technologies, 5(2), (2019), 90–99.
doi: 10.6084/m9.figshare.8796941

[41]. Covault J.A., Fildani A., Romans B.W., McHargue T. "The natural range of submarine canyon-and-channel longitudinal profiles", Geosphere, 7, (2011), 313–332.
doi:10.1130/GES00610.1

[42]. Clark M.J., Small R.J. Slopes and weathering: Cambridge University Press, Cambridge, England, (1982).

[43]. Jones O.P., Simons R.R., Jones E.J.W., Harris J.M. "Influence of seabed slope and Coriolis effects on the development of sandbanks near headlands", Journal of Geophysical Research, 111, (2006), 1–23.
doi: 10.1029/2005JC002944

[44]. Dadson S., Hovius N., Pegg S., Dade W.B., Horng M.J., Chen H. "Hyperpycnal river flows from an active mountain belt", Journal of Geophysical Research Earth Surface, 110 (F4), (2005).
doi: 10.1029/2004JF000244

[45]. Karig D.E., Sharman G.F. "Subduction and accretion in trenches", Geological Society of America Bulletin, 86 (3), (1975), 377–389.

[46]. Mayer L. Introduction to Quantitative Geomorphology: Prentice Hall, Englewood Cliffs, NJ, (1990).

[47]. Lemenkova P., Promper C., Glade T. Economic Assessment of Landslide Risk for the Waidhofen a.d. Ybbs Region, Alpine Foreland, Lower Austria. In E. Eberhardt, C. Froese, A. K. Turner, & S. Leroueil (Eds.), Protecting society through improved understanding, (2012), 279-285.
doi: 10.6084/m9.figshare.7434230

[48]. Schenke H.W., Lemenkova P. “Zur Frage der Meeresboden-Kartographie: Die Nutzung von AutoTrace Digitizer für die Vektorisierung der Bathymetrischen Daten in der Petschora-See”, Hydrographische Nachrichten, 25(81), (2008), 16–21. doi: 10.6084/m9.figshare.7435538.v2

[49]. Myers J.L. Well A.D. Research Design and Statistical Analysis. Ed. 2, Lawrence Erlbaum, U.S., (2003).

[50]. Cowan G. Statistical Data Analysis. Oxford Science Publications. Clarendon Press, Oxford, UK, (1998).

[51]. Brownlee K.A. Statistical theory and methodology in science and engineering. 2nd ed., New York: John Wiley & Sons, (1965).

[52]. Klaučo M., Gregorová B., Stankov U., Marković,V., Lemenkova P. “Determination of ecological significance based on geostatistical assessment: a case study from the Slovak Natura 2000 protected area”, Central European Journal of Geosciences, 5(1), (2013), 28-42. doi: 10.2478/s13533-012-0120-0

[53]. Suetova I.A., Ushakova L.A., Lemenkova P. Geoinformation mapping of the Barents and Pechora Seas. Geography and Natural.

MANAS Journal of Engineering
ISSN 1694-7398 | e-ISSN 1694-7398

*Volume 7 (Issue 2) (2019) Pages 114-120*

# Accelerating renewable energy generation over industry 4.0

Hasan Huseyin Coban

Ardahan University, Engineering Faculty, Department of Electrical Engineering, 75000. Ardahan, Turkey,
huseyincoban@ardahan.edu.tr, ORCID: 0000-0002-5284-0568

**ABSTRACT**

The "Industry 4.0" (the fourth industrial revolution) is recognized as a new industrial step in which horizontal and vertical manufacturing progress combination and product connectivity may supply benefit producers to achieve higher technical achievement. However, especially in developing countries; limited information is known about how industries could meet the implementation possibilities of the Industry 4.0 associated technologies to achieve industrial production and performance.

This paper briefly reviews and describes industry 4.0 and environment for modernization. The paper also discusses what are the current objections met by companies especially energy generator companies according to hydropower plant operators' experiments. The paper offers an approach from strategic planning to operational level for the implementation of industry 4.0 for all manufacturers especially the energy sector. Also new opportunities, applications and scenarios examined by introducing the technologies and tools for Industry 4.0. Finally, it referred a conclusion and brief look of the future work.

**ARTICLE INFO**

***Research article***

*Received: 19.07.2019*
*Accepted:15.10.2019*

***Keywords:***
*IoT,*
*Industry 4.0,*
*hydropower,*
*renewable energy,*
*sensors*

## 1. Introduction

The Industrial Revolution is one of the most famed and revered milestones in human history [1]. They are mostly accompanied not only by technical and scientific innovations but also by the essential aspects involved in the Industrial Revolution were technological, cultural and socioeconomic [2].

In order to explicate the theory and perception of technological revolution, initially, we need to define the notion of technology. It represents a set of technological knowledge about how to conceive, produce, use and even commercialize goods or services or their elements; or in the accomplishment of objectives, such as scientific investigation, as well as any possible aggregation of these operations [2]. Industrial Revolutions, basically, is a period in which machines bring meaningful developments to the people's way of life particularly in the manufacturing environment [3]. As history provides [4].

The first Industrial Revolution launched in the 18$^{th}$ century when agricultural communities became more modern, technical and urban. The first mechanical revolution occurred in the middle of the 19$^{th}$ century and was accompanied by a process of economic growth as a result of the industrialization of North America and Europe [2,5].

Industry 2.0 also known as the Technological Revolution began from the end of the nineteenth century continued up to the 1980s [6]. It was the period when industrial products started to increase both in variety and volume. Major technological innovations included the transcontinental railroad, the cotton gin, electricity, mechanical devices, cars, and other inventions permanently changed society. Industry 2.0 products are still effective today [7].

Industry 3.0 began in the 1980s and also known as the Digital Revolution. It is characterized by technological innovations such as the change from analog to digital, which had considerable influence, especially on the electronics industry [8]. By this revolution; production of automation had increased, people empowered to "higher-level jobs" – i.e. programming and automotive industry had use of robotics. The demand for goods during Industry 3.0 increased to three dimensions which are volume, variety and delivery time [7].

Organizations that want to be ahead of the global competition in the world of the future have to achieve with smart robots that will work in production and distribution processes, research and development, sales marketing and management processes to be used with artificial intelligence systems. Nowadays the world is witnessing the 4th technological

revolution; namely Industry 4.0. Fig. 1 shows main transformation areas in the world.

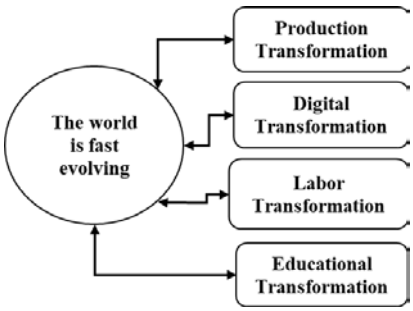


**Figure 1**. *Fast-evolving world*

Many different definitions exist for Industry 4.0 by companies and various groups according to their wishes and understanding. The main idea of industry 4.0 demonstrates how complex production processes can be optimized using new Technologies. A formal definition of industry 4.0 is defined in [9] as follows: It is understood as a new industrial stage with technology innovations such as manufacturing operations systems and information and communication technologies (ICT) – especially rapid developments in the fields of the Internet of Things (IoT), Big Data, robotics, blockchain technology, sensors, artificial intelligence, augmented reality and rapid prototyping technologies. We define Industry 4.0 as a revolution enabled by the application of advanced technologies (like IT) at the manufacturing level to bring new values and services for customers and the organization itself. Many aspects of Industry 4.0 are undefined, undiscovered and uncertain, such as the demand dimensions of customers and the future product architecture of electricity generation and electric vehicles [7]. If we Google "fourth Industrial Revolution," that's somewhat synonymous with industry 4.0. The idea is after the digital age, the computer age, what we've got now is a collision of the digital and physical ages. We have Internet of Things devices. We have data analytics, machine learning, artificial intelligence, and all of those are changing the relationship, we have to each other and to the machines around us, both the physical machines and the ethereal machines, like cloud computing systems. So industry 4.0 is one in which standard manufacturing, standard production of goods is being superseded by the idea that you can use digital technologies to change the whole dynamics and calculus of manufacturing. And 3D printing is actually a very good example of that. The industrial revolutions are depicted in Fig 2.

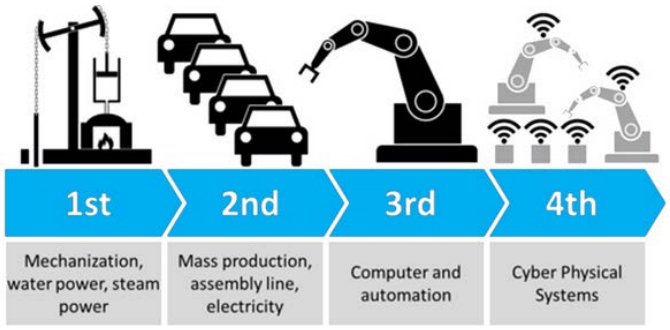


**Figure 2**. *Stages of industrial revolution [10]*

## 2. Importance of industry 4.0

While 4th technological revolution has been developing at a dizzying pace in recent years, the public is divided into 'worries' and 'hopefuls'. So, what kind of future will artificial intelligence offer us? How does the world use these technologies? The world and Turkey, at which point the Industry 4.0 fields? The most curious question for academics, professionals, and entrepreneurs is: whether the machines can think? The British mathematician Alan Turing, who introduced this question for the first time in 1650, had not imagined the point reached today [11].

But today computers can beat the chess champion. Or in the quiz, it can make a slam to its competitors. Thousands of years of the strategy game can defeat the champion in “Go”. They can even quickly move and open the doors. But sometimes they can make mistakes. Just like the “Robot Mini Ada”, which had an accident in the past days in Konya City, Turkey.

Industry 4.0 has been developing at a swift pace in recent years. Because artificial intelligence is fed by data, and there is much more data than before. It is made by imitating human movements and behaviors by software and algorithms. When it comes to this revolution, many people think of robots that we are familiar with from movies. But in fact, we use them in almost every aspect of our daily lives.

Robotics and automation systems provide the muscle for Industry 4.0, cameras and other sensors provide the senses, and connectivity and data are its central nervous system. But in the background, the real brains of this industrial revolution is Artificial Intelligence [12, 13]. When we use each search engine, we also benefit from artificial intelligence. Or we use artificial intelligence again when using virtual assistants on smartphones. For example, artificial intelligence algorithms for diagnosing disease from medical images work very well.

For example, this artificial intelligence technology used in the IOWA university clinic in the United States can identify and prevent the corals from sugar diseases [14]. This area is becoming increasingly popular, and the countries are interested in it [15].

Countries that make the most investment in artificial intelligence in the world at the beginning of the United States and China is coming [16]. The same two countries lead the academic publications [17].

Many countries have announced their national artificial intelligence strategies. The first was explaining Canada and followed by China [18]. For example, China said it aimed to be the world's largest artificial intelligence force by 2030 [19]. It focuses on a number of issues, most notably the funds allocated to artificial intelligence studies. After that, the important thing is that people who develop artificial intelligence technologies.

In Turkey, many institutions producing national artificial intelligence projects. One of them is Turkcell [20]. The company is preparing to market the first virtual assistant in Turkey. There are also artificial intelligence entrepreneurs. Sercan Esen, a 28-year-old from the private sector, who spent 4 years working on his own project, is one of them. The two young entrepreneurs developed the award-winning project namely “intenseye” in Istanbul Technical University.

Performing a first time in Turkey with this artificial intelligence video recording applications, gender and emotion analysis can be done. It can also use magazines to do customer analysis. Or in the contact and transportation points for smart cities, airports, metros can use this solution. For example, in the production facilities, businesses can analyze the emotions of their employees. When working with a tool; they understand how intense and stressful you are and can intervene and prevent accidents. Civil-society organizations are also doing all works for widespread use of artificial intelligence in Turkey. “Deep Learning Turkey” is one of them, bringing together professionals, academics and entrepreneurs. They have a lot of members in the community, and they share information with each other, and they do projects together. In summary; Turkey is closely following the work of artificial intelligence. So what's the next step?

In fact, in general, like every developing country, Turkey also needs an artificial intelligence strategy as a nation in order for these studies to come together and to provide them with more benefits.

What kind of future will artificial intelligence offer us? There is no doubt that it will enter many areas of our lives. How can we do many things that exist in our daily lives when electricity is found, how we can do it? That's exactly what countries need to do right now. How can we do even the most complex things in our daily life with artificial intelligence? Applying artificial intelligence to everyday life. Machines can be part of our daily life. According to some, there is nothing to fear, but the number of those who are concerned is not small. For example, in the state of Arizona, on March 13, 2018, the fact that Uber's driverless vehicle caused the death of a pedestrian opened the door to a new debate [21]. Nowadays the scenarios that robots take control are also very popular. There are different views about how artificial intelligence will transform the world.

-The development of artificial intelligence can lead to the end of humanity. (Stephen Hawking) [22,23]

-We can use artificial intelligence to create heaven or hell. That still depends on us. (Yuval Noah Harari) [24]

-There will be very, very little work that Robots cannot do better than people. (Elon Musk) [25]

According to the US-based Mckinsey consulting firm, by 2030 robots could leave 800 million unemployed. Automatic cash registers, driverless cars, robot security guards are already starting to enter our lives [26].

We be aware or not; we have an industrial revolution. But this does not mean that systems are created to completely replace people. The aim should not create systems that replace human beings with artificial intelligence algorithms, but create the capabilities of people, the characteristics of people and the systems that develop and integrate. Therefore, it shouldn’t be imagined where the environments of only the people work, or the machines work. But we imagine the systems where people and machines can work together, people work where people are good, machine can be used where the machine is good.

What will the manufacturing of tomorrow look like? There is no clear answer to how Industry 4.0 will transform the world. But it is obvious that the transformation has already begun and the energy sector has the chance to be part of it and will be on our agenda for many years. This is not going to be the same likes before. There's going to be a huge change. It's not about the steam that feeds our plants in the first revolution, or dominant mass-production model in the second, or even computerized systems come out of the third revolution that we live today. The basic principle of Industry 4.0 is about automated connectivity which manufacturers worldwide are connecting their machines to the cloud and progressing their owned industrial Internet of Things. It's an opportunity to radically change the way industry impacts the needs of individuals and societies. The advancement of Industry 4.0 will be guided by an intelligent, interdependent and widespread environment, as innovations in production processes and systems are led by earlier industrial revolutions. Those left behind the revolution will feel it keenly for the jobs are today might be dramatically different in the not too distant future. There is still a space for leaders of this new revolution to emerge, but the race has already started. [27]

Industrial parts are becoming smaller. Products get to market with less waste, faster, and on-time. Even the most manual processes are turning towards automation. Innovations in deep learning, machine vision, fuzzy logic, and robotics are

revolutionizing production lines and supply chains. The machines now produce vast amounts of Big Data, accessible via the cloud. As the information and machines, they produce become connected, new cyber-physical systems will glint a modern-day Industrial Revolution. This is Industry 4.0. In the Industry Revolution, machines become smarter and learn from their environments and take corrective actions to optimize production. These machines work without regard to a central controller, collaborating and communicating with other devices. Industry 4.0 facilities produce new organizational intelligence, which expands across facilities. The result: nothing short of total transformation of production lines and business performance. Machine vision will be at the mainline of this new manufacturing paradigm. [28]

The power network is also changing. With the increase of renewable energy generation technologies and drive to make a better demand response, the grid's current environment must change to realize the promise of the IoT.

## 3. Industry 4.0 for energy generation

To meet the need for greater flexibility in hydraulic systems and to maximize overall equipment efficiency, production processes must automatically adapt to changing demand. This requires smart devices that communicate with each other in real-time and a controller platform that serves as a hub for seamless providing two-way communication from the corporate network up to the actuators. Today, important steps have been taken on Industry 4.0 theory in hydraulic applications. The most important of these is to connect the hydraulic equipment to the digital control electronics to process the steps in the software. In addition, all the features of fluid technology have been stored in the form of algorithms in the software.

There are 5 important points for the application of Industry 4.0 in power systems. These are:

- Compatibility of power system components for the current structure of Industry 4.0,
- Easy control of the structure of the power plant and consequently to increase the efficiency of the system,
- It can be controlled from a single point, so that operating costs can be reduced,
- Easy monitoring of plant equipment,
- producing alternative solutions with advanced control applications.

Today's many Central Station controlled power grids operate on update cycles that are as long as 15 minutes. Approximately every 15-minute outage information is updated, and Central Station estimates the power and sets its generators to meet the load. Unlike conventional power from fossil fuels, renewable power sources such as wind turbines or hydropower plant a predictable output at the same time. Fast loads like plugging in electric cars are also hard to predict. If the grid drops below the needed power, it can fail. So; to ensure sufficient power grid operators maintain extra power plant reserves to compensate for these fluctuations. That keeps the lights on, but it wastes fossil fuels. It means the renewables are not lowering the carbon footprint as much as they should. To deliver on the promise of renewable energy, the Industrial Internet Consortium (IIC) started a new initiative named the communication and control testbed for microgrid applications to enable the efficient use of renewable energy resources at a large scale. This is an ambitious goal. But when the expertise and the technology come together, the dream can become a reality [29]. The industrial Internet of things provides a disruptive technology that will change the way the grid operates. Three members of the IIC are lending their expertise to the microgrid communication and control testbed Project. Real-time Innovations (RTI) is providing real-time data bus software. National Instruments is providing the intelligent nodes for edge control in analytics. Cisco is providing network equipment and security expertise. The open FMB project at the smart grid interoperability panel is defining communications data model and services standards. Duke Energy Southern California Edison and CPS Energy will take the architecture through performance and security testing to prepare it for real-world challenges. The goal of the new initiative is to prove the viability of real-time communications and control framework which combines distributed edge located processing and control applications with intelligent analytics. A real-time secure connectivity framework enables machine-to-machine, machine to control center and machine to cloud data connectivity. The framework will run in real-world power applications and interface with operational equipment. At the core of the new smart microgrid, critical infrastructure is a high-speed field data bus that connects devices and intelligent nodes. The data bus also interacts with the Central Station and the cloud taking advantage of both local and remote state to optimize operations. The data bus streamlines the delivery of real-time to analytics to any node on the network edge or cloud. It is based on the data distribution service protocol (DDS).

Things like Uber and Airbnb and things like Pandora or Spotify, which are kind of examples of Industry 4.0. So what about; does Industry 4.0 mean to sort of a power producer? It's kind of that collision between cyber and physical. Maybe a simpler way to put some of this is that smart manufacturing, IOT, Industry 4.0, is all an attempt to help take the information that you generate every day in companies — from electric energy producer processes — take that information and make some value from that information; feed that back into processes, whether it's in terms of supply chain, whether it's in terms of better-improved processes. Being able to model those processes to improve the output, the expectation of a higher-quality product. Be able to lower costs in some way, shape, or

form through lower energy, through lower material use, through reduced scrap. The idea is to take information and make value from that information. The challenge that all of these aggregator companies have is to be able to make sure that anytime hydropower or wind farms change a requirement for one of their parts that these facilities manufacture, that that is appropriately fed through the process, that there are, the plans are appropriately changed. This is a very large problem when you're talking thousands of parts for a generator, turbines, governor, controller, transformers.

Hydropower has played an important part as the critical electricity generation source of renewable energy for over a century. The digitalization of hydropower plants is transforming the way power facility will be operated and maintained in the future. It guarantees to bring substantial values to the renewable energy sector, and it is an industry-wide trend that can positively influence power networks around the world. By 2030 over half of the world's existing hydropower facilities will have undergone, upgrading and modernization, according to International Hydropower Association (IHA) [30].

Machine learning, neural network, cyber-physical systems, data mining, the Internet of Things and the Internet of Services are some of the keywords related to digitalization. It improves performance with intelligent design and common sense and reduces costs by means of save millions in hydropower operation and maintenance costs. The algorithms and models help the companies to analyze and classify the faults or, more precisely, future faults in the facility. The figure shows steps of the data collection for smart operation and maintenance of a power facility.

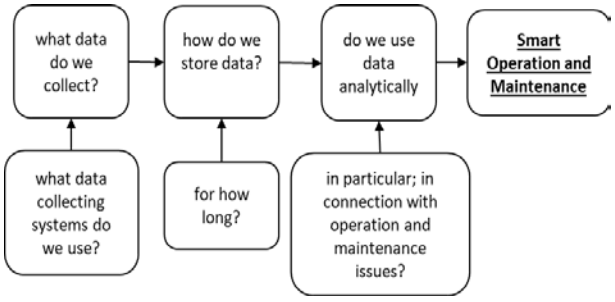


**Figure 3**. *The steps of the data collection*

As shown in Fig. 3; initially, all parts and items of the power plant, whether in the air or underwater, should be digitalized by means of a laser scan and documented regularly on a special data platform.

These stored data will later be connected to algorithms with the existing information and the multiplicity of ongoing measurement values from the facility. In order to get a precisely comprehensive picture of the whole facility, let's start by considering where and how the IoT is becoming enmeshed across the hydropower industry. Even cheap sensors without maintenance overheads are appearing right across the hydropower operational landscape as components of the industrial IoT. Location isn't truly restricted; it can be upstream and downstream, sensors can now transmit continually, for instance, to provide water level in the reservoir, water inflow of data. When the industrial IoT begins to be shaped, the use of sensors in the hydroelectric plant also increases. The sensors can provide a continuous, high-speed data stream to inform the operation personnel of everything from stability to heat generation in turbine bearings.

Nowadays most power plant uses Supervisory Control and Data Acquisition (SCADA) which PLC boards gather data and push it to SCADA systems. However, Industry 4.0 and the growing number of internet-enabled devices in use offers facilities a fantastic opportunity to significantly increase their generation, flexibility and enhanced security with innovative solutions based on the latest technologies. The internet-of-things sensor technology and big data are advancing a new breed of power plants. A smart power plant is one which is data-rich has interconnected systems that enhanced management capabilities for property owners managers and user experience of the space customers. Smart power plants are sometimes referred to as automated plants, intelligent plants or plants that incorporate smart technology. The unit connected system found within a smart power plant work cohesively to deliver accurate and useful data that is used for enhancing operational performance personalized comfort measurable health and well-being outcomes and connected operator experiences largely mobile-phone technology. These power plants operate using integrated communication networks. It connects the systems and shares data for increased visibility and management capability enhanced operational performance and connected place experience.

There are 5 important issues in the application of Industry 4.0 in hydraulic systems. Basically:

1. Developments: The current structure of hydraulic system components is compatible with Industry 4.0,
2. Advantages: To be able to control the hydraulic structure easily in an intelligent system and to increase the system efficiency accordingly,
3. 3.Cost: Since the control from a single point is provided, the reduction in operating costs can be easily obtained,
4. Convenience: Easy monitoring of hydraulic types of equipment,
5. Alternativity: Producing alternative solutions with advanced hydraulic applications.

Major operative advantages of Artificial Intelligence with respect to hydropower facilities include limited to none a priori knowledge of involved physical experience, high level

of flexibility when managing different sets of versions and fluctuations related to discharge energy generation, and quick setup time of the forecast system. Fig. 4 illustrates a smart hydropower control system.

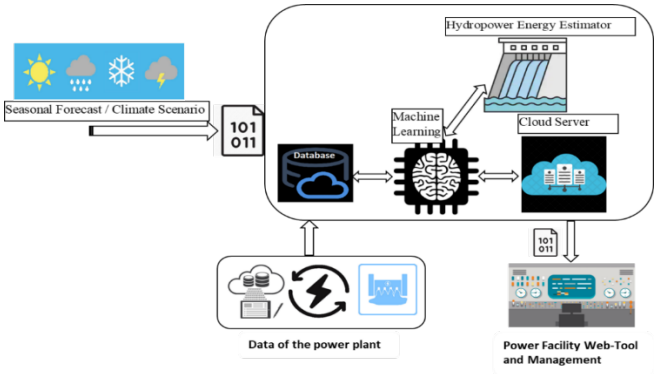


**Figure 4.** *Hydropower plant control system.*

The goal of this control system is to operate and manage the water reservoirs and flow rates in real-time for a continuous stable and optimal electricity production for maximizing the profit, on the global level. The dilemma here is the complex and nonlinear dynamics of hydropower plant control system.

The nonlinear dynamics of hydropower facility system can be classified as follows; firstly, on the powerhouse has its own water turbine, governor, generator, and other electromechanical equipment where any uncontrollable release of hydraulic mass by reason of water hammer can disturb the balance of the system and transfer the oscillations to the electric power grid.

Secondly the system may take time-dependent variable and random inputs such as rainfall or sudden increase or decrease of electricity market prices and water sources, in this case the system's control strategy and the operational input data have to be modified so that the variable water inflow data conditions and the electricity market prices are always utilized for optimal electricity production with negligible water losses and do not exceed the penstocks' operational capacities and reservoirs' level which means water does not run uselessly.

Thirdly it has nonlinear mathematical relationships between water inflow rates and electricity market price, in addition to the relationships between the reservoirs' levels and the consequence of generated powers are also nonlinear. Furthermore, the system has to handle uncertain requires or rejections from the grid where the input data for frequency and power adjustments may always be required.

IoT is complementary to SCADA and Distributed control systems (DCS). The data achieved from SCADA systems acts as one of the data points of supply for IoT. SCADA's target is on control and monitoring, IoT's focus is firmly on analyzing machine data to develop work rate, generation and impact top line. The Global System for Mobile communications (GSM) module or any telemetry system to feedback the community for monitoring.

## 4. Conclusion

As a renewable energy source; hydropower is well-positioned to continue to supply reliable and sustainable energy. In a power facility, the noise is the voice of the machines. The voice tells us how the machines are feeling. Inspection personnel understands the voice of the machine. But who listens to the machines between the inspection rounds? Smart sensors tell us how the machine is feeling. Vibration sensors, sound recorders detect abnormalities by intelligent algorithms and machine learning. Inspectors check if something has happened in the power plant.

The digitization of hydropower plants, control systems, and power grids is an emerging industry trend that promises to optimize asset management and performance. By utilizing digitalization and the correct concepts, the hydropower industry will be able to rationalize its maintenance processes, reduction in costs and expansion of hydropower capabilities. And millions will be saved in maintenance costs! The digitization of hydropower plants, control systems, and power grids is an emerging industry trend that promises to optimize asset management and performance. Industry 4.0 can play a key role in reducing climate change.

In this study, Industry 4.0 design fundamentals, implementing and conceptual approaches as an electric energy producer in power plant analysis are given. Nowadays nations and industry companies collaborate to gain new technology with energy generation and aggregator companies. The most important reason is to use skilled sensors and to contribute actively to the power plants. Therefore, the components of power facilities should be linked to Industry 4.0 concepts is very important in terms of being able to adapt to smart, cheap operation and maintenance.

**Acknowledgement**

I would like to extend great appreciation to the academic staff of the Ardahan University Engineering faculty for their help in offering me the resources making this research successful and complete.

## References

[1]. Allen R.C. "Why the industrial revolution was British: commerce, induced invention, and the scientific revolution 1", The Economic History Review, 64(2), (2011), 357-384. doi.org/10.1111/j.1468-0289.2010.00532.x

[2]. Viorel O. Considerations on the Contemporary Revolution in Military Affairs.

[3]. Technological change is coming: The Fourth Industrial Revolution, Labor Market Intelligence Report, TESDA: Technical Education and Skills Development Authority, December 2016

[4]. Peter O., Mbohwa, C. "Correlation between Future Energy Systems and Industrial Revolutions", (2018), 1953-1961.

[5]. Hillstrom K. The Industrial Revolution. Greenhaven Publishing LLC. (2008).

[6]. Mokyr J. "The second industrial revolution, 1870-1914. Storia dell'economia Mondiale", (1998), 219-45.

[7]. Yin Y., Stecke K.E., Li D. "The evolution of production systems from Industry 2.0 through Industry 4.0". International Journal of Production Research, 56(1-2), (2018), 848-861. doi.org/10.1080/00207543.2017.1403664

[8]. Brunet-Thornton R., Martinez F. (Eds.). Analyzing the Impacts of Industry 4.0 in Modern Business Environments. IGI Global. (2018), 42.

[9]. Khan A., Turowski K., "A Preliminary Study on Industry 4.0", Journal of Industrial and Intelligent Information, 4 (3), (2016), 230-234. doi: 10.18178/jiii.4.3.230-234.

[10]. Charlie Ashton, August 16, 2017, Solving Critical Business Challenges for "Industry 4.0"

[11]. Machinery C. "Computing machinery and intelligence-AM Turing", Mind, 59(236), 433. (1950), 433–460.

[12]. Dopico M., Gomez A., De la Fuente D., García N., Rosillo, R., Puche, J. (2016). A vision of industry 4.0 from an artificial intelligence point of view. In Proceedings on the International Conference on Artificial Intelligence (ICAI) (p. 407). The Steering Committee of the World Congress in Computer Science, Computer Engineering and Applied Computing (WorldComp). ISBN: 1-60132-438-3

[13]. Lee J., Davari H., Singh J., Pandhare V. "Industrial Artificial Intelligence for industry 4.0-based manufacturing systems", Manufacturing letters, 18, (2018), 20-23. doi.org/10.1016/j.mfglet.2018.09.002

[14]. Dankwa-Mullan I., Rivo M., Sepulveda M., Park Y., Snowdon, J., Rhee K. (2018). Transforming Diabetes Care Through Artificial Intelligence: The Future Is Here. Population health management. doi.org/10.1089/pop.2018.0129

[15]. Jiang F., Jiang Y., Zhi H., Dong Y., Li H., Ma S, Wang Y. "Artificial intelligence in healthcare: past, present and future", Stroke and vascular neurology, 2(4), (2017), 230-243. doi: 10.1136/svn-2017-000101

[16]. Private Equity Investment in Artificial Intelligence, OECD, December (2018).

[17]. Lucas L., Waters, R. The AI arms race: China and US compete to dominate big data. (2018).

[18]. Tim Dutton, Building an AI World Report on National and Regional AI Strategies. (2018).

[19]. Kewalramani M. China's Quest for AI Leadership: Prospects and Challenges. (2018).

[20]. Dijital yasam Journal 2018 Issue:17, Will Artificial Intelligence save or destroy humanity?

[21]. Griggs T., Wakabayashi D. (2018). How a self-driving Uber killed a pedestrian in Arizona. The New York Times.

[22]. Cellan-Jones R. Stephen Hawking warns artificial intelligence could end mankind. BBC news, 2, (2014).

[23]. Bundy A. Smart machines are not a threat to humanity. Commun. ACM, 60(2), (2017), 40-42.

[24]. Noah H.Y. Homo Deus: A brief history of tomorrow. London: Harvill Secker. (2016).

[25]. Mclay R. Managing the rise of Artificial Intelligence. Retrieved November, 10, (2018).

[26]. Report Mckinsey Co (2017).

[27]. Rüßmann M., Lorenz M., Gerbert P., Waldner M., Justus J., Engel P., Harnisch M. "Industry 4.0: The future of productivity and growth in manufacturing industries", Boston Consulting Group, 9(1), (2015), 54-89.

[28]. Bloch M., Blumberg S., Laartz J. "Delivering large-scale IT projects on time, on budget, and on value", Harvard Business Review, (2012), 2-7.

[29]. Outcomes, Insights, and Best Practices from IIC Testbeds: Microgrid Testbed, IIC Journal of Innovation, September (2017).

[30]. Hydropower operators discuss 'new reality' of digitalization. Posted on 1st October 2018 by IHA communications team.

MANAS Journal of Engineering
ISSN 1694-7398 | e-ISSN 1694-7398

*Volume 7 (Issue 2) (2019) Pages 121-125*

# Finite element analysis of thermal stress of laminated composite plates using Taguchi method

Savaş Evran

Canakkale Onsekiz Mart University, Department of Machine and Metal Technologies, Vocational School of Canakkale Technical Sciences, Canakkale, sevran@comu.edu.tr, ORCID 0000-0002-7512-5997

**ABSTRACT**

In present study, thermal stress behavior of laminated composite plates subjected to constant temperature load was investigated using Taguchi method according to von Mises stress. Numerical thermal stress analyses were conducted based on L8 orthogonal array including four control factors with two levels. Fiber orientation angles of laminates for the plates were used to be control factors. Finite element analysis of the plates was carried out using ANSYS software. Fiber angles with optimum levels and their effects on thermal stress of plates were detected using analysis of signal to noise (S/N) ratio. Level of importance of laminates and percentage effect ratio of each laminate on von Mises stress were determined according to analysis of variance (ANOVA).

**ARTICLE INFO**

***Research article***

*Received: 14.05.2019*
*Accepted:02.11.2019*

***Keywords:***
*Laminated composite,*
*plate,*
*thermal stress,*
*finite element,*
*Taguchi method*

## 1. Introduction

Laminated composite plates can be used in different application areas of engineering. The plates made of laminated composite materials have some superior properties compared to metal and ceramic materials. Therefore the need for these materials is increasing. In addition, the increase in temperature can limits the use characteristics of laminated composite plates. Because of that, thermal stress behavior of these plates is important. Finite element approach was used in some of these analyses [1]. In literature, there are many studies about thermal stress of laminated composite plates. Thangaratnam et al. [2] investigated the thermal stress behavior of plates and shells made from laminated composite. Savoia and Reddy [3] evaluated the thermal behavior of laminated composite plates subjected to thermal load according to three dimensional. Tungikar and Rao [4] reported an exact solution stress of rectangular composite laminate subjected to temperature load according to three dimensional approach. Sayyad et al. [5] analyzed of thermal stress of plates made of laminated composite based on exponential shear deformation approach. Bektas and Sayman [6] presented the analytical approach about elasto-plastic stress of thermoplastic laminated plates under simply supported boundary condition. Sit et al. [7] examined the thermal stress behavior of plates made from laminated composite based on third order shear deformation approach. Wu et al. [8] investigated the thermal stress of plates made from laminates according to actual temperature field. Khdeir and Reddy [9] analyzed the thermal stress and deflection behaviors of plates made from cross-ply laminates according to refined plate methods. Kant and Khare [10] presented a study about finite element approach of thermal stress of composite laminates based on a higher-order technique. Raju and Kumar [11] carried out the thermal behavior of plates made from laminated composite according to higher-order shear deformation approach which having zig-zag function. In this study, von Mises stress analysis of laminated composite plates subjected to temperature load was determined using finite element and Taguchi methods. Numerical analyses were conducted using finite element software ANSYS. Tests were performed using L8 orthogonal array based on Taguchi method. Each laminate groups has two laminates and their fiber orientation angles were assumed to be control parameters.

## 2. Materials and methods

The square laminated composite plate has eight laminates and it were made from graphite/epoxy materials. The material constants were given in Table 1.

**Table 1.** *Material constants [12-14]*

| $E_1$ | $E_2 = E_3$ | $G_{12} = G_{13}$ | $G_{23}$ | $\nu_{12} = \nu_{13}$ | $\nu_{23}$ | $\alpha_1$ | $\alpha_2 = \alpha_3$ |
|---|---|---|---|---|---|---|---|
| 155 GPa | 8.07 GPa | 4.55 GPa | 3.25 GPa | 0.22 | 0.373 | $-0.07 \times 10^{-6}\,^0C^{-1}$ | $30.1 \times 10^{-6}\,^0C^{-1}$ |

The planar dimension of plates made of laminated composite and thickness of each laminate were determined to be 150 mm and 0.125 mm [12] respectively. Thermal stress analysis of laminated composite plates were conducted using L8 orthogonal array based on Taguchi method. The orthogonal array consists of four control factors with two levels. Fiber orientation angles of composite laminates were considered to be control factors and each control factor was assumed to be two laminates. Eight analyses were performed numerically and statically. The control parameters with different levels were tabled in Table 2.

**Table 2.** *Control factors with different levels*

| Control Factors | Symbol | Unit | Levels | |
|---|---|---|---|---|
| First Two Laminates | A | Degree | 0 | 10 |
| Second Two Laminates | B | Degree | 20 | 30 |
| Third Two Laminates | C | Degree | 40 | 50 |
| Fourth Two Laminates | D | Degree | 60 | 70 |

In order to obtain the optimum levels of fiber orientation angles of each laminate groups according to the maximum thermal stress for von Mises stress, "higher is better" quality characteristic was used. Analysis of S/N ratio was carried out using Minitab R15 [15] statistical software. The quality characteristic was given in Equation 1 [16].

$$(S/N)_{HB} \text{ for } \sigma_T = -10.\log\left(n^{-1}\sum_{i=1}^{n}(y_i^2)^{-1}\right) \qquad (1)$$

According to Equation 1, n is determined to be the number of thermal stress analyses based on a trial and yi was used to be ith data analyzed.

## 3. Numerical approach

Finite element thermal stress analysis of laminated composite plates was analyzed using finite element software ANSYS [17]. Thermal stress results were determined for maximum data according to von Mises stress. Right and left edges of plates were assumed to be clamped boundary conditions whereas top and bottom edges of plates were considered to be free boundary conditions. Fiber orientation angles with 0 in degree were employed in x axis direction. Laminated composite plates were subjected to constant temperature load with $\Delta T = 70\ ^0C$ on surface area of the plates. Problem dimensionality was determined as three dimensional. Degrees of freedom was studied to be UX, UY, UZ, ROTX, ROTY, and ROTZ. Globally assembled matrix was taken to be symmetric. In finite element analyses, SHELL 281 element type [18] in modelling of plates was used. This element type includes eight nodes which having six degree of freedom according to each node: translations based on the x, y, and z axes, and rotations for the x, y, and z-axes [18]. The laminated composite plates with clamped-clamped boundary conditions of right and left edges and SHELL 281 geometry [18] were shown in fig. 1.

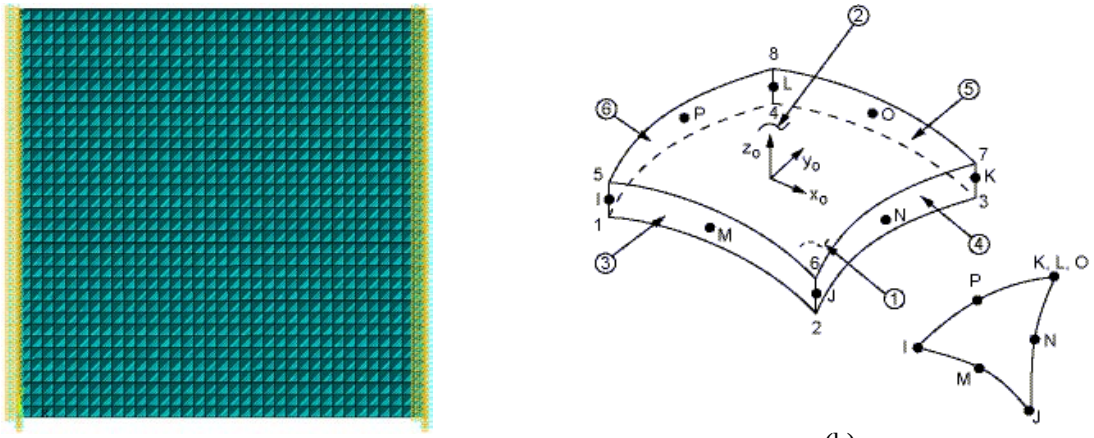


(a) (b)

**Figure 1.** *a) laminated composite plates and b) SHELL281 geometry [18]*

## 4. Results and discussions

Numerical thermal stress behavior of laminated composite plates was conducted using finite element software ANSYS according to Taguchi's L8 orthogonal array. Finite element results for thermal stress and their data for signal to noise ratio were given in Table 3.

**Table 3.** *Finite element and S/N ratio results*

| Test | Designation | Control Factors | | | | Results | |
|---|---|---|---|---|---|---|---|
| | | A | B | C | D | Von Mises Stress $\sigma_T$ (MPa) | S/N Ratios $\eta$ (dB) |
| 1 | $A_1B_1C_1D_1$ | 0 | 20 | 40 | 60 | 310.873 | 49.8517 |
| 2 | $A_1B_1C_2D_2$ | 0 | 20 | 50 | 70 | 354.209 | 50.9852 |
| 3 | $A_1B_2C_1D_2$ | 0 | 30 | 40 | 70 | 320.124 | 50.1064 |
| 4 | $A_1B_2C_2D_1$ | 0 | 30 | 50 | 60 | 305.509 | 49.7005 |
| 5 | $A_2B_1C_1D_2$ | 10 | 20 | 40 | 70 | 405.287 | 52.1553 |
| 6 | $A_2B_1C_2D_1$ | 10 | 20 | 50 | 60 | 392.913 | 51.8859 |
| 7 | $A_2B_2C_1D_1$ | 10 | 30 | 40 | 60 | 358.235 | 51.0834 |
| 8 | $A_2B_2C_2D_2$ | 10 | 30 | 50 | 70 | 404.968 | 52.1484 |
| Overall Mean ($\overline{T_{\sigma_T}}$) | | | | | | 356.5148 | - |

### 4.1. Effect of Fiber Angles

In order to analyze of effect of fiber orientation angles of composite laminates on thermal stress, average results of each control factor for each level based on numerical and S/N ratio values of thermal stress were calculated. The average results for numerical and S/N ratio were tabulated in Table4.

**Table 4.** *Response Table for S/N ratio and thermal stress*

| Level | S/N ratios in dB | | | | Means in MPa | | | |
|---|---|---|---|---|---|---|---|---|
| | A | B | C | D | A | B | C | D |
| 1 | 50.16 | 51.22 | 50.8 | 50.63 | 322.7 | 365.8 | 348.6 | 341.9 |
| 2 | 51.82 | 50.76 | 51.18 | 51.35 | 390.4 | 347.2 | 364.4 | 371.1 |
| Delta | 1.66 | 0.46 | 0.38 | 0.72 | 67.7 | 18.6 | 15.8 | 29.3 |
| Rank | 1 | 3 | 4 | 2 | 1 | 3 | 4 | 2 |

According to Table 4, the control factors with the optimum levels were found to be A with second level, B with first level, C with second level, and D with second level. In order to see the effects of fiber orientation angles on the thermal stress, average results of S/N ratio for each levels of control factors were used. The average results were plotted in Fig. 2. It can be seen from Figure 2 that the increase of fiber orientation angles for the first two laminates, the third two laminates, and the fourth two laminates causes the increase of thermal stress of laminates composite plates. However, the increase of the fiber angles of the second two laminates provides the decrease of thermal stress of laminated composite plates.

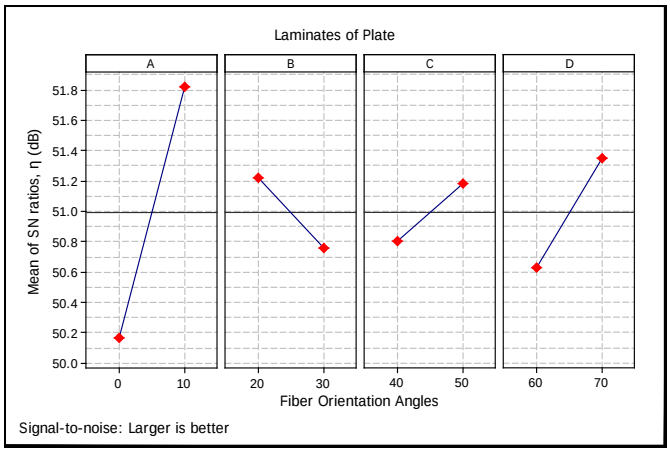


**Figure 2.** *Effect of fiber orientation angles*

### 4.2. Analysis of Variance

Laminated composite plates were designed to be eight laminates and fiber orientation angle of each two laminates was assumed to be control factor. In order to examine significance level and contribution ratio the fiber orientation angles of laminates of the plates, analysis of variance (ANOVA) was employed at 95 % confidence level using finite element results for thermal stress based on von Mises stress. The ANOVA result for R-Sq = 99.95 %, and R-Sq(adj) = 99.88 % was shown in Table 5.

**Table 5.** *ANOVA result*

| Source | DF | Seq SS | Adj SS | Adj MS | F | P | % Effect |
|---|---|---|---|---|---|---|---|
| A | 1 | 9159 | 9159 | 9159.0 | 4151.88 | 0.000 | 75.89 |
| B | 1 | 692.8 | 692.8 | 692.8 | 314.04 | 0.000 | 5.74 |
| C | 1 | 497.4 | 497.4 | 497.4 | 225.47 | 0.001 | 4.12 |
| D | 1 | 1712.8 | 1712.8 | 1712.8 | 776.44 | 0.000 | 14.19 |
| Error | 3 | 6.6 | 6.6 | 2.2 | | | 0.06 |
| Total | 7 | 12068.6 | | | | | 100 |
| S = 1.48526, R-Sq = 99.95 %, and R-Sq(adj) = 99.87 % | | | | | | | |

As can be seen from ANOVA result, the most effective laminates groups on the thermal stress were obtained to be A with 75.89 % effect, D with 14.19 % effect, B with 5.74 % effect, and C with 4.12 effect, respectively. Each laminate groups was found to be the significance control parameter because P value was smaller than 0.05 data.

### 4.3. Estimation of Optimum Thermal Stress

The optimum result of thermal stress of laminated composite plates for the maximum value based on von Mises stress was only predicted considering the influence of the significant control factors. The optimum value of thermal stress was obtained using A with second level, B with first level, C with second level, and D with second level. The estimated mean of

thermal stress of laminated composite plates can be calculated using Equation 2 [16].

$$\mu_{\sigma_T} = \overline{A_2} + \overline{B_1} + \overline{C_2} + \overline{D_2} - 3\overline{T_{\sigma_T}} \quad (2)$$

where, $\overline{A_2}$ = 390.4, $\overline{C_2}$ = 364.4, and $\overline{D_2}$ = 371.1 are average data of numerical thermal stress at the second levels of laminate groups such as A, C, and D. These average values were taken from Table 4. In addition, $\overline{B_1}$ = 365.8 is average result of numerical thermal stress at the first level of laminate groups such as B. ($\overline{T_{\sigma_T}}$) = 356.5148 is overall mean according to L8 orthogonal array and this result was taken from Table 3. Substituting these values of different terms in Equation 2, $\mu_{\sigma_T}$ is calculated to be 422.156 MPa. 95 % confidence intervals of confirmation numerical thermal stress behavior and population were solved by using Equation 3 and Equation 4 [16] respectively.

$$CI_{CA} = \left(F_{\alpha;1;n_2} V_{error} \left[\frac{1}{n_{eff}} + \frac{1}{R}\right]\right)^{1/2} \quad (3)$$

$$CI_{POP} = \left(\frac{F_{\alpha;1;n_2} V_{error}}{n_{eff}}\right)^{1/2} \quad (4)$$

$$n_{eff} = \frac{N}{(1 + T_{DOF})} \quad (5)$$

where, $\alpha = 0.05$ is determined as risk and $n_2 = 3$ is analyzed as the error data for the degree of freedom in ANOVA. $F_{0.05;1;3}$ is employed as 10.13 [16] for F ratio table at 95 % CI. $V_{error}$ is investigated to be the error result of variance based on ANOVA data and it is found to be 2.2 value. R is achieved as the sample size of confirmation analyses of numerical thermal stress and it is studied to be 1. N represents the total number of analyses of numerical thermal stress and it was evaluated to be 8 depending on Taguchi's L8 orthogonal array. $T_{DOF}$ is analyzed as the total number of degrees of freedom according to the important control parameters and it was conducted to be 4. $n_{eff}$ was solved to be 1.6 value so $CI_{CA}$ and $CI_{POP}$ were solved to be ± 6.018 and ± 3.732 respectively. The estimated confidence interval according to confirmation analyses for finite element thermal stress [16] is:

$$\text{Mean } \mu_{\sigma_T} - CI_{CA} < \mu_{\sigma_T} < CI_{CA} + \text{Mean } \mu_{\sigma_T}$$

The population depending on the 95 % confidence interval [16] is:

$$\text{Mean } \mu_{\sigma_T} - CI_{POP} < \mu_{\sigma_T} < CI_{POP} + \text{Mean } \mu_{\sigma_T}$$

The estimated and finite element optimal results depending on predicted confidence intervals were tabulated in Table 6.

**Table 6.** *Optimal results for numerical and estimated data*

| Designation | Numerical Result | Predictive Result | Estimated Confidence Intervals for 95% Confidence Level |
|---|---|---|---|
| $A_2B_1C_2D_2$ | 423.301 MPa | 422.156 MPa | $416.138 < \mu_{\sigma_T} < 428.174$ for $CI_{CA}$ |
| | | | $418.424 < \mu_{\sigma_T} < 425.888$ for $CI_{POP}$ |

## 5. Conclusion

In this study, von Mises stress of laminated composite plates subjected to constant temperature load was investigated by using finite element software ANSYS and Taguchi method. Fiber orientation angles of laminates of the plates were designed based on L8 orthogonal array consisting of four control factors with two levels. The optimal fiber angles and their effects were investigated using analysis of signal to noise ratio. ANOVA was used in order to analyze the significant laminate groups of composite plates and their percentage effects on the thermal stress. The following conclusions were drawn for this numerical and statistical study:

- Stress based on von Mises was found to be 356.5148 MPa according to L8 orthogonal array.
- Thee increase of fiber orientation angles for the first two laminates, the third two laminates, and the fourth two laminates leads to the increase of thermal stress of laminates composite plates whereas the increase of the fiber angles of the second two laminates causes the decrease of thermal stress.
- The optimum laminate groups were determined to be $A_2B_1C_2D_2$ according to Taguchi method.
- According to ANOVA, the most effective laminates groups on the thermal stress were found to be A with 75.89 % effect, D with 14.19 % effect, B with 5.74 % effect, and C with 4.12 effect, respectively.
- All of the laminate groups were determined as significant control parameters since P value in ANOVA was smaller than 0.05 data.
- Estimated confidence intervals for 95% confidence level were carried out to be $416.138 < \mu_{\sigma_T} < 428.174$ for $CI_{CA}$ and $418.424 < \mu_{\sigma_T} < 425.888$ for $CI_{POP}$.
- Numerical and estimated optimum thermal stress results were solved to be 423.301 MPa and 422.156 MPa respectively.

**References**


[1]. Zhang Y.X., Yang C.H., "Recent developments in finite element analysis for laminated composite plates", Composite Structures, 88, (2009), 147-57.

[2]. Thangaratnam R.K, Palaninathan, Ramachandran J. "Thermal stress analysis of laminated composite plates and shells", Computers & Structures, 30, (1988), 1403-11.

[3]. Savoia M, Reddy J.N, "Three-dimensional thermal analysis of laminated composite plates", International Journal of Solids and Structures, 32, (1995), 593-608.

[4]. Tungikar V.B., Rao K.M., "Three dimensional exact solution of thermal stresses in rectangular composite laminate", Composite Structures, 27, (1994), 419-30.

[5]. Sayyad A.S., Ghugal Y.M., Shinde B.M. "Thermal stress analysis of laminated composite plates using exponential shear deformation theory", International Journal of Automotive Composites, 2, (2016), 23-40.

[6]. Bektas N.B., Sayman O., "Thermal Elastic-Plastic Stress Analysis in Simply Supported Thermoplastic Laminated Plates", Journal of Reinforced Plastics and Composites, 21, (2002), 639-52.

[7]. Sit M., Ray C., Biswas D. "Thermal Stress Analysis of Laminated Composite Plates Using Third Order Shear Deformation Theory", New Delhi: Springer India; (2015), 149-56.

[8]. Wu Z., Cheng Y.K., Lo S.H., Chen W. "Thermal stress analysis for laminated plates using actual temperature field", International Journal of Mechanical Sciences, 49, (2007), 1276-88.

[9]. Khdeir A.A., Reddy J.N., "Thermal stresses and deflections of cross-ply laminated plates using refined plate theories", Journal of Thermal Stresses, 14, (1991), 419-38.

[10]. Kant T., Khare R.K., "Finite element thermal stress analysis of composite laminates using a higher-order theory", Journal of Thermal Stresses, 17, (1994), 229-55.

[11]. Raju T.D., Kumar J.S., "Thermal analysis of composite laminated plates using higher-order shear deformation theory with zig-zag function", Int J Sci Emerg Technol, 2, (2011), 53-7.

[12]. Meyers C.A., Hyer M.W., "Thermal Buckling And Postbuckling Of Symmetrically Laminated Composite Plates", Journal of Thermal Stresses, 14, (1991), 519-40.

[13]. Meyers C.A., Hyer M.W., "Thermally-induced, geometrically nonlinear response of symmetrically laminated composite plates", Composites Engineering, 2, (1992), 3-20.

[14]. Averill R.C., Reddy J.N., Thermomechanical Postbuckling Analysis Of Laminated Composite Shells. Proceedings of the 34th AIAA/ASME/ASCE/AHS/ASC Structures, Structural Dynamics and Materials Conference: AIAA-93-1337-CP; (1993), 351-60.

[15]. MINITAB. Software (Minitab Inc State College, PA, USA) (www.minitab.com).

[16]. Ross PJ. Taguchi Techniques for Quality Engineering: McGraw-Hill International Editions, 2nd Edition, New York, USA; (1996).

[17]. ANSYS. Software (ANSYS Inc, Canonsburg, PA, USA) (www.ansys.com).

[18]. ANSYS. Help (Version 13).

Manas Journal of Engineering
ISSN 1694-7398 | e-ISSN 1694-7398

*Volume 7 (Issue 2) (2019) Pages 126-135*

# Green supplier selection of a textile manufacturer: a hybrid approach based on AHP and VIKOR

Billur Ecer[1], Ahmet Aktas[2,*], Mehmet Kabak[3]

[1]Ankara Yildirim Beyazit University, Department of Industrial Engineering, Ankara, Turkey, becer@ybu.edu.tr, ORCID: 0000-0001-9692-1450

[2]Gazi University, Department of Industrial Engineering, Ankara, Turkey, aaktas@gazi.edu.tr, ORCID: 0000-0002-4394-121X

[3]Gazi University, Department of Industrial Engineering, Ankara, Turkey, mkabak@gazi.edu.tr, ORCID: 0000-0002-8576-5349

**ABSTRACT**

Because of the increasing popularity on protecting the environment, consumers prefer environmentally friendly products in recent years. Due to the trend among consumers, companies have changed their production processes. The first necessity for production of an environmentally friendly product is to supply less harmless raw materials. Therefore, companies have to supply production inputs from green suppliers in order to produce environmentally friendly products. Since the wide use range of textile products make them products that are desired to be green products, green supplier selection of a textile manufacturer was examined in this study. The main aim in this study is to propose a decision model for determination of the best green suppliers. In the proposed model, Analytic Hierarchy Process (AHP) and Vise Kriterijumska Optimizacija I Kompromisno Resenje (VIKOR) methods were integrated. AHP was used to determine criteria weights and VIKOR was used to evaluate alternative suppliers. Seven alternative green suppliers were evaluated by taking 5 main criteria and 17 sub-criteria into account according to the opinions of planning department experts of the company. Alternative green suppliers were ranked by using the proposed methodology and the study was concluded with suggestions for further studies and by giving some managerial implications.

**ARTICLE INFO**

***Research article***

*Received: 26.03.2019*
*Accepted: 05.09.2019*

***Keywords:***
*Multiple criteria decision-making, green supplier selection, Analytic Hierarchy Process, VIKOR*

*Corresponding author

## 1. Introduction

In the past, companies have been choosing suppliers by considering some features such as price, speed, quality, references, flexibility, size of supplier, and cultural compatibility between manufacturer and supplier. Now, in addition to the given features, they also consider the working places of the producers, characteristics of the products they produce, production conditions and legal arrangements.

The addition of new features into the supplier selection is a result of increasing environmental awareness. Now, consumers tend to choose more environmentally friendly products. This trend among consumers led companies to change their production processes to produce green products. Environmentally friendly raw materials usage is the first necessity in order to produce environmentally friendly products. In short, companies should prefer green suppliers who supply environmentally friendly production inputs.
Environmentally friendly clothing is made by using environmentally friendly and sustainable resources to manage green clothing production effectively, companies have to consider all stages of production, including design, purchasing of raw materials, production processes, distribution to market and also reverse logistics and waste. Textile industry is one of the largest polluters in the world. Therefore, it should be said that making textile and clothing production more environmentally friendly could be possible by environmentally friendly management. That is why determination of suitable and green suppliers and logistics structures along the textile supply chain have become a key strategic consideration during recent years.

Selection of green suppliers was confronted in the literature within the last 20 years. Some of these studies can be summarized as follows: Green supplier selection was made by Lu et al. [1] by using AHP in electronic industry. Lee et al. [2] proposed a Delphi and fuzzy extended AHP approach for green supplier selection in high tech electronics industry. Fuzzy ANP (Analytic Network Process) and PROMETHEE techniques were integrated as a hybrid decision-making

approach for green supplier selection in manufacturing industry [3]. Hashemi et al. [4] proposed a green supplier selection approach, which integrates ANP and Grey Relational Analysis techniques for automobile manufacturing. Kuo et al. [5] developed a green supplier selection model for electronics industry based on DEMATEL, ANP and VIKOR techniques. Luthra et al. [6] used an AHP – VIKOR integrated decision-making approach for green supplier selection in automobile manufacturing. Song et al. [7] considered decision maker's psychology to be changing over time for green supplier decision, so, they proposed a green supplier selection framework in a dynamic environment. They used Third Generation Prospect Theory for supplier evaluation. Haeri and Rezaei [8] used grey cognitive maps to determine the best green supplier by considering economic and environmental factors. Six sigma quality indices were included in green supplier selection under fuzzy uncertainty by Chen et al. [9].

In this study, the selection of the green suppliers of a textile company was discussed. In the green supplier selection process, there are different criteria to consider and different alternative companies to evaluate as a supplier. Multi-criteria decision-making approaches are used in such kind of decision problems to find a compromise solution. In order to find the most appropriate supplier company, a hybrid multi-criteria decision-making approach was proposed in this study. Within the proposed approach, criteria weights were calculated with the Analytical Hierarchy Process (AHP) and Vise Kriterijumska Optimizacija I Kompromisno Resenje (VIKOR) method was used to select the most suitable green supplier.

The rest of the paper was organized as follows: in the 2nd part, a brief explanation of methodology of the proposed approach was introduced. A case study of green supplier selection in a textile company was presented in detail in the 3rd part. The paper was concluded in the 4th part with conclusions and suggestions for further studies.

## 2. Methodology

Complex decision problems require considering different criteria simultaneously. Multiple criteria decision-making (MCDM) approaches are useful in such problems to obtain a compromise solution. Green supplier decision is one of such kind of decisions that needs to take various criteria into consideration for selection between alternatives. In this study, green supplier selection was made by using a hybrid MCDM methodology based on AHP and VIKOR methods. AHP was used to calculate main and sub criteria weights and alternative suppliers were evaluated via VIKOR. A flowchart of the proposed decision model is given in Figure 1 as follows:

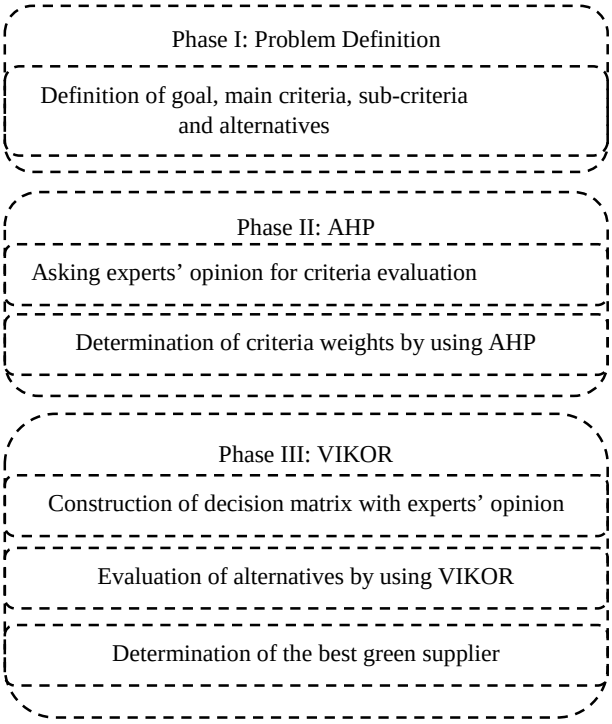


**Figure 1**. *Flowchart for the proposed decision model*

### *2.1. Problem Definition*

First action in this step is to define the aim of the decision precisely. Then, decision criteria and sub-criteria to take into account must be identified and a set of alternatives should be formed.

### *2.2. AHP*

AHP was used for calculation of criteria weights. The AHP is a widely used MCDM method for solving complex decision problems and it is introduced by Thomas L. Saaty [10]. The Analytical Hierarchy Process method has a wide range of applications, including marketing [11], human resources [12], economics [13], information technology selection [14], planning [15], production [16], purchasing [17], health [18], environmental sciences [19] and many other applications. The procedure of AHP consists of five steps. These steps of AHP are explained as follows:

*Step 1. Determination of decision criteria and alternatives*

Decision criteria and alternatives can be determined by conducting a literature review for the studies related to the decision problem or by asking experts of the field.
In the problem description step of the AHP method, a one-way hierarchical structure from the goal to decision criteria and to alternatives is constructed. An example hierarchical structure, which represents a decision problem with n criteria and m alternatives, is shown in Figure 2.

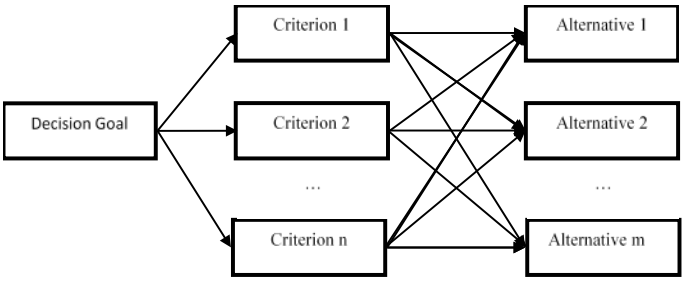


**Figure 2.** *Hierarchical structure of a MCDM problem with n criteria and m alternatives*

*Step 2. Construction of pair wise comparison matrices*

Pairwise comparison matrices are formed by using the 1 – 9 scale of Saaty. Elements of 1 – 9 scale are given in Table 1 with their definitions.

Row element of the matrix is compared with the column element and the relative importance score is written into the cell. If the column element has importance over the row element, multiplicative inverse of the corresponding importance score is written into the cell. In addition, symmetrical elements of the pairwise comparison matrix are multiplicative inverse of each other. Elements on the main diagonal are equal to one, which means the comparison of element with itself.

**Table 1.** *1 – 9 scale for pairwise comparisons*

| Importance Score | Definition |
|---|---|
| 1 | Equal importance |
| 3 | Moderate importance |
| 5 | Strong importance |
| 7 | Very strong importance |
| 9 | Absolute importance |
| 2, 4, 6, 8 | Intermediate values |

*Step 3. Calculation of priorities of decision criteria and alternatives*

Criteria weights can be obtained by using different approaches. Some of these approaches can be listed as follows:

- Logarithmic least squares method
- Least squares method
- Eigenvector/eigenvalue method
- Matrix operations method

In this study, Eigenvector/eigenvalue method is used to obtain criteria weights (priority values). Steps of Eigenvector/eigenvalue method to obtain priorities are as follows:

- Step 3.1: Sum of elements in each column of the pairwise comparison matrix is calculated.
- Step 3.2: Each column is normalized by dividing each element with the corresponding column sum.
- Step 3.3: Arithmetic mean of each row gives the priority value of the row element.

Sum of priority values must be equal to 1. Correction of the obtained priorities can be made by checking sum of priorities.

*Step 4. Determination of the consistency index of the matrix*

Consistency index is an important issue to consider in AHP applications. If pairwise comparison matrix is inconsistent, the matrix should be formed again. Consistency index is calculated by following the five steps:

- Step 4.1: Each element of pairwise comparison matrix is multiplied by the weight of the corresponding column element. Then, weighted sums vector is obtained by adding elements in each row.
- Step 4.2: Elements of weighted sums vector is divided by the corresponding weight values.
- Step 4.3: The arithmetic mean of the obtained values in Step 4.2 is calculated. This value is called as $\lambda_{max}$. $\lambda_{max}$ is defined as the maximum equivalent of the pairwise comparison matrix. The closer value of $\lambda_{max}$ to n means the pairwise comparison matrix is more consistent.
- Step 4.4: Consistency index (CI) is calculated according to the following formula:

$$CI = \frac{\lambda_{\max} - n}{n - 1}$$

- Step 5.5: Consistency ratio (CR) is determined by the following formula. If the consistency ratio is less than 0.1, the pairwise comparison matrix is consistent. Otherwise, the pairwise comparison matrix is inconsistent and a new pairwise comparison matrix must be constructed as follows:

$$CR = \frac{CI}{RI}$$

Where the RI (Random Index) values are presented in the Table 2 as follows:

**Table 2.** *Random Index (RI) values*

| n | 1 | 2 | 3 | 4 | 5 | 6 | 7 | 8 | 9 | 10 |
|---|---|---|---|---|---|---|---|---|---|---|
| RI | 0 | 0 | 0.58 | 0.90 | 1.12 | 1.24 | 1.32 | 1.41 | 1.45 | 1.48 |

*Step 5. Making the decision*

In the AHP method, decision is made according to the relative weights of alternatives vector. Relative weights of alternatives vector is calculated by the matrix product of alternative weights based on each criterion matrix and criteria weights vector. The best alternative is the alternative with the highest priority value. The AHP method was used for obtaining criteria weights in this study and pairwise comparison matrices for alternative evaluation were not constructed. For this reason, this step is not a part of our application.

### 2.3. VIKOR

Alternative evaluations were made by using VIKOR. VIKOR is a MCDM methodology, which is firstly proposed by Opricovic and Tzeng [20]. Translation of its name from Serbian to English is multi-criteria optimization and compromise solution. In the literature, VIKOR was used for evaluation of alternative buses for public transport [21], bank performance evaluation [22] and water resources planning [23], supplier selection [24], mobile services evaluation [25], industrial robots selection [26] etc. VIKOR is a method of determining a compromise order and achieving compromise resolution under specified weights. The compromise solution statement indicates the most appropriate result that the decision makers will achieve in complex decision problems by considering different criteria. VIKOR is applied on decision problems by following six steps:

*Step 1: Construction of the decision matrix*

Decision matrix of the problem (F) consists of alternative scores in views of each criteria. Score of alternative i with respect to criterion j is defined as $f_{ij}$. Scores can be written as the numerical values of alternatives or as a result of evaluation of experts. In this study, alternatives are evaluated by using a 2 – 10 scale, which is proposed by Tayyar and Arslan [27]. 2 – 10 scale is presented in Table 3 as follows:

**Table 3.** *Alternative evaluation scale*

| **Number** | 2 | 4 | 6 | 8 | 10 |
|---|---|---|---|---|---|
| **Linguistic Equivalent** | Very poor | Poor | Moderate | Good | Very Good |

An example decision matrix can be shown as follows:

$$F = \begin{bmatrix} f_{11} & f_{12} & \cdots & f_{1n} \\ f_{21} & f_{22} & \cdots & f_{2n} \\ \vdots & \vdots & \ddots & \vdots \\ f_{m1} & f_{m2} & \cdots & f_{mn} \end{bmatrix}$$

*Step 2: Normalization of the decision matrix*

Normalization of the decision matrix is made for obtaining normalized decision matrix (R). Elements of R are shown as $r_{ij}$. To calculate $r_{ij}$ values, the following formula is used:

$$r_{ij} = \frac{f_j^+ - f_{ij}}{f_j^+ - f_j^-}$$

Where $f_j^+ = \max_i f_{ij}$ and $f_j^- = \min_i f_{ij}$.

$$R = \begin{bmatrix} r_{11} & r_{12} & \cdots & r_{1n} \\ r_{21} & r_{22} & \cdots & r_{2n} \\ \vdots & \vdots & \ddots & \vdots \\ r_{m1} & r_{m2} & \cdots & r_{mn} \end{bmatrix}$$

*Step 3: Weighted normalized decision matrix*

In this step, weighted normalized decision matrix (V) is obtained by multiplication of $r_{ij}$ values with the weight of corresponding criteria ($w_j$). In this study, criteria weights are calculated by using AHP. AHP and VIKOR are integrated in this step.

$$v_{ij} = r_{ij} w_j$$

$$V = \begin{bmatrix} v_{11} & v_{12} & \cdots & v_{1n} \\ v_{21} & v_{22} & \cdots & v_{2n} \\ \vdots & \vdots & \ddots & \vdots \\ v_{m1} & v_{m2} & \cdots & v_{mn} \end{bmatrix}$$

*Step 4: Calculation of $S_i$ and $R_i$ values*

To define the rank between alternatives, VIKOR uses $S_i$ and $R_i$ values. $S_i$ is defined as the utility value and $R_i$ is defined as the regret value. These values are used in the next step for calculation of $Q_i$ values. The formulas for $S_i$ and $R_i$ values are given as follows:

$$S_i = \sum_{j=1}^{n} w_j \frac{f_j^+ - f_{ij}}{f_j^+ - f_j^-} = \sum_{j=1}^{n} v_{ij}$$

$$R_i = \max_j \left( w_j \frac{f_j^+ - f_{ij}}{f_j^+ - f_j^-} \right) = \max_j v_{ij}$$

*Step 5: Calculation of $Q_i$ values*

$Q_i$ values are calculated in order to be able to make decision by aggregating $S_i$ and $R_i$ values. Alternative ranks may change according to $S_i$ and $R_i$ values, so an aggregated measure would help decision makers. The alternative with the minimum value of $Q_i$ is the best alternative. Alternatives are ranked according

to this information. Formula of $Q_i$ integrates normalized $S_i$ and $R_i$ values with a weighting multiplier (v) and is given as follows, Where $S_i^+ = \min_i S_i$, $S_i^- = \max_i S_i$ $R_i^+ = \min_i R_i$ and $R_i^- = \max_i R_i$:

$$Q_i = v \times \frac{S_i - S^+}{S^- - S^+} + (1 - v) \times \frac{R_i - R^+}{R^- - R^+}$$

*Step 6: Checking the results*

Obtained rank is checked in the last step of VIKOR. To check the rank, we should control whether the results satisfy the following two conditions:

- Condition 1: Acceptable advantage

Let us define Q (a') is the $Q_i$ value of the best alternative and Q (a'') is the $Q_i$ value of the second best alternative, respectively. Also, let us define DQ is equal to 1 / (m – 1). If $Q(a'') - Q(a') \geq DQ$, acceptable advantage condition is met.

- Condition 2: Acceptable stability in decision making

Alternative a' must also be the best ranked by S or/and R.

If both of these conditions are satisfied, alternative rank according to the $Q_i$ values is said to be true.

## 3. Case study of green supplier selection in a textile company

Green supplier selection of a textile manufacturer was made in this study by using the proposed AHP - VIKOR approach. Steps of application are explained in this part in detail as follows:

### *3.1. Definition of the Problem*

Goal of the problem is determination of the most appropriate green supplier. 5 main criteria and 17 sub criteria were taken into account. Determination of green supplier selection criteria, assessments about criteria and alternatives were made collecting opinions of a decision making group of four planning experts of the company. Decision criteria of the problem can be listed as follows:

- Green Image (C1)
  - Social Responsibility (C11)
  - Protection of Current Customers (C12)
  - Perception of Environment (C13)
  - Market Share (C14)
- Environmental Management System (C2)
  - Quality Certificates (C21)
  - Adaptation to Regulations (C22)
  - Existence of Environmental Policy (C23)
- Green Production (C3)
  - Less Usage of Harmful Material (C31)
  - Energy Saving (C32)
  - Waste Disposal (C33)
- Green Design (C4)
  - Long Life Product (C41)
  - Recoverable Product (C42)
  - Quality Product (C43)
  - Recycling (C44)
- Green Packaging (C5)
  - Green Pack (C51)
  - Less Usage of Package (C52)
  - Transportation Costs (C53)

Hierarchical structure of decision problem was given in Figure 3. According to the hierarchy, criteria and sub-criteria weights were determined with AHP and seven alternative suppliers were evaluated by using VIKOR.

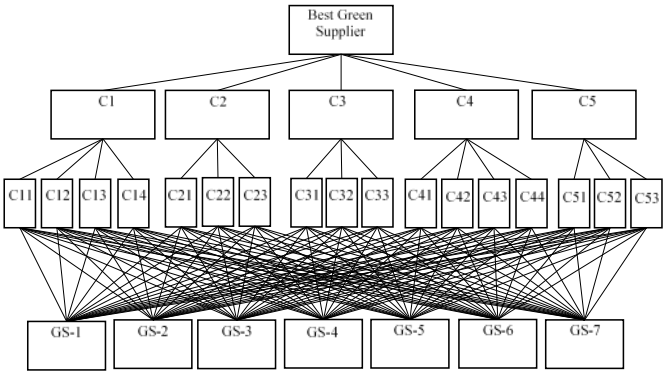


**Figure 3.** *Hierarchical structure of decision problem*

### *3.2. Calculation of Criteria Weights with AHP*

In this step, criteria and sub-criteria weights were calculated by using pairwise comparison matrices. Pairwise comparison matrices were formed according to opinion of planning experts, and then weights were determined by applying AHP calculations on Microsoft Excel software. Pairwise comparison of main criteria was given in Table 4 with calculated weights and consistency ratio as follows:

**Table 4.** *Pairwise comparison of main criteria with respect to goal*

| | C1 | C2 | C3 | C4 | C5 | Weights |
|---|---|---|---|---|---|---|
| C1 | 1 | 3 | 1/3 | 1/5 | 3 | 0.146 |
| C2 | 1/3 | 1 | 1/3 | 1/5 | 2 | 0.085 |
| C3 | 3 | 3 | 1 | 1/3 | 3 | 0.227 |
| C4 | 5 | 5 | 3 | 1 | 5 | 0.478 |
| C5 | 1/3 | 1/2 | 1/3 | 1/5 | 1 | 0.063 |
| | | | | CR Value | | 0.069 |

As it is seen from Table 4, the most important criterion for green supplier selection was determined as Green Design (C4) since it has the highest weight value. Green Production (C3),

Green Image (C1), Environmental Management System (C2) and Green Package (C5) followed Green Design criterion, respectively. Consistency ratio was calculated as 0.069 and it is less than 0.1. Therefore, the pairwise comparison matrix is consistent. Similar to the Table 4, pairwise comparison matrices for sub-criteria were presented in Table 5 – 9 as follows:

**Table 5.** *Pairwise comparison of Green Image sub-criteria with respect to Green Image criterion*

| | C11 | C12 | C13 | C14 | Weights |
|---|---|---|---|---|---|
| C11 | 1 | 1/4 | 1/3 | 1/2 | 0.095 |
| C12 | 4 | 1 | 2 | 2 | 0.424 |
| C13 | 3 | 1/2 | 1 | 3 | 0.314 |
| C14 | 2 | 1/2 | 1/3 | 1 | 0.167 |
| | | | | CR Value | 0.044 |

**Table 6.** *Pairwise comparison of sub-criteria of C2 with respect to C2*

| | C21 | C22 | C23 | Weights |
|---|---|---|---|---|
| C21 | 1 | 1 | 2 | 0.411 |
| C22 | 1 | 1 | 1 | 0.328 |
| C23 | 1/2 | 1 | 1 | 0.261 |
| | | | CR Value | 0.046 |

**Table 7.** *Pairwise comparison of sub-criteria of C3 with respect to C3*

| | C31 | C32 | C33 | Weights |
|---|---|---|---|---|
| C31 | 1 | 1/2 | 3 | 0.334 |
| C32 | 2 | 1 | 3 | 0.525 |
| C33 | 1/3 | 1/3 | 1 | 0.142 |
| | | | CR Value | 0.046 |

**Table 8.** *Pairwise comparison of sub-criteria of C4 with respect to C4*

| | C41 | C42 | C43 | C44 | Weights |
|---|---|---|---|---|---|
| C41 | 1 | 1/3 | 1/2 | 2 | 0.169 |
| C42 | 3 | 1 | 1 | 2 | 0.350 |
| C43 | 2 | 1 | 1 | 4 | 0.367 |
| C44 | 1/2 | 1/2 | 1/4 | 1 | 0.114 |
| | | | | CR Value | 0.044 |

**Table 9.** *Pairwise comparison of sub-criteria of C5 with respect to C5*

| | C51 | C52 | C53 | Weights |
|---|---|---|---|---|
| C51 | 1 | 2 | 1/2 | 0.312 |
| C52 | 1/2 | 1 | 1/2 | 0.198 |
| C53 | 2 | 2 | 1 | 0.490 |
| | | | CR Value | 0.046 |

According to the Table 5 – 9, all pairwise comparisons are consistent, since CR values were less than 0.1. After determination of criteria and sub-criteria weights, global weights of sub-criteria were calculated by multiplication of sub-criteria weight with the corresponding main criterion weight. Global weights of sub-criteria were presented in Table 10 as follows:

**Table 10.** *Global weights of sub-criteria*

| Criteria | Weight | Sub-criteria | Local Weight | Global Weight |
|---|---|---|---|---|
| C1 | 0.1456 | C11 | 0.0947 | 0.0138 |
| | | C12 | 0.4244 | 0.0618 |
| | | C13 | 0.3141 | 0.0457 |
| | | C14 | 0.1667 | 0.0243 |
| C2 | 0.0855 | C21 | 0.4111 | 0.0351 |
| | | C22 | 0.3278 | 0.0280 |
| | | C23 | 0.2611 | 0.0223 |
| C3 | 0.2274 | C31 | 0.3338 | 0.0759 |
| | | C32 | 0.5247 | 0.1193 |
| | | C33 | 0.1416 | 0.0322 |
| C4 | 0.4783 | C41 | 0.1689 | 0.0808 |
| | | C42 | 0.3501 | 0.1675 |
| | | C43 | 0.3672 | 0.1756 |
| | | C44 | 0.1139 | 0.0545 |
| C5 | 0.0632 | C51 | 0.3119 | 0.0197 |
| | | C52 | 0.1976 | 0.0125 |
| | | C53 | 0.4905 | 0.0310 |

According to the Table 10, Quality Product (C43) was the most important sub-criterion among all 17 sub-criteria. Its global weight was calculated as 0.1756. It was followed by Recoverable Product (C42) with the weight value of 0.1675 and Energy Saving (C32) sub-criterion, respectively. Less usage of Package (C52) sub-criterion was considered the least important since its weight is found as 0.0125.

### *3.3. Evaluation of Alternatives by using VIKOR*

Evaluation of alternatives was made by using VIKOR within the proposed algorithm. In this part of the study, we presented steps of VIKOR application. Expert group was asked to evaluate alternative green suppliers in views of sub-criteria by using 2-10 scale given in Table 3.

By using the given scale, evaluation of alternatives was made and at the end of this evaluation decision matrix of the problem (F) was obtained. In addition to the alternative values, the best ($f_i^+$) and the worst ($f_i^-$) values of each column were presented in Table 11 as follows:

**Table 11.** *Decision matrix of the problem (F)*

| Sub-criteria | C11 | C12 | C13 | C14 | C21 | C22 | C23 | C31 | C32 | C33 | C41 | C42 | C43 | C44 | C51 | C52 | C53 |
|---|---|---|---|---|---|---|---|---|---|---|---|---|---|---|---|---|---|
| GS1 | 6 | 8 | 8 | 6 | 6 | 4 | 6 | 8 | 6 | 4 | 6 | 4 | 10 | 4 | 4 | 4 | 2 |
| GS2 | 8 | 6 | 6 | 4 | 8 | 4 | 8 | 6 | 2 | 8 | 8 | 10 | 6 | 6 | 8 | 4 | 8 |
| GS3 | 10 | 8 | 8 | 6 | 4 | 8 | 6 | 8 | 10 | 10 | 6 | 8 | 10 | 8 | 6 | 2 | 4 |
| GS4 | 8 | 4 | 6 | 6 | 8 | 10 | 8 | 10 | 6 | 8 | 8 | 6 | 10 | 8 | 8 | 10 | 8 |
| GS5 | 6 | 4 | 4 | 8 | 8 | 4 | 6 | 4 | 2 | 6 | 4 | 10 | 8 | 4 | 6 | 6 | 6 |
| GS6 | 4 | 6 | 8 | 4 | 6 | 10 | 4 | 2 | 4 | 2 | 4 | 6 | 6 | 8 | 6 | 8 | 8 |
| GS7 | 8 | 10 | 8 | 6 | 10 | 8 | 6 | 6 | 8 | 4 | 10 | 8 | 8 | 6 | 8 | 8 | 6 |
| $f_i^+$ | 10 | 10 | 8 | 8 | 10 | 10 | 8 | 10 | 10 | 10 | 10 | 10 | 10 | 8 | 8 | 10 | 8 |
| $f_i^-$ | 4 | 4 | 4 | 4 | 4 | 4 | 4 | 2 | 2 | 2 | 4 | 4 | 6 | 4 | 4 | 2 | 2 |

Decision matrix was normalized according to the normalization procedure described in the 2nd part of the paper. An example of normalized value calculation was given for GS1 alternative and C11 sub-criterion ($r_{11}$) and normalized decision matrix (R) was presented in Table 12 as follows:

$$r_{11} = \frac{f_1^+ - f_{11}}{f_1^+ - f_1^-} = \frac{10-6}{10-4} = \frac{4}{6} = 0.667$$

**Table 12.** *Normalized decision matrix (R) of the problem*

| Sub-criteria | C11 | C12 | C13 | C14 | C21 | C22 | C23 | C31 | C32 | C33 | C41 | C42 | C43 | C44 | C51 | C52 | C53 |
|---|---|---|---|---|---|---|---|---|---|---|---|---|---|---|---|---|---|
| GS1 | 0.667 | 0.333 | 0.000 | 0.500 | 0.667 | 1.000 | 0.500 | 0.250 | 0.500 | 0.750 | 0.667 | 1.000 | 0.000 | 1.000 | 1.000 | 0.750 | 1.000 |
| GS2 | 0.333 | 0.667 | 0.500 | 1.000 | 0.333 | 1.000 | 0.000 | 0.500 | 1.000 | 0.250 | 0.333 | 0.000 | 1.000 | 0.500 | 0.000 | 0.750 | 0.000 |
| GS3 | 0.000 | 0.333 | 0.000 | 0.500 | 1.000 | 0.333 | 0.500 | 0.250 | 0.000 | 0.000 | 0.667 | 0.333 | 0.000 | 0.000 | 0.500 | 1.000 | 0.667 |
| GS4 | 0.333 | 1.000 | 0.500 | 0.500 | 0.333 | 0.000 | 0.000 | 0.000 | 0.500 | 0.250 | 0.333 | 0.667 | 0.000 | 0.000 | 0.000 | 0.000 | 0.000 |
| GS5 | 0.667 | 1.000 | 1.000 | 0.000 | 0.333 | 1.000 | 0.500 | 0.750 | 1.000 | 0.500 | 1.000 | 0.000 | 0.500 | 1.000 | 0.500 | 0.500 | 0.333 |
| GS6 | 1.000 | 0.667 | 0.000 | 1.000 | 0.667 | 0.000 | 1.000 | 1.000 | 0.750 | 1.000 | 1.000 | 0.667 | 1.000 | 0.000 | 0.500 | 0.250 | 0.000 |
| GS7 | 0.333 | 0.000 | 0.000 | 0.500 | 0.000 | 0.333 | 0.500 | 0.500 | 0.250 | 0.750 | 0.000 | 0.333 | 0.500 | 0.500 | 0.000 | 0.250 | 0.333 |

The next step of VIKOR was weighting the normalized decision matrix. To do so, each value in the normalized decision matrix was multiplied by the global weight value of corresponding sub-criterion calculated via AHP. C11 sub-criterion value of alternative GS1 was calculated below as an example and weighted normalized decision matrix (V) was presented in Table 13 as follows:

$$v_{11} = r_{11} w_1 = 0.667 * 0.0138 = 0.009$$

**Table 13.** *Weighted normalized decision matrix (V) of the problem*

| Sub-criteria | C11 | C12 | C13 | C14 | C21 | C22 | C23 | C31 | C32 | C33 | C41 | C42 | C43 | C44 | C51 | C52 | C53 |
|---|---|---|---|---|---|---|---|---|---|---|---|---|---|---|---|---|---|
| GS1 | 0.009 | 0.021 | 0.000 | 0.012 | 0.023 | 0.028 | 0.011 | 0.019 | 0.060 | 0.024 | 0.054 | 0.167 | 0.000 | 0.054 | 0.020 | 0.009 | 0.031 |
| GS2 | 0.005 | 0.041 | 0.023 | 0.024 | 0.012 | 0.028 | 0.000 | 0.038 | 0.119 | 0.008 | 0.027 | 0.000 | 0.176 | 0.027 | 0.000 | 0.009 | 0.000 |
| GS3 | 0.000 | 0.021 | 0.000 | 0.012 | 0.035 | 0.009 | 0.011 | 0.019 | 0.000 | 0.000 | 0.054 | 0.056 | 0.000 | 0.000 | 0.010 | 0.012 | 0.021 |
| GS4 | 0.005 | 0.062 | 0.023 | 0.012 | 0.012 | 0.000 | 0.000 | 0.000 | 0.060 | 0.008 | 0.027 | 0.112 | 0.000 | 0.000 | 0.000 | 0.000 | 0.000 |
| GS5 | 0.009 | 0.062 | 0.046 | 0.000 | 0.012 | 0.028 | 0.011 | 0.057 | 0.119 | 0.016 | 0.081 | 0.000 | 0.088 | 0.054 | 0.010 | 0.006 | 0.010 |
| GS6 | 0.014 | 0.041 | 0.000 | 0.024 | 0.023 | 0.000 | 0.022 | 0.076 | 0.089 | 0.032 | 0.081 | 0.112 | 0.176 | 0.000 | 0.010 | 0.003 | 0.000 |
| GS7 | 0.005 | 0.000 | 0.000 | 0.012 | 0.000 | 0.009 | 0.011 | 0.038 | 0.030 | 0.024 | 0.000 | 0.056 | 0.088 | 0.027 | 0.000 | 0.003 | 0.010 |

Weighted normalized decision matrix was used to calculate $S_i$ and $R_i$ values of alternatives. $S_i$ and $R_i$ values are used for calculation of $Q_i$ values, which is an important determinant for alternative ranks. $S_i$ and $R_i$ values of GS1 was given to show the calculation and values for all alternatives were presented in Table 14.

$$S_1 = \sum_{j=1}^{n} w_j \frac{f_j^+ - f_{1j}}{f_j^+ - f_j^-} = \sum_{j=1}^{n} v_{1j} = 0.543$$

$$R_1 = \max_j \left( w_j \frac{f_j^+ - f_{1j}}{f_j^+ - f_j^-} \right) = \max_j v_{1j} = 0.167$$

**Table 14.** *$S_i$ and $R_i$ values of alternatives*

| Alternatives | $S_i$ | $R_i$ |
|---|---|---|
| GS1 | 0.543 | 0.167 |
| GS2 | 0.537 | 0.176 |
| GS3 | 0.260 | 0.056 |
| GS4 | 0.319 | 0.112 |
| GS5 | 0.609 | 0.119 |
| GS6 | 0.704 | 0.176 |
| GS7 | 0.313 | 0.088 |

As it is mentioned before, alternative ranks were determined according to the $Q_i$ values. To calculate Qi values, we need $S^-$, $S^+$, $R^-$, and $R^+$ values. The values were given in Table 15 as follows:

**Table 15.** *$S^-$, $S^+$, $R^-$, $R^+$ values*

| Measure | $S^-$ | $S^+$ | $R^-$ | $R^+$, |
|---|---|---|---|---|
| Value | 0.704 | 0.260 | 0.176 | 0.056 |

By using the formula given in VIKOR explanation part, $Q_i$ values of alternatives were calculated. For v=0.5, $Q_i$ value of alternative GS1 can be calculated as:

$$Q_1 = 0.5 \times \frac{S_1 - S^+}{S^- - S^+} + (1 - 0.5) \times \frac{R_1 - R^+}{R^- - R^+}$$
$$= 0.5 \times \frac{0.543 - 0.260}{0.704 - 0.260} + 0.5 \times \frac{0.167 - 0.056}{0.176 - 0.056} = 0.7850$$

$Q_i$ values of other alternatives were presented in Table 16 as follows:

**Table 16.** *$Q_i$ values of alternatives (v=0.5)*

| Alternatives | $Q_i$ | Rank |
|---|---|---|
| GS1 | 0.7850 | 5 |
| GS2 | 0.8123 | 6 |
| GS3 | 0.0000 | 1 |
| GS4 | 0.2998 | 3 |
| GS5 | 0.6588 | 4 |
| GS6 | 1.0000 | 7 |
| GS7 | 0.1938 | 2 |

At the last step of VIKOR, acceptable advantage and acceptable stability in decision making conditions were investigated.

For the first condition; Q (a') value was determined as 0.0000 and Q (a'') value was 0.1938. DQ was equal to 0.1667, which is calculated as 1 / (7 – 1). Q (a'') – Q (a') = 0.1938 and it was greater than 0.1667. Therefore, acceptable advantage condition was met.

For the second condition; $S_i$ and $R_i$ values of alternative GS3 were the minimum values, which means that the alternative gets the best rank for $S_i$ and $R_i$ values, too. Hence, the second condition to check the obtained rank was met.

Alternative GS3 was determined as the best alternative, after the evaluation with the proposed methodology.

## 4. Conclusion

In recent years, development of the consumers' environmental awareness and legal obligations have caused the enterprises to produce environmentally friendly products. Raw material selection is the most important stage of production, which directly effects the characteristics of product. The selected raw material has a direct impact on the production process as well as a direct impact on the environmental effects of the product. In this study, the most appropriate green supplier for a textile manufacturer in order to produce an environmentally friendly product was examined. Selection among alternative suppliers was made by using the proposed decision making methodology based on AHP and VIKOR.

AHP evaluation was made for determination of importance degree of supplier selection criteria. Quality product sub-criteria of green design criterion was seen as the most important sub-criterion for selection of a green supplier. VIKOR analysis showed the best alternative supplier as GS3 among the seven alternatives. The alternative rank obtained by VIKOR was corrected by checking both two conditions of VIKOR method are satisfied.

In further studies, this work can be extended by making a comparison study for alternative ranks obtained as a result of different MCDM applications to the problem. Effect of criteria weight changes can be analysed with different experts' opinion or by conducting a sensitivity analysis on current criteria weights.

## References


[1]. Lu L.Y.Y., Wu C.H., Kuo T.C. "Environmental principles applicable to green supplier evaluation by using multi-objective decision analysis, International Journal of Production Research, 45, (2007), 4317-4331.

[2]. Lee A.H.I., Kang H.Y., Hsu C.F., Hung H.C. "A green supplier selection model for high-tech industry", Expert Systems with Applications, 36, (2009), 7917-7927.

[3]. Tuzkaya G., Özgen A., Özgen D., Tuzkaya U.R., Environmental performance evaluation of suppliers: A hybrid fuzzy multi-criteria decision approach, International Journal of Environmental Science and Technology, 6,(2009), 477-490.

[4]. Hashemi S.H., Karimi A., Tavana M. "An integrated green supplier selection approach with analytic network process and improved Grey relational analysis", International Journal of Production Economics, 159,(2015),178–191.

[5]. Kuo T.C., Hsu C.W. and Li J.Y. "Developing a green supplier selection model by using the DANP with VIKOR", Sustainability, 7, (2015), 1661–1689.

[6]. Luthra S., Govindan K., Kannan D., Mangla S.K., Garg C.P. "An integrated framework for sustainable supplier selection and evaluation in supply chains", Journal of Cleaner Production, 140, (2016), 1686-1698.

[7]. Song, W., Song, W., Chen, Z., Liu, A., Zhu, Q., Zhao, W., Tsai, S. B., Lu, H. "A Study on Green Supplier Selection in Dynamic Environment", Sustainability, 10, (2018), 1226-1247.

[8]. Haeri, S. A. S., Rezaei J. "A grey-based green supplier selection model for uncertain environments", Journal of Cleaner Production, 221, (2019), 768-784.

[9]. Chen, K. S., Wang,C. H., Tan K. H. "Developing a fuzzy green supplier selection model using six sigma quality indices", International Journal of Production Economics, 212, (2019), 1–7.

[10]. Saaty, T. L. The analytic hierarchy process. New York: McGraw-Hill.1980.

[11]. Wu, Y., Chen, S. C., Lin, I. C. "Elucidating the impact of critical determinants on purchase decision in virtual reality products by Analytic Hierarchy Process approach", Virtual Reality, 23, (2019), 187–195.

[12]. Çelikbilek, Y. "A grey analytic hierarchy process approach to project manager selection", Journal of Organizational Change Management, 31, (2018), 749-765.

[13]. Banda, W. "Economic analysis of Zambia's ad valorem copper mineral royalty reforms using an analytic hierarchy process framework", Mineral Economics, 32, (2019), 1–18.

[14]. Alava, M. V., Figueroa, S. P. D., Alcivar, H. M. B., Vázquez, M. L. "Single Valued Neutrosophic Numbers and Analytic Hierarchy Process for Project Selection", Neutrosophic Sets and Systems, 21, (2018), 122-130.

[15]. Ahmad, I., Verma, M. K. "Application of Analytic Hierarchy Process in Water Resources Planning: A GIS Based Approach in the Identification of Suitable Site for Water Storage", Water Resources Management, 32, (2018), 5093–5114.

[16]. Amin Nikkhah A., Firouzi, S., El Haj Assad M., Ghnimi S. "Application of analytic hierarchy process to develop a weighting scheme for life cycle assessment of agricultural production", Science of the Total Environment, 665, (2019), 538–545.

[17]. Thaker, H. M. T., Sakaran, K. C. "Prioritisation of key attributes influencing the decision to purchase a residential property in Malaysia: An analytic hierarchy process (AHP) approach", International Journal of Housing Markets and Analysis, 9, (2016), 446-467.

[18]. Sahin, T., Ocak, S., Top, M. "Analytic hierarchy process for hospital site selection", Health Policy and Technology, 8, (2019), 42–50.

[19]. Akay, O. A., Demir M., Akgul, M. "Assessment of risk factors in forest road design and construction activities with fuzzy analytic hierarchy process approach in Turkey", Environmental Monitoring and Assessment, 190, (2018), 561-572.

[20]. Opricovic, S., Tzeng, G.H. "Compromise Solution by MCDM Methods: A Comparative Analysis of VIKOR and TOPSIS", European Journal of Operational Research, 156, (2004), 445-455.

[21]. Aydin, S., Kahraman, C. "Vehicle selection for public transportation using an integrated multi criteria decision making approach: A case of Ankara", Journal of Intelligent & Fuzzy Systems, 26, (2014), 2467–2481.

[22]. Beheshtinia, M.A., Omidi, S. "A hybrid MCDM approach for performance evaluationin the banking industry", Kybernetes, 46, (2017), 1386-1407.

[23]. Opricovic, S. "Fuzzy VIKOR with an application to water resources planning", Expert Systems with Applications, 38, (2011). 12983-12990.

[24]. Joshi, R., Kumar, S. "An intuitionistic fuzzy information measure of order (α, β) with a new approach in supplier selection problems using an extended VIKOR method", Journal of Applied Mathematics and Computing, 60, (2019), 27–50.

[25]. Suh Y., Park Y., Kang D. "Evaluating mobile services using integrated weighting approach and fuzzy VIKOR", PLoS ONE, 14, (2019), e0217786.

[26]. Narayanamoorthy, S., Geetha, S., Rakkiyappan, R., Joo, Y. H. "Interval-valued intuitionistic hesitant fuzzy entropy based VIKOR method for industrial robots selection", Expert Systems With Applications, 121, (2019), 28–37.

[27]. Tayyar, N., Arslan, P. "Hazır Giyim Sektöründe En İyi Fason İşletme Seçimi İçin AHP ve VIKOR Yöntemlerinin Kullanılması", Celal Bayar Üniversitesi Sosyal Bilimler Dergisi, 11, (2013), 340-358.

MANAS Journal of Engineering
ISSN 1694-7398 | e-ISSN 1694-7398

*Volume 7 (Issue 2) (2019) Pages 136-140*

# Antioxidant activity of galangal powder and the effect of addition on some quality characteristics of meatball

Recep Palamutoğlu[1,*], Cemal Kasnak[2]

[1]Afyonkarahisar Health Sciences University, Zafer Health Campus Dörtyol District, Afyonkarahisar, Turkey, receppalamutoglu@hotmail.com, ORCID: 0000-0002-1168-081X

[2]Afyonkarahisar Health Sciences University, Zafer Health Campus Dörtyol District, Afyonkarahisar, Turkey, ckasnak@gmail.com, ORCID: 0000-0002-8312-7829

**ABSTRACT**

In this research, the effect of dried galangal powder addition (% 0.1, % 0.25, % 0.5 w/w) on oxidative stability as measured by thiobarbituric acid-reactive substances (TBA) and conjugated diene of meatballs were investigated at different days (Day 0, 3, 7). There was no significant difference were found between the TBA values of control and BHT added samples at the end of the storage but significant difference ($p<0.05$) were found the galangal added samples. The lowest TBA value observed at % 0.5 galangal powder added samples (0.2 mg malonaldehyde/ kg meat sample). When the conjugated dienes results were examined, it was determined that the highest value was obtained at % 0.5 galangal powder added group (0.0273 µmole/mg meat) and there was no significant difference ($p>0.05$) were found between the other galangal powder added samples. There was a significant difference ($p<0.01$) was found between the % 0.5 galangal added and control or BHT added samples (0.0151 and 0.017 µmole/mg meat respectively). Also color analysis and sensorial evaluations of the meatball samples were done.

**ARTICLE INFO**

***Research article***

*Received: 21.12.2018*
*Accepted: 03.05.2019*

***Keywords:***
*Conjugated dienes,*
*galangal powder,*
*meatball,*
*TBA*

**Corresponding author*

## 1. Introduction

Buckley, Morissey, & Gray [1] concluded that lipid hydroperoxides formed during the propagation phase of the process are unstable and are reductively cleaved by the trace elements to give a range of free radicals and other non-radical compounds including alkoxyl, alkyl radicals, aldehydes, ketones and a range of carboxyl compounds. These compounds adversely affect the texture, color, flavor, nutritive value and safety of muscle food. Addition of antioxidative compounds required for preserving the food quality [2]. Synthetic antioxidants are widely used in the food industry such as butylated hydroxyanisole (BHA), butylated hydroxytoluene (BHT), propile gallate (PG), tert-butyl hydroquinone (TBHQ) [2-3]. Synthetic antioxidants have long been used but their use has recently come into the dispute to a suspected carcinogenic potential [4] and the general rejection of synthetic food additives by consumers [2]. A multitude of natural antioxidants has already been isolated from different kinds of plant materials such as; oilseeds, cereal corp, vegetables, fruits, leaves, roots, spices, herbs [5]. Currently, there is an increasing demand for new ethnic foods. Some of the popular emerging ingredients for developing these foods include galangal, cardamom, lemongrass, etc. [6].

Lu, Yuan, Zeng, & Chen [7] studied the antioxidant capacity and phenolic compounds of spices used in China. They found that galangal has the highest antioxidant capacity between the 19 dried culinary spices. Galangal (Alpinia galanga), a rhizome related to the ginger family and used for stir-fries, curries, soups of South East Asia [6].

The study aimed to determine the effects of dried galangal powder addition on oxidative stability of meatballs as measured by thiobarbituric acid reactive substances, conjugated dienes during storage at 4°C. Also, some quality characteristics of meatballs were determined

## 2. Materials and methods

Galangal rhizomes were purchased from a supermarket in Afyonkarahisar/ Turkey. Beef meat was purchased from local butchers in Afyonkarahisar. The rest of the chemicals and standards were analytical grades and obtained from Sigma or Merck (Darmstadt, Germany) unless otherwise stated. Duplicate determinations were carried out for all analysis.

Rhizomes were cleaned and cut into small pieces and ground by using a grinder (Bosch, MKM6000), and stored at

refrigerated conditions in an airtight, screw-capped plastic container until use.

Phenolic isolation of samples was done by the method of Shahidi, Chavan, Naczk, & Amarowicz [8]. According to this method, one gram sample extracted 3 times with 10 mL of aqueous methanol (70%) using a homogenizer (Daihan HG-15D) at 11.000 rpm for 1 min. Then the slurry centrifuged at 4000 rpm for 15 min. Supernatants were collected and evaporated by the rotary evaporator (Scilogex- RE100) at 45 °C under vacuum. Extracted phenolics were dissolved in 25 mL of methanol and filtered by filter paper (Whatmann No:1). Methanolic solutions of extracted materials were then used for further analysis.

Total phenolic contents were determined according to Kaur & Kapoor [9]. The methanolic solution of extracts (0.5 mL), distilled water (7 mL) and Folin Ciocalteu reagent (0.5mL) were added to the test tube and mixed. After 3 min, 2 mL of sodium carbonate (20%) was added and mixed again. The solution was read at 720 nm after 1 h standing at 25°C in a water bath. Results were expressed as mg catechin of kg weight sample using a standard calibration curve of catechin ($r2>0.99$).

The DPPH radical scavenging assay with some modifications was used Choi, Kozukue, Kim, & Friedman [10]. The methanolic DPPH solution was prepared and 1.6 mL of sample was added to DPPH (0.4 mL, 96mg/L). After 30 min incubation period at room temperature, the absorbance was measured by UV-Vis spectrophotometer at 517 nm against the blank. Antioxidant activity (AA) (%) was calculated according to the equation given below;

Antioxidant activity (%)= [(Ablank-Asample)/Ablank]x100

Duplicate treatments were done for the meatball dough preparation. Meat divided into 5 groups. Control, BHT added and 3 different galangal added meat doughs prepared. Galangal powder (previously ground galangal powders) added to meat at a concentration of 0.1% (P1), 0.25 % (P2) and 0.5 % P3) of the meat weight. Each group sample was divided into 25 g of meatballs on a plastic tray and sealed with stretch film and stored in a refrigerator at 4°C. Meat samples were evaluated at 0, 3, 7 days for TBA, Conjugated dienes, color values. Also, sensory parameters evaluated on Day 0.

**Table 1.** *Meatball preparation*

| Ingredients | Control | BHT | P1 | P2 | P3 |
|---|---|---|---|---|---|
| Meat (g) | 1000 | 1000 | 1000 | 1000 | 1000 |
| Salt (g) | 20 | 20 | 20 | 20 | 20 |
| BHT (ppm) | - | 200 | - | - | - |
| Galangal Powder (g) | - | - | 1 | 2,5 | 5 |

CIE color values (L*, a*, b*) of the meatballs were determined by X-Rite (Ci6X) colorimeter. The colorimeter was calibrated using a standard white plate. The color was measured at three positions of the samples. The color was measured from uncooked meatball samples during the storage and cooked meatballs on day 0.

To determine lipid oxidation, a 10 g sample was homogenized with 97.5 mL distilled water at 50°C and put into a Kjeldahl flask. The volume was completed to 100 mL by adding a 2.5 mL 4 N HCl solution (1:2 37% HCl : distilled H2O) to it. Soybean oil was used as the antifoaming agent. Fifty mL of distillate was collected with steam distillation in a precise manner. Five mL was taken from the distillate and 5 mL 0.02 M TBA reactive was added to it; it was kept in a boiling water bath for 35 min. The absorbance values of the cooled samples were read in the UV spectrophotometer at 538 nm wavelength. The amount of malondialdehyde (MDA) (mg MDA/kg sample) formed in the product was calculated by multiplying the absorbance values by the factor 7.8 [11].

The formation of conjugated dienes was determined according to the procedure described by 2. Meat samples (0.5 g) were suspended in 5 mL of distilled water and homogenized to form a smooth slurry. A 0.5 mL aliquot of this suspension was mixed with 5 mL of extracting solution (3:1 hexane: isopropanol) for 1 min. after centrifugation at 2000 g for 5 min, the absorbance of the supernatant was measured at 223 nm. The concentration of conjugated diene was calculated using the molar extinction coefficient of 25.200/Mcm and the results were expressed as µmole per mg meat sample.
Sensory evaluation was conducted according to IFT (Institute of Food Technologists) [12]. Meatball samples were grilled at 80°C internal temperature and served in random order. The serving temperature was approximately 60°C. Water and bread were served for cleaning the mouth between samples. Consumer panelists were 12 volunteers from the Nutrition and Dietetics department and a nine-point hedonic scale was used.

The obtained data were presented as means and standard deviation (mean±SD) and subjected to analysis of variance (one way/ two way-ANOVA). Means were compared with Tukey test.

## 3. Results and discussion

The total phenolic content of galangal rhizomes was 17,729.16 mg catechin equivalent/ kg sample and antioxidant activity was 89.62 %. These results showed that the galangal methanolic extracts have strong antioxidant activity.

**Table 2.** *Color values of Stored Meatballs*

| Treatment | L* | a* | b* |
|---|---|---|---|
| Control | 44.45± 4.41 | 12.42$^{a}$±4.57 | 13.09±1.37 |
| BHT | 43.64±2.73 | 11.25$^{ab}$±4.38 | 13.01±2.14 |
| P1 | 47.55±5.25 | 8.41$^{b}$±6.49 | 12.37±3.94 |
| P2 | 41.22±2.02 | 10.34$^{ab}$±5.23 | 11.88±3.64 |
| P3 | 41.85±3.69 | 11.45$^{ab}$±5.04 | 12.61±3.18 |
| Sig | n.s. | * | n.s. |
| Day | | | |
| 0 | 44.30±1.71 | 15.66$^{a}$±1.55 | 15.84$^{a}$±1.06 |
| 3 | 43.40±5.01 | 5.69$^{c}$±1.95 | 11.33$^{b}$±1.20 |
| 7 | 43.53±5.3 | 10.98$^{b}$±4.42 | 10.61$^{b}$±2.32 |
| Sig | n.s. | ** | ** |
| Treatment* Day Interaction | | | |
| Sig | n.s. | * | * |

$^{a–c}$ Means in the same column with different superscripts are significantly different.
* p<0.05, **p<0.01

When the L* values of meatballs were compared, results showed that there was no significant (p>0.05) difference found between treatment groups, days and "Treatment*Day" interactions. Also, treatment does not affect the b*values of meatballs. Table 3 shows that the a* value of the meatballs significantly affected a partial the treatment (p<0.05) and storage (p<0.01). The highest a* value was seen in the control group (12.42±4.57) but there was no difference seen between the other groups except P1. Maybe the quantity of galangal powder in the meat matrix is inadequate for the prevention of color.

Discoloration in meat is interrelated with lipid oxidation and metmyoglobin production through the action of free radicals [13]. Cheah & Abu Hasim [3] concluded that samples with galangal extract showed increasing a* values with increasing concentration. Addition of BHT or alfa-tocopherol didn't affect the L* and b* values.

According to Tironi et al. [14] The red color decreased in both untreated and rosemary extract-treated samples as a function of storage time; a minor decrease was observed in treated muscles, as evidenced by the increase in a*. These results indicate partial red color preservation by the rosemary extract. Rosemary extract produces only partial preservation of red color because there are other causes for color modification in addition to the oxidative processes investigated in this work. Possible causes for the decrease of a* include the conversion of oxy- and deoxyhemoglobin to methemoglobin, denaturation of myofibrillar proteins that produce a change upon interaction with hemoglobin, and surface dehydration.

**Table 3.** *Color values of Cooked Meatballs*

| Treatment | L* | a* | b* |
|---|---|---|---|
| Control | 33.48±2.09 | 6.82±0.06 | 9.28±0.52 |
| BHT | 29.95±1.40 | 5.63±0.51 | 6.84±1.14 |
| P1 | 32.16±0.55 | 6.86±0.51 | 8.90±0.64 |
| P2 | 28.76±2.41 | 6.59±0.30 | 7.55±1.08 |
| P3 | 30.27±0.74 | 5.79±0.49 | 7.17±1.28 |

a–c Means in the same column with different superscripts are significantly different.
* p<0.05, **p<0.01

There was no significant (p>0.05) difference found between the color values of cooked control and treatment groups of meatballs. The highest L* value (33.48±2.09) was seen in the control g highest a* (6.86±0.51) and the highest b* values (8.90±0.64) were seen in the P1 group.

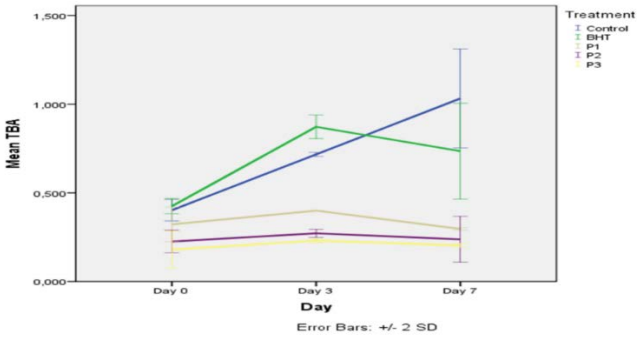


**Figure 1.** *TBA values (mg MDA/kg meat) of meatballs*

TBA values, which can be used as a measure of the concentrations of secondary lipid oxidation products such as aldehydes or ketones in samples. Many spices contain phenolic substances which exhibit antioxidant activities. Several studies showed the antioxidant effect of galangal extract in model systems. Cheah & Abu Hasim [3] also showed the galangal extracts at higher concentrations (like 5-10 %) retarded the lipid oxidation in meat. But 1% concentration of galangal extract was not effective on retarding the lipid oxidation (Fig. 1). In this research, TBA values decrease by the dose increase. The TBA value of the control group increases linearly by the storage time. BH added groups TBA value increase during the beginning of the storage and then decrease by the time. At the same time, galangal powder added samples lowers the TBA values by the increase of their concentration. That can be said the inhibitory effect of galangal powder is dose-dependent.

**Table 4.** *Conjugated dienes values of meatballs*

| Treatment | Conjugated Dienes (µmole/mg meat) |
|---|---|
| Control | $0.0162^{c}$±0.001 |
| BHT | $0.0170^{bc}$±0.004 |
| P1 | $0.0213^{abc}$±0.012 |
| P2 | $0.0250^{ab}$±0.018 |
| P3 | $0.0273^{a}$±0.026 |
| Sig | ** |
| Day | |
| 0 | $0.0143^{b}$±0.002 |
| 3 | $0.0133^{b}$±0.001 |
| 7 | $0.0359^{a}$±0.018 |
| Sig | ** |
| Treatment*Day Interaction | |
| Sig | ** |

[a–c] Means in the same column with different superscripts are significantly different (**p<0.01)

Lipid oxidation in meat can result in quality deterioration and decreases in sensory and nutritional factors [2]. Unsaturated lipids that have non-conjugated double bonds transform into conjugated dienes after peroxides are formed during lipid oxidation. Hydroperoxides hardly decompose during the early stage of lipid oxidation and decompose into secondary products at the later stage [15].

Table 4 shows that there was a significant (p<0.01) difference found between the conjugated diene values of galangal added meatballs compared with the control group. But there was no difference found between each other. At the beginning of the storage, the conjugated dienes value lowers but increase by the time. The effect of time on the conjugated dienes values of the samples was significant (p<0.01) different.

Conjugated dienes values of the galangal powder added samples have an opposite situation with the TBA results. Meatball samples which have the lowest TBA value have the highest conjugated diene value. This can be explained with the transformation of the lipid peroxidation products during the storage because the compounds don't stable.

**Table 5.** *Sensorial values of Meatballs*

| Treatment | Appearance | Color | Odor | Taste | Texture | Overall Acceptabil |
|---|---|---|---|---|---|---|
| Control | 5.73±1.10 | 6.82±1.08 | 4.73±1.49 | 5.00±1.79 | 6.09±0.70 | 5.72±1.10 |
| BHT | 4.91±1.22 | 6.73±1.10 | 4.28±2.24 | 4.55±1.51 | 5.64±1.03 | 4.90±1.22 |
| P1 | 4.27±1.42 | 6.64±1.36 | 3.45±1.97 | 3.73±1.62 | 5.45±1.44 | 4.27±1.42 |
| P2 | 5.09±0.83 | 6.64±1.03 | 3.90±1.76 | 4.36±1.75 | 6.09±1.04 | 5.09±0.83 |
| P3 | 5.36±1.43 | 6.55±1.13 | 5.27±1.80 | 4.82±1.99 | 5.55±0.93 | 5.36±1.43 |

[a–c] Means in the same column with different superscripts are significantly different. * p<0.05, **p<0.01

Sensorial analysis results (Table 5) indicate that there was no significance (p>0.05) difference found between appearance, color, odor, taste, texture, overall acceptability values of the control and the treatment groups.

## 4. Conclusion

Generally dried galangal powder has a protective effect against lipid oxidation of meatballs during storage at 4 °C for 7 days. These results suggest that the addition of galangal powder to meatballs enhance the oxidative stability of meat or other lipid-containing food systems.

Dried galangal powder addition to meatballs lowers the TBARS values. Galangal, used in Asian countries cuisine for centuries. But some countries like Turkey don't use in their cuisine especially in their meatballs. Sensory analysis showed that no differences were found between control and galangal added samples. The consumer wants to use natural ingredients in their foods. Galangal can be used as a natural antioxidant without any known toxic effects. In this research, only galangal usage showed the antioxidant activity but the consumer will use the spice with other spices. As conclusion, further investigations are needed.

**Funding**
This research funded by Afyon Kocatepe University Scientific Projects Coordination Department under grant number of 17.KARİYER.149.

## References

[1]. Buckley D.J., Morissey P.A., Gray J.I. "Influence of dietary vitamin E on the oxidative stability and quality of pig meat", J. Anim. Sci., 73, (1995), 122–130.

[2]. Juntachote T., Berghofer E., Siebenhandl S., Bauer F. "The effect of dried galangal powder and its ethanolic extracts on oxidative stability in cooked ground pork", LWT - Food Sci. Technol., 40, (2007), 324–330.

[3]. Cheah P.B., Abu Hasim N.H. "Natural antioxidant extract from galangal (Alpinia galanga) for minced beef", J. Sci. Food Agric., 80, (2000), 1565–1571.

[4]. Chen C.H., Pearson A.M., Gray J.I. "Effects of synthetic antioxidants (BHA, BHT and PG) on themutagenicity of IQ-like compounds", Food Chem., 45, (1992), 177–183.

[5]. Ramarathnam N., Osawa T., Ochi H., Kawakishi S. "The contribution of plant food antioxidants to human health", Trends Food Sci. Technol., 6, (1995), 75–82.

[6]. Uhl S. "Ingredients: the building blocks for developing `new' ethnic foods", Food Technol. 6, (1996), 79–84.

[7]. Lu M., Yuan B., Zeng M., Chen J. "Antioxidant capacity and major phenolic compounds of spices commonly

consumed in China", Food Res. Int., 44, (2011), 530–536.

[8]. Shahidi F., Chavan U.D., Naczk M., Amarowicz R. "Nutrient distribution and phenolic antioxidants in air-classified fractions of beach pea (Lathyrus maritumus L.)", J. Agric. Food Chem., 49, (2001), 926–933.

[9]. Kaur C., Kapoor H.C. "Anti-oxidant activity and total phenolic content of some Asian vegetables", Int. J. Food Sci. Technol., 37, (2002), 153–161.

[10]. Choi S.-H., Kozukue N., Kim H.-J., Friedman M. "Analysis of protein amino acids, non-protein amino acids and metabolites, dietary protein, glucose, fructose, sucrose, phenolic, and flavonoid content and antioxidative properties of potato tubers, peels, and cortexes (pulps)", J. Food Compos. Anal., 50, (2016).

[11]. Tarladgis B.G., Watts B.M., Younathan M.T., Dugan J. "A distillation method for the quantitative determination of malonaldehyde in rancid foods", J. Am. Oil Chem. Soc., 37, (1960), 44–48.

[12]. IFT. Guidelines for the preparation and review of papers reporting sensory evaluation data. J. Food Sci., 60, (1985), 210–211.

[13]. O'Grady M.N., Monahan F.J., Brunton N.P. "Oxymyoglobin oxidation and lipid oxidation in bovine muscle - Mechanistic studies", J. Food Sci., 66, (2001), 386–392.

[14]. Tironi V., Tomás M., Añón M. "Lipid and protein changes in chilled sea salmon (Pseudopercis semifasciata): Effect of previous rosemary extract (Rossmarinus officinalis L.) application", Int. J. Food Sci. Technol., 44, (2009), 1254–1262.

[15]. Kulås E., Ackman R.G. "Different tocopherols and the relationship between two methods for determination of primary oxidation products in fish oil", J. Agric. Food Chem., 49, (2001), 1724–1729.

Manas Journal of Engineering
ISSN 1694-7398 | e-ISSN 1694-7398

*Volume 7 (Issue 2) (2019) Pages 141-146*

# Assisting Tool for Essay Grading for Turkish Language Instructors

Mustafa Alp Çetin[1], Rita Ismailova[2,*]

[1]Kyrgyz-Turkish Manas University, Computer Engineering Department, Bishkek, Kyrgyzstan, mustafaalpcetin1@gmail.com

[2]Kyrgyz-Turkish Manas University, Computer Engineering Department, Bishkek, Kyrgyzstan, rita.ismailova@manas.edu.kg, ORCID: 0000-0003-0308-2315

**ABSTRACT**

When learning languages, writing an essay is one of the main methods for assessing students' knowledge. However, with the development of information and communication technologies, language learning is also being transferred to online platforms. At the same time, as the number of students increases, the problem of evaluating students' essays arises. In this paper, we offer an automated system that facilitates instructors while evaluating students' essays. Currently, the system works for essays written in Turkish. The system was built using the Zemberek library. It allows one to extract text features the essay of several people at the same time on several indicators, namely, morphological analysis, vocabulary, the use of different language structures, etc. Currently, many automated essay grading tools are proposed, and one of the main factors that defined their accuracy it the extraction of text features. Thus, as further work, it is planned to use the data obtained using this essay assessment system together with instructors' evaluation to create an expert system for automatic essay evaluation using machine learning techniques.

**ARTICLE INFO**

***Research article***

*Received: 17.12.2019*
*Accepted: 23.12.2019*

***Keywords:***
*Natural language processing, automated tool, essay evaluation, Computer-assisted language learning*

*Corresponding author

## 1. Introduction

Nowadays, natural language processing is becoming a widespread subject and many types of research are being carried out in this field. This technique deals with the conversion of human language into a form that eases the computer manipulations on the language [9]. Another definition by Chowdhury (2003) emphasizes that the technique of natural language processing aims at developing tools so that computer systems could manipulate natural languages to perform desired tasks [8]. Processing techniques differ by their complexity, starting from text categorization and word frequency count [5, 7, 10, 12] to text translation [2, 4, 13, 18, 23] smart text annotation [21] and generating meaningful responses to human questions [3]. As natural language processing techniques develop, its usage area is also expanding.

Despite the popularity of natural language processing, it has not been fully completed for any language today. The most NLP solutions are offered for the English language. Though there are studies presented for other languages as well [1, 11, 24].

Looking at the application of NLP from the other end, and considering the way people learn languages, essay writing is one of the most effective methods that allow evaluating how much the language learners are adapting to the language they are learning. However, evaluation and grading written works is a hard task, especially as the number of students increases. Besides, human rating in some cases can be considered as bias [25]. In addition, grading essays is an expensive task [14]. Especially this issue becomes very acute when using massive open online courses, where students expect feedback for their writing assignments.

In this article, the use of language processing techniques for the evaluation of essay assignments is considered. We aimed to develop a fast automatic evaluation system by using Turkish natural language processing tools. For that, the Zemberek Turkish natural language processing library by Akın and Akın, developed in 2007, and its modules were utilized for the morphological analysis of essays written in Turkish. However, since prose evaluation is more than a count of a spelling error, in the frame of the current study, the software was developed for segregating the text assignments.

Thus, the tool serves as an assisting tool for language teachers.

The article is organized as follows. Section 2 starts with an overview of essay grading techniques and software. After that, the methodology, utilized in the current work is described along with materials. Results are presented in Section 4.Section 5 concludes the work.

## 2. Related works

An essay evaluation program was first proposed in 1966 by Page [14, 15]. The author proposed to grade essays in two dimensions – by analyzing content and writing style. In order to predict an essay grading, initially, 272 essays were evaluated by four independent instructors. Next, the text features such as number of words, number of parts of speech or length of words of the essays were extracted and analyzed by a multiple regression method. Finally, a multivariate relationship between human and machine evaluations was analyses to make essay grading more accurate. With the development of computer science, this approach was further modified by the author by adding grammar checking, dictionaries, tagger and parsers [16].

As for the practical implementation of essay grading software, Shermis et al. proposed a web-system, which served for placement tests for English learners by extending the idea by Page et al. in 1997 [17]. The system was tested based on the work of 807 students' text assignments. The results of the study suggested that computer evaluation was as accurate, as that of humans [20].

In 2003, Burstein et al. [6] also proposed an online application consisting of two components, an essay scoring component, and a writing analysis tool. The scoring component was built using content vector analysis while the writing analysis part utilized NLP and statistical machine learning techniques. The evaluation was done based on the grammar, repetition of word usage and disclosure structures. As early essay evaluation was mostly based on spelling error count, Schraudner proposed to correct students' errors by collecting students' assignments using Google forms, which were further analyzed using three different online services for correcting grammar errors [19].

However, later works in this field are done using achievements in machine learning. For example, the automated essay scoring system, proposed by Taghipour and Ng in 2016 utilizes recurrent neural networks [22]. Zupanc and Bosnić in 2017 proposed a system that increases the evaluation accuracy by enhancing the semantic scoring [26]. Thus, as can be seen, mostly algorithms that serve as a basis for written task evaluation are based on partitioning and putting prose into some framework [20]. Thus, the correct partitioning can serve as a good basis for the further text assignment evaluation system.

## 3. Materials and methodology

### *3.1. Materials and Workflow*

The system has been developed in NetBeans development environment using Java programming language. In addition, for the language processing, Morphology, Tokenization and Normalization modules of Zemberek Turkish natural language processing framework by Akın and Akın, developed in 2007 [1] was utilized. The choice of these modules was due to a task that was aimed while developing the software.

For the evaluation, first, the text is divided into sentences by the Tokenization module and the incorrect usage within the sentence is corrected with the Normalization module. However, before normalization, these usages are counted, and the number of errors is displayed in an output file. Then, all the elements of the sentence are separated using the Morphology module; the following morphological outputs are determined:

- the morphological output of the vocabulary used in the text;
- morphological word wealth (parts of spech);
- use of indicative moods (tenses);
- use of subjunctive moods;
- the total number of sentences used;
- the total number of words used.

The choice of outputs was due to the scaling used by the language preparatory school. However, since some evaluation scales such as relevance or redundancy of words and sentences or disclosure of the topic of the essay could not be implemented, the list of outputs was limited to the above measurements. Yet, the keywords entered by the instructor can be identified in the list of vocabulary knowledge obtained as a result of these processes.

In addition, to detect incorrect spelling of words in the text the Turkish Spell Checker method within the normalization module was utilized. The data obtained here is saved in the Excel file format using the Apache POI application programming interface.

### *3.2. Research Hypotheses and Questions*

As was mentioned above, the project aimed to develop an essay evaluation software that could assist language instructors in the evaluation of essay assignments. However, to be able to build a system that would have a high accuracy in the essay grading, the proper component extraction is needed. Therefore, in the scope of current work, the text

feature extraction was carried out. While designing the tool, the following research questions were formulated:

1. What are the specific criteria for essay evaluation?
2. What methods of natural language processing can be used for essay evaluation?
3. What barriers does one face while using Turkish natural language processing methods?

In the current study, the first research question was considered. However, results obtained by answering the first research question would shed a light to the hypotheses for further works formulated as follows:

1. By evaluating the essay assignment of the language learners, an instructor can comment on how much the student mastered the subject based on the use (or disuse) of keywords, provided by the instructor.
2. By evaluating the essay assignment of the language learners, an instructor can determine exactly where the student has deficiencies in language learning through the spelling errors that the student has made repeatedly.
3. By evaluating the essay assignment of the language learners, an instructor can measure by how many different words the student can express himself/herself and measure the sufficiency of the vocabulary wealth on the given subject. In addition, these words can be analyzed morphologically by counting the number of nouns, verbs, adjectives and so on. Thus, the morphological correctness of sentences can be observed.
4. Since in the Turkish language, multiple, recursively addable derivational suffixes are used for word formation, by determining the modalities of indicative moods and subjunctive moods usage in the Turkish language, an instructor can measure how many moods the student can use while writing an essay in Turkish and the ability to use certain Turkish suffixes.
5. Comparing the total number of unique words that a student used in an essay with the total number of words used, an instructor can measure whether the student constantly makes statements using the same words.

The system, developed in the frame of the current study, provides a technical background to estimating these hypotheses.

## 4. Results

The software, developed for essay feature extraction, works on a base of written assignments. The developed tool takes as input files in XML format. Thus, for essay submission, the special text editor was developed, where essays are recorded in XML file format. In addition, the system allows the instructor (or system administrator) to include several essays (files) and keywords in the main program as well (Fig. 1).

The results of the essay evaluation are recorded in the Excel file format. The system separates each submission by recording them in separate rows, thus, several files can be graded simultaneously. However, although the feature extraction is done for each file (essay) separately, an output is provided in a single file, with each essay features in one row. In addition, it is possible to see the program output on the text editor screen as well as demonstrated in Fig. 1

In the Excel file, there are several fields, reflecting identification information such as the student's surname, student ID number; the next sections include information related to the current essay topic in form of several keywords. While extracting features, the program counts keywords' usage by language learners and provides this information to the instructor. Thus, the instructor can check the relevance of the essay to the given topic.

Grammar features of text assignments are provided in the field reflecting spelling errors. Finally, the semantic structure of sentences, used by language learners are given by morphological vocabularies, the number of sentences using indicative moods and subjunctive moods, the total number of words, the total number of sentences and evaluation information, which can be seen in separate rows for each student (Table 1).

.

**Table 1.** *Sample software output in excel format (the simplified transposed form)*

| Name Surname | Student 1 | Student 2 | Student 3 | Student 4 |
|---|---|---|---|---|
| **Student ID** | xxxx.xxxx | xxxx.xxxx | xxxx.xxxx | xxxx.xxxx |
| **Keywords** | gelmek<br>gitmek<br>dil<br>öğrenmek | gelmek<br>gitmek<br>dil<br>öğrenmek | gelmek<br>gitmek<br>dil<br>öğrenmek | gelmek<br>gitmek<br>dil<br>öğrenmek |
| **Spelling errors** | uyanırır,<br>baktığınğz,<br>bakasanız,<br>…<br>Number of errors: 10 | şoyle,<br>büyüklerimzden,<br>soyler,<br>…<br>Number of errors: 14 | Hintler,<br>Çinliler,<br>Amerikalılarla ,<br>…<br>Number of errors: 21 | Bügün,<br>dı,<br>hokabaz,<br>sehitliğe ,<br>…<br>Number of errors: 9 |
| **Morphological Word Wealth** | Nouns: 45<br>Verbs: 33<br>…<br>Unknown: 1 | Nouns: 31<br>Verbs: 24<br>…<br>Unknown : 0 | Nouns: 82<br>Verbs: 49<br>…<br>Unknown: 1 | Nouns: 79<br>Verbs: 63<br>…<br>Unknown: 1 |
| **Vocabulary Wealth** | // unique words listed<br>// number of unique words | | | |
| **indicative moods (tenses)** | // list of moods<br>// the number of sentences in an indicative moods | | | |
| **Subjunctive moods** | // list of moods<br>// the number of sentences in a subjunctive mood | | | |
| **Total Words Used** | 176 | 140 | 432 | 465 |
| **Total Number of Sentences** | 27 | 16 | 67 | 75 |
| **Evaluation** | - | - | - | - |

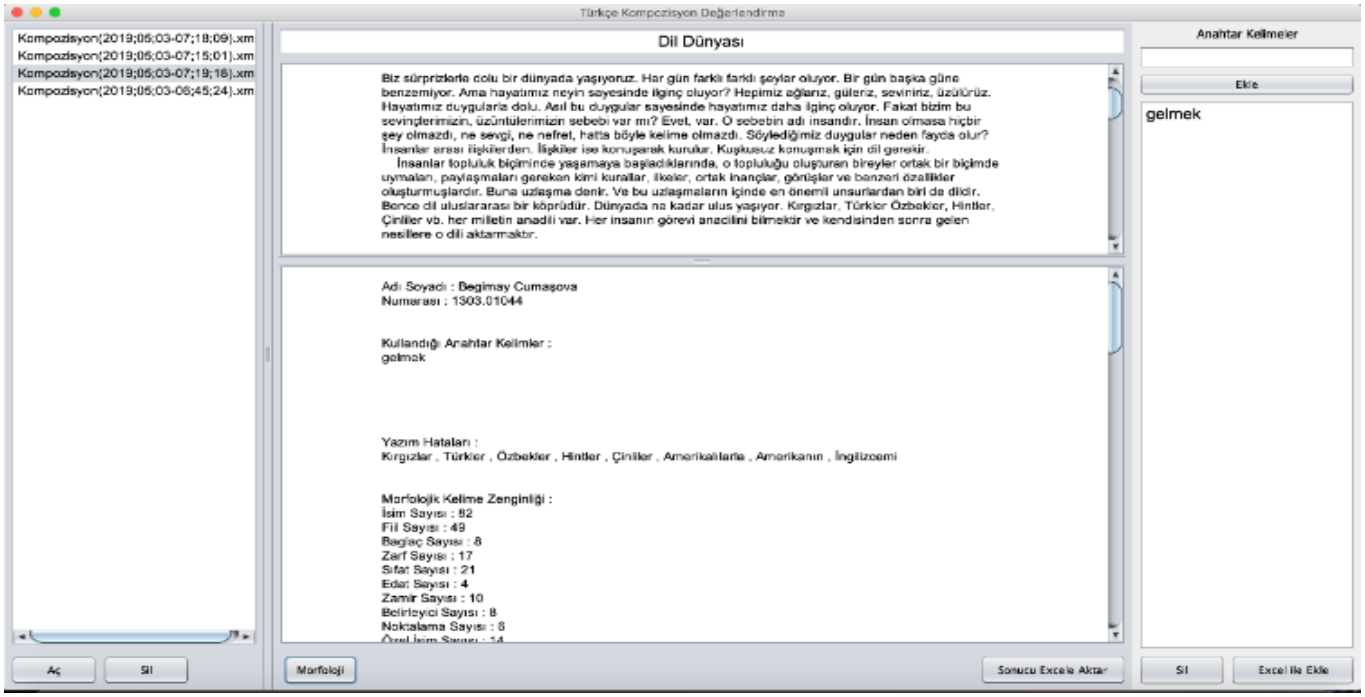


**Figure 1**. *The interface of the feature extraction tool for essay evaluation*

As can be seen from Table 1, an instructor can evaluate how much the student mastered the subject based on the use (or disuse) of keywords. In the output table, the use of keywords is indicated. The spelling errors are also listed.

The semantic structure of sentences is extracted using the Zemberek library, according to which, the count of parts of the speech is carried out. However, despite the normalization process, the proposed system was unable to determine the part of speech of some words. Yet, the success rate was approximately 98%, with maximum 2 words with undefined classification at each of tested essays.

In addition, comparing the total number of unique words that a student used in an essay with the total number of words used, an instructor can measure whether the student constantly makes statements using the same words. In addition, the number of sentences, where the modalities of indicative moods and subjunctive moods were used, allows an instructor to measure how many moods the student can use and the ability to use certain Turkish suffixes.

## 5. Conclusion

In this work, we present a simple tool that can help teachers to evaluate students' essays. Although there are studies in the field of Turkish natural language processing, there is no study such as the evaluation of an essay written by Turkish language learners with natural language processing methods. As mentioned before, at the current stage of natural language processing techniques, it is infeasible to implement some text evaluation measurements. Instead, as many works suggest, for further implementation of statistical machine learning techniques, it is necessary to extract text features. Therefore, in current work, in addition to assisting language instructors, the list of essay evaluation scales was proposed and software was developed to extract these features. Yet, the list of features was limited to six measurements.

The limitation of the current work is that some evaluation scales such as relevance or redundancy of words and sentences or disclosure of the topic of the essay were not implemented. The difficulty of this task was widely discussed in the literature. Yet, as mentioned above, in the scope of the current work, the attempt to solve this issue was done by counting usage of keywords, provided by language instructor for a given topic.

Nevertheless, these measurements can more or less predict the grade given to an essay. Therefore, as future work, it is planned to use the developed software and extracted text features for building a model for automatic essay evaluation using machine learning techniques.

## References

[1]. Akın A.A., Akın M.D. “Zemberek, an open-source NLP framework for Turkic languages”, Structure, 10, (2007), 1-5.

[2]. Bahdanau D., Cho K., Bengio Y. “Neural machine translation by jointly learning to align and translate”, arXiv preprint arXiv:1409.0473, (2014).

[3]. Bird S., Klein E., Loper E. “Natural language processing with Python: analyzing text with the natural language toolkit”, Sebastopol: O'Reilly Media, Inc., (2009).

[4]. Brants T., Popat A.C., Xu P., Och F.J., Dean J. “Large language models in machine translation”, In Proceedings of the 2007 Joint Conference on Empirical Methods in Natural Language Processing and Computational Natural Language Learning (EMNLP-CoNLL), (2007, June), 858-867.

[5]. Brown P.F., Desouza P.V., Mercer R.L., Pietra V.J. D., Lai J.C., “Class-based n-gram models of natural language”, Computational linguistics, 18(4), (1992), 467-479.

[6]. Burstein J., Chodorow M., Leacock C. “CriterionSM Online Essay Evaluation: An Application for Automated Evaluation of Student Essays”, In IAAI, (2003, August), 3-10.

[7]. Cavnar W.B., Trenkle, J.M. “N-gram-based text categorization”, In Proceedings of SDAIR-94, 3rd annual symposium on document analysis and information retrieval, Vol. 161175, (1994, April).

[8]. Chowdhury G.G. Natural language processing”, Annual review of information science and technology, 37(1), (2003), 51-89.

[9]. Collobert R., Weston J. “A unified architecture for natural language processing: Deep neural networks with multitask learning”, In Proceedings of the 25th international conference on Machine learning. ACM, (2008, July), 160-167.

[10]. Goyal A., Jagarlamudi J. Daumé III, H., & Venkatasubramanian, S. “Sketching techniques for large scale NLP”, In Proceedings of the NAACL HLT 2010 Sixth Web as Corpus Workshop, (2010, June), 17-25. Association for Computational Linguistics.

[11]. Habash N.Y. “Introduction to Arabic natural language processing”, Synthesis Lectures on Human Language Technologies, 3(1), (2010), 1-187.

[12]. Khreisat L. “A machine learning approach for Arabic text classification using N-gram frequency statistics”, Journal of Informetrics, 3(1), (2009), 72-77.

[13]. Koehn P., Hoang H., Birch A., Callison-Burch C., Federico M., Bertoldi N., Cowan B., Shen W., Moran

Ch., Zens R., Dyer Ch., Bojar O., Constantin A., Herbst E. “Moses: Open source toolkit for statistical machine translation”, In Proceedings of the 45th annual meeting of the association for computational linguistics companion volume proceedings of the demo and poster sessions, (2007, June), 177-180.

[14]. Page E.B. “The imminence of... grading essays by computer”, The Phi Delta Kappan, 47(5), (1966), 238-243.

[15]. Page E.B. “Grading essays by computer: Progress report”, In Proceedings of the Invitational Conference on Testing Problems, (1967).

[16]. Page E.B. “Computer grading of student prose, using modern concepts and software”, The Journal of experimental education, 62(2), (1994), 127-142.

[17]. Page E.B. Poggio, J. P., Keith, T. Z., “Computer analysis of student essays: Finding trait differences in the student profile”, Paper presented at the annual meeting of the American Educational Research Association, Chicago, (1997, March).

[18]. Papineni K., Roukos S., Ward, T., Zhu W.J., “BLEU: a method for automatic evaluation of machine translation“, In Proceedings of the 40th annual meeting on association for computational linguistics, (2002, July), 311-318. Association for Computational Linguistics.

[19]. Schraudner M. “The online teacher’s assistant: Using automated correction programs to supplement learning and lesson planning”, CELE Journal, 22, (2014), 128-140.

[20]. Shermis M.D., Koch C.M., Page E.B., Keith T.Z., Harrington S. “Trait ratings for automated essay grading“, Educational and Psychological Measurement, 62(1), (2002), 5-18.

[21]. Stenetorp P., Pyysalo S., Topić G., Ohta T., Ananiadou S., Tsujii J.I. “BRAT: a web-based tool for NLP-assisted text annotation”, In Proceedings of the Demonstrations at the 13th Conference of the European Chapter of the Association for Computational Linguistics, (2012, April), 102-107. Association for Computational Linguistics.

[22]. Taghipour K., Ng H.T. “A neural approach to automated essay scoring”, In Proceedings of the 2016 Conference on Empirical Methods in Natural Language Processing, (2016, November), 1882-1891.

[23]. Tayirova N., Tekerek M., Brimkulov U. “Statistical machine translation implementation and performance tests between Kyrgyz and Turkish Languages”, MANAS Journal of Engineering, 3 (2), (2015), 59-68.

[24]. Tyers F.M., Alperen M.S. “South-east European times: A parallel corpus of Balkan languages”, In Proceedings of the LREC Workshop on Exploitation of Multilingual Resources and Tools for Central and (South-) Eastern European Languages, (2010), 49-53.

[25]. Van Ewijk R. “Same work, lower grade? Student ethnicity and teachers’ subjective assessments”, Economics of Education Review, 30(5), (2011), 1045-1058.

[26]. Zupanc K., Bosnić Z. “Automated essay evaluation with semantic analysis”, Knowledge-Based Systems, 120, (2017), 118-132

.

Manas Journal of Engineering
ISSN 1694-7398 | e-ISSN 1694-7398

*Volume 7 (Issue 2) (2019) Pages 147-156*

# On the recursive sequence $x_{n+1}=\dfrac{x_{n-20}}{1+x_{n-2}x_{n-5}x_{n-8}x_{n-11}x_{n-14}x_{n-17}}$

Dağıstan Şimşek[1], Burak Oğul[2,*]

[1]Konya Technical University, Faculty of Engineering and Natural Sciences, Department of Industrial Engineering, Konya, Turkey, dsimsek@ktun.edu.tr

[2]Kyrgyz Turkish Manas University, Graduate School of Natural Sciences, Bishkek, Kyrgyzstan, burak_1745@hotmail.com, ORCID: 0000-0002-3264-4340

**ABSTRACT**

The behaivour of the solutions of the following system of difference equations is examined,

$$x_{n+1}=\frac{x_{n-20}}{1+x_{n-2}x_{n-5}x_{n-8}x_{n-11}x_{n-14}x_{n-17}},$$

where the initial conditions are positive real numbers. The initial conditions of the equation are arbitrary positive real numbers. Also, we discuss and illustrate the stability of the solutions in the neighborhood of the critical points and the periodicity of the considered equations.

**ARTICLE INFO**

***Research article***

*Received: 28.02.2019*
*Accepted: 15.10.2019*

***Keywords:***
*Difference equation recursive sequence, semicycle*

**Corresponding author*

## 1. Introduction

Recently there has been a lot of interest in studying the global attractivity, boundedness character, periodicity and the solution form of nonlinear difference equations. For some results in this area, for example: [1-40].
Elabbasy et al. [8-9] investigated the global stability, periodicity character and gave the solution of some special cases of the following difference equations

$$x_{n+1}=ax_n-\frac{bx_n}{cx_n-dx_{n-1}},\quad x_{n+1}=\frac{\alpha x_{n-k}}{\beta+\gamma\prod_{i=0}^{k}x_{n-i}}.$$

In [13] Elsayed dealed with the dynamics and found the solution of the following rational recursive sequences

$$x_{n+1}=\frac{x_{n-5}}{\pm1\pm x_{n-1}x_{n-3}x_{n-5}}.$$

Simsek et. al. [28,29,30,33], studied the following problems with positive initial values

$$x_{n+1}=\frac{x_{n-3}}{1+x_{n-1}},\quad x_{n+1}=\frac{x_{n-5}}{1+x_{n-2}},\quad x_{n+1}=\frac{x_{n-5}}{1+x_{n-1}x_{n-3}},\quad x_{n+1}=\frac{x_{n-3}}{1+x_nx_{n-1}x_{n-2}}$$

respectively.

In this work the following non linear difference equation was studied

$$x_{n+1}=\frac{x_{n-20}}{1+x_{n-2}x_{n-5}x_{n-8}x_{n-11}x_{n-14}x_{n-17}} \tag{1}$$

where $x_{-20},x_{-19},...,x_{-1},x_0\in(0,\infty)$ is investigated.

## 2. Main results

Let $\overline{x}$ be the unique positive equilibrium of the equation (1), then clearly

$$\overline{x}=\frac{\overline{x}}{1+\overline{xxxxxx}}\Rightarrow\overline{x}+\overline{x}^7=\overline{x}\Rightarrow\overline{x}^7=0\Rightarrow\overline{x}=0$$

so, $\overline{x}=0$ can be obtained.
For any $k\geq 0$ and $m>k$ notation $i=\overline{k,m}$ means $i=k,k+1,...,m$.

**Theorem 1:** Consider the difference equation (1). Then the following statements are true.

a) The sequences

$$\left(x_{21n-20}\right),\left(x_{21n-19}\right),\ldots,\left(x_{21n-1}\right),\left(x_{21n}\right)$$

are being decreasing and

$$a_1,a_2,\ldots,a_{20},a_{21}\geq 0$$

are existed and such that

$$\lim_{n\to\infty}x_{21n-20+k}=a_{1+k}\ \text{ for }\ k=\overline{0,20}.$$

b) $\left(a_1,a_2,a_3,a_4,a_5,a_6,a_7,a_8,a_9,a_{10},a_{11},a_{12},a_{13},a_{14},a_{15},a_{16},a_{17},a_{18},a_{19},a_{20},a_{21},...\right)$ is a solution of Eq. (1) having period 21.

c) $\prod_{k=0}^{6}\lim_{n\to\infty}x_{21n-20-j+3k}=0,\ j=\overline{0,2}$ or $\prod_{k=0}^{6}a_{3k+i}=0,\ i=\overline{1,3}$.

d) If there exist $n_0\in\mathbb{N}$ such that $x_{n-17}\geq x_{n+1}$ for all $n\geq n_0$, then

$$\lim_{n\to\infty}x_n=0.$$

e) The following formulas below are

$$x_{21n+1+k}=x_{-20+k}\left(1-\frac{x_{-2+k}x_{-5+k}x_{-8+k}x_{-11+k}x_{-14+k}x_{-17+k}}{1+x_{-2+k}x_{-5+k}x_{-8+k}x_{-11+k}x_{-14+k}x_{-17+k}}\sum_{j=0}^{n}\prod_{i=1}^{7j}\frac{1}{1+x_{3i-17+k}x_{3i-14+k}x_{3i-11+k}x_{3i-8+k}x_{3i-5+k}x_{3i-2+k}}\right),$$

$$x_{21n+4+k}=x_{-17+k}\left(1-\frac{x_{-2+k}x_{-5+k}x_{-8+k}x_{-11+k}x_{-14+k}x_{-20+k}}{1+x_{-2+k}x_{-5+k}x_{-8+k}x_{-11+k}x_{-14+k}x_{-17+k}}\sum_{j=0}^{n}\prod_{i=1}^{7j+1}\frac{1}{1+x_{3i-17+k}x_{3i-14+k}x_{3i-11+k}x_{3i-8+k}x_{3i-5+k}x_{3i-2+k}}\right),$$

$$x_{21n+7+k}=x_{-14+k}\left(1-\frac{x_{-2+k}x_{-5+k}x_{-8+k}x_{-11+k}x_{-17+k}x_{-20+k}}{1+x_{-2+k}x_{-5+k}x_{-8+k}x_{-11+k}x_{-14+k}x_{-17+k}}\sum_{j=0}^{n}\prod_{i=1}^{7j+2}\frac{1}{1+x_{3i-17+k}x_{3i-14+k}x_{3i-11+k}x_{3i-8+k}x_{3i-5+k}x_{3i-2+k}}\right),$$

$$x_{21n+10+k}=x_{-11+k}\left(1-\frac{x_{-2+k}x_{-5+k}x_{-8+k}x_{-14+k}x_{-17+k}x_{-20+k}}{1+x_{-2+k}x_{-5+k}x_{-8+k}x_{-11+k}x_{-14+k}x_{-17+k}}\sum_{j=0}^{n}\prod_{i=1}^{7j+3}\frac{1}{1+x_{3i-17+k}x_{3i-14+k}x_{3i-11+k}x_{3i-8+k}x_{3i-5+k}x_{3i-2+k}}\right),$$

$$x_{21n+13+k}=x_{-8+k}\left(1-\frac{x_{-2+k}x_{-5+k}x_{-11+k}x_{-14+k}x_{-17+k}x_{-20+k}}{1+x_{-2+k}x_{-5+k}x_{-8+k}x_{-11+k}x_{-14+k}x_{-17+k}}\sum_{j=0}^{n}\prod_{i=1}^{7j+4}\frac{1}{1+x_{3i-17+k}x_{3i-14+k}x_{3i-11+k}x_{3i-8+k}x_{3i-5+k}x_{3i-2+k}}\right),$$

$$x_{21n+16+k}=x_{-5+k}\left(1-\frac{x_{-2+k}x_{-8+k}x_{-11+k}x_{-14+k}x_{-17+k}x_{-20+k}}{1+x_{-2+k}x_{-5+k}x_{-8+k}x_{-11+k}x_{-14+k}x_{-17+k}}\sum_{j=0}^{n}\prod_{i=1}^{7j+5}\frac{1}{1+x_{3i-17+k}x_{3i-14+k}x_{3i-11+k}x_{3i-8+k}x_{3i-5+k}x_{3i-2+k}}\right),$$

$$x_{21n+19+k}=x_{-2+k}\left(1-\frac{x_{-5+k}x_{-8+k}x_{-11+k}x_{-14+k}x_{-17+k}x_{-20+k}}{1+x_{-2+k}x_{-5+k}x_{-8+k}x_{-11+k}x_{-14+k}x_{-17+k}}\sum_{j=0}^{n}\prod_{i=1}^{7j+6}\frac{1}{1+x_{3i-17+k}x_{3i-14+k}x_{3i-11+k}x_{3i-8+k}x_{3i-5+k}x_{3i-2+k}}\right),$$

$k=\overline{0,2}$ holds.

f) If $x_{21n+1+k}\to a_{1+k}\neq 0$, $x_{21n+4+k}\to a_{4+k}\neq 0$, $x_{21n+7+k}\to a_{7+k}\neq 0$, $x_{21n+10+k}\to a_{10+k}\neq 0$, $x_{21n+13+k}\to a_{13+k}\neq 0$, $x_{21n+16+k}\to a_{16+k}\neq 0$ then $x_{21n+19+k}\to a_{19+k}=0$ as $n\to\infty$. $k=\overline{0,2}$.

**Proof**

a) Firstly, from the (1)

b)

$$x_{n+1}\left(1+x_{n-2}x_{n-5}x_{n-8}x_{n-11}x_{n-14}x_{n-17}\right)=x_{n-20}$$

is obtained. If $x_{n-2}x_{n-5}x_{n-8}x_{n-11}x_{n-14}x_{n-17}\in(0,\infty)$, then $1+x_{n-2}x_{n-5}x_{n-8}x_{n-11}x_{n-14}x_{n-17}\in(1,\infty)$. Since

$$x_{n+1}<x_{n-20},$$

$n\in\mathbb{N}$,

$$\lim_{n\to\infty}x_{21n-20+k}=a_{1+k},\ \text{for}\ k=\overline{0,20}$$

existed formulas are obtained.

c) $(a_1,a_2,a_3,a_4,a_5,a_6,a_7,a_8,a_9,a_{10},a_{11},a_{12},a_{13},a_{14},a_{15},a_{16},a_{17},a_{18},a_{19},a_{20},a_{21},...)$ is a solution of (1) having period 21.

d) In wiew of (1),

$$n=21n\Rightarrow x_{21n+1}=\frac{x_{21n-20}}{1+\prod_{k=0}^{5}x_{21n-17+3k}}$$

is obtained. If the limits are put on both sides of the above equality,

$$\prod_{k=0}^{6}\lim_{n\to\infty}x_{21n-20+3k}=0\ \text{ or }\ \prod_{k=0}^{6}a_{3k+1}=0$$

is obtained. Similarly for $n=21n+1$ and $n=21n+2$, we can obtain $x_{21n+2}$ and $x_{21n+3}$.

e) If there exist $n_0\in\mathbb{N}$ such that $x_{n-17}\geq x_{n+1}$ for all $n\geq n_0$, then,

$a_1\leq a_4\leq a_7\leq a_{10}\leq a_{13}\leq a_{16}\leq a_{19}\leq a_1$, $a_2\leq a_5\leq a_8\leq a_{11}\leq a_{14}\leq a_{17}\leq a_{20}\leq a_2$, $a_3\leq a_6\leq a_9\leq a_{12}\leq a_{15}\leq a_{18}\leq a_{21}\leq a_3$.

Using (c), we get

$$\prod_{k=0}^{6}a_{3k+i}=0,\ i=\overline{1,3}.$$

Then we see that

$$\lim_{n\to\infty} x_n = 0 .$$

Hence the proof of (d) completed.

f) Subracting $x_{n-20}$ from the left and right-hand sides in (1)

$$x_{n+1} - x_{n-20} = \frac{1}{1 + x_{n-2}x_{n-5}x_{n-8}x_{n-11}x_{n-14}x_{n-20}}\left(x_{n-1} - x_{n-22}\right)$$

and the following formula

$$n \geq 3 \text{ for } \begin{cases} x_{3n-8} - x_{3n-29} = \left(x_1 - x_{-20}\right)\prod_{i=1}^{n-3} \frac{1}{1 + x_{3i-2}x_{3i-5}x_{3i-8}x_{3i-11}x_{3i-14}x_{3i-17}} \\ x_{3n-7} - x_{3n-28} = \left(x_2 - x_{-19}\right)\prod_{i=1}^{n-3} \frac{1}{1 + x_{3i-1}x_{3i-4}x_{3i-7}x_{3i-10}x_{3i-13}x_{3i-16}} \\ x_{3n-6} - x_{3n-27} = \left(x_3 - x_{-18}\right)\prod_{i=1}^{n-3} \frac{1}{1 + x_{3i}x_{3i-3}x_{3i-6}x_{3i-9}x_{3i-12}x_{3i-15}} \end{cases} \tag{2}$$

hold. Replacing n by 7j in (2) and summing from $j = 0$ to $j = n$, we obtain:

$$x_{21n+1+k} - x_{-20+k} = \left(x_{1+k} - x_{-20+k}\right)\sum_{j=0}^{n}\prod_{i=1}^{7j} \frac{1}{1 + x_{3i-2+k}x_{3i-5+k}x_{3i-8+k}x_{3i-11+k}x_{3i-14+k}x_{3i-17+k}}, \; k = \overline{0,2}$$

Also, $7j+1$ inserted in (2) by replacing $n$, $j = 0$ to $j = n$ is obtained by summing

$$x_{21n+4+k} - x_{-17+k} = \left(x_{4+k} - x_{-17+k}\right)\sum_{j=0}^{n}\prod_{i=1}^{7j+1} \frac{1}{1 + x_{3i-2+k}x_{3i-5+k}x_{3i-8+k}x_{3i-11+k}x_{3i-14+k}x_{3i-17+k}}, \; k = \overline{0,2}$$

Also, $7j+2$ inserted in (2) by replacing $n$, $j = 0$ to $j = n$ is obtained by summing

$$x_{21n+7+k} - x_{-14+k} = \left(x_{7+k} - x_{-14+k}\right)\sum_{j=0}^{n}\prod_{i=1}^{7j+2} \frac{1}{1 + x_{3i-2+k}x_{3i-5+k}x_{3i-8+k}x_{3i-11+k}x_{3i-14+k}x_{3i-17+k}}, \; k = \overline{0,2}.$$

Also, $7j+3$ inserted in (2) by replacing $n$, $j = 0$ to $j = n$ is obtained by summing

$$x_{21n+10+k} - x_{-11+k} = \left(x_{10+k} - x_{-11+k}\right)\sum_{j=0}^{n}\prod_{i=1}^{7j+3} \frac{1}{1 + x_{3i-2+k}x_{3i-5+k}x_{3i-8+k}x_{3i-11+k}x_{3i-14+k}x_{3i-17+k}}, \; k = \overline{0,2}.$$

Also, $7j+4$ inserted in (2) by replacing $n$, $j = 0$ to $j = n$ is obtained by summing

$$x_{21n+13+k} - x_{-8+k} = \left(x_{13+k} - x_{-8+k}\right)\sum_{j=0}^{n}\prod_{i=1}^{7j+4} \frac{1}{1 + x_{3i-2+k}x_{3i-5+k}x_{3i-8+k}x_{3i-11+k}x_{3i-14+k}x_{3i-17+k}}, \; k = \overline{0,2}.$$

Also, $7j+5$ inserted in (2) by replacing $n$, $j = 0$ to $j = n$ is obtained by summing

$$x_{21n+16+k}-x_{-5+k}=\left(x_{16+k}-x_{-5+k}\right)\sum_{j=0}^{n}\prod_{i=1}^{7j+5}\frac{1}{1+x_{3i-2+k}x_{3i-5+k}x_{3i-8+k}x_{3i-11+k}x_{3i-14+k}x_{3i-17+k}},\ k=\overline{0,2}.$$

Also, $7j+6$ inserted in (2) by replacing $n$, $j=0$ to $j=n$ is obtained by summing

$$x_{21n+19+k}-x_{-2+k}=\left(x_{19+k}-x_{-2+k}\right)\sum_{j=0}^{n}\prod_{i=1}^{7j+6}\frac{1}{1+x_{3i-2+k}x_{3i-5+k}x_{3i-8+k}x_{3i-11+k}x_{3i-14+k}x_{3i-17+k}},\ k=\overline{0,2}.$$

Now we obtained of the above formulas:

$$x_{21n+k+1}=x_{-20+k}\left(1-\frac{x_{-2+k}x_{-5+k}x_{-8+k}x_{-11+k}x_{-14+k}x_{-17+k}}{1+x_{-2+k}x_{-5+k}x_{-8+k}x_{-11+k}x_{-14+k}x_{-17+k}}\sum_{j=0}^{n}\prod_{i=1}^{7j}\frac{1}{1+x_{3i-17+k}x_{3i-14+k}x_{3i-11+k}x_{3i-8+k}x_{3i-5+k}x_{3i-2+k}}\right),$$

$$x_{21n+4+k}=x_{-17+k}\left(1-\frac{x_{-2+k}x_{-5+k}x_{-8+k}x_{-11+k}x_{-14+k}x_{-20+k}}{1+x_{-2+k}x_{-5+k}x_{-8+k}x_{-11+k}x_{-14+k}x_{-17+k}}\sum_{j=0}^{n}\prod_{i=1}^{7j+1}\frac{1}{1+x_{3i-17+k}x_{3i-14+k}x_{3i-11+k}x_{3i-8+k}x_{3i-5+k}x_{3i-2+k}}\right),$$

$$x_{21n+7+k}=x_{-14+k}\left(1-\frac{x_{-2+k}x_{-5+k}x_{-8+k}x_{-11+k}x_{-17+k}x_{-20+k}}{1+x_{-2+k}x_{-5+k}x_{-8+k}x_{-11+k}x_{-14+k}x_{-17+k}}\sum_{j=0}^{n}\prod_{i=1}^{7j+2}\frac{1}{1+x_{3i-17+k}x_{3i-14+k}x_{3i-11+k}x_{3i-8+k}x_{3i-5+k}x_{3i-2+k}}\right),$$

$$x_{21n+10+k}=x_{-11+k}\left(1-\frac{x_{-2+k}x_{-5+k}x_{-8+k}x_{-14+k}x_{-17+k}x_{-20+k}}{1+x_{-2+k}x_{-5+k}x_{-8+k}x_{-11+k}x_{-14+k}x_{-17+k}}\sum_{j=0}^{n}\prod_{i=1}^{7j+3}\frac{1}{1+x_{3i-17+k}x_{3i-14+k}x_{3i-11+k}x_{3i-8+k}x_{3i-5+k}x_{3i-2+k}}\right),$$

$$x_{21n+13+k}=x_{-8+k}\left(1-\frac{x_{-2+k}x_{-5+k}x_{-11+k}x_{-14+k}x_{-17+k}x_{-20+k}}{1+x_{-2+k}x_{-5+k}x_{-8+k}x_{-11+k}x_{-14+k}x_{-17+k}}\sum_{j=0}^{n}\prod_{i=1}^{7j+4}\frac{1}{1+x_{3i-17+k}x_{3i-14+k}x_{3i-11+k}x_{3i-8+k}x_{3i-5+k}x_{3i-2+k}}\right),$$

$$x_{21n+16+k}=x_{-5+k}\left(1-\frac{x_{-2+k}x_{-8+k}x_{-11+k}x_{-14+k}x_{-17+k}x_{-20+k}}{1+x_{-2+k}x_{-5+k}x_{-8+k}x_{-11+k}x_{-14+k}x_{-17+k}}\sum_{j=0}^{n}\prod_{i=1}^{7j+5}\frac{1}{1+x_{3i-17+k}x_{3i-14+k}x_{3i-11+k}x_{3i-8+k}x_{3i-5+k}x_{3i-2+k}}\right),$$

$$x_{21n+19+k}=x_{-2+k}\left(1-\frac{x_{-5+k}x_{-8+k}x_{-11+k}x_{-14+k}x_{-17+k}x_{-20+k}}{1+x_{-2+k}x_{-5+k}x_{-8+k}x_{-11+k}x_{-14+k}x_{-17+k}}\sum_{j=0}^{n}\prod_{i=1}^{7j+6}\frac{1}{1+x_{3i-17+k}x_{3i-14+k}x_{3i-11+k}x_{3i-8+k}x_{3i-5+k}x_{3i-2+k}}\right),\ k=\overline{0,2}\ \text{holds.}$$

g) Suppose that $a_1=a_4=a_7=a_{10}=a_{13}=a_{16}=a_{19}=0$. By e) we have

$$\lim_{n\to\infty}x_{21n+1}=\lim_{n\to\infty}x_{-20}\left(1-\frac{x_{-2}x_{-5}x_{-8}x_{-11}x_{-14}x_{-17}}{1+x_{-2}x_{-5}x_{-8}x_{-11}x_{-14}x_{-17}}\sum_{j=0}^{n}\prod_{i=1}^{7j}\frac{1}{1+x_{3i-17}x_{3i-14}x_{3i-11}x_{3i-8}x_{3i-5}x_{3i-2}}\right)$$

$$a_1=x_{-20}\left(1-\frac{x_{-2}x_{-5}x_{-8}x_{-11}x_{-14}x_{-17}}{1+x_{-2}x_{-5}x_{-8}x_{-11}x_{-14}x_{-17}}\sum_{j=0}^{\infty}\prod_{i=1}^{7j}\frac{1}{1+x_{3i-17}x_{3i-14}x_{3i-11}x_{3i-8}x_{3i-5}x_{3i-2}}\right)$$

$$a_1=0\Rightarrow\frac{1+x_{-2}x_{-5}x_{-8}x_{-11}x_{-14}x_{-17}}{x_{-2}x_{-5}x_{-8}x_{-11}x_{-14}x_{-17}}=\sum_{j=0}^{\infty}\prod_{i=1}^{7j}\frac{1}{1+x_{3i-17}x_{3i-14}x_{3i-11}x_{3i-8}x_{3i-5}x_{3i-2}}\qquad(3)$$

Similarly;
$$a_4=0\Rightarrow\frac{1+x_{-2}x_{-5}x_{-8}x_{-11}x_{-14}x_{-17}}{x_{-2}x_{-5}x_{-8}x_{-11}x_{-14}x_{-20}}=\sum_{j=0}^{\infty}\prod_{i=1}^{7j+1}\frac{1}{1+x_{3i-17}x_{3i-14}x_{3i-11}x_{3i-8}x_{3i-5}x_{3i-2}}\qquad(4)$$

Similarly;
$$a_7=0\Rightarrow\frac{1+x_{-2}x_{-5}x_{-8}x_{-11}x_{-14}x_{-17}}{x_{-2}x_{-5}x_{-8}x_{-11}x_{-17}x_{-20}}=\sum_{j=0}^{\infty}\prod_{i=1}^{7j+2}\frac{1}{1+x_{3i-17}x_{3i-14}x_{3i-11}x_{3i-8}x_{3i-5}x_{3i-2}}\qquad(5)$$

Similarly;
$$a_{10}=0\Rightarrow\frac{1+x_{-2}x_{-5}x_{-8}x_{-11}x_{-14}x_{-17}}{x_{-2}x_{-5}x_{-8}x_{-14}x_{-17}x_{-20}}=\sum_{j=0}^{\infty}\prod_{i=1}^{7j+3}\frac{1}{1+x_{3i-17}x_{3i-14}x_{3i-11}x_{3i-8}x_{3i-5}x_{3i-2}}\qquad(6)$$

Similarly;
$$a_{13}=0\Rightarrow\frac{1+x_{-2}x_{-5}x_{-8}x_{-11}x_{-14}x_{-17}}{x_{-2}x_{-5}x_{-11}x_{-14}x_{-17}x_{-20}}=\sum_{j=0}^{\infty}\prod_{i=1}^{7j+4}\frac{1}{1+x_{3i-17}x_{3i-14}x_{3i-11}x_{3i-8}x_{3i-5}x_{3i-2}} \tag{7}$$

Similarly;
$$a_{16}=0\Rightarrow\frac{1+x_{-2}x_{-5}x_{-8}x_{-11}x_{-14}x_{-17}}{x_{-2}x_{-8}x_{-11}x_{-14}x_{-17}x_{-20}}=\sum_{j=0}^{\infty}\prod_{i=1}^{7j+5}\frac{1}{1+x_{3i-17}x_{3i-14}x_{3i-11}x_{3i-8}x_{3i-5}x_{3i-2}} \tag{8}$$

Similarly;
$$a_{19}=0\Rightarrow\frac{1+x_{-2}x_{-5}x_{-8}x_{-11}x_{-14}x_{-17}}{x_{-5}x_{-8}x_{-11}x_{-14}x_{-17}x_{-20}}=\sum_{j=0}^{\infty}\prod_{i=1}^{7j+6}\frac{1}{1+x_{3i-17}x_{3i-14}x_{3i-11}x_{3i-8}x_{3i-5}x_{3i-2}} \tag{9}$$

From (3) and (4),
$$\begin{aligned}\frac{1+x_{-2}x_{-5}x_{-8}x_{-11}x_{-14}x_{-17}}{x_{-2}x_{-5}x_{-8}x_{-11}x_{-14}x_{-17}}&=\sum_{j=0}^{\infty}\prod_{i=1}^{7j}\frac{1}{1+x_{3i-17}x_{3i-14}x_{3i-11}x_{3i-8}x_{3i-5}x_{3i-2}}>\\ \frac{1+x_{-2}x_{-5}x_{-8}x_{-11}x_{-14}x_{-17}}{x_{-2}x_{-5}x_{-8}x_{-11}x_{-14}x_{-20}}&=\sum_{j=0}^{\infty}\prod_{i=1}^{7j+1}\frac{1}{1+x_{3i-17}x_{3i-14}x_{3i-11}x_{3i-8}x_{3i-5}x_{3i-2}}\end{aligned} \tag{10}$$

thus, $x_{-20}>x_{-17}$. From the (4) and (5),
$$\begin{aligned}\frac{1+x_{-2}x_{-5}x_{-8}x_{-11}x_{-14}x_{-17}}{x_{-2}x_{-5}x_{-8}x_{-11}x_{-14}x_{-20}}&=\sum_{j=0}^{\infty}\prod_{i=1}^{7j+1}\frac{1}{1+x_{3i-17}x_{3i-14}x_{3i-11}x_{3i-8}x_{3i-5}x_{3i-2}}>\\ \frac{1+x_{-2}x_{-5}x_{-8}x_{-11}x_{-14}x_{-17}}{x_{-2}x_{-5}x_{-8}x_{-11}x_{-17}x_{-20}}&=\sum_{j=0}^{\infty}\prod_{i=1}^{7j+2}\frac{1}{1+x_{3i-17}x_{3i-14}x_{3i-11}x_{3i-8}x_{3i-5}x_{3i-2}}\end{aligned} \tag{11}$$

thus, $x_{-17}>x_{-14}$. From the (5) and (6),
$$\begin{aligned}\frac{1+x_{-2}x_{-5}x_{-8}x_{-11}x_{-14}x_{-17}}{x_{-2}x_{-5}x_{-8}x_{-11}x_{-17}x_{-20}}&=\sum_{j=0}^{\infty}\prod_{i=1}^{7j+2}\frac{1}{1+x_{3i-17}x_{3i-14}x_{3i-11}x_{3i-8}x_{3i-5}x_{3i-2}}>\\ \frac{1+x_{-2}x_{-5}x_{-8}x_{-11}x_{-14}x_{-17}}{x_{-2}x_{-5}x_{-8}x_{-14}x_{-17}x_{-20}}&=\sum_{j=0}^{\infty}\prod_{i=1}^{7j+3}\frac{1}{1+x_{3i-17}x_{3i-14}x_{3i-11}x_{3i-8}x_{3i-5}x_{3i-2}}\end{aligned} \tag{12}$$

thus, $x_{-14}>x_{-11}$.From the (6) and (7),
$$\begin{aligned}\frac{1+x_{-2}x_{-5}x_{-8}x_{-11}x_{-14}x_{-17}}{x_{-2}x_{-5}x_{-8}x_{-14}x_{-17}x_{-20}}&=\sum_{j=0}^{\infty}\prod_{i=1}^{7j+3}\frac{1}{1+x_{3i-17}x_{3i-14}x_{3i-11}x_{3i-8}x_{3i-5}x_{3i-2}}>\\ \frac{1+x_{-2}x_{-5}x_{-8}x_{-11}x_{-14}x_{-17}}{x_{-2}x_{-5}x_{-11}x_{-14}x_{-17}x_{-20}}&=\sum_{j=0}^{\infty}\prod_{i=1}^{7j+4}\frac{1}{1+x_{3i-17}x_{3i-14}x_{3i-11}x_{3i-8}x_{3i-5}x_{3i-2}}\end{aligned} \tag{13}$$

thus, $x_{-11}>x_{-8}$.From the (7) and (8),
$$\begin{aligned}\frac{1+x_{-2}x_{-5}x_{-8}x_{-11}x_{-14}x_{-17}}{x_{-2}x_{-5}x_{-11}x_{-14}x_{-17}x_{-20}}&=\sum_{j=0}^{\infty}\prod_{i=1}^{7j+4}\frac{1}{1+x_{3i-17}x_{3i-14}x_{3i-11}x_{3i-8}x_{3i-5}x_{3i-2}}>\\ \frac{1+x_{-2}x_{-5}x_{-8}x_{-11}x_{-14}x_{-17}}{x_{-2}x_{-8}x_{-11}x_{-14}x_{-17}x_{-20}}&=\sum_{j=0}^{\infty}\prod_{i=1}^{7j+5}\frac{1}{1+x_{3i-17}x_{3i-14}x_{3i-11}x_{3i-8}x_{3i-5}x_{3i-2}}\end{aligned} \tag{14}$$

thus, $x_{-8}>x_{-5}$.From the (8) and (9),
$$\begin{aligned}\frac{1+x_{-2}x_{-5}x_{-8}x_{-11}x_{-14}x_{-17}}{x_{-2}x_{-8}x_{-11}x_{-14}x_{-17}x_{-20}}&=\sum_{j=0}^{\infty}\prod_{i=1}^{7j+5}\frac{1}{1+x_{3i-17}x_{3i-14}x_{3i-11}x_{3i-8}x_{3i-5}x_{3i-2}}>\\ \frac{1+x_{-2}x_{-5}x_{-8}x_{-11}x_{-14}x_{-17}}{x_{-5}x_{-8}x_{-11}x_{-14}x_{-17}x_{-20}}&=\sum_{j=0}^{\infty}\prod_{i=1}^{7j+6}\frac{1}{1+x_{3i-17}x_{3i-14}x_{3i-11}x_{3i-8}x_{3i-5}x_{3i-2}}\end{aligned} \tag{15}$$

thus, $x_{-5}>x_{-2}$.

From here we obtain $x_{-20} > x_{-17} > x_{-14} > x_{-11} > x_{-8} > x_{-5} > x_{-2}$. Similarly, we can obtain $x_{-19} > x_{-16} > x_{-13} > x_{-10} > x_{-7} > x_{-4} > x_{-1}$ and $x_{-18} > x_{-15} > x_{-12} > x_{-9} > x_{-6} > x_{-3} > x_0$. We arrive at a contradiction which completes the proof of theorem.

## 3. Example

**Example 3.1:** If the initial conditions are selected in accordance with Lemma 1 and Theorem 1;

x[-20] = 0.99999999999999999999; x[-19] = 0.99999999999999999999; x[-18] = 0.888888888888888888888;
x[-17] = 0.99999999999999999999;
x[-16] = 0.99999999999999999999; x[-15] = 6; x[-14] = 0.99999999999999999; x[-13] = 0.9999999999999999;
x[-12] = 0.999999999999999; x[-11] = 0.77777777777777; x[-10] = 0.9999999999999; x[-9] = 0.999999999999;
x[-8] = 0.99999999999; x[-7] = 0.9999999999; x[-6] = 0.999999999; x[-5] = 0.99999999; x[-4] = 0.9999999;
x[-3] = 0.999999; x[-2] = 0.99999; x[-1] = 0.9999; x[0] = 0.999.

$$x_n = \{0.562502,0.500025,0.127093,0.695653,0.666678,5.32403,0.766667,0.750006,0.596669,$$
$$0.598291,0.800004,0.71259,0.847826,0.833336,0.776754,0.867925,0.857145,0.817496,$$
$$0.883324,0.874903,0.844688,0.465877,0.400026,0.0574,0.610812,0.579722,5.25524,$$
$$0.690279,0.672085,0.534988,0.530552,0.728998,0.655823,0.785099,0.767906,0.723852,$$
$$0.809425,0.796355,0.76781,0.828458,0.818062,0.797762,0.416792,0.350257,0.0315814,$$
$$0.565378,0.533888,5.22954,0.647651,0.629177,0.510473,0.491094,0.688476,0.632191,$$
$$0.747529,0.729414,0.700968,0.773522,0.759638,0.745588,0.794046,0.782923,0.776142,$$
$$0.385004,0.318321,0.0187474,0.535283,0.503755,5.21674,0.618892,0.600421,0.497984,$$
$$0.463926,0.660873,0.619944,0.721314,0.702817,0.688931,0.748166,0.733941,0.733742,$$
$$0.769474,0.758042,0.764474,0.361907,0.295245,0.0115556,0.513141,0.481689,...\}$$

solutions are obtained and the graphs of the solutions are shown below.

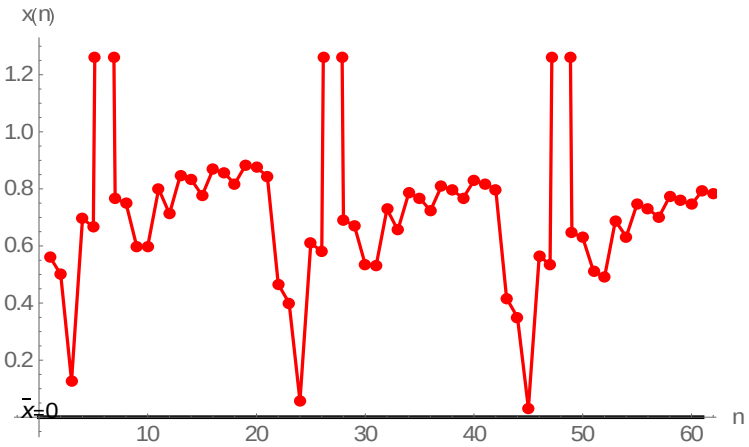


**Figure 1.** *$x_n$ solutions graph*

## References

[1]. Amleh A.M., Grove E.A., Ladas G., Georgiou D.A. "On the recursive sequence $x_{n+1} = \alpha + \frac{x_{n-1}}{x_n}$". J. Math. Anal. Appl., 233 (2), (1999), 790-798.

[2]. Belhannache F., Nouressadat T., Raafat A. "Dynamics of a third-order rational difference equation". Bull. Math. Soc. Sci. Math. Roumanie, 59 (1), (2016).

[3]. Cinar C., "On the positive solutions of the difference equation $x_{n+1}=\frac{x_{n-1}}{1+ax_nx_{n-1}}$". Appl. Math. Comp., 158 (3), (2004), 809–812.

[4]. Cinar C. "On the positive solutions of the difference equation $x_{n+1}=\frac{x_{n-1}}{-1+ax_nx_{n-1}}$". Appl. Math. Comp., 158 (3), (2004), 793–797.

[5]. Cinar C. "On the positive solutions of the difference equation $x_{n+1}=\frac{ax_{n-1}}{1+bx_nx_{n-1}}$". Appl. Math. Comp., 156 (3), (2004), 587–590.

[6]. DeVault R., Ladas G., Schultz W.S. "On the recursive sequence $x_{n+1}=\frac{A}{x_n}+\frac{1}{x_{n-2}}$". Proc. Amer. Math. Soc., 126 (11), (1998), 3257-3261.

[7]. Elabbasy E.M., El-Metwally H., Elsayed E.M. "On the difference equation $x_{n+1}=ax_n-\frac{bx_n}{cx_n-dx_{n-1}}$". Advances in Difference Equation, Article number: 082579, (2006), 1-10.

[8]. Elabbasy E.M., El-Metwally H., Elsayed E.M. "Qualitative behavior of higher order difference equation". Soochow Journal of Mathematics, 33(4), (2007), 861-873.

[9]. Elabbasy E.M., El-Metwally H., Elsayed E. M. "Global attractivity and periodic character of a fractional difference equation of order three". Yokohama Mathematical Journal, 53, (2007), 89-100.

[10]. Elabbasy E.M., El-Metwally H., Elsayed E.M. "On the difference equation $x_{n+1}=\frac{\alpha x_{n-k}}{\beta+\gamma\prod_{i=0}^{k}x_{n-i}}$". J. Conc. Appl. Math., 5(2), (2007), 101-113.

[11]. Elabbasy E.M., Elsayed E.M. "On the Global Attractivity of Difference Equation of Higher Order". Carpathian Journal of Mathematics, 24 (2), (2008), 45–53.

[12]. Elsayed E.M. "On the Solution of Recursive Sequence of Order Two". Fasciculi Mathematici, 40, (2008), 5–13.

[13]. Elsayed E.M. "Dynamics of a rational recursive sequences". International Journal of Difference Equations, 4(2), (2009), 185–200,.

[14]. Elsayed E.M. "Dynamics of a Recursive Sequence of Higher Order". Communications on Applied Nonlinear Analysis, 16 (2), (2009), 37–50.

[15]. Elsayed E.M. "Solution and atractivity for a rational recursive sequence". Discrete Dynamics in Nature and Society, (2011), 17.

[16]. Elsayed E.M. "On the solution of some difference equation". European Journal of Pure and Applied Mathematics, 4 (3), (2011), 287–303.

[17]. Elsayed E.M. "On the Dynamics of a higher order rational recursive sequence". Communications in Mathematical Analysis, 12 (1), (2012), 117–133.

[18]. Elsayed E.M. "Solution of rational difference system of order two". Mathematical and Computer Modelling, 55, (2012), 378–384.

[19]. Gibbons C.H., Kulenović M.R.S., Ladas G. "On the recursive sequence $x_{n+1}=\frac{\alpha+\beta x_{n-1}}{\chi+x_n}$". Math. Sci. Res. Hot-Line, 4 (2), (2000), 1-11.

[20]. Ibrahim T.F. “Periodicity and analytic solution of a recursive sequence with numerical examples”. Journal of Interdisciplinary Mathematics, 12 (5), (2009), 701-708.

[21]. Ibrahim T.F. “On the third order rational difference equation”. Int. J. Contemp. Math. Sciences 4 (27), (2009), 1321-1334.

[22]. Ibrahim T.F., Touafek N. “On a third order rational difference equation with variable coefficients”. DCDIS Series B: Applications & Algorithms 20, (2013), 251-264.

[23]. Ibrahim T.F. “Periodicity and Global Attractivity of Difference Equation of Higher Order”. Journal of Computational Analysis & Applications, 16 (1), (2014).

[24]. Khaliq A, Alzahrani F., Elsayed E.M. “Global attractivity of a rational difference equation of order ten”. J. Nonlinear Sci. Appl, 9 (6), (2016), 4465-4477.

[25]. Kulenović M.R.S., Ladas G., Sizer W.S. “On the recursive sequence $x_{n+1}=\frac{\alpha x_n+\beta x_{n-1}}{\chi x_n+\delta x_{n-1}}$”. Math. Sci. Res. Hot-Line, 2, 5, (1998), 1-16.

[26]. Kulenovic M.R.S., Moranjkic S., Nurkanovi, Z. “Naimark-Sacker bifurcation of second order rational difference equation with quadratic terms”. J. Nonlinear Sci. Appl, 10, (2017), 3477-3489.

[27]. Stevic S. “On the recursive sequence $x_{n+1}=\frac{x_{n-1}}{g(x_n)}$”. Taiwanese J. Math., 6, 3, (2002), 405-414.

[28]. Simsek D., Cinar C., Yalcinkaya I. “On the recursive sequence $x_{n+1}=\frac{x_{n-3}}{1+x_{n-1}}$”. Int. J. Contemp. Math. Sci., 1, 9-12, (2006), 475-480.

[29]. Simsek D., Cinar C., Karatas R., Yalcinkaya I. “On the recursive sequence $x_{n+1}=\frac{x_{n-5}}{1+x_{n-2}}$”. Int. J. Pure Appl. Math., 27, 4, (2006), 501-507.

[30]. Simsek D., Cinar C., Karatas R., Yalcinkaya I. "n the recursive sequence $x_{n+1}=\frac{x_{n-5}}{1+x_{n-1}x_{n-3}}$”. Int. J. Pure Appl. Math., 28, 1, (2006), 117-124.

[31]. Simsek D., Cinar C., Yalcinkaya I. “On The Recursive Sequence x(n+1) = x[n-(5k+9)] / 1+x(n-4)x(n-9) x[n-(5k+4)]”. Taiwanese Journal of Mathematics, Vol. 12, 5, (2008), 1087-1098.

[32]. Simsek D., Dogan A. “On A Class of Recursive Sequence”. Manas Journal of Engineering, 2, 1, (2014), 16-22.

[33]. Simsek D., Eröz M. “Solutions of The Rational Difference Equations $x_{n+1}=\frac{x_{n-3}}{1+x_n x_{n-1}x_{n-2}}$”. Manas Journal of Engineering, 4, 1, (2016), 12-20.

[34]. Simsek D., Oğul B. “Solutions of The Rational Difference Equations $x_{n+1}=\frac{x_{n-(2k+1)}}{1+x_{n-k}}$”. Manas Journal of Engineering, 5, 3, (2017), 57-68.

[35]. Şimşek D., Oğul B., Abdullayev F. “Solutions of The Rational Difference Equations $x_{n+1}=\frac{x_{n-11}}{1+x_{n-2}.x_{n-5}x_{n-8}}$”. AIP Conference Proceedings, 1880(1), 040003, (2017).

[36]. Simsek D., Abdullayev F. “On The Recursive Sequence $x_{n+1}=\frac{x_{n-(4k+3)}}{1+\prod_{t=0}^{2}x_{n-(k+1)t-k}}$”. Journal of Mathematics Sciences, 6, 222, (2017), 762-771.

[37]. Simsek D., Abdullayev F.G. "On the Recursive Sequence $x_{n+1}=\frac{x_{n-(k+1)}}{1+x_n x_{n-1}...x_{n-k}}$". Journal of Mathematical Sciences, 234 (1), (2018), 73-81.

[38]. Takahasi S., Yasuhide M., Takeshi M. "On Convergence of a Recursıve Sequence x_ {n+ 1}= f (x_ {n-1}, x_n)". Taiwanese Journal of Mathematics, 10 (3), (2006), 631-638.

[39]. Yan X., Wan-Tong L., Zhu Z. "On the recursive sequencex n+ 1= α-(x n/x n− 1)". Journal of Applied Mathematics and Computing, 17 (1), (2005), 269-282.

[40]. Zhang L., Guang Z., Hui L. "Periodicity and attractivity for a rational recursive sequence". Journal of Applied Mathematics and Computing 19 (1-2), (2005), 191-201.

Manas Journal of Engineering
ISSN 1694-7398 | e-ISSN 1694-7398

*Volume 7 (Issue 2) (2019) Pages 157-165*

# Generalized solution of boundary value problem with an inhomogeneous boundary condition

Elmira Abdyldaeva[1,*], Gulbarchyn Taalaibek kyzy[2], Bermet Anarkulova[3]

[1]Kyrgyz – Turkish Manas University, Faculty of Science, Department of Mathematics, Bishkek, Kyrgyzstan, efa_69@mail.ru; elmira.abdyldaeva@manas.edu.kg, ORCID: 000-0002-3874-9055

[2]Kyrgyz – Turkish Manas University, Faculty of Science, Department of Mathematics, Bishkek, Kyrgyzstan, gylbarchunt.@gmail.com

[3]Kyrgyz – Turkish Manas University, Faculty of Science, Department of Mathematics, Bishkek, Kyrgyzstan, jemchujina.96@gmail.com

**ABSTRACT**

A solution to boundary value problem is investigated for a controlled oscillation process, described by Fredholm integro-differential equation with inhomogeneous boundary conditions. An algorithm is developed for constructing a generalized solution of boundary value problem. It is proved that a weak generalized solution is an element of Hilbert space. Approximate solutions of the boundary value problem are determined and their convergence to the exact solution is proved.

**ARTICLE INFO**

***Research article***

*Received: 04.01.2019*
*Accepted: 19.09.2019*

***Keywords:***
*Boundary value problem,*
*Boundary control condition,*
*Generalized solution,*
*İntegral equation,*
*Fourier series,*
*Approximate solution*

**Corresponding author*

## 1. Introduction

Natural phenomena and technology processes are usually described by differential equations, integral equations and integro-differential equations. When investigating these processes, apart from the description by equations, additional conditions are required too [1-3]. These additional conditions could be given as an initial condition or as a boundary condition [4-7]. Therefore, equations satisfying the initial and boundary conditions, in other words, boundary value problems play an important role in practice.

Nowadays, boundary value problems with differential equations are relatively well understood [6-9], but boundary value problems with integral equations and integro-differential equations are not yet sufficiently investigated. Therefore, we study the boundary value problem for the oscillation process described by Fredholm integro-differential equations [10] with inhomogeneous boundary condition.

## 2. Generalized solution ofthe boundary value problem

Consider the Oscillaton process described by following integro-differential equation

$$V_{tt} = V_{xx} + \lambda \int_0^T K(t,\tau)V(\tau,x)d\tau\,, 0 < x < 1, 0 < t \leq T, \tag{1}$$

subject to initial

$$V(0,x)=\psi_1(x), V_t(0,x)=\psi_2(x), 0<x<1, \tag{2}$$

and boundary

$$V_x(t,0)=0, V_x(t,1)+\alpha V(t,1)=u(t), 0<t\le T, \tag{3}$$

conditions. Here $K(t,\tau)$ is a given function defined in domain $D=\{0\le t\le T, 0\le\tau\le T\}$ andsatisfies the condition

$$\int_0^T\int_0^T K^2(t,\tau)d\tau dt=K_0<\infty; \tag{4}$$

$\psi_1(x)\in H_1(0,1)$, $\psi_2(x)\in H(0,1)$ are given functions; $\lambda$ is a parameter, $T$ is a fixed moment of time, $\alpha>0$ is a constant. $H(Y)$ is a Hilbert space of square-integrable functions defined on the set $Y$.
Solution to boundary value problem [1-3] will be found in form of Fourier series:

$$V(t,x)=\sum_{n=1}^{\infty}V_n(t)z_n(x), \tag{5}$$

where

$$V_n(t)=\langle V(t,x),z_n(x)\rangle=\int_Q V(t,x)z_n(x)dx$$

is a Fouruier coefficient.

Functions $z_n(x)$are solutions to following problem

$$z_n''+\lambda_n^2 z_n(x)=0,\ \ z_n'(0)=0,\ \ z_n'(1)+\alpha z_n(1)=0,$$

for each fixed $n=1,2,3,\dots$ . Solving this boundary value problem, we have following functions which called *eigenfunctions*

$$z_n(x)=C_n cos\lambda_n x, \qquad n=1,2,3,\dots \tag{6}$$

Using boundary conditions we find that

$$C_n=\sqrt{\frac{2(\lambda_n^2+\alpha^2)}{\lambda_n^2+\alpha^2+\alpha}},$$

then $z_n(x)=\sqrt{\frac{2(\lambda_n^2+\alpha^2)}{\lambda_n^2+\alpha^2+\alpha}}cos\lambda_n x$ and $\{z_n(x)\}$ is an orthonormal system.

The numbers $\lambda_n$ are called an *eigenvalues* of eigenfnctions. They are positive roots of transcendental equations $tg\lambda_n=\frac{\alpha}{\lambda_n}$. It is known that we can't analytically solve these transcendental equations, so we have solved they graphically as the following Fig 1.

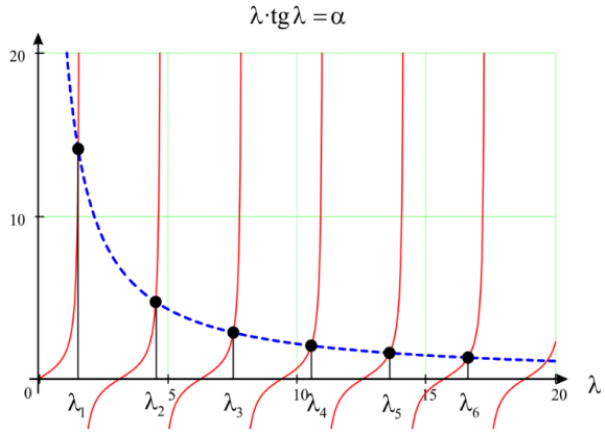


**Figure 1.** *Solutions of transcendental equations*

As shown in Fig. 1 values of eigenvalues $\lambda_n$are increase with growing value of *n*. To see that Eigenvalues $\lambda_n$ depend on parameter$\alpha$, we have calculated values of $\lambda_n$ using program MATLAB for $\alpha = 0.5;\ 1.5;\ 2.5;\ 3;\ 5$and obtain following table (Table 1). Similarly, values of eigenfunctions $z_n(x) = \sqrt{\frac{2(\lambda_n^2+\alpha^2)}{(\lambda_n^2+\alpha^2+\alpha)}}\cos\lambda_n x$ corresponding to eigenvalues $\lambda_n$was calculated and given in Table 1.

**Table 1.** *Eigenvalues and eigenfunctions*

| № | $\lambda_1$ | $\lambda_2$ | $\lambda_3$ | $\lambda_4$ | $\lambda_5$ | $\lambda_6$ | $\lambda_7$ | $\lambda_8$ | $\lambda_9$ | $\lambda_{10}$ |
|---|---|---|---|---|---|---|---|---|---|---|
| | | | | | $\alpha$=0.5 | | | | | |
| $\lambda_n(x)$ | 0.653 | 3.292 | 6.362 | 9.477 | 12.606 | 15.740 | 18.876 | 22.014 | 25.153 | 28.292 |
| $Z_n(x)$ | 1.0725 | 1.384 | 1.406 | 1.410 | 1.412 | 1.4128 | 1.4132 | 1.4135 | 1.4137 | 1.4138 |
| | | | | | $\alpha$=1.5 | | | | | |
| $\lambda_n(x)$ | 0.9882 | 3.5422 | 6.5097 | 9.5801 | 12.6841 | 15.8026 | 18.9286 | 22.059 | 25.1922 | 28.3272 |
| $Z_n(x)$ | 1.1685 | 1.3476 | 1.3910 | 1.4031 | 1.4078 | 1.410 | 1.4113 | 1.4121 | 1.4125 | 1.4129 |
| | | | | | $\alpha$=2.5 | | | | | |
| $\lambda_n(x)$ | 1.1422 | 3.7318 | 6.6431 | 9.6776 | 2.7598 | 15.8643 | 18.9805 | 22.1038 | 25.2315 | 28.3623 |
| $Z_n(x)$ | 1.2558 | 1.3340 | 1.3804 | 1.3968 | 1.4039 | 1.4074 | 1.4094 | 1.4106 | 1.4115 | 1.4120 |
| | | | | | $\alpha$=3 | | | | | |
| $\lambda_n(x)$ | 1.1925 | 3.8088 | 6.704 | 9.724 | 12.7966 | 15.8945 | 19.0061 | 22.1259 | 25.251 | 28.3797 |
| $Z_n(x)$ | 1.2462 | 1.3318 | 1.3765 | 1.3942 | 1.4021 | 1.4062 | 1.4085 | 1.4099 | 1.4109 | 1.4116 |
| | | | | | $\alpha$=5 | | | | | |
| $\lambda_n(x)$ | 1.3138 | 4.0336 | 6.9096 | 9.8927 | 12.9352 | 16.0107 | 19.1055 | 22.2126 | 25.3276 | 28.4483 |
| z(x) | 1.298 | 1.3356 | 1.3679 | 1.3863 | 1.3962 | 1.4018 | 1.4052 | 1.4074 | 1.4089 | 1.4099 |

From this table, we see that the more value of parameter $\alpha$the more values of eigenfunctions$z_n(x)$ and eigenvalues$\lambda_n$. As given boundary value problem (1) - (3) hasn't a classical solution, we use the notion of generalized solution of boundary value problem.

By multiplying both sides of tequation (4) by any function $\Phi(t,x)$ and using integral in parts we have integral identity

$$\int_0^1 [V_t\Phi(t,x) - V\Phi_t(t,x)]|_{t_1}^{t_2}dx \equiv \int_{t_1}^{t_2}\int_{t_1}^{t_2}(-V\Phi_{tt}(t,x) + V\Phi_{xx}(t,x))dxdt + \quad (7)$$

$$+\int_{t_1}^{t_2}\int_{0}^{1}(\lambda\int_{0}^{T}K(t,\tau)V(\tau,x)d\tau)\,\Phi(t,x)dxdt+$$

$$+\int_{t_1}^{t_2}(u(t)\Phi(t,1)+V(t,0)\Phi_x(t,0)-V(t,1)(\propto\Phi(t,1)+\Phi_x(t,1))dt;$$

***Definition.*** Function $V(t,x)\in H(Q_T)$, which satisfies the integral identity (7) and initial conditions in the weak sense ( i.e. for any functions $\phi_0(x)\in H(0,1),\phi_1(x)\in H(0,T)$ equalities

$$\lim_{t\to+0}\int_Q V(t,x)\phi_0(x)dx=\int_Q\psi_1(x)\phi_0(x)dx\ \lim_{t\to+0}\int_Q V_t(t,x)\phi_1(x)dx=\int_Q\psi_2(x)\phi_1(x)dx,$$

fulfile), is called a generalized solution of boundary value problem (1) - (3).

As function $\Phi(t,x)$ is arbitrary since the, we take $\Phi(t,x)\equiv z_n(x)$ in (7), and by direct calculations we have the following problem

$$V_n"(t)+\lambda_n^2V_n(t)=\lambda\int_0^T K(t,\tau)V_n(\tau)d\tau+u(t)z_n(1),$$

$$V_n(t)|_{t=t_1}=<V(t_1,x),z_n(x)>,$$

$$V_n'(t)|_{t=t_1}=<V_t(t_1,x),z_n(x)>.$$

We reduce this problem to Fredholm integral equation of the second kind

$$V_n(t)=\psi_{1n}cos\lambda_nt+\frac{1}{\lambda_n}\psi_{2n}sin\lambda_nt+$$

$$+\frac{1}{\lambda_n}\int_0^t sin\lambda_n(t-\tau)\left[\lambda\int_0^T K(t,\eta)V_n(\eta)d\eta+z_n(1)u(\tau)\right]d\tau. \tag{8}$$

Here, $\psi_{1n}$, $\psi_{2n}$are Fourier coefficients of functions $\psi_1(x)$, $\psi_2(x)$respectively.
Using the notations

$$q_n(t)=\psi_{1n}cos\lambda_nt+\frac{1}{\lambda_n}\psi_{2n}sin\lambda_nt+\frac{1}{\lambda_n}\int_0^t sin\lambda_n(t-\tau)z_n(1)u(\tau)\,d\tau; \tag{9}$$

$$K_n(t,s)=\frac{1}{\lambda_n}\int_0^t sin\lambda_n(t-\tau)K(\tau,s)\,d\tau; \tag{10}$$

we obtain the following integral equation

$$V_n(t)=\lambda\int_0^T K_n(t,s)\,V_n(s)ds+q_n(t), \tag{11}$$

Solution of this equation (11) will be found by following formula [6]`

$$V_n(t) = \lambda \int_0^T B_n(t,s,\lambda) q_n(s)\, ds + q_n(t); \tag{12}$$

Here

$$B_n(t,s,\lambda) = \sum_{i=1}^{\infty} \lambda^{i-1} K_{n,i}(t,s), \tag{13}$$

is a resolvents of repeated kernels $K_{n,i}(t,s)$. Repeated kernels $K_n(t,s) \equiv K_{n,i}(t,s)$are defined by formulas

$$K_{n,i+1}(t,s) = \int_0^T K_n(t,\tau) K_{n,i}(\tau,s)\, d\tau, \quad i = 1,2,3\ldots, \qquad K_{n,1}(t,s) = K_n(t,s). \tag{14}$$

for each fixed$n = 1,2,3, \ldots,$. By (10) - (14) equations, we get the following estimates:

$$|B_n(t,s,\lambda)| \le \sqrt{T} \frac{\sqrt{\int_0^T K_n^2(\tau,s) d\tau}}{\lambda_n - |\lambda| T\sqrt{K_0}}, \tag{15}$$

which hold for values of $\lambda$ satisfying the inequality

$$|\lambda| \frac{T}{\lambda_n} \sqrt{K_0} < 1. \tag{16}$$

Using inequality (15), we obtain inequalities:

$$\int_0^T |B_n(t,s,\lambda)|^2\, ds \le \frac{K_0 T}{(\lambda_n - |\lambda| T\sqrt{K_0})^2}. \tag{17}$$

Neumann series absolutely convergence for parameters, satisfying the condition

$$|\lambda| < \frac{\lambda_n}{T\sqrt{K_0}} \tag{18}$$

for each $n = 1,2,3, \ldots$, from which we can see that the radius of convergence $|\lambda| < \frac{\lambda_n}{T\sqrt{K_0}}$ of the Neumann series increases with growth $n$. As the sum of an absolutely convergent series, resolvent $B_n(t,s,\lambda)$ is a continuous function. As we have seen, when the condition $|\lambda| < \frac{\lambda_1}{T\sqrt{K_0}}$is met, the Neumann series absolutely converges to the continuous function for any $n = 1,2,3$. Thus, we find the solution of the boundary value problem (1) - (3) by the formula (5), where $V_n(t)$ is defined as solution of the integral equation (12) by the formula (13).
Substituting (11) into (12) by direct calculations we obtain

$$V_n(t) = \lambda \int_0^T B_n(t,s,\lambda) q_n(s) ds + q_n(t) =$$

$$= \lambda \int_0^T B_n(t,s,\lambda)\left[\psi_{1n} cos\lambda_n s + \frac{1}{\lambda_n}\psi_{2n} sin\lambda_n s + \frac{1}{\lambda_n}\int_0^s sin\lambda_n(s-\tau) z_n(1)u(\tau)\, d\tau\right] +$$

$$+\psi_{1n} cos\lambda_n t + \frac{1}{\lambda_n}\psi_{2n} sin\lambda_n t + \frac{1}{\lambda_n}\int_0^t sin\lambda_n(t-\tau) z_n(1)u(\tau)\, d\tau =$$

$$= \psi_n(t,\lambda) + \frac{1}{\lambda_n}\left[\int_0^t \int_\tau^T B_n(t,s,\lambda) sin\lambda_n(s-\tau) z_n(1)u(\tau) ds d\tau +\right.$$

$$\left. + \int_t^T \int_\tau^T B_n(t,s,\lambda) sin\lambda_n(s-\tau) z_n(1)u(\tau) ds d\tau + \int_0^t sin\lambda_n(t-\tau) z_n(1)u(\tau) d\tau\right].$$

Denoting the expression by

$$\psi_n(t,\lambda) = \psi_n\left[cos\lambda_n s + \lambda\int_0^t B_n(t,s,\lambda) cos\lambda_n\, sds\right] + \frac{1}{\lambda_n}\psi_{2n}\left[sin\lambda_n t + \lambda\int_0^t B_n(t,s,\lambda) sin\lambda_n\, sds\right], \tag{19}$$

$$D_n(t,\tau,\lambda) = \begin{cases} sin\lambda_n(t-\tau) + \int_0^t B_n(t,s,\lambda) sin\lambda_n(s-\tau) ds, & 0 \le \tau \le t, \\ \int_0^t B_n(t,s,\lambda) sin\lambda_n(s-\tau) ds, & t \le \tau \le T, \end{cases} \tag{20}$$

we get the formula for finding the Fourier coefficient

$$V_n(t) = \psi_n(t,\lambda) + \frac{1}{\lambda_n}\int_0^T D_n(t,\tau,\lambda)\, z_n(1)u(\tau) d\tau. \tag{21}$$

Then solution $V(t,x)$to boundary value problem (1) - (3) is determined by the formula

$$V(t,x) = \sum_{n=1}^{\infty} V_n(t) z_n(x) =$$

$$= \sum_{n=1}^{\infty}\left[\psi_n(t,\lambda) + \frac{1}{\lambda_n}\int_0^T D_n(t,\tau,\lambda)\, z_n(1)u(\tau) d\tau\right] z_n(x); \tag{22}$$

***Lemma 1.*** The solution of boundary value problem (1) - (3) defined by formula (22) is an element of the Hilbert space $H(Q)$.

***Proof:*** To proof Lemma 1 we should show that following equality is fulfill

$$\int_0^T V^2(t,x) dx dt < \infty.$$

Taking equations (10) and (11) into account we get the following inequalities:

$$\int_t^T\int_\tau^T V^2(t,x)dxdt = \int_t^T\int_\tau^T [V_n(t)z_n(x)]^2 dxdt = \int_0^T \sum_{n=1}^{\infty} V_n^2(t)dt \le$$

$$\le 2\left[3T\lambda^2 \frac{K_0 T}{\left(\lambda_1 - |\lambda|T\sqrt{K_0}\right)^2}\left(\|\psi_1(x)\|^2_{H(0,1)} + \frac{1}{\lambda_1^2}\|\psi_2(x)\|^2_{H(0,1)} + \frac{1}{\lambda^2_1}\|z_n(1)\|^2\|u(t)\|^2_{H(0,T)}\right) + \right.$$

$$\left. +3T\left(\|\psi_{1n}\|^2 + \frac{1}{\lambda^2_1}\|\psi_{2n}\|^2 + \frac{1}{\lambda^2_1}\|z_n(1)\|^2\|u\|^2\right)\right] \le$$

$$\le 6T\left[\|\psi_{1n}\|^2 + \frac{1}{\lambda_1^2}\|\psi_{2n}\|^2 + \frac{1}{\lambda_1^2}\|z_n(1)\|^2\|u\|^2\right]\left(\lambda^2 \frac{K_0 T}{\left(\lambda_1 - |\lambda|T\sqrt{K_0}\right)^2} + 1\right) < \infty,$$

from which it follows that $V(t,x) \in H(Q)$.

## 3. Approximate solution of boundary value problem

When defining the functions $V_n(t), n = 1,2,3,\ldots$, by formulas (20)-(22), due to infinity of the Neumann series, it is not always possible to find the exact value of resolvent $R_n(t,s,\lambda)$. Therefore, approximations of the resolvent are usually used. Truncated series in the form

$$B_n^m(t,s,\lambda) = \sum_{i=1}^{m} \lambda^{i-1} K_{n,i}(t,s) \tag{23}$$

is called an $m$ th *approximation of the resolvent* or a *resolvental approximation* for each fixed$n = 1,2,3,\ldots$ The function $V_n^m(t)$defined by formula

$$V_n^m(t) = \lambda \int_0^T B_n^m(t,s,\lambda)q_n(s)ds + q_n(t), \ n = 1,2,3,\ldots, \tag{24}$$

and it is called the *m*th *approximation* of the function $V_n(t)$ for each fixed$m = 1,2,3,\ldots$ .
According to formulas (5) and (23), function is defined by the formulas

$$V^m(t,x) = \sum_{n=1}^{\infty} V_n^m(t)z_n(x)$$

and it is called an *m*th approximation of the solution to boundary value problem (1)-(3) .

To prove that mth approximate solutions $V^m(t,x)$ to boundary value problem (1) - (3) converge to their exact $V(t,x)$ solution with respect to the norm of the space, we do the following calculations :

$$\|V(t,x) - V^m(t,x)\|^2_{H(Q)} = \int_0^T\int_0^1 \left(V(t,x) - V^m(t,x)\right)^2 dxdt \le \int_0^T\int_0^1 \left(\sum_{n=1}^{\infty}[V_n(t) - V_n^m(t)]z_n(x)\right)^2 dxdt \le$$

$$\le \int_0^T \sum_{n=1}^{\infty}[V_n(t) - V_n^m(t)]^2\, dt \le \int_0^T \sum_{n=1}^{\infty}\{\psi_{1n} + \left(\lambda\int_0^T [B_n(t,s,\lambda) - B_n^m(t,s,\lambda)]\cos\lambda_n s ds\right)$$

$$+\frac{\psi_{2n}}{\lambda_n}\left(\lambda\int_0^T [B_n(t,s,\lambda) - B_n^m(t,s,\lambda)]\cos\lambda_n s ds\right) + \frac{1}{\lambda_n}\int_0^T D_n[(t,s,\lambda) - D_n^m(t,s,\lambda)]z_n(1)u(\tau)d\tau\Big\}^2 dt \le$$

$$\leq 3T\sum_{n=1}^{\infty}\left(\psi_{1n}^2+\frac{\psi_{2n}^2}{\lambda_n^2}+\frac{2T}{\lambda_n^2}\|u(t)\|_{H(0,T)}^2\right)\frac{\lambda^2K_0T}{\lambda_n^2}\left(\sum_{i=m+1}^{\infty}\left[|\lambda|\frac{\sqrt{K_0T^2}}{\lambda_n}\right]^{i-1}\right)^{2m}\left(1-\frac{1}{\ln\frac{|\lambda|\sqrt{K_0T^2}}{\lambda_n}}\right)^2\leq \quad (25)$$

$$\leq C_3(\lambda)\left(|\lambda|\frac{\sqrt{K_0T^2}}{\lambda_1}\right)^{2m}\to\infty,\quad m\to\infty,$$

$$C_3(\lambda)=3T\left(\|\psi_1(x)\|_{H(0,1)}^2+\frac{2}{\lambda_n^2}\|\psi_2(x)\|_{H(0,1)}^2+\frac{2T}{\lambda_1^2}\|u(t)\|_{H(0,T)}^2\right)\lambda^2K_0T\times\left(1-\frac{1}{\ln|\lambda|\frac{\sqrt{K_0T^2}}{\lambda_1}}\right)\left(\frac{1}{\lambda_1^2}+\frac{1}{6}\right).$$

The solution of boundary value problem, defined by truncated Fourier series,

$$V^{m,k}(t,x)=\sum_{n=1}^{k}V_n^{m,k}(t)\,z_n(x)=\sum_{n=1}^{k}(\lambda\int_0^T B_n^{m,k}(t,s,\lambda)q_n(s)ds+q_n(t)) \quad (26)$$

is called an *m,k[th] approximate* solution of boundary value problem for each fixed $m,k=1,2,3,\ldots$. Proof of convergence these *m,k [th] approximate* solutions *to m [th] approximate* solutions follows from following inequality:

$$\|V^m(t,x)-V^{m,k}(t,x)\|_{H(Q)}^2=\int_0^T\int_0^1(\sum_{n=1}^{\infty}V^m(t,x)-V^{m,k}(t,x))^2\,dxdt\leq$$

$$\leq\int_0^T\int_0^1\left(\sum_{n=1}^{\infty}\left[V_n^m(t)-V_n^{m,k}(t)\right]z_n(x)\right)^2dxdt\leq\int_0^T\sum_{n=1}^{\infty}\left[V_n^m(t)-V_n^{m,k}(t)\right]^2dt\leq$$

$$\leq\int_0^T\sum_{n=1}^{\infty}\{\psi_{1n}+\left(\lambda\int_0^T\left[B_n^m(t,s,\lambda)-B_n^{m,k}(t,s,\lambda)\right]\cos\lambda_n s ds\right)$$

$$+\frac{\psi_{2n}}{\lambda_n}\left(\lambda\int_0^T[B_n(t,s,\lambda)-B_n^m(t,s,\lambda)]\cos\lambda_n s ds\right)+\frac{1}{\lambda_n}\int_0^T D_n[(t,s,\lambda)-D_n^m(t,s,\lambda)]z_n(1)u(\tau)d\tau\Bigg\}^2dt\leq$$

$$\leq 2\int_0^T\sum_{n=k+1}^{\infty}(\lambda^2\frac{K_0T^2}{\left(\lambda_n-|\lambda|T\sqrt{K_0}\right)^2}+1)\int_0^T q_n^2(t)dt\leq$$

$$\leq 2\sum_{n=k+1}^{\infty}(\lambda^2\frac{K_0T^2}{\left(\lambda_n-|\lambda|T\sqrt{K_0}\right)^2}+1)\int_0^T\left(\psi_{1n}\cos\lambda_n t+\frac{\psi_{2n}}{\lambda_n}\sin\lambda_n t++\frac{1}{\lambda_n}\int_0^t\sin\lambda_n(t-\tau)z_n(1)u(\tau)\,d\tau\right)^2dt\leq$$

$$\leq 6\left(1+\lambda^2\frac{K_0T^2}{\left(\lambda_n-|\lambda|T\sqrt{K_0}\right)^2}\right)\sum_{n=k+1}^{\infty}\left(\psi_{1n}^2+\frac{\psi_{1n}^2}{\lambda}+\frac{2}{\lambda_n^2}\int_0^T\sin^2(T-\tau)d\tau\int_0^T u^2(\tau)\,d\tau\right)\underset{k\to\infty}{\to}0,\ \ m=1,2,3,\ldots \quad (27)$$

Convergence of that *m,k [th]* approximate solutions $V^{m,k}(t,x)$of BVP(1)-(3) to exact solutions $V(t,x)$ is proved as follows

$$\|V(t,x)-V^{m,k}(t,x)\|_H=\|V(t,x)-V^m(t,x)\|_H+\|V^m(t,x)-V^{m,k}(t,x)\|_H\underset{k,m\to\infty}{\to}0,$$

As according to formulas (25) qnd (27), we obtain

$$||V(t,x) - V^m(t,x)||_{H(Q)} \underset{m\to\infty}{\to} 0,$$

$$||V^m(t,x) - V^{m,k}(t)||_{H(Q)} \underset{k\to\infty}{\to} 0, \qquad m = 1,2,3,\ldots.$$

## 4. Conclusion

- An algorithm is developed for finding generalized solutions of the inhomogeneous boundary value problem with Frodholm integro-differential operator;
- Approximate solutions, which used in sientific researches and in practice, are found;
- Convergence of approximate solutions of boundary value problem to its exact solutions is proved;
- By numerical calculations using Matlab, we investigated the dependence of the solution of given boundary value problem on a parameter.

## References

[1] Vladimirov V.S.," Matematicheskie zadachi odnoskorostnoi toerii perenosa chastis", Trudy MİAN, T. 61, (1961), 130-158.

[2] Volterra V., Teoriya funksionalov, integrelnyhi integro- differensiyalnyh uravneniy. Moskva, Nauka, (1982).

[3] Tyn Myint-U, Lokenath, Partial Differential Equations for Scientists and Engineers, Prentice Hall, (1987).

[4] Sharma J.N., Kehar Singh, Partial Differential Equations for Engineers and Scientists, Alpha Science İnternational Ltd. UK. (2000).

[5] Denemeyer R. Introduction to: Partial Differential Equations and Boundary Value Problems, McGraw-Hill Book Company, New York, (1968).

[6] Snedon I.N., Elements of Partial Differential Equations, dover Publications, INC.,New York , (2006).

[7] Chaglıyan M., Chelebi O., Kysmi Diferensiyel Denklemler, Uludag Üniversitesi Guchlendirme Vakfı,Yayın No:196,VİPASH A.SH.,Yayın No:72,2002.

[8] Koca K., Kısmi Diferensiyel Denklemler, Gunduz Egitim ve Yayıncılık, Ankara, (2001).

[9] Anar E., Kısmi Diferensiyel Denklemler, Palme Yayıncılık, Ankara, (2005).

[10] Kerimbekov A., Abdyldaeva E., "On the Solvability of a Nonlinear Tracking Problem Under Boundary Control for the Elastic Oscillations Described by Fredholm Integro-Differential Equations", System Modeling and Optimization. 27th IFIP TC 7 Conference, CSMO 2015. Sophia Antipolis, France, June 29–July 3, 2015. Revised Selected Papers. Sprınger. (2017). 312-322.